Enhanced Utilization of Pyrolysis Products from Waste Tyre for the Generation of Fuels

Vincent Kok Yeow, Tan

A thesis submitted for the degree of

Doctor of Philosophy

Department of Chemical Engineering
Monash University

2019

Copyright notice

Contents

Abstract

Pyrolysis process is an optimal recycling route to convert waste scrap tyre into high-value resources such as liquid oil that is low in oxygen-containing hydrocarbons and solid char that is rich in metallic species. Although many studies have been conducted for the pyrolysis for tyre, the understanding of the fundamental science underpinning the pyrolysis of scrap tyre chip, in particular the reaction mechanism of tyre volatiles is still far from complete.

This PhD project has examined the mild pyrolysis of scrap tyre in an integrated manner by examining the co-effects of several operating conditions including terminal temperature, heating rate, volatile residence time, tyre particle size and non-inert gases (CO_2 and/or H_2O). These crucial operating conditions and the resulting heat transfer efficiencies was taken into consideration in the development of a mechanistic kinetic model that considers the inherent molecular structure of tyre rubbers, and the reaction mechanism of tyre volatiles that ultimately affects the qualities of tars. In addition, this PhD project has investigated the catalytic performance and mechanism of tyre char upon the pyrolysis of lignites.

It has been confirmed that in a simulated fixed-bed reactor with the absence of carrier gas, the temperature discrepancy between particle and reactor environment can be correlated exponentially with the extent of secondary cracking of tyre volatiles. The temperature discrepancy of 115 °C resulted in the loss of tar with up to 17 wt%. Upon an increase in the temperature discrepancy by either increasing the heating rate or tyre chip size, the inherent long-chain aliphatics preferentially underwent scission, cyclisation and even polymerisation, leading to the formation of abundant heavy aromatics and light gases that are rich in methane. In the presence of steam, the long-chain aliphatics was reactive enough to undergo steam

reforming reaction even at 600°C, upon the catalytic effect of the nascent char derived from scrap tyre chips. The catalytic effect of the char from tyre chips were further extended to the pyrolysis of lignites in various operating conditions -reactor terminal temperature, heating rate and steam environment. The catalytic effect of tyre char is profound in the fast pyrolysis scheme, and from a minimum temperature of 700^{o}C. The catalyst is also highly size selective for the upgrading of primary volatile vapours. The heavy molecules of lignites are preferentially easily trapped within the catalyst matrix, and hence, upgraded via catalytic scission and decarbonylation reactions even in inert argon. The coke deposit derived from the cracking of heavy volatiles is also catalysed for the respective char-steam gasification. The nano-sized Zn-bearing species are responsible for the co-production of H_2-rich syngas and upgraded liquid oil via steam-reforming reactions, whereas the S-bearing active sites are essential and responsible for most of the decarbonylation reaction.

Declaration

This thesis contains no material which has been accepted for the award of any other degree or diploma at any university or equivalent institution and that, to the best of my knowledge and belief, this thesis contains no material previously published or written by another person, except where due reference is made in the text of the thesis.

Signature:

Print Name:

Date:

Acknowledgements

Firstly, I would like to express my gratitude to my supervisor, Prof. Lian Zhang for his continued support and encouragement throughout the length of my candidature. I would also like to thank my friends and colleagues in our research group: Dr. Anthony De Girolamo, Dr. Bai Qian Dai, Ms. Iman Ja'baz, Ms. Miriam Issac, Dr. Song Zhou, Dr. Tahereh Hosseini, Ms. Rabeeh Golmohammadzadeh, Mr. Binbin Qian, Ms. Qiaoqiao Zhou.

Thank you to all the Chemical Engineering department staff, particularly Ross Ellingham, Kim Phu and Lilyanne Price. More important, a huge appreciation towards the senior learning skills advisor, Lilian Khaw who is always willing to help me with my writing even though she has a busy schedule.

I am grateful to Coal Energy Australia (CEA) and Department of Industry, Innovation and Science, Australian Government for the research fund support. This research was supported by the Australian Research Council (ARC) under its Industrial Research Training Hub (170100009) and (150100006) schemes for the joint project between Monash and Advanced Fuel Innovation Pty Ltd. The scrap tyre used in this project was provided by the Tyrecycle Pty Ltd, Australia. Their contributions to this PhD study are highly appreciated.

Last but not least, a big thank you to my family for their continuous support and encouragement.

Publications during enrolment

Published work

V. Tan, A. De Girolamo, T. Hosseini, J. Alhesan, L. Zhang, Scrap tyre pyrolysis: Modified chemical percolation devolatilization (MCPD) to describe the influence of pyrolysis conditions on product yields, Waste Manage. 76 (2018) 516–527. doi: 10.1016/j.wasman.2018.03.013

V. Tan, A. De Girolamo, T. Hosseini, J. Alhesan, Q. Zhou, L. Zhang, *Secondary reactions of volatiles upon the influences of particle temperature discrepancy and gas environment during the pyrolysis of scrap tyre chips*, Fuel. doi: 10.1016/j.fuel.2019.116291

Thesis including published works declaration

I hereby declare that this thesis contains no material which has been accepted for the award of any other degree or diploma at any university or equivalent institution and that, to the best of my knowledge and belief, this thesis contains no material previously published or written by another person, except where due reference is made in the text of the thesis.

This thesis includes one original paper published and one accepted in peer reviewed journals, and one submitted publications. The core theme of the thesis is the pyrolysis of waste tyres and low-rank coals. The ideas, development and writing up of all the papers in the thesis were the principal responsibility of myself, the student, working within the Department of Chemical Engineering under the supervision of Prof. Lian Zhang.

The inclusion of co-authors reflects the fact that the work came from active collaboration between researchers and acknowledges input into team-based research.

In the case of Chapter 4 and 5 my contribution to the work involved the following:

Thesis Chapter	Publication Title	Status	Nature and % of student contribution	Co-author name(s) Nature and % of Co-author's contribution*	Co-author(s), Monash student
4	Scrap tyre pyrolysis: Modified CPD model to describe the influence of pyrolysis conditions	Published	85%. Concept and collecting data and writing first draft	1) Anthony De Girolamo, experimental work 5% 2) Tahereh Hosseini, revised manuscript, 5% 3) Jameel Aljariri Alhesan, 5%	Yes Yes Yes

	on product yields			4) Lian Zhang, supervisor	No
5	Secondary reactions of volatiles upon the influences of particles temperature discrepancy and gas environment during the pyrolysis of scrap tyre chips	Published	80%. Concept and collecting data and writing first draft	1) Anthony De Girolamo, experimental work 5% 2) Tahereh Hosseini, revised manuscript, 5% 3) Jameel Aljariri Alhesan, 5% 4) Qiaoqiao Zhou, concept provided, 5% 5) Lian Zhang, supervisor	Yes Yes Yes Yes No

I have renumbered sections of submitted or published papers in order to generate a consistent presentation within the thesis.

Student signature: **Date:**

The undersigned hereby certify that the above declaration correctly reflects the nature and extent of the student's and co-authors' contributions to this work. In instances where I am not the responsible author, I have consulted with the responsible author to agree on the respective contributions of the authors.

Main Supervisor signature: **Date:**

List of Figures

List of Tables

Table 21 Elemental analysis of YL lignite tars with respect to the cyclic test of tyre char in the steam-assisted pyrolysis at 800°C, upon a fast heating.

Abbreviations and nomenclature

amu = atomic mass unit, 1 g/mol

A_b = Frequency factor for bridge breaking (s^{-1})

A_{cross} = Frequency factor for cross-linking (s^{-1})

A_g = Frequency factor for gas release (s^{-1})

A_s = Pre-exponential factor of secondary cracking reaction (s^{-1})

C_p = Specific heat ($J \cdot kg^{-1} \cdot K^{-1}$)

$C_{p,tyre}$ =Tyre specific heat ($J \cdot kg^{-1} \cdot K^{-1}$)

$C_{p,carbon}$ =Carbon specific heat ($J \cdot kg^{-1} \cdot K^{-1}$)

C_o = Initial fraction of char bridges (-)

E_{cross} = Activation energy for cross-linking ($kcal \cdot mol^{-1}$)

E_b = Activation energy for bridge breaking ($kcal.mol^{-1}$)

E_g = Activation energy for gas formation ($kcal \cdot mol^{-1}$)

E_s = Activation energy for secondary cracking ($kcal \cdot mol^{-1}$)

fal= Aliphaticity (fraction, [-])

fa = Aromaticity (fraction, [-])

fa^c = The carboxyl and carbonyl region (fraction, [-])

fa' = The main aromatic ring region (fraction, [-])

fa^o = Aldehyde and ketone region (fraction, [-])

fa^{oo} = Acid, ester, amide region (fraction, [-])

fa^H = Aromatic ring carbons with an attached proton (fraction, [-])

fa^N = Non-protonated aromatic carbons (fraction, [-])

fa^P = Aromatic ring carbons with an attached oxygen (fraction, [-])

fa^S = Aromatic ring carbons with an attached alkyl group (fraction, [-])

fa^B= Bridge head carbons (fraction, [-])

fal^* = Methyls and methoxy methyls (fraction, [-])

fal^H = Methylene and methane groups (fraction, [-])

fal^o =Total aliphatic carbon bonded to an oxygen atom (fraction, [-])

k= Thermal conductivity ($W \cdot m^{-1} \cdot K^{-1}$)

k_{tyre} = Tyre thermal conductivity ($W \cdot m^{-1} \cdot K^{-1}$))

k_{carbon} = Carbon thermal conductivity ($W \cdot m^{-1} \cdot K^{-1}$)

k_δ/k_c = Ratio of bridge breaking to char bridge formation (-)

MW_{cl} =Average number of aromatic carbons per cluster (-)

MW_{side} =Average molecular weight of a side chain (-)

h= Convection coefficient ($W \cdot m^{-2} \cdot K^{-1}$)

ΔH_{rxn}= Heat of reaction ($kJ \cdot kg^{-1}$)

P_o = Initial number of bridges in the tyre lattice matrix (-)

r = Radius of particle (m)

r_i= radius at point i (m)

R= Gas constant ($kcal \cdot K^{-1} \cdot mol^{-1}$)

T= Temperature (K)

T_∞= Reactor temperature (K)

T_s= Tyre surface temperature (K)

VM= Volatile matter (daf) from proximate analysis (fraction, [-])

x_i= Primary tar amount at each point i across the tyre particle (s^{-1})

X_i= Averaged amount of primary tar (s^{-1})

X= Tar amount after cracking (s^{-1})

Greek Symbols

ρ_{tyre}=Density of tyre ($kg \cdot m^{-3}$)

ε= Emissivity (-)

σ =Stefan-Boltzmann constant (5.67×10^{-8} $J \cdot m^{-2} \cdot s^{-1} \cdot K^{-4}$)

α = Mass loss of tyre at different pyrolysis conditions (fraction, [-])

σ+1 = Lattice coordination number (-)

σ_b = Standard deviation in E_b ($kcal \cdot mol^{-1}$)

σ_g = Standard deviation in E_g ($kcal \cdot mol^{-1}$)

Chapter 1 - Introduction

This page is intentionally left blank

1.1 Overview

The disposal of waste tyre is a serious environmental issue, predominantly due to its poor biodegradability [1]. In Australia, on average, 51 million of waste tyre are generated each year in which only 5 % of waste tyre is properly reused whereas the rest are simply piled in large quantities [2]. Random disposal of waste tyre can easily cause fires. Tyre fires are very difficult to control, which can create a great deal of hazardous smoke, causing a health risk through the inhalation of particles and chemicals. Various technologies have been developed to recycle waste tyre, among which, pyrolysis has received a great deal of attention due to its ability to recover the energy content and valuable chemicals [3, 4]. Specifically, three value-added products can be generated via tyre pyrolysis, solid semi-coke (char), liquid oil (tar) and light gases ($<C_5$).

However, the utilisation of these pyrolysis product from waste tyre could be a challenging process. Although it is reported that tyre tar has high potential to be used as a direct fuel, added to petroleum refinery stocks or upgraded using catalysts to a premium grade fuel, it also contains a large number of heavy matters such as coke and asphaltene [5] that is associated with high concentration of sulphur element [6], which causes serious blockage of volatile production line, and becomes a huge threat to the environment upon combustion. Not only that, although it is reported that tyre char could be used as carbon black, it contains metallic species as large as 15*wt%* which will result in relatively low energy value. Despite the low utilisation of these by-products as shown in previous studies, these pyrolysis by-products have great potential to be reused which should be further explored and enhanced.

Therefore, this PhD project aims to enhance the utilization of these pyrolysis products, tar and char from waste tyre chips, by focusing on understanding the kinetic behaviour of tyre chip upon the pyrolysis process, the reaction mechanism and properties of tar oils resulted from various operating conditions, and the potential use of tyre char as catalyst to upgrade the quality of tar oils derived from other carbonaceous materials.

This project is based on three major hypotheses that embody the project:

1. It is hypothesized that the heat transfer efficiency will significantly be affected by the operating conditions – the terminal temperature, heating rate, particle size and flowrate of carrier gas and presence of non-inert gases.
2. The second hypothesis is that fast heating in *large* volatile residence time will generate a large amount of asphaltene in the tar as compared to slow heating in the same volatile residence time, as opposed to previous findings that fast heating generates a better quality of tar in terms of the light oil fraction and higher H/C ratio.
3. The third hypothesis is that the ash-forming elements in tyre char can deoxygenate the oils from *low-rank coals*, as opposed to what previous studies have concluded --- tyre char promotes the production of hydrogen [7] and produces a lower oxygen content of tar oil [8] from *biomass*, although the catalytic mechanism was not mentioned.

To test all hypotheses mentioned above, a large number of experimental and characterisation techniques were employed for quantitative and qualitative analysis of the raw materials and the resultant tar and char products. Large scales of fixed bed vertical and horizontal reactors were used for all waste tyre and Victorian brown coals pyrolysis experiments. ^{13}C-NMR (carbon-nuclear magnetic resonance) was used for the molecular footprint of the organics for the raw tyre while ^{1}H-NMR (Proton- nuclear magnetic resonance), FT-IR (Fourier-

transform infrared spectroscopy) and GC-MS (Gas Chromatography-Mass Spectrometry) were used for the molecular footprint of organics for the tar oils from both tyre and brown coal. The method of solvent fractionation by n-hexane and toluene was used to fractionate the overall tar into light oil, asphaltene and pre-asphaltene. X-ray powder diffraction (XRD), X-ray fluorescence (XRF) and Transmission Electron Microscopy (TEM) were used for the clarification of the active sites in the tyre chars for the catalytic reactions.

It is believed that the outcomes of this project could provide some valuable insights into the pyrolysis reaction mechanism of tyre chips, optimisation of the properties of tyre tars, and catalytic capability of tyre char, which in turn enhances the utilisation of the pyrolysis products from waste tyre.

1.2 Research aims

The overall aim of this PhD research program is to design an effective approach for the utilisation of waste tyre upon pyrolysis process. Specific aims to bridge the knowledge gaps are described as follows:

1. Develop a modified CPD model for tyre pyrolysis based on the conventional CPD model by integrating heat transfer and the secondary reactions of primary tar, so as to make it fit for the pyrolysis of scrap tyre chips under a broad range of critical pyrolysis conditions including the particle size, carrier gas flow rate, terminal temperature, heating rate and non-inert carrier gas (pure argon versus 15-30 *vol%* CO_2 and/or steam balanced by argon) in a lab-scale fixed bed pyrolyzer.

2. Study the influences of temperature discrepancy between particle and gas environment, which provides insights into the optimisation of the properties of liquid tars derived from waste scrap chips.

3. Explore the catalytic potential of tyre char on low-rank coals, and investigate the catalytic mechanism of the char-volatile interaction between the roles of minerals in tyre char and the exact chemical species in coal volatiles.

1.3 Thesis outline

Chapter 1 gives an overview of the area of research and highlights the main research aims.

Chapter 2 presents a review of the literature, in relation to the kinetic modelling of waste tyre, pyrolysis process of waste tyre and low-rank coals, influence of operating conditions on the physiochemical properties of tars derived from tyre and coal, and state-of-the-art technologies for tar upgrading in terms of deoxygenation or thermal cracking using different types of catalysts. This review ultimately leads to the identification of research gaps that form the foundation of this PhD project.

Chapter 3 is a summary of the experimental and analytical methods used during the course of this research project.

Chapter 4 develops a modified chemical percolation devolatilization (M-CPD) model that can include the heat transfer, primary pyrolysis and secondary cracking reactions of volatiles to describe the pyrolysis of waste scrap tyre chip, as well as to examine the influence of operating conditions on the product yields.

Chapter 5 conducts the mild pyrolysis of scrap tyre at 600^{o}C, in an integrated manner by examining the co-effects of several operating conditions including the heating rate, volatile residence time, tyre particle size and non-inert gases (CO_2 and/or H_2O) on the quality of tars. In particular, it is aimed to elucidate the influences of particle temperature discrepancy (to the surrounding gas environment) and reactive gas on the quality of tars.

Chapter 6 examines the catalytic performance of tyre char on different Victorian brown coals as well as the catalytic reaction mechanism interacting between the active sites of tyre char and chemical species of the coal volatiles.

Chapter 7 presents the conclusions of the study and recommendations for future works related to the further development of the heat transfer model, cost analysis of tar upgrading process, and catalytic mechanism for individual tarry species.

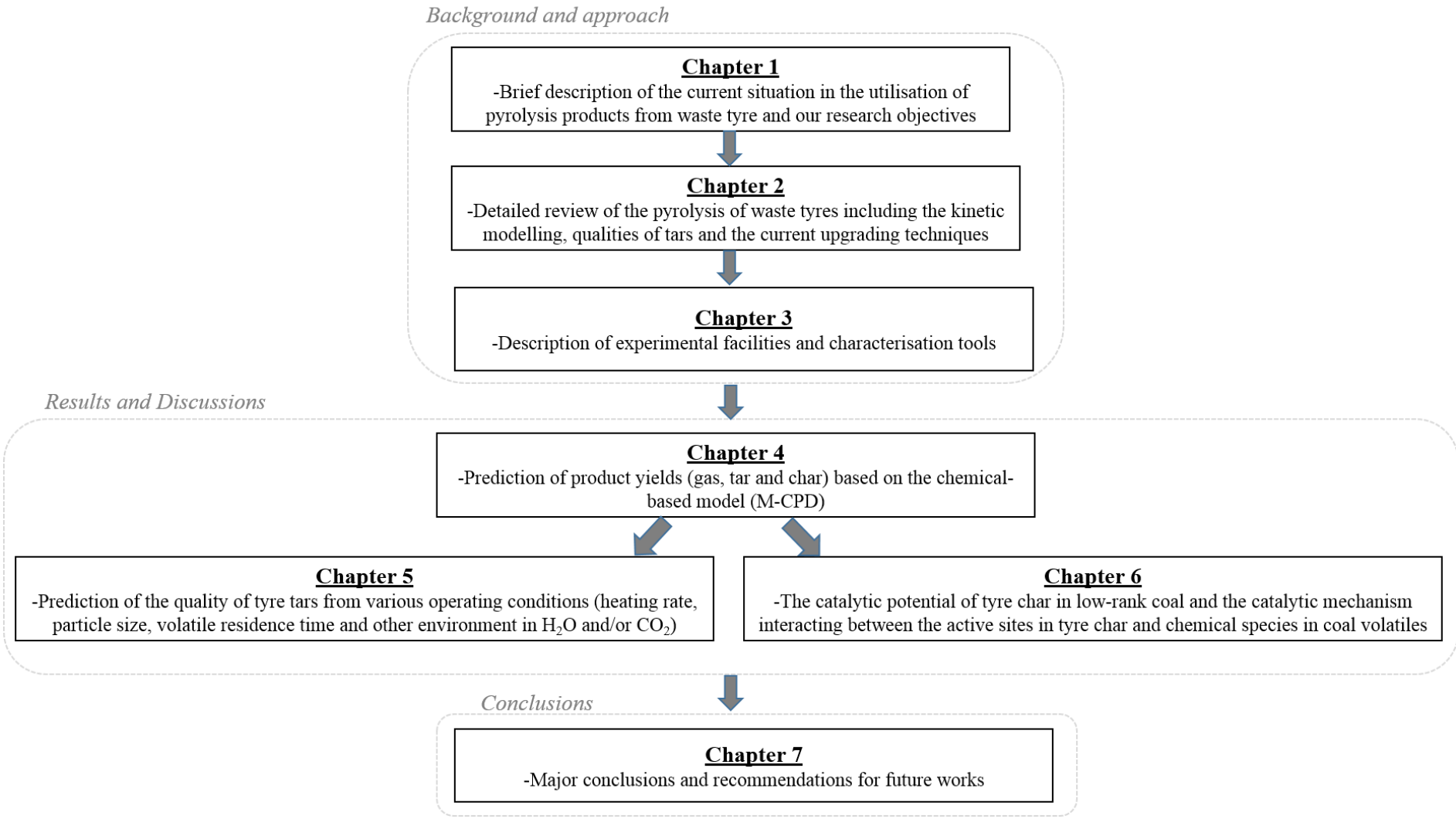

Figure 1 Thesis structure

This page is intentionally left blank

This page is intentionally left blank

1.4 References

1. Lopez, G., et al., *Waste truck-tyre processing by flash pyrolysis in a conical spouted bed reactor.* Energy Conversion and Management, 2017. **142**(Supplement C): p. 523-532.
2. Emma Mountjoy, D.H., Tom Freeman, *STOCKS & FATE OF END OF LIFE TYRES - 2013-14 STUDY*. 2012, Hyder Consulting Pty Ltd.
3. Purcell, A.H., *Tire recyling: Research trends and needs.* Conservation & Recycling, 1978. **2**(2): p. 137-143.
4. Shulman, V.L., *Chapter 21 - Tyre Recycling A2 - Letcher, Trevor M*, in *Waste*, D.A. Vallero, Editor. 2011, Academic Press: Boston. p. 297-320.
5. Williams, P.T., *Pyrolysis of waste tyres: A review.* Waste Management, 2013. **33**(8): p. 1714-1728.
6. Williams, P.T. and R.P. Bottrill, *Sulfur-polycyclic aromatic hydrocarbons in tyre pyrolysis oil.* Fuel, 1995. **74**(5): p. 736-742.
7. Al-Rahbi, A.S. and P.T. Williams, *Hydrogen-rich syngas production and tar removal from biomass gasification using sacrificial tyre pyrolysis char.* Applied Energy, 2017. **190**: p. 501-509.
8. Zhou, Q., et al., *Catalytic performance of scrap tyre char for the upgrading of eucalyptus pyrolysis derived bio-oil via cracking and deoxygenation.* Journal of Analytical and Applied Pyrolysis, 2019. **139**: p. 167-176.

Chapter 2- Literature Review

This page is intentionally left blank

Scope of literature review

This literature review covers the motivation for this study of the enhanced utilization of pyrolysis products from waste tyre for the generation of fuels derived from waste tyre and brown coal. Therefore, the general background information on waste tyre is firstly presented in Section 2.1. Then, a comprehensive literature survey regarding the kinetic modelling for tyre pyrolysis along with their limitations upon different process conditions is reviewed in Section 2.2. The influence of process conditions on the physiochemical properties of tyre-derived tars is also presented in Section 2.3. Later, the general background information of brown coals and the influence of process operating conditions on the properties of coal-derived tars are discussed in Section 2.4 and 2.5, respectively. Last but not least, the common advanced technologies for the tar upgrading *via* hydrogenation, hydrocracking, deoxygenation and thermal cracking reactions using various types of catalysts is also reviewed in Section 2.6. Based on the literature review, the research gaps are identified and presented in Section 2.7.

2.1 Background of waste tyre

The disposal of waste tyre is a global concern. It is estimated that around more than 51 million passenger tyre reach the end of their life each year in Australia. However, only <5% of waste tyre are recovered and properly managed in Australia, whereas the rest is just simply dumped, which increases the risk of hazardous toxic gases being produced upon extreme heat. Tyre is made of rubbers (60-65 *wt%*), carbon black (25-35 *wt%*) and the rest consists of accelerators and organic fillers [1]. The composition of tyre is difficult to be generalised, as rubbers are mainly a blend of different types of elastomers, such as isoprene natural rubber (NR), synthetic styrene-butadiene (SBR) and butadiene (BR) polymers mixed at different ratios depending on the manufacturing requirement [2].

The traditional methods of treating those non-biodegradable waste tyre, including stockpiling, illegal dumping or landfilling are only short-term solutions causing the secondary hazards to the environment. However, there is a renewed interest in the research and development of alternative technologies for recycling these waste tyre [3]. Among these technologies, pyrolysis has been researched intensively, owing to its simpleness, cost-effectiveness and remarkable advantage of transforming waste into energy [3].

Pyrolysis is a thermal devolatilization process in which tyre chips are heated in an inert environment at an elevated temperature to remove organic matters, producing products known as light gas, solid char and liquid tar. The valuable pyrolysis product such as light gas is rich in methane, hydrogen and other light hydrocarbons (C_2-C_6), whilst the solid fraction (char) contains a great amount of fixed carbon and metal-containing ash, and may be used as a precursor for carbon black, activated charcoal and metal recovery [4]. The liquid tar, accounting for 45- 60 *wt%*, could be potentially used as an alternative fuel in the internal combustion engines as well as the chemical feedstock in a wide variety of applications. Although liquid tar is rich in valuable chemicals such as limonene, styrene, etc., it is an undesirable product as it also contains a wide range of polyaromatic hydrocarbons that is responsible for the formation of heavy by-products such as coke and asphaltene, resulting in the blockage of volatile production line, and thus making the tyre pyrolysis process hard to be commercialised. Therefore, substiantial research aims to address the issues by acquiring in-depth knowledge regarding the considered reaction systems in the pyrolysis process of waste tyre through the study of kinetic modelling and devolatilization of volatiles species.

2.2 Kinetic modelling of tyre pyrolysis

To date, a variety of empirical kinetic models have been developed to describe the pyrolysis process of tyre, and each is designed with a different end-use in mind. In general, the variety of kinetic model for tyre pyrolysis can be classified into two types; empirical model and chemical-based models. The main difference for both models is, the empirical model assumes that the various polymers (NR, BR, SBR) have no interaction during the pyrolysis process whereas the chemical-based model required the understanding and the chemical input of the molecular structure for the raw tyre feedstocks (including NR, BR, SBR polymers) for the simulation to be carried out. Empirical models for tyre pyrolysis could be classified into single-reaction, single-component and multi-component model, which were reviewed in Section 2.2.1. As for chemical-based model, in particular CPD (Chemical percolation devolatilization) model targeting a variety of carbonaceous feedstocks were reviewed in Section 2.2.2.

2.2.1 Empirical models

2.2.1.1 Single-reaction models

Among the large variety of tyre modelling studies on pyrolysis, the single-reaction model is considered as the simplest kinetic model, in which the entire waste tyre pyrolysis is treated as a single reaction route [5-7]. The model regards pyrolysis as a first-order decomposition reaction, with the kinetic rate is being controlled by an Arrhenius expression as per Equation 2.1- 2.3.

$$\frac{dx}{dT} = k(1 - X)^n \qquad \text{Equation 2.1}$$

$$k = Ae^{-\frac{Ea}{RT}} \qquad \text{Equation 2.2}$$

$$X = \frac{m_o - m}{m_o - m_\infty}$$ Equation 2.3

Where $\frac{dx}{dT}$, the rate of reaction is proportional to the nth order of the mass concentration of the reactant; X is the mass concentration of the tyre sample; k is the rate constant; A is the pre-exponential factor (min^{-1}), R is the gas constant (8.314 $Jmol^{-1}K^{-1}$); E_a is the activation energy of reaction (J/mol); m_o, m_∞, m are the initial mass of tyre sample, the final mass after complete pyrolysis and the mass at any time during the pyrolysis.

Although this approach is relatively simple and it works well at a low pyrolysis temperature range (<450°C), it has been highly doubted by many researchers who argued that the pyrolysis process involved multiple reactions at higher temperatures, with different mechanisms occurring simultaneously. Zabaniotou et al [8] modelled the flash pyrolysis (1100°C/s) of tyre particles in a helium atmosphere as one reaction, but obtained a value for the activation energy that is much lower than others reported in the literature. Other than that, a closer look at the experimental thermo-balance data reveal that while the mass loss profiles for heating rates of 2°C/min and 10°C/min follow each other very closely, the mass loss profile for 5°C/min does not fall in between these two rates. Besides, Aguado et al. [9] used a microreactor and measured different products evolved for tyre pyrolyzed under a helium atmosphere. It was indicated that different kinetic parameters were found for thirteen volatiles evolved from tyre pyrolysis under an inert atmosphere at 10°C/min, proving that tyre was highly heterogeneous and its pyrolysis rate was not a singular reaction.

2.2.1.2 Single-component models

The comparison between the single-reaction and single-component model was made by Sachin et al [9]. The author used the same linearized equation to calculate the activation energies for the pyrolysis of cis-1,4 polybutadiene polymer with a cobalt catalyst and without a catalyst under high-temperature conditions. However, the authors found no difference in the pyrolysis rates between the two conditions, noting that the rate of reaction cannot be simply described by assuming one single reaction. However, the author also reported that a consensus seems to appear in the literature on tyre pyrolysis when the tyre pyrolysis was deconvoluted by independent single-component reaction. This corresponds to the evolution of major components of a tyre, such as oil, natural rubber and manufactured rubbers. It is assumed that the tyre components (processing oil, polyisoprene, poly-butadiene and styrene-butadiene copolymer) are decomposed individually without any interaction among one another. It is also assumed that each of these decomposition reactions follows only one mechanism and is irreversible. This approach was also used by Aylon [10] and Seidelt [11] who attempted to use kinetic constants for each of the tyre components to fit experimental data. While the fit by them was reasonably good, the overlapping region for NR and SBR did not show a good fit. This was also the case when DTG data of each component was used to fit into DTG data for tyre pyrolysis. A good fit at the two ends was achieved, except in the overlapping region in middle temperature range (400-565°C). Senneca et al [12] who applied this approach to tyre pyrolysis from 5 to 900 °C/min indicated that the two peaks in the experimental DTG data merged into one at the higher heating rates (1000°C/s) and attributed this merging to the increasing extent of cyclisation/cross-linking as the heating rate was raised. They then argued that there is interaction between different components, particularly when they all released at a high temperature environment (>450°C).

2.2.1.3 Multi-reaction routes models

The same group of researchers later proposed a scheme that included intermediate and parallel reactions in the formation of products during the pyrolysis of tyre. Five final products were considered as gas, liquids, aromatics, char and their intermediates, as illustrated in **Figure 2 [14]**. The proposed scheme consisted of four primary reactions in parallel, whose reactant was original tyre and another three secondary reactions (also in parallel) whose reactant was the intermediate. Using an error-minimization function, seven sets of kinetic parameters for the seven equations were obtained. The calculated parameters showed the highest value of activation energies for the formation of aromatics (254 kJ/mol) and lowest for the formation of tar from intermediates (48 kJ/mol). As a result, this method is able to deconvolute the TGA/DTG data of tyre with a high fitting agreement and has been further extended to include other considerations, including heat transfer limitation and reactor designs [13, 14]. Besides that, this model was also applied to cooperate with the iso-conversional model to predict the pyrolysis of biomass and plastics [15].

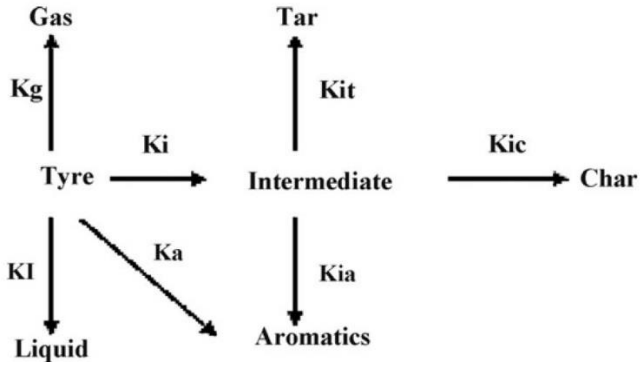

Figure 2 Scheme of kinetic reactions for multi-reaction models [14]

2.2.2 Chemical-based models

In contrast to the empirical models, chemical-based models describe the pyrolysis process by considering the chemical composition in terms of functional groups and structures, making the

predictions more sensible and applicable over a wide range of solid fuels. With the recent development of kinetic modelling, several models for other carbonaceous material such as coal were built to study their devolatilization behaviour. These models are known as chemical percolation devolatilization (CPD), FG-FVC, and FLASHCHAIN. Among these models, CPD model is the most advanced due to the consideration of the bond-breaking reactions, re-polymerisation of the metaplast, vapour equilibrium and the theory of lattice statistics percolation. Besides, by knowing the properties of the raw material through ^{13}C-NMR experiments, the conventional CPD model can predict the yield of char, tar and gasses, as well as the formation of the metaplast and some properties such as radical concentration of the tar and gasses. The CPD model seems promising for use in this work due to its code availability and wide implementation, including integration into CFD (Computational fluid dynamics) software ANSYS Fluent 42. The CPD model was originally developed for the pyrolysis of bituminous coal [16], but has recently been extended to other materials including low-rank coal [17], biomass [18], black liquor [18] and oil shale [19].

2.2.2.1 CPD (Chemical percolation devolatilization) model [16]

During pyrolysis, labile (i.e., breakable) bridges are cleaved as the temperature increases. Dependent upon the lattice structure, cleaving one bridge does not necessarily release pyrolysis products. Therefore, treatment of the relationship between the lattice structure and the probability of creating liberated fragments is necessary. The liberated fragments may contain one or more aromatic clusters, and hence they will contain a molecular weight distribution. The liberated fragments with a high molecular weight may not vaporize, depending upon the temperature and pressure, and hence vapour pressures of the different fragments must be used to determine phase behaviour [20]. Fragments that do not vaporize may cross-link with

remaining solids to form char. Side chains are likely released at a different rate than the rate of cleavage of labile bridges, because the side chains have a different chain length.

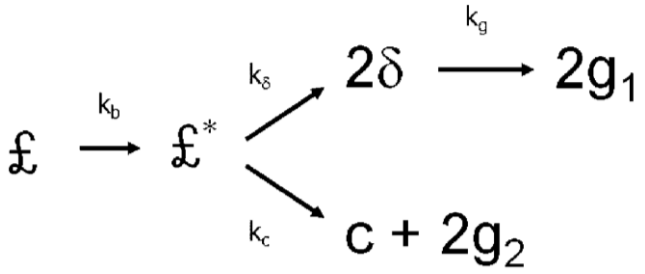

Figure 3 Reaction routes for the CPD model [16]

Figure 3 shows the reaction sequence of the CPD model. An aliphatic "labile" bridge (£) is activated (£*) and is either cleaved to form two side chains (δ) with rate k_δ or transformed into a stable bridge (c) (such as a biaryl bridge) while releasing the aliphatic material (with rate k_c). The side chains will eventually degrade to form gases as well (with rate k_g). Experimental findings from previous studies have shown that the ratio of k_δ/k_c is relatively constant [16]. The gas that is produced by the side chains that break off is referred to as g_1, whereas the gas that is produced by the bridge transformation to a char bridge is referred to as g_2. Two types of bridges exist between aromatic clusters, known as labile bridges and char bridges (c). Bridges initially present as labile bridges, and will decompose to form an active intermediate *. This intermediate bridge is unstable so that it will react immediately via one of two competitive reactions. In the first, the labile bond is cleaved, and two side chains are formed, δ. This can then undergo a cracking reaction to form a light gas g1. In the second reaction, the reactive labile bond will form a stable char bridge with the concurrent formation of a light gas g_2. The rate of labile bridge breaking, k_b, and rate of gas release from side chains, k_g are both determined by Arrhenius expressions whereby the activation energy is given a standard deviation. The ratio of bridge breaking to char bridge formation (k_δ/k_c) is fixed at 0.9 based on experimental data. As bridges are cleaved, clusters are completely detached from the lattice

network and create tar precursor fragments, also known as the metaplast. Depending on the temperature, pressure and molecular weight of the metaplast, it may be vaporised by means of a flash vaporization scheme which uses vapour/liquid phase equilibration. Lower molecular weight compounds such as benzene and naphthalene will have a higher vapour pressure and are more readily vaporised. Higher molecular weight compound's vapour pressure is predicted based on a simple form of Raoult's Law. A simple cross-linking mechanism was implemented into the model which describes the re-polymerisation of the metaplast with the coal matrix and is based on a first-order Arrhenius expression.

The use of the CPD model requires the measurement of the chemical structure parameters (MW_{cl} MW_{side}, $\sigma+1$, P_o, C_o) of the parent tyre, which was the first step for the modelling procedure. The average values of these five structure parameters were measured from ^{13}C-NMR (solid-state carbon-13 nuclear magnetic resonance analysis). Besides these five parameters, other parameters are used internally in the model such as the vapour pressure correlation, and rates of gas formation, labile bridge breaking, cross-linking, and these should theoretically be independent of coal type [16].

2.3 The influence of operating conditions on yields and physiochemical properties of tyre pyrolysis oils

Tyre pyrolysis is an overall endothermic process that is maintained by temperature in the reactor. Thus, temperature imposes a remarkable effect on the behaviour of volatile volatilization, and due to this reason, it is the governing variable with major influence on pyrolysis. However, other variables such as particle size, heating rate and volatiles residence time involved in the process also exert a considerable effect, as they affect the heat transfer phenomena- having a direct relation with the temperature, and consequently influencing not

only the product yield distributions but their physicochemical properties. Other than that, the pyrolysis environment has also an important effect in the process, controlling the occurrence of secondary pyrolysis reactions such as thermal cracking, gasification, tar/ methane reforming reactions and etc. **Table 1** shows an extensive review of different results and remarkable observations on the waste tyre pyrolysis conducted under different process conditions. From the scientific research perspective, most researches listed in **Table 1** was conducted at slow heating of 5-10^{o}C/min [21-32], with some exceptions on the use of faster heating of 20-80^{o}C/min [33-35] and two cases using 200-300^{o}C/min [10, 36]. A broad range of different sizes of tyre chips have been tested, whilst the volatile residence time was limited to a maximum nine minutes, mainly due to the employment of micro-scale pyro-probe and bench-scale fixed-bed reactors in these studies. With regards to the tar quality, it is unambiguous that the primary devolatilization of the scrap tyre completes at 550 - 600°C. At such temperatures, a broad variety of secondary reactions are also proposed for the volatiles, such as self-scission, hydrogenation, cyclisation (also known as Diel-alders), aromatisation, polymerisation and coking. In terms of the heating rate, it has been believed that slow pyrolysis requires a low heating rate and longer residence time is beneficial to minimise these secondary reactions, thereby increasing the tar yield remarkably [4].

Table 1 Literature survey on the studies related to the yields, composition and properties of tyre derived tars at 450-800°C

Heating rate (°C/min)	Volatile residence time (min)	Particle size range (mm)	Reactor	Carrier gas type	Conclusive observation	Study
5, 20, 40, 80	1.8	14-22	Fixed-bed	N_2	The largest yield of tyre tar (55 *wt%*) was obtained at 600°C. When the heating rate was increased from 5 to 80°C/min, the molecular mass range of the tars notably increased.	[16]
5, 20, 60	2.5	10-17	Fixed-bed	N_2	A significant increase (~600 ppm) of benzothiophenes (sulphur-polyaromatics) was noticed as the heating rate was increased from 5 to 60°C/min at 550°C.	[3]
5	2.0	15-30	Fixed-bed	N_2	The tar formed at 600°C contained a high concentration (2 *wt%*) of biologically active polyaromatics such as fluorene, phenanthrene and chrysene.	[4]
200	1.8	3	Pyro-probe	N_2	As the final temperature was increased from 450 to 550°C in 200°C/min, a 7 *wt%* of tyre tar was lost, corresponding to the increment of light gas.	[18]
5, 20	9.0	0.2-1.6	Fixed-bed	N_2	A maximum of tyre yields was obtained at 575°C in both heating rates. Further increasing the temperature resulted in the production of light gases due to strong cracking of tyre volatiles.	[17]

15	0.9	20-30	Pyro-probe	N_2	The tyre tars consisted of 10 *wt%* of the heavy tar fraction which has a boiling point of larger than 370°C.	[13]
10	7.7	-	Fixed-bed	N_2	The yields of tar and element sulphur were increased by 8.0 and 0.3 *wt%* as the temperature was increased from 350 to 550°C.	[8]
10	1.5	25-30	Fixed-bed	N_2	The tars from seven different brands of tyre showed very similar compositional properties.	[12]
12	2.4	20	Pyro-probe	N_2	A maximum of tyre yield was obtained at 550°C and above.	[6]
300	0.8	2-5	Pyro-probe	N_2	A maximum of tyre yield was obtained at the temperature of 500°C and above at the heating rate of 300°C/min.	[19]
10	0.5	0.25	Pyro-probe	N_2	The concentration of single-aromatic hydrocarbons including styrene, toluene and ethylbenzene in the tars reached 120, 20 and 5 ppm at 500°C.	[11]
10	4.0	2	Fixed-bed	N_2	The tyre tars consisted of the hydrocarbons in the carbon number of 5-15 predominantly in the form of aromatics.	[9]
5, 35	2.2	1-4	Fixed-bed	N_2	There was no significant influence of the heating rates of 5 and 35°C/min on the physiochemical properties of the tyre tars. The fuel properties of the tars were similar to those of the commercial diesel in terms of the heating value, density and viscosity, except for sulphur content.	[5]
10	1.1	1-2	Fixed-bed	N_2	The tars from 500 to 800°C mainly consisted of limonene, xylene and sulphuric hydrocarbons such as benzothiazole which accounted for 0.9 *wt%*.	[7]

20	<2.0	10-30	Fixed-bed	N_2	Major identified hydrocarbons in the tars derived from light, medium and heavy vehicle tyre at the temperatures of 500-700°C predominantly contained benzene, toluene, xylene, *dl*-limonene and double-ring aromatics.	[10]
5, 15, 25	1.0	0.6-0.8, 2.8-3.4	Pyro-probe	N_2	Increasing the heating rate from 5 to 25°C/min led to a decrease of tar fraction due to the secondary cracking reaction of tyre volatiles.	[14]
Slow	9.8	5-6	Rotary Kiln	N_2	The tars generated from 550°C in slow heating condition contained 47 *wt%* of heavy matters whose boiling point was larger than 200 °C.	[15]

#: Averaged volatile residence time is calculated based on the reactor dimension and the flow rate of purging gas/ volatiles (min)

2.4 Background of Victorian brown coals

Low-rank coal is known as one of the world abundant resources, which is projected to last until the year 2100 at current growth rates. Compared to higher-rank coals, it is characterised by having a high moisture content and a low heating value. Consequently, it is used almost exclusively for power generation at adjacent power plants, owing to the cost of transport and spontaneous combustion risk. In its crude form, it combusts relatively inefficiently and has the highest greenhouse gas emissions per unit of electricity produced from common sources. Low-rank coals are inexpensive, owing to their low cost of extraction. This cost difference, as well as a secure supply, presents an opportunity to more effectively utilise low-rank coal by upgrading through a pyrolysis process that will produce a beneficiated solid product, char, as well as value-added gas and liquid tar products. In the Latrobe Valley, Victoria, Australia, Victorian brown coals form a family of various low-rank coals in which they are known as Yallourn, Morwell and Loy Yang coal.

The elemental oxygen content of Victorian brown coals is generally up to 22 *wt%* (dry basis), manifesting the abundance of oxygen in the coal. Studies showed that the high oxygen content of coal would result in the oxygen content of the coal-derived tars to be very high - causing the tars to have lower calorific value, viscous, acidic and corrosive. It has been widely identified that coal-derived tars contain more than hundred types of organic hydrocarbon compounds such as BTX, naphthalene and phenol, cresol, long-chain hydrocarbon and polyaromatic (three-five fused rings) compounds [38]. In addition, the other drawbacks such as the relatively high water content, high viscosity and poor product stability make it unsuitable for direct use as a liquid fuel [39]. As for the physiochemical properties, it has been analyzed by Wailes et al [40] for tar derived from carbonization of briquette Yallourn brown coal in a slow heating

(10^{o}C/min) and 800^{o}C. As reported, the tar yield only reaches 7 *wt%*. The oxygen content in tar reaches around 10 *wt%*, while C and H account for 79.4 *wt%* and 9.2 *wt%*, respectively. The highly polar nature of the tar is evident from the results that 66 *wt%* is methanol-soluble fraction (C: 76.5; H: 7.9; O: 16%) whereas only 34 *wt%* of tar is non - polar hydrocarbon (C: 85.1; H: 11.2; O: <4%). In regards to boiling characteristic, it has 28% of dry tar which is not distillable even at the temperature up to 320^{o}C. It contains large number of heavy matters such as asphaltenes (>C_{30}) that have a very low commercial value [40].

2.5 The governing variables in the pyrolysis process of carbonaceous materials including coal and biomass, and its impact on the mechanism and product yields

Table 2 tabulated the findings of previous studies on the effect of governing process variables on the product yields and properties, which are also described in detail in Section 2.5.1 and 2.5.2.

Table 2 Summarized literatures concerning the effects of heating rate, particle size and metallic species in feedstock

Feedstocks	Experiment conditions	Findings/Observations	References
Biomass	3.7 -33.3°C/min 600°C 10-100 µm Tubular furnace reactor	• All biomass materials formed higher tar yield in fast heating rate compared to slow heating rate upon a large residence time (no mentioned). • The long-chain oxygenated fraction of oil increased with the rise of heating rate from 3.7 -33.3°C/min.	[41]
Bituminous coal Subbituminous coal	0.1 - 10^6 °C/s 900°C 10-100 µm Drop tube furnace	• Upon a short residence time (<20 s), the yields of light gases increased with the heating rate and the extent of secondary cracking reaction. • As for the light gases, C_2H_2 (weak double bond) are mainly found in the fast heating scheme (10^6 °C/s); whereas CH_4 (strong single bond) is the main constituent in slow heating condition (0.1°C/s).	[42]
Australian low-rank coals	0.5-20°C /s 1000°C <149µm Thermogravimetric	• The spectrum from FT-IR analysis revealed that the number of aromatic ring compounds	[43]

	analyzer coupled with gas chromatography	was more prevalent along with the rise of the heating rate.	
Bituminous coal	5-25°C/min 800°C 1 mm Fixed bed reactor	• The gas yield was increased from 7.24 to 18.04 *wt%* when the heating rate was increased from 5 to 25°C/min. • The yield of coal tar is favoured in lower heating rate, although the volatile residence time was not mentioned. • Heavy hydrocarbons were less for fast-heating-derived tars. • The concentration of CH_4 is higher than that of C_4H_8 as a gas product at 25°C/min than in 5°C/min.	[44]
Olivehusk Cornbub	10°C/s 978°C 0.5-2.2 mm Fixed bed reactor	• The yield of char derived from olive husk increased from 19.4 - 35.6 *wt%* when sizes reduced from 0.5 to 2.2 mm in 10°C/s. • Similarly, corncob derived char yield was increased from 5.7 to 16.6 *wt%* when the particle size increased from 0.5 to 2.2 mm. • It was claimed that smaller particle size created higher heat flux across the particle.	[45]
Wheat straw	5-20°C/min 900°C 0.25-1.35 mm Thermogravimetric analyzer	• The yield of char increased by increasing the particle size from 0.25 to 0.475 mm and heating rate.	[46]
Elbistan lignite	10°C/min 200-900°C 38- 2360 µm Thermogravimetric analyzer	• Moisture loss occurred at a higher temperature for larger particle from TG/DTG results.	[47]

		• The apparent activation energy of coking reaction (600-900 °C) was higher for smaller particle size.	
Woody biomass Cynara cardunculus L.	Rapid heating rate 0.4-2.0 mm 300-800°C Fixed bed reactor	• The highest yield of tar and the lowest yield of char was attained at 400°C. • There was no significant change in product yields when the final temperature was increased from 400-800°C in rapid heating scheme. • The char resulted from the same range of temperature bear the same properties in terms of heating value, surface area and mineral contents.	[48]
Australian oil mallee biomass	Slow heating 500°C 0.18-5.6 mm Fluidized bed reactor	• The yield of tar decreased at the final temperatures between 0.3 and 1.5 mm, due to the enhanced cracking reaction. • However, no further drop by further increasing the size to 5.6 mm. • The results of GC-MS for bio-tars indicated that the fraction of light hydrocarbon was increased along with the increment of particle sizes from 0.3 to 1.5 mm.	[49]
Bituminous coal	10, 1000°C/min 1000°C <74 μm-1.4 mm Thermogravimetric analyzer	• The yield of tar increased with the heating rate between 10 and 1000°C/min. • The mechanism governing the reduced intra-residence time of volatile precursor compared to dense-packed small particles was proposed.	[50]
Loy yang coal	Rapid pyrolysis 1173°C Drop-tube reactor	• The yield of tar was increased by 5 *wt%* after removal of inherent metallic species and ash content by 1.5 *wt%*.	[37, 51]

Yallourn coal	74-125 μm	• It was claimed that the metallic species in coal suppressed the release of volatile precursor, resulting in incomplete devolatilization.	
Loy yang coal	10 and 1000°C/min 600-900°C 106-150 μm Wire-mesh reactor	• Both heating rate (10 and 1000°C/min) showed the positive impact in increasing the tar yield (by 3 *wt%*) after the acid-washed of the metallic species in coal. • The same conclusion was drawn –The metallic species in coal served as a cross-linking point to the volatile precursor from the cleavage of a covalent bond.	[51]

2.5.1 Effect of heating rate

Pyrolysis is generally classified as two different processes. Slow heating generally takes place at a heating rate close to and even smaller than 10°C/min whereas a fast heating rate is considered as heating at the rate larger than 100°C/min [52]. Slow heating primarily optimizes char production through carbonization. It promotes the secondary pyrolysis reaction such as polymerization of volatile or charring reaction [53]. Conversely, the primary goal of the fast pyrolysis is to maximize the production of tar (liquid oil) or gas. It requires a very short residence time of volatiles in the reaction chamber and rapid quenching of the volatiles to minimize the secondary reactions for the volatiles [4].

The reason that the heating rate influences the product distribution is attributed to the fact that reaction mechanism during the process changes significantly upon the variation of the heating rate. It is agreed that fast heating rate causes much quicker generation of volatile precursors,

resulting in the increase in the driving force of transportation due to the large pressure and concentration build-up within the particles [54]. On the contrary, in a slow heating mode, volatile tends to further experience intra-particle thermal cracking to form lighter species and polymerisation leading to the formation of extra char particles (i.e. secondary cracking pyrolysis) [55].

2.5.2 Effect of metallic species in feedstock

Low-rank coal is well known for the relatively low ash content within it, which typically accounts for 1-2 *wt%* on a dry basis. More specifically, the ash-forming elements are dominated by alkali and alkaline metal species [56]. Nevertheless, the removal of the metallic species in the coal largely affect the pyrolysis product distribution and properties [57, 58].

Several studies reported that the tar yield is increased by the removal of metallic species [51] [59]. The results were explained by the fact that metallic species serve as cross-linking points in the coal matrix, causing difficulty for the fragmentation and release of the volatiles out of the char matrix. The mechanism of metallic species during pyrolysis is shown as Reaction 2.1 – 2.3 below. Originally, metallic species exist as a carboxylate - form in the brown coal matrix, which easily decomposes to release CO_2 even at a low temperature such as 300^{o}C [60]. The resultant metallic-bearing radicals then bonds to the coal macromolecule (CM) matrix forming a new, rigid structure. As a result, it makes the formation and release of volatile fairly difficult.

$$(\text{-COO-Ca-OOC-}) + (\text{-CM}) = (\text{-COO-Ca-CM}) + CO_2 \qquad \text{Reaction 2.1}$$

$$(\text{-COO-Ca-CM}) + (\text{-CM}) = (\text{CM-Ca-CM}) + CO_2 \qquad \text{Reaction 2.2}$$

(-COO-Na) + (-CM) = (CM-Na) + CO_2 Reaction 2.3

2.6 Common upgrading method of pyrolysis tar oils by means of in-situ operating conditions or *in-situ* and *ex-situ* catalytic reactions

With respect to the crude tar derived from low-rank coal that is rich in oxygen-bearing compounds, the most crucial way to improve the quality and reduce the oxygen content is by means of hydrogenation reaction. Two common process designs to upgrade pyrolysis oil can be classified into '*Ex-situ*' and '*In-situ*' process systems. "*Ex-situ*' is a focus on the upgrading of the crude oil externally outside the pyrolyzer, whereas '*In-situ'* system focuses on the upgrading of the crude tar internally in the pyrolysis bed and during the pyrolysis process [39]. Several techniques derived from '*Ex-situ*' and '*In-situ*' process systems are discussed below.

2.6.1 *Ex-situ* methods for tar quality upgrading

2.6.1.1 Adjustment of operating conditions

As learning from section and section, the parameters including heating rate, particle size, volatile re time and different gas environment can work in upgrading the properties of tars from both tyre and coal.

2.6.1.2 Catalytic hydrogenation

Hydrogenation is the most common deoxygenation technique to upgrade the quality of tar by hydrogenating unsaturated bonds without cracking the organics as well as removing the heteroatoms such as sulphur, nitrogen and oxygen. This method takes place under mild

conditions, 200-250^{o}C and atmospheric pressure. However, the yield of the refined oil is relatively low. The catalysts commonly used include CoMo, Pt/C, Ru/C or NiMo with the use of silica or alumina as the supporter [61]. Many researchers have used model compounds such as cresol, phenol, dibenzofuran, carboxylic acid and ketone that are the main constitute in the pyrolysis oil to examine the appropriate catalyst to hydrogenate the pyrolysis oil [62, 63]. The study of deoxygenation of Victorian brown coal was conducted by Trimm et al [64]. The use of NiMo catalyst was found effective to remove the oxygen meanwhile saturates the aromatic ring to alkane [56]. One disadvantage of this technique is that the char, coke (8-25%) and heavy tar resulted from the deoxygenation caused the catalyst deactivation and even reactor clogging. Also, all the experiment requires the extra input of valuable H_2 to undergo the hydrogenation reaction. Zhang et al [65] reported that a significant amount of coke (14 *wt%*) was deposited on the catalyst after four sequential use of the NiCu /SiO2. A similar observation was reported from Gao et al [66] who revealed that 17 *wt%* of coke was found depositing on the Ru/C catalyst after only one single use.

2.6.1.3 Catalytic hydrocracking

Hydrocracking is a less popular technique than hydrogenation is. It is a thermal process in which hydrogenation accompanies the thermal cracking. Hydrocracking occurs at much higher temperature and pressure than hydrogenation does, and it is responsible for hydrogenating the heavy tar followed by cracking into light oil that is suitable for incorporation into gasoline and diesel. The catalysts to be used are commonly SiO_2/Al_2O_3, platinum oxide and nickel. It is effective to produce larger amount of light hydrocarbon. However, the oxygen content in the resultant product is not sufficiently low. The process also requires high energy consumption, *e.g.* >350^{o}C, and 7-140 bar. Hertan et al [66] studied the hydrocracking of asphaltene (>C_{30})

fraction derived from the pyrolysis of Morwell coal. A batch reactor was used and the temperature of 375-450ºC and the addition of NiMo catalyst at 10MPa were employed. It was indicated that up to 12 *wt%* of oxygen content is initially in the asphaltene fraction, which slightly dropped to 10 *wt%* after the catalytic cracking. The catalyst was not effective in reducing the oxygen content, although in fact more light oil will be generated through the process.

2.6.2 *In-situ* methods for tar quality upgrading

2.6.2.1 Char as co-feed material

In recent years, some researchers also utilised char as the catalyst to co - feed with raw coal together into the pyrolyzer to improve the quality of the crude tar. It is believed that the introduction of char will promote the tar reforming reaction, due to the catalysis effect of the ash-forming elements within the char. Besides, Min et al [67] determined that the char has the catalyst effect to reform the tar into lighter hydrocarbons due to the porous nature of the char prolonged the residence time of the crude tar within the char matrix and therefore, the secondary reactions such as reforming reaction of tar was enhanced.

Another observation was reported by Han et al [68]. It was declared that the total tar yield was decreased by using black coal char as the co-feed material with coal together into the pyrolyzer. However, the light tar fraction, in which mostly consists of BTX and naphthalene, was increased. Zhang et al [69] investigated the in-situ tar reforming by using Loy Yang char under pyrolysis process in drop tube furnace. It was given as the explanation that the major components of light tar after reforming with char were mostly benzene and naphthalene as a

result of the metallic species. Extra injection of steam promoted the reforming to a higher extent but not significantly. There were two possible mechanisms involving the decomposition of nascent tar over char surface at elevated temperatures: catalytic cracking of heavy volatiles to smaller fragment [70], and reforming/hydrogenation by reacting with steam, CO_2 or H_2 [71]. For both reactions, the inherent ash-forming elements including the metallic species in particular iron in brown coal were the catalysts.

2.6.2.2 Co-pyrolysis process with tyre

It has been reported that the co-pyrolysis of different fuels simultaneously can improve the liquid tar yield and/or quality effectively. In this section, studies concerning co-pyrolysis of coal and biomass with scrap tyre are reviewed, as summarized in **Appendix C**.

Onay et al [72] indicated that less polar substance and more aromatics were present in the resultant tar when 10 *wt%* of waste tyre was added with the lignite and pyrolyzed at condition, 500^{o}C and 300 ^{o}C/min. A similar phenomenon was found by Martinez et al for the co-pyrolysis of biomass and waste tyre in a fixed bed reactor using a fast heating rate of 80^{o}C/min and 500^{o}C [73]. Less oxygenated compounds such as ketone and phenols and increment of BTX compounds were found in the upgraded bio-oil. The stability of the tar was also improved remarkably as the viscosity of the bio-oil remained unchanged after several months. Cao et al [74] stated that the synergetic mechanism of co-pyrolysis was due to the hydrogen radical transferring from polymer in scrap tyre to biomass volatiles. Furthermore, Ucar et al [75] reported that the water content in co-pyrolyzed tar was less than that of both pure biomass and pure tyre - derived tar, ascribed to the hydrogenation reaction. Acevedo et al [76] further optimized the synergetic effect of tyre and coal in pyrolysis process. It was found that a longer

residence in the reactor significantly promoted the interaction between the volatiles from two different fuels. As a result, the quality of the tar was improved, and more aromatic and small amount of oxygenated compounds were formed due to the hydrogenation reaction.

2.7 Research gaps based on the previous literature review

This chapter has given an in-depth literature review of the current state of knowledge regarding the pyrolysis of waste tyre and low-rank coals as well as the physio-chemical properties of tyre and brown coal resultant tars. Based on this literature review, several gaps in the knowledge base have been identified as follows:

1. Firstly, it is of interest to understand the pyrolysis behaviour of waste tyre in greater detail. Previous studies have particularly focused on developing the kinetic model based on empirical methods without considering the molecular structure of tyre rubbers and their interaction.
2. The integration of intra-particle heat transfer with pyrolysis modelling has become well understood for coal and biomass pyrolysis, whereas waste tyre has not been considered as a fuel to be upgraded. With the growing capacity of abandoned waste tyre, this has attracted much industrial attention in recent years; however, more knowledge is needed.
3. Although a broad range of different sizes of tyre chips have been tested, whilst the volatile residence time is limited to a maximum nine minutes, mainly due to the employment of micro-scale pyro-probe and bench-scale fixed-bed reactors in these studies.
4. Although it was confirmed that syngas could be produced from the use of pure CO_2 and H_2O as carrier gas, it is still unknown how the injection of flue gas affects yield and properties of the liquid tar, in particular at the mild temperatures of 550-600^oC where tyre pyrolysis is conducted.
5. Although the co-pyrolysis of tyre chip and coal have been studied extensively, the co-pyrolysis of tyre char and coal has never been explored.

6. Recently, the use of tyre chars on biomass pyrolysis has been examined. It is believed that tyre char is a good catalyst to upgrade the quality of oil due to its abundant mineral metallic species; however, the catalytic reaction mechanism has not been studied.

This page is intentionally left blank

This page is intentionally left blank

2.8 References

1. Leung DYC, Wang CL. Kinetic study of scrap tyre pyrolysis and combustion. Journal of Analytical and Applied Pyrolysis. 1998 1998/05/01/;45(2):153-69.
2. Martínez JD, Puy N, Murillo R, García T, Navarro MV, Mastral AM. Waste tyre pyrolysis – A review. Renewable and Sustainable Energy Reviews. 2013 2013/07/01/;23(Supplement C):179-213.
3. Williams PT. Pyrolysis of waste tyres: A review. Waste Management. 2013 2013/08/01/;33(8):1714-28.
4. Martínez JD, Puy N, Murillo R, García T, Navarro MV, Mastral AM. Waste tyre pyrolysis – A review. Renewable and Sustainable Energy Reviews. 2013 2013/07/01/;23:179-213.
5. Zabaniotou A, Lagoudakis J, Toumanidou E, Stavropoulos G. Energetic Utilization of Used Tires. Energy Sources. 2002 2002/09/01;24(9):843-54.
6. Gupte SL, Madras G. Catalytic degradation of polybutadiene. Polymer Degradation and Stability. 2004 2004/12/01/;86(3):529-33.
7. Unapumnuk K, Keener T, Lu M, Khang S-J. Pyrolysis Behavior of Tire-Derived Fuels at Different Temperatures and Heating Rates2006. 618-27 p.
8. Zabaniotou A, Stavropoulos G. Pyrolysis of used automobile tires and residual char utilization. Journal of Analytical and Applied Pyrolysis. 2003 12/01;70:711-22.
9. Aguado R, Olazar M, Vélez D, Arabiourrutia M, Bilbao J. Kinetics of scrap tyre pyrolysis under fast heating conditions. Journal of Analytical and Applied Pyrolysis. 2005 2005/06/01/;73(2):290-8.
10. Murillo R, Aylón E, Navarro MV, Callén MS, Aranda A, Mastral AM. The application of thermal processes to valorise waste tyre. Fuel Processing Technology. 2006 2006/01/01/;87(2):143-7.
11. Seidelt S, Müller-Hagedorn M, Bockhorn H. Description of tire pyrolysis by thermal degradation behaviour of main components. Journal of Analytical and Applied Pyrolysis. 2006 2006/01/01/;75(1):11-8.
12. Senneca O, Salatino P, Chirone R. A fast heating-rate thermogravimetric study of the pyrolysis of scrap tyres. Fuel. 1999 1999/10/01/;78(13):1575-81.
13. Cheung K-Y, Lee K-L, Lam K-L, Lee C-W, Hui C-W. Integrated kinetics and heat flow modelling to optimise waste tyre pyrolysis at different heating rates. Fuel Processing Technology. 2011 2011/05/01/;92(5):856-63.

14. Olazar M, Lopez G, Arabiourrutia M, Elordi G, Aguado R, Bilbao J. Kinetic modelling of tyre pyrolysis in a conical spouted bed reactor. Journal of Analytical and Applied Pyrolysis. 2008 2008/01/01/;81(1):127-32.
15. Narobe M, Golob J, Klinar D, Francetič V, Likozar B. Co-gasification of biomass and plastics: Pyrolysis kinetics studies, experiments on 100kW dual fluidized bed pilot plant and development of thermodynamic equilibrium model and balances. Bioresource technology. 2014 2014/06/01/;162:21-9.
16. Fletcher TH, Kerstein AR, Pugmire RJ, Solum MS, Grant DM. Chemical percolation model for devolatilization. 3. Direct use of carbon-13 NMR data to predict effects of coal type. Energy & Fuels. 1992 1992/07/01;6(4):414-31.
17. Liu G, Song H, Wu J. Prediction of low-rank coal pyrolysis behavior by chemical percolation devolatilization model. Environmental Progress & Sustainable Energy. 2016 02/01;35:n/a-n/a.
18. Wooters T, Baxter L, Fletcher T. CPD model calculations of black liquor and biomass pyrolysis. Prepr Symp - Am Chem Soc, Div Fuel Chem. 2005 01/01;50:108-9.
19. Fletcher TH, Barfuss D, Pugmire RJ. Modeling Light Gas and Tar Yields from Pyrolysis of Green River Oil Shale Demineralized Kerogen Using the Chemical Percolation Devolatilization Model. Energy & Fuels. 2015 2015/08/20;29(8):4921-6.
20. Solum MS, Sarofim AF, Pugmire RJ, Fletcher TH, Zhang H. 13C NMR Analysis of Soot Produced from Model Compounds and a Coal. Energy & Fuels. 2001 2001/07/01;15(4):961-71.
21. Cunliffe AM, Williams PT. Composition of oils derived from the batch pyrolysis of tyres. Journal of Analytical and Applied Pyrolysis. 1998 1//;44(2):131-52.
22. Banar M, Akyıldız V, Özkan A, Çokaygil Z, Onay Ö. Characterization of pyrolytic oil obtained from pyrolysis of TDF (Tire Derived Fuel). Energy Conversion and Management. 2012 2012/10/01/;62:22-30.
23. Berrueco C, Esperanza E, Mastral FJ, Ceamanos J, García-Bacaicoa P. Pyrolysis of waste tyres in an atmospheric static-bed batch reactor: Analysis of the gases obtained. Journal of Analytical and Applied Pyrolysis. 2005 2005/08/01/;74(1):245-53.
24. Choi G-G, Jung S-H, Oh S-J, Kim J-S. Total utilization of waste tire rubber through pyrolysis to obtain oils and CO2 activation of pyrolysis char. Fuel Processing Technology. 2014 2014/07/01/;123:57-64.

25. Diez C, Martinez O, Calvo LF, Cara J, Moran A. Pyrolysis of tyres. Influence of the final temperature of the process on emissions and the calorific value of the products recovered. Waste Manag. 2004;24(5):463-9. PubMed PMID: 15120430.
26. Kar Y. Catalytic pyrolysis of car tire waste using expanded perlite. Waste Management. 2011 2011/08/01/;31(8):1772-82.
27. Kumar Singh R, Ruj B, Jana A, Mondal S, Jana B, Kumar Sadhukhan A, et al. Pyrolysis of three different categories of automotive tyre wastes: Product yield analysis and characterization. Journal of Analytical and Applied Pyrolysis. 2018 2018/10/01/;135:379-89.
28. Kwon E, Castaldi MJ. Investigation of Mechanisms of Polycyclic Aromatic Hydrocarbons (PAHs) Initiated from the Thermal Degradation of Styrene Butadiene Rubber (SBR) in N2 Atmosphere. Environmental Science & Technology. 2008 2008/03/01;42(6):2175-80.
29. Kyari M, Cunliffe A, Williams PT. Characterization of Oils, Gases, and Char in Relation to the Pyrolysis of Different Brands of Scrap Automotive Tires. Energy & Fuels. 2005 2005/05/01;19(3):1165-73.
30. Laresgoiti MF, Caballero BM, de Marco I, Torres A, Cabrero MA, Chomón MJ. Characterization of the liquid products obtained in tyre pyrolysis. Journal of Analytical and Applied Pyrolysis. 2004 2004/06/01/;71(2):917-34.
31. Mkhize NM, van der Gryp P, Danon B, Görgens JF. Effect of temperature and heating rate on limonene production from waste tyre pyrolysis. Journal of Analytical and Applied Pyrolysis. 2016 2016/07/01/;120:314-20.
32. Yazdani E, Hashemabadi SH, Taghizadeh A. Study of waste tire pyrolysis in a rotary kiln reactor in a wide range of pyrolysis temperature. Waste Management. 2019 2019/02/15/;85:195-201.
33. Williams PT, Besler S, Taylor DT. The pyrolysis of scrap automotive tyres. Fuel. 1990 1990/12/01;69(12):1474-82.
34. Williams PT, Bottrill RP. Sulfur-polycyclic aromatic hydrocarbons in tyre pyrolysis oil. Fuel. 1995 1995/05/01/;74(5):736-42.
35. González JF, Encinar JM, Canito JL, Rodríguez JJ. Pyrolysis of automobile tyre waste. Influence of operating variables and kinetics study. Journal of Analytical and Applied Pyrolysis. 2001 2001/04/01/;58-59:667-83.

36. Napoli A, Soudais Y, Lecomte D, Castillo S. Scrap tyre pyrolysis: Are the effluents valuable products? Journal of Analytical and Applied Pyrolysis. 1997 1997/05/01/;40-41:373-82.
37. Hayashi J-i, Takahashi H, Doi S, Kumagai H, Chiba T, Yoshida T, et al. Reactions in Brown Coal Pyrolysis Responsible for Heating Rate Effect on Tar Yield. Energy & Fuels. 2000 2000/03/01;14(2):400-8.
38. Rathsack P. Analysis of pyrolysis liquids obtained from the slow pyrolysis of a German brown coal by comprehensive gas chromatography mass spectrometry. Fuel. 2017;191:312-21.
39. Ruddy DA, Schaidle JA, Ferrell Iii JR, Wang J, Moens L, Hensley JE. Recent advances in heterogeneous catalysts for bio-oil upgrading via "ex situ catalytic fast pyrolysis": catalyst development through the study of model compounds. Green Chem. 2014;16(2):454-90.
40. Wailes PC, Bell AP, Triffett ACK, Weigold H, Galbraith MN. Continuous hydrogenation of Yallourn brown-coal tar. Fuel. 1980 1980/02/01;59(2):128-32.
41. Tao P, Ma XB, Chen DZ, Wang H. Pyrolysis of Waste Plastics: Effect of Heating Rate on Product Yields and Oil Properties. Advanced Materials Research. 2013;666:1-10.
42. Yan B-H, Cao C-X, Cheng Y, Jin Y, Cheng Y. Experimental investigation on coal devolatilization at high temperatures with different heating rates. Fuel. 2014;117:1215-22.
43. Okumura Y. Effect of heating rate and coal type on the yield of functional tar components. Proceedings of the Combustion Institute. 2017;36(2):2075-82.
44. Akkouche N, Balistrou M, Loubar K, Awad S, Tazerout M. Heating rate effects on pyrolytic vapors from scrap truck tires. Journal of Analytical and Applied Pyrolysis. 2017;123:419-29.
45. Demirbas A. Effects of temperature and particle size on bio-char yield from pyrolysis of agricultural residues. Journal of Analytical and Applied Pyrolysis. 2004;72(2):243-8.
46. Mani T, Murugan P, Abedi J, Mahinpey N. Pyrolysis of wheat straw in a thermogravimetric analyzer: Effect of particle size and heating rate on devolatilization and estimation of global kinetics. Chemical Engineering Research and Design. 2010;88(8):952-8.

47. Ozbas KE. Effect of particle size on pyrolysis characteristics of Elbistan lignite. Journal of Thermal Analysis and Calorimetry. 2008 2008//;93(2):641-9.
48. Encinar JM, González JF, González J. Fixed-bed pyrolysis of Cynara cardunculus L. Product yields and compositions. Fuel Processing Technology. 2000 12//;68(3):209-22.
49. Shen J, Wang X-S, Garcia-Perez M, Mourant D, Rhodes MJ, Li C-Z. Effects of particle size on the fast pyrolysis of oil mallee woody biomass. Fuel. 2009;88(10):1810-7.
50. Tian B, Qiao Yy, Tian Yy, Liu Q. Investigation on the effect of particle size and heating rate on pyrolysis characteristics of a bituminous coal by TG–FTIR. Journal of Analytical and Applied Pyrolysis. 2016;121:376-86.
51. Sathe C, Hayashi J-i, Li C-Z, Chiba T. Release of alkali and alkaline earth metallic species during rapid pyrolysis of a Victorian brown coal at elevated pressures☆. Fuel. 2003;82(12):1491-7.
52. Haykiri-Acma H, Yaman S, Kucukbayrak S. Effect of heating rate on the pyrolysis yields of rapeseed. Renewable Energy. 2006;31(6):803-10.
53. Kök MV, Özbas E, Hicyilmaz C, Karacan Ö. Effect of particle size on the thermal and combustion properties of coal. Thermochimica Acta. 1997 1997/10/22;302(1):125-30.
54. Sathe C, Pang Y, Li C-Z. Effects of Heating Rate and Ion-Exchangeable Cations on the Pyrolysis Yields from a Victorian Brown Coal. Energy & Fuels. 1999 1999/05/01;13(3):748-55.
55. Miura K, Hashimoto K, Silveston PL. Factors affecting the reactivity of coal chars during gasification, and indices representing reactivity. Fuel. 1989 1989/11/01;68(11):1461-75.
56. Jones JC. Chapter 9 - PYROLYSIS A2 - Durie, R.A. The Science of Victorian Brown Coal: Butterworth-Heinemann; 1991. p. 465-516.
57. Takarada T, Tamai Y, Tomita A. Reactivities of 34 coals under steam gasification. Fuel. 1985 1985/10/01;64(10):1438-42.
58. Miura K, Mae K, Asaoka S, Yoshimura T, Hashimoto K. A new coal flash pyrolysis method utilizing effective radical transfer from solvent to coal. Energy & Fuels. 1991 1991/03/01;5(2):340-6.
59. Hayashi Ji, Takahashi H, Iwatsuki M, Essaki K, Tsutsumi A, Chiba T. Rapid conversion of tar and char from pyrolysis of a brown coal by reactions with steam in a drop-tube reactor. Fuel. 2000 2//;79(3–4):439-47.

60. Wornat MJ, Sakurovs R. Proton magnetic resonance thermal analysis of a brown coal: effects of ion-exchanged metals. Fuel. 1996 1996/05/01;75(7):867-71.
61. Nava R, Pawelec B, Castaño P, Álvarez-Galván MC, Loricera CV, Fierro JLG. Upgrading of bio-liquids on different mesoporous silica-supported CoMo catalysts. Applied Catalysis B: Environmental. 2009;92(1-2):154-67.
62. Ghampson IT, Sepúlveda C, Garcia R, Radovic LR, Fierro JLG, DeSisto WJ, et al. Hydrodeoxygenation of guaiacol over carbon-supported molybdenum nitride catalysts: Effects of nitriding methods and support properties. Applied Catalysis A: General. 2012;439-440:111-24.
63. Echeandia S, Arias PL, Barrio VL, Pawelec B, Fierro JLG. Synergy effect in the HDO of phenol over Ni–W catalysts supported on active carbon: Effect of tungsten precursors. Applied Catalysis B: Environmental. 2010;101(1-2):1-12.
64. Trimm DL. Catalyst design for reduced coking (review). Applied Catalysis. 1983 1983/03/15;5(3):263-90.
65. Gao D, Schweitzer C, Hwang HT, Varma A. Conversion of Guaiacol on Noble Metal Catalysts: Reaction Performance and Deactivation Studies. Industrial & Engineering Chemistry Research. 2014;53(49):18658-67.
66. Hertan PA, Jackson WR, Larkins FP. Hydrogenation of brown coal: 7. The chemical nature of the products from the hydrogenation of asphaltenes. Fuel. 1986 3//;65(3):368-73.
67. Min Z, Yimsiri P, Asadullah M, Zhang S, Li C-Z. Catalytic reforming of tar during gasification. Part II. Char as a catalyst or as a catalyst support for tar reforming. Fuel. 2011 7//;90(7):2545-52.
68. Han J, Wang X, Yue J, Gao S, Xu G. Catalytic upgrading of coal pyrolysis tar over char-based catalysts. Fuel Processing Technology. 2014 6//;122:98-106.
69. Zhang L-x, Matsuhara T, Kudo S, Hayashi J-i, Norinaga K. Rapid pyrolysis of brown coal in a drop-tube reactor with co-feeding of char as a promoter of in situ tar reforming. Fuel. 2013;112:681-6.
70. Hosokai S, Kumabe K, Ohshita M, Norinaga K, Li C, Hayashi J. Mechanism of decomposition of aromatics over charcoal and necessary condition for maintaining its activity. Fuel. 2008;87(13-14):2914-22.

71. Hayashi J-I, Iwatsuki M, Morishita K, Tsutsumi A, Li C-Z, Chiba T. Roles of inherent metallic species in secondary reactions of tar and char during rapid pyrolysis of brown coals in a drop-tube reactor. Fuel. 2002 10/1/;81(15):1977-87.
72. Onay O, Koca H. Determination of synergetic effect in co-pyrolysis of lignite and waste tyre. Fuel. 2015;150:169-74.
73. Martínez JD, Veses A, Mastral AM, Murillo R, Navarro MV, Puy N, et al. Co-pyrolysis of biomass with waste tyres: Upgrading of liquid bio-fuel. Fuel Processing Technology. 2014;119:263-71.
74. Cao Q, Jin Le, Bao W, Lv Y. Investigations into the characteristics of oils produced from co-pyrolysis of biomass and tire. Fuel Processing Technology. 2009;90(3):337-42.
75. Uçar S, Karagöz S. Co-pyrolysis of pine nut shells with scrap tires. Fuel. 2014;137:85-93.
76. Acevedo B, Barriocanal C, Alvarez R. Pyrolysis of blends of coal and tyre wastes in a fixed bed reactor and a rotary oven. Fuel. 2013;113:817-25.

Chapter 3- Experimental and Analytical Methods

This page is intentionally left blank

The section covers the experimental and analytical methods used in this thesis. They can be classified into three groups, experimental facilities that consist of two lab-scale heating devices, modelling part including one-dimensional modelling and the analytical methods used in sample characterisation.

3.1 Experimental facilities

3.1.1 Vertical shaft furnace

All pyrolysis experiment was conducted in either vertical fixed-bed shaft furnace as shown in **Figure 4**. The shaft furnace can reach temperatures up to 1000 °C. The furnace itself can heat at 10 °C/min, while loading the quartz reactor directly into the pre-heated furnace facilitates a higher heating rate. A quartz reactor of 1 *m* length and 55 *mm* inner diameter was used. Argon at a flow rate of 0.6-0.9 L/min is used to purge the reactor for 20 *min* prior to heating and during the pyrolysis process to sweep both the light gasses and condensable tar gasses to the collection system. The carrier gas used in this study includes argon, CO_2 and steam. The collection system is made up of three impingers surrounded by an acetone-dry ice cooling bath, and kaowool was also placed close to the outlet of the impingers to trap liquid entrained in the gas flow. Water in the crude tar collected in impingers was quantified using the Karl-Fischer titration method. The remaining fraction was identified as tar. Gasses exiting the impinger system enter a gas analyser which can measure O_2, CH_4, CO, CO_2 and H_2 real-time.

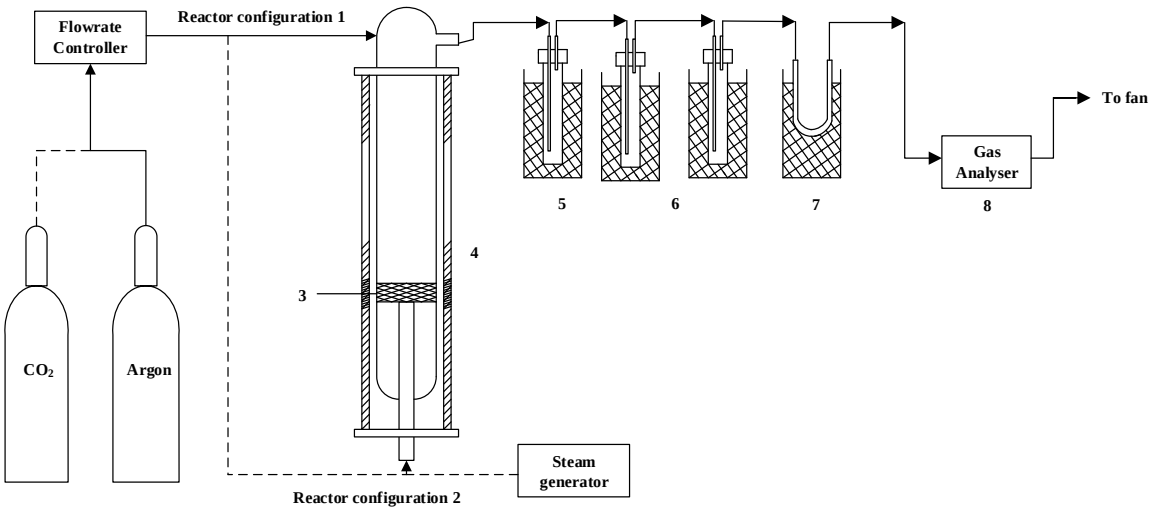

Figure 4 Shaft furnace schematic of two reactor configurations (1-2. Reactor configurations; 3. Feed; 4. Heating furnace; 5. Condensed system with ice and water as cooling agent; 6. Condensed system with dry ice and acetone as cooling agent; 7. U-tube filled with kaowool.

3.2 Kinetic modelling

3.2.2 1-D numerical modelling

The software used for numerical calculations is MATLAB R2016b. MATLAB R2016b is a computing environment that uses its own programming language which contains many built-in maths functions, graphing tools and solving methods including error minimisation and solving of simultaneous partial and ordinary differential equations.

One of the primary functions used in MATLAB for this work is “pdepe”. Pdepe is useful for solving systems of parabolic and elliptic PDEs that have one space dimension and one time dimension as well as combining ODEs with one time dimension. The PDE must fit into the following form:

$$c\left(x,t,u,\frac{\partial u}{\partial x}\right)\frac{\partial u}{\partial t}=x^{-m}\frac{\partial}{\partial x}\left(x^{m}f\left(x,t,u,\frac{\partial u}{\partial x}\right)\right)+s(x,t,u,\frac{\partial u}{\partial x})$$

Where *x* is the space variable, t is the time variable, *u* is the variable to be solved, and m is the geometry of the problem which can be set to 0, 1, or 2 corresponding to a slab, cylinder or sphere respectively.

3.3 Characterization analysis of samples

3.3.1 Proximate and ultimate analysis

The proximate analysis is used to determine the composition of the coal or char sample in terms of moisture, volatile matter, fixed carbon and ash. While the ultimate analysis determines the composition in terms of carbon, hydrogen, nitrogen and sulphur and oxygen. These elements can be assumed to be contained within the volatile matter and fixed carbon. It is important to understand the different bases that are used to report these results and how to convert between them. Under different circumstances, a certain basis may be more useful for comparing samples. For example, dry basis could be used to determine the composition of the sample after drying.

The following terms are commonly used in this thesis:

Air-dried or ad: This basis assumes the sample has been dried although some moisture is remaining. In terms of the proximate analysis, the moisture, volatile matter, ash content and fixed carbon will sum to 100%. Similarly, as for the ultimate analysis, all elements including carbon, hydrogen, nitrogen and sulphur and oxygen will sum to 100%.

Dry basis or db: This basis reports the components that would be remaining once moisture is removed. Therefore, for the proximate analysis, the volatile matter, ash content and fixed

carbon will sum to 100%, while carbon, hydrogen, nitrogen and sulphur and oxygen will sum to 100%.

Dry ash free or daf: This basis excludes both moisture and ash. Therefore, it will indicate on a basis of all the combustible matter in the sample. For the proximate analysis, only volatile matter and fixed carbon are reported and these sum to 100%. For the ultimate analysis, carbon, hydrogen, nitrogen and sulphur and oxygen will sum to 100%.

Table 3 can be used to convert between these bases.

Table 3 Conversion between air-dried, dry and dry ash free bases.

To obtain:	**ad**	**db**	**daf**
Multiply			
ad by	-	$100/(100-M_{ad})$	$100/(100-M_{ad}-A_{ad})$
db by	$(100-M_{ad})/100$	-	$100/(100-A_{db})$
daf by	$(100-M_{ad}-A_{ad})/100$	$(100-A_{db})/100$	-

Where A is ash and M is moisture.

The proximate analysis procedure was carried out per ASTM Standard D3172-136. Firstly, the sample needs to be ground so that it passes through a 250 μm sieve. The sample should have already been air dried. A muffle furnace, capable of temperatures up to 950 °C is needed, a desiccator for cooling samples and ceramic crucibles with lids to hold the samples. The moisture in the sample is determined per ASTM Standard D3173 – 117. The sample is placed in a 105 °C oven and held for 1 *h*. Just prior to its removal, a cap is placed on top to prevent moisture being reabsorbed while cooling. Once the sample reaches room temperature, it is weighed and the difference in mass before and after heating, divided by the initial weight, will

give the moisture fraction. For the ash content, ASTM Standard D3174 – 128 is used. Either air dried, or dried coal can be used for this test as well as the following volatile matter test, and the result will be reported on that basis (e.g. ad or db). The sample is placed in the muffle furnace at room temperature. The furnace will then be heated so that 500 °C is reached at the end of 1 *h* and 750 °C by the end of the second hour. It is then held for an additional 2 *hrs*. The sample can then be removed, cooled down and weighed. The fraction of ash is taken as the remaining mass divided by the initial mass. Following this, the volatile matter is determined per ASTM Standard ASTM D3175 – 11 9. The furnace is preheated to 950 °C. The sample is placed inside the crucible with its lid on and placed inside the 950 °C furnace. The lid will prevent air from entering the container and oxidising the sample. Oxygen should theoretically be consumed first by flammable volatile vapours being released. At the end of 7 min, the sample is removed from the furnace and allowed to cool. The difference in initial and final mass, divided by the initial mass, is the fraction of volatile matter. From here, the fixed carbon can be determined as the remaining fraction besides moisture, ash and volatile matter on an air-dried basis. Or the remaining fraction after accounting for ash and volatile matter on a dry basis. The ultimate analysis was outsourced to an analytical services company. The analysis was performed using a CHNS elemental analyser, which oxidises the sample and evaluates the compounds generated by thermal conductivity. CHNS composition is determined directly, and oxygen is assumed to be the remainder of the sample after CHNS, ash and moisture are measured.

3.3.2 Thermogravimetric analysis (TGA)

TGA was carried out in a Shimadzu DTG-60H. It allows for simultaneous measurement of temperature, mass and differential thermal analysis (DTA). The temperature can be increased up to 1500 °C, and the heating rate can be set between 1 and 50 °C/min. Mass is measured to

a precision of 0.001 *mg*. DTA measures the difference in temperature between a reference and the sample and quantifies this as electric potential difference (voltage). This reading will indicate the extent to which the sample absorbs or releases heat, i.e. whether the reaction is endothermic or exothermic. The entering the TGA may be inert (nitrogen or argon) or reactive (air or carbon dioxide). Three main analysis types were conducted in the TGA (ignition temperature analysis, kinetic analysis and burnout determination) and these are detailed below.

For all experiments, the samples do not require drying since this process can be carried out by the instrument. The flow rate of the inert or reactive gas was set to 100 ml/min. For the ignition test and kinetic analysis, the particle size was fixed at 63-105 μm and the amount of sample was varied between 1.5-5 *mg*. It is important that the heating rate remains linear; using too much sample in an oxidative environment will cause the sample to heat faster than intended. However, enough sample should be provided so that a high resolution can be obtained for the measurement of the mass loss derivative or the DTA signal compared to the noise or baseline drift. Generally, samples with a higher calorific value and low volatile matter will require less sample to be used. Also, samples with a higher activation energy will react in a well-defined temperature region. Therefore less sample is needed as the peak will be strong.

3.3.3 Solvent fractionation

As outlined in **Figure 5**, the method of solvent fractionation was applied to separate pyrolysis derived tars into different fractions, including light oil and heavy oils including asphaltene and pre-asphaltene [1]. Each tar sample was firstly mixed with n-hexane solution at a fixed ratio of 1:2 (mass: volume) in a 100 ml Erlenmeyer flask, which was subsequently stirred vigorously for 30 *min* at 290 *rpm* until a clear solid-liquid layer was formed. The vacuum filtration was carried out to filter out the n-hexane soluble and n-hexane insoluble. The n-hexane soluble was

considered as light oil hereafter. The n-hexane insoluble was further mixed with toluene based on the same procedure as the mixing with hexane. The toluene-soluble and insoluble were considered as asphaltene and pre-asphaltene, respectively. After vacuum filtration, the separated insoluble products were dried in a vacuum oven at 110°C to remove the solvent for a minimum 5 *hrs* before weighing.

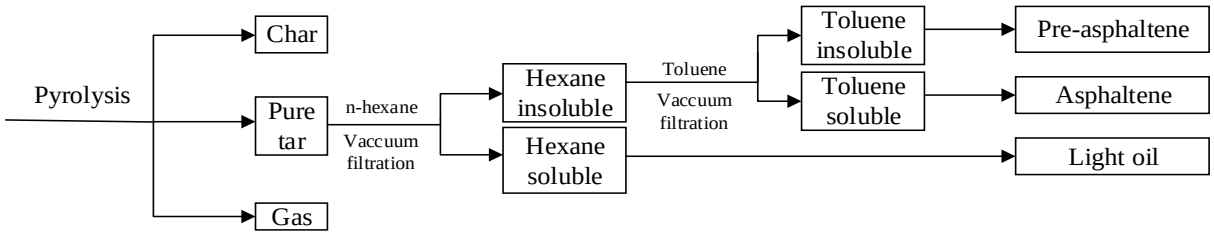

Figure 5 Method of solvent fractionation for the separation of light oil, asphaltene and pre-asphaltene for tars from tyre and coal.

3.3.4 Gas chromatography-mass spectrometer (GC-MS)

Elemental composition of the tar samples was determined using a CHNS Elementary Vario EL III. The chemical compositions of tars were identified by gas chromatography-mass spectrometer (GC-MS) on an HP6890 instrument in a splitless auto mode. Helium was used as the carrier gas at a flow rate of 1 mL/min. For GC analysis, the capillary column used is HP 19091S-433 (HP-5MS with 5% phenylmethyl siloxane) with a dimension of 30 *m* long, 0.25 *mm* inner diameter, and 0.25 μm nominal film thickness. The GC oven temperature was initially held at 50°C for 2 min, then heated to 200°C at 4 °C/min and on hold for 2 *min*. Finally, the oven was raised to 300°C at 8°C/min and on hold for 3 *min*. MS was operated in electron ionisation (EI) mode at 70 eV; the mass ratio scanning range is from 45-600 m/z; the accelerating voltage is 1.9 kV and the ion source is at a temperature range of 200-250°C. The chromatographic peaks were identified by using the Agilent MSD Chemstation software.

3.3.5 Fourier-transform infrared spectroscopy (FT-IR)

The functional group analysis of the liquid tars were carried out by Perkin Elmer spectrum 2000 FT-IR. For each analysis, a thin uniform layer of a tar sample was placed on the sample cell, and peak heights were normalised to the major C-H peak with a normalisation order of two.

3.3.6 Karl-fischer titration

The water content in the crude tar collected was determined by a Karl Fischer Volumetric Titration (Mettler Toledo) at least twice for accuracy. Special reagent for acetone were used for Karl fischer titration, namely combitrant 5 keto one component reagent and combisolvent keto solvent.

3.3.7 ^{13}C-nuclear magnetic resonance (^{13}C-NMR)

The solid state ^{13}C NMR spectra for samples were determined using a Bruker 400 (^{1}H)/100 (^{13}C) MHz spectrometer with cross polarization-magic angle spinning (CP/MAS). The acquisition time was 1000 min with 20000 scans averaged and a repetition time of 3.0 s, sample spinning rate 30 kHz.

3.3.8 ^{1}H- nuclear magnetic resonance (^{1}H-NMR)

The ^{1}H-NMR spectrum of tyre tars were obtained at an H frequency of 400 MHz with a 90^{o} pulse flip angle using a Bruker AVANCE instrument. The samples were dissolved in deuterated chloroform as an internal standard. The solid-state ^{13}C-NMR spectra for the raw

tyre was determined using a Bruker 400 (^{1}H)/100 (^{13}C) MHz spectrometer with cross polarisation-magic angle spinning (CP/MAS). The acquisition time was 1000 *min* with 20000 scans averaged and a repetition time of 3.0 s, a sample spinning rate of 30 kHz. All spectra from ^{1}H and ^{13}C-NMR were integrated based on the standard chemical shift ranges using the Topspin7.0 software.

3.3.9 Transmission Electron Microscopy (TEM)

Images and SAED patterns were recorded using TEM (Model FEI Tecnai G2 T20 TWIN TEM) with an accelerating voltage of 200 kV at the Monash Centre for Electron Microscopy.

3.4 References

1. Aljariri Alhesan, J.S., et al., *Long time, low temperature pyrolysis of El-Lajjun oil shale.* Journal of Analytical and Applied Pyrolysis, 2018. **130**: p. 135-141.

This page is intentionally left blank

This page is intentionally left blank

Chapter 4- Scrap tyre pyrolysis: Modified CPD model to describe the influence of pyrolysis conditions on products yields

The literature review in Chapter 2 has reviewed the current state-of-art of the kinetic modelling for tyre pyrolysis. It is learnt that all the kinetic models for tyre pyrolysis were empirical models which is required no consideration of the chemical structure of raw materials. In contrast to the empirical model, mechanistic CPD models describe the pyrolysis process by considering the chemical composition in terms of functional groups and structures, making the predictions more sensible and applicable over a wide range of solid fuels. Therefore, the first point of interest is to consider to develop a chemical percolation devolatilization (M-CPD) model that can include heat transfer, primary pyrolysis and the secondary cracking reactions of volatiles together to describe the pyrolysis of waste scrap tyre chip. This chapter has been reformatted from a manuscript submitted to Waste Management journal. The publication form is presented in Appendix A.

Abstract

This paper attempted to develop a modified chemical percolation devolatilization (M-CPD) model that can include heat transfer, primary pyrolysis and the secondary cracking reactions of volatiles together to describe the pyrolysis of waste scrap tyre chip, as well as to examine the influence of operating conditions on the scrap tyre pyrolysis product yields. Such a study has yet to be conducted in the past, thereby leading to a large knowledge gap failing to understand the pyrolysis of coarse feedstock appropriately. To validate the developed model, a number of operating parameters including reactor configurations, carrier gas compositions (argon and argon blended with CO_2 and/or steam), scrap tyre chip size (0.5 to 15.0 mm), terminal pyrolysis temperature (400-800 °C) and heating rate (10 °C/min and 110 °C/min) were examined in a lab-scale fixed-bed pyrolyzer, with a particular focus on the secondary cracking extents of the liquid tar. Through both experimental investigation and modelling approach, it was found that significant secondary cracking extent occurred upon the increase on the feedstock size, heating rate and residence time. Upon the fast pyrolysis, the average temperature gap between the centres of the coarse particle and reactor wall in that case could reach a maximum of 115 °C for the tyre chips of 6-15 mm. Consequently, its primary volatiles underwent the secondary cracking reaction at an overall extent of 17 % at a terminal temperature of 600 °C and a fast heating rate of 110 °C/min. Consequently, the yield of light gases including methane was increased remarkably. The flow rate of inert carrier gas was also influential in the secondary cracking, in which a maximum tar yield (54 *wt%*) was reached at a carrier gas flow rate of 1.5 L/min. This indicates the occurrence of secondary cracking has been largely minimised. At a pyrolysis temperature of 600 °C, the addition of CO_2 in carrier gas had an insignificant effect on the product yield distribution under the slow heating scheme. In contrast, the addition of steam resulted in a slight increase of carbon monoxide, presumably due to the occurrence of gasification reaction.

Keywords

Waste Tyre, Pyrolysis, M-CPD model, Secondary Cracking Reaction.

4.1 Introduction

The disposal of waste tyre is a serious environmental issue, predominantly due to its poor biodegradability [1]. In Australia, on average 51 million of waste tyre is generated each year in which only 5 % of waste tyre is properly reused whereas the rest are simply piled in large quantities [2]. Tyre fires are very difficult to control, which can create a great deal of hazardous smoke, causing a health risk through the inhalation of particles and chemicals. Various technologies have been developed to recycle waste tyre, among which, pyrolysis is receiving a great deal of attention due to its ability to recover the energy content and valuable chemicals [3, 4]. Specifically, three value-added products can be generated via tyre pyrolysis, solid semi-coke (char), liquid oil (tar) and light gases ($<C_5$).

Tyre is made of rubbers (60-65 *wt%*), carbon black (25-35 *wt%*) and the rest consists of accelerators and organic fillers [5]. The composition of tyre is difficult to be generalised, as rubbers are mainly a blend of different types of elastomers, such as isoprene natural rubber (NR), synthetic styrene-butadiene (SBR) and butadiene (BR) polymers mixed at different ratios depending on the manufacturing requirement [6]. Regardless of the chemical composition of the tyre, a great deal of kinetic studies of the tyre upon pyrolysis process has been completed, as reviewed previously [7].

Among the large variety of tyre modelling studies on pyrolysis, the single-kinetic-rate model is considered as the simplest kinetic model, in which the entire waste tyre pyrolysis is treated as a single reaction route [8-10]. However, this approach has been argued to only work at a high pyrolysis temperature range, while the mass loss is more diffusion limited at lower temperatures [8]. Aguado et al. [11] also indicated that different kinetic parameters were found

for thirteen volatiles evolved from tyre pyrolysis under an inert atmosphere, proving that tyre is highly heterogeneous and its pyrolysis rate is not a singular reaction.

Besides the single-reaction-route, other kinetic studies proposed a series of reaction routes to account for the entire tyre pyrolysis process. It is assumed that the tyre components (additive, NR, SBR and BR) are decomposed individually without any interaction among one another. Through the comparison of thermo-gravimetric analyser (TGA) and differential thermos-gravimetry (DTG) profiles, the predicted results from the model showed a good fit at two ends of temperatures, though the overlapping regions around 250-500 °C did not show a good agreement [12], particularly under fast heating conditions. An improvement was made by Lah, Klinar [13] who considered additional tyre components (volatiles, fabric and other additives), showing a satisfactory agreement with the TGA results of tyre composites. It is also acknowledged that the pyrolysis reactions are not being simple monomolecular and first-order decompositions. Another common method is to assume that the tyre pyrolysis process is competing multi-series/parallel reactions with several intermediates and products. This method is able to deconvolute the TGA/DTG data of tyre with a high fitting agreement and has been further extended to include other considerations, including heat transfer limitation and reactor designs [14, 15]. Besides that, multistep reaction kinetics can also be accounted for by the isoconversional model to predict the pyrolysis of biomass and plastics [16].

In contrast to the empirical model, chemical based models describe the pyrolysis process by considering the chemical composition in terms of functional groups and structures, making the predictions more sensible and applicable over a wide range of solid fuels. The most renowned chemical based model, namely the chemical percolation devolatilization (CPD) works

effectively to describe the devolatilization behaviour of a variety of bituminous coals [17]. The CPD model has shown a high accuracy on the pyrolysis rate over primary devolatilization reactions. However, the secondary reactions for the primary volatiles are not included. Our previous study on the pyrolysis of low-rank brown coal (*i.e.* lignite) briquette discovered that the internal heat transfer is the limiting factor, which lowers the heating rate of coarse particle and leads to an increase in the cross-linking extent and a decrease in the tar fraction compared to the fine coal particles [18].

This work aims to develop a modified CPD model for tyre pyrolysis based on the conventional CPD model by integrating heat transfer and the secondary reactions of primary tar, so as to make it fit for the pyrolysis of scrap tyre chips under a broad range of critical pyrolysis conditions in a lab-scale fixed bed pyrolyzer, including three granule sizes (0.5 to 15.0 mm), carrier gas flow rate (0 to 3.0 L/min), four terminal temperatures (400 to 800 °C), two different heating rates (10 °C/min versus 100 °C/min) and different carrier gases (pure argon versus 15-30 *vol%* CO_2/steam balanced by argon). All the experimental conditions are expected to be encountered in an industry-scale pyrolyzer; some have yet to be tested and understood previously. In respect to the modelling approach, a first-order kinetic reaction is applied to tackle the secondary reactions of primary volatiles, incorporating the heat transfer mechanism to predict the time-resolved particle temperature as well as its radial distribution to track the overall pyrolysis rate and product yield profiles. Since the modified model has been validated by a broad range of experimental conditions, it is desirable that the modified model can be used for the scale – up and proper design of an industry-scale reactor, as well provides insights on the fundamentals underpinning the pyrolysis of scrap tyre chip, a feedstock that is far more heterogeneous than coal and biomass [19].

4.2 Material and methods

4.2.1 Properties of the scrap tyre feedstock

The scrap tyre collected from Tyrecycle Pty Ltd (Australia) is a mixture of different tyres which were grouped into three particle size bands, 0.5-1.5, 4 and 6-15 *mm*. The steel and wires were removed prior to the experiments. The proximate and ultimate properties of these tyre are displayed in **Table 4**. As can be seen, the three sizes possess very similar properties expect the ash content. The slight differences between the three sizes are not expected to cause any considerable difference in the pyrolysis behaviour.

Table 4 Proximate and Ultimate analysis of scrap tyre in different sizes.

Size bands (mm)	0.5-1.5	4	6-15
Proximate analysis, *wt%*			
Moisture (ad)	0.85	1.07	0.89
Volatile matter (db)	68.49	66.27	66.64
Fixed carbon (db)	25.17	29.59	30.12
Ash (db)	6.34	4.14	3.24
Ultimate analysis (db), *wt%*			
C	82.10	83.19	84.57
H	7.56	7.65	7.35
O (by difference)	0.75	0.74	0.70
N	1.93	1.77	2.01
S	1.32	2.51	2.13

4.2.2 Pyrolysis conditions

A lab-scale fixed-bed pyrolyzer shown in **Figure 4** was employed. The reactors are made of quartz with an inner diameter of 55 *mm* and a total length of 1 *m*. For the reactor configuration 1, an argon stream of 0.8 L/min was purged continuously from the top of the reactor which meets the released tar and gases from the inside of the reactor. The argon gas, in this case, is merely used to minimise the deposition of tar on the reactor wall as well inside the connecting tubes. However, it is not supposed to flow back inside the reactor once the tyre pyrolysis occurs, considering that the pyrolysis gases and the hot tar are generally ejected and flow upwards based on their concentration/pressure gradient. Such a configuration aims to mimic the indirect heating mode for an industry-scale pyrolyzer without any carrier gas inside [20]. Based on the amount and reactor configuration, the released volatiles were expected to have a residence time of approximately 300 s inside the reactor.

Conversely, the reactor configuration 2 uses a continuous carrier gas flow starting from the bottom of the reactor and passing through the tyre chip bed, thus sweeping away the gaseous and tarry species instantaneously once they are released out from solid particles [20]. This process aims to mimic the direct heating mode for an industry-scale pyrolyzer inside of which a portion of the products burns to provide heat. The resultant hot flue gas flows through the reactor bed (Bergman et al., 2005). To simulate the flue gas compositions derived from the internal combustion in configuration 2, argon is also blended with 15-30 *vol%* CO_2 and/or steam as a carrier gas for this study.

After leaving the pyrolyzer, both condensable (tar) and non-condensable (gas) species enter a three-stage impinger train. The first impinger is surrounded by ice and water mixture as a cooling agent whereas dry ice/acetone mixture is used in the second and third impingers. U-

tube filled with alumino silicate wool is further used downstream to trap the remaining tarry species. The exiting gases enters to a gas analyser (Sensotec Rapidox 5100) which can measure O_2, CH_4, CO, CO_2 and H_2 real-time. Tar yield is calculated based on the mass of the condensable volatiles collected in the impinger train, plus those deposits on the reactor wall (*i.e.* the reactor was weighed before and after each run to calculate the tarry depositions on its wall). The content of water in each tar sample is quantified by a pre-calibrated Karl-Fischer volumetric titrator (Mettler Toledo EasyPlus). The solid char yield is calculated, on a dry-ash-free (*daf*) basis, as the weight difference of the reactor before and after each run.

Regarding the pyrolysis conditions, the final pyrolysis temperature varies between 400 °C and 700 °C at two heating rates, slow pyrolysis (10 °C/min) and fast pyrolysis (110 °C/min) under an atmospheric pressure. The slow heating rate is used to mimic the industry – scale pyrolyzer such as a coking oven that bakes slowly, whereas the fast heating rate is expected to mimic particles entering a pre-heated oven or those close to the hot reactor wall that is heated up quickly. For the slow heating mode, the tyre chips are loaded inside the reactor and heated together, whereas for the fast heating mode, the furnace is pre heated to a set temperature before the tyre chips – laden reactor was quickly inserted inside. Regardless the heating mode, the total reaction time is approximately 88 min for every single run, including the time reaching the target temperature and holding time, whilst the carrier gas flow rate is fixed at 0.8 L/min. Some experiments were repeated twice and the standard deviations were averaged and listed in the corresponding figures. The average error of the overall material balance was as high as 6 *wt%*, presumably due to the disability of gas analyser which treats all the non-condensable C_2-C_6 hydrocarbons as methane gas (CH_4).

4.2.3 M-CPD model for waste tyre chip pyrolysis

Figure 6 shows the overall calculation flow for the modelling development of the M-CPD, which is further detailed below. The MATLAB codes are presented in Appendix B.

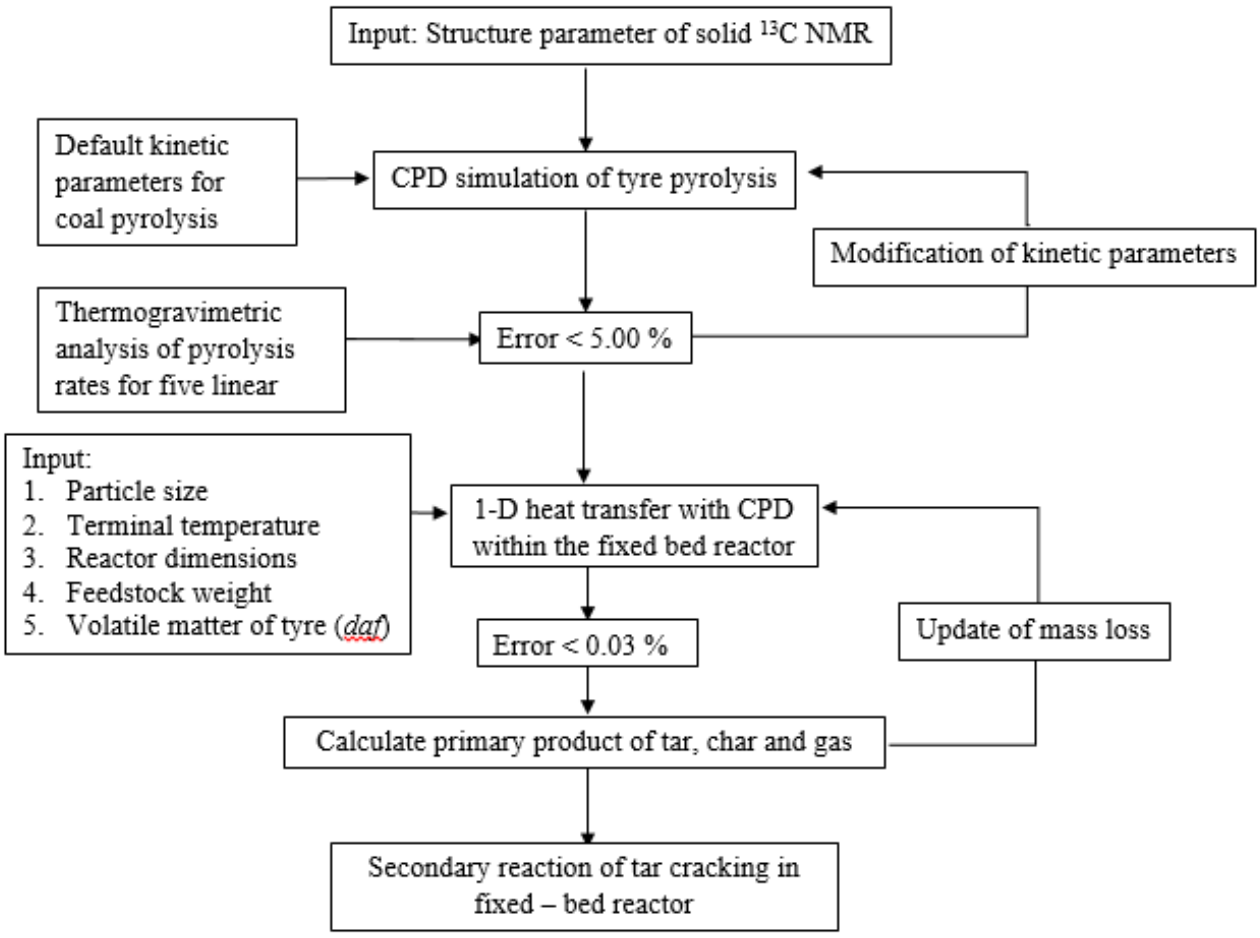

Figure 6 The calculation flow for the M-CPD model.

4.2.3.1 Chemical Structure Parameters

The use of the CPD model requires the measurement of the chemical structure parameters (MW_{cl} MW_{side}, $\sigma+1$, P_o, C_o) of the parent tyre, which was the first step for the modelling procedure in **Figure 6**. The average values of these structure parameters were measured from the solid-state carbon-13 nuclear magnetic resonance analysis (^{13}C NMR).

The solid state ^{13}C NMR spectra for samples were determined using a Bruker 400 (^{1}H)/100 (^{13}C) MHz spectrometer with cross polarization-magic angle spinning (CP/MAS). The acquisition time was 1000 min with 20000 scans averaged and a repetition time of 3.0 s, sample spinning rate 30 kHz.

Through NMR analysis, the ^{13}C NMR CP-MAS chromatograph of the tyre of 0.5-1.5 mm is presented in **Figure 7**. The abundant peaks in the spectra were integrated based on the standard chemical shift ranges using Topspin 3.5 pl 7 software. The relative areas are tabulated in **Table** 5, corresponding to the characteristics of each peak in terms of organic structures and functional group [21, 22]. With these area fractions, the four chemical structure parameters (P_o, $\sigma+1$, MW_{cl} *and* MW_{side}) were determined by means of the mathematical equations by Solum et al [21]. However, the last fifth parameter (C_o) has not been measured directly and was set to nil for this tyre sample, as most of the previous CPD work.

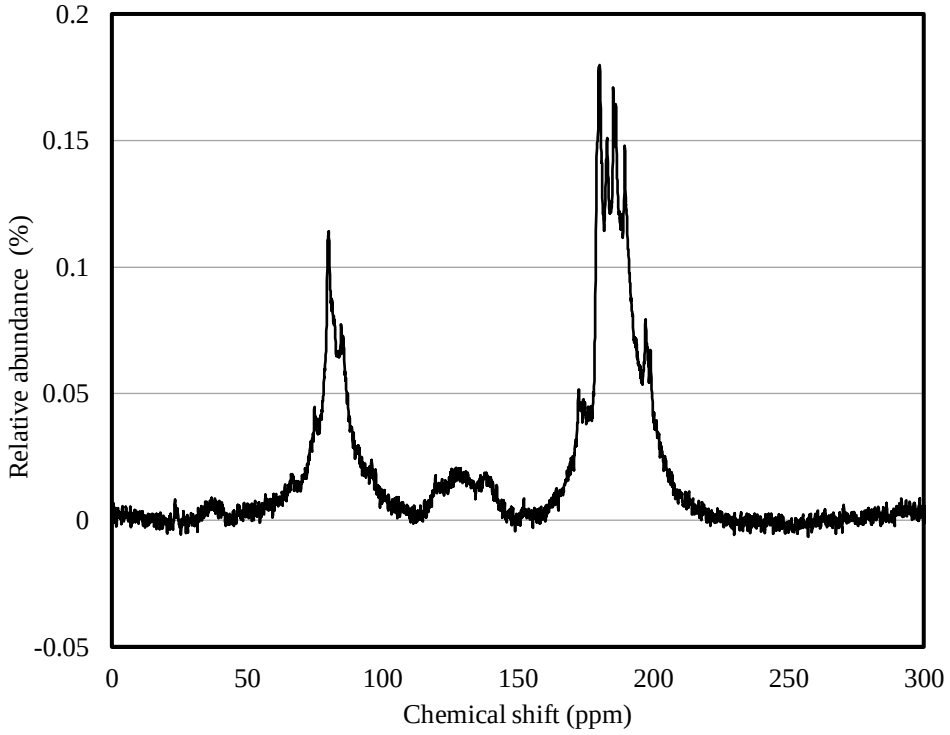

Figure 7 NMR chromatogram of tyre rubber of 0.5-1.5mm after deconvolution.

Table 5 The integrated peaks for the organic functional regions.

Parameters	Chemical Shift range (ppm)	Area fraction
Fal	0-90	0.645
Fa	90-240	0.355
fa^{c}	165-240	0.042
fa'	90-165	0.313
fa^{o}	185-240	0.036
fa^{oo}	165-185	0.006
fa^{H}	90-130	0.199
fa^{N}	130-165	0.114
fa^{P}	150-165	0.018
fa^{S}	135-150	0.052
fa^{B}	130-135	0.044
fal^{*}	50-60	0.014
fal^{*}	0-22	0.166
fal^{H}	60-90	0.080
fal^{H}	22-50	0.385
fal^{o}	50-90	0.094

A modification was also made to the theoretical coordination number, $\sigma+1$ which was found to be 1.87 experimentally. According to Solum et al. [21], the percolation threshold for a lattice is defined as $\sigma = 1/P_o$, representing the point at which the bridges are broken up to the point that no connected lattice exists. The value of $\sigma+1$ was thus calculated to be 2.30 to compromise with the value of P_o. A similar attempt was made by the CPD simulation for black liquor [23].

Besides the five structure parameters, there is a sixth parameter used to correct the molecular weight of side-chain of scrap tyre, MW_{side}. The molecular weight of side chain is subject to the reduction by a correlation factor as some functional groups (such as fraction of tightly-bound a-methyl groups), which were counted as side chains in the NMR measurements and should be considered as part of the aromatic clusters [17]. To ensure a good agreement between model prediction and experimental data, this correlation factor was defaulted to be 7.0. However, this factor was noted to vary between -8.25 to 19.73 for the bituminous coals from different sources [24]. In this case, the correlation factor was found to be 49.0 for tyre CPD simulation by fitting with the TGA data (to be shown later). For comparison, the structure parameters for other solid fuels were also included in **Table 6**. Clearly, the structure for scrap tyre differs significantly from those that have been studied extensively.

Table 6 Chemical Structure Parameters of the tyre samples determined from solid-NMR measurement

Structure Parameters	Zap coal [17]	Xinjiang coal [25]	Celluloses [26]	Green river oil Shale 1.9 [27]	Present work
MW_{cl}	277.00	320.96	81.00	776.00	391.00
MW_{side}	40.00	37.55	22.70	131.00	153.00
P_o	0.63	0.60	1.00	0.50	0.80
C_o	0.40	0.07	0.00	0.00	0.00
σ+1	3.90	5.11	3.00	4.50	2.30
Correlation factor of MW_{side}	7.00	14.95	7.00	7.00	49.00

4.2.3.2 Intrinsic and Primary Reaction Routes of Tyre Pyrolysis

The intrinsic kinetic parameters related to the primary pyrolysis of tyre were determined after modifying its structural parameters. The conventional CPD model characterises the primary

devolatilization reactions as several first-order bridge-breaking and bridge-forming reaction routes based on the theory of percolation lattice statistics [17]. The rates of the reaction routes were defined as the rate of labile bridge scission (k_b), light gas release (k_g), cross-linking (k_{cross}) and the competing reaction coefficient of bridge breaking to char bridge formation (k_δ/k_c) [17].

In this study, a major modification was made on the inherent reaction routes of CPD model. By definition, CPD assumes that light gas is derived from the side-chain molecules whose molecular weight was as small as around 12 to 52 amu [17]. However, the molecular weight of the side chain of scrap tyre was found to be 139 amu. (**Table 7).** Modification was thus made by taking the product derived from breakage of side-chain molecules in scrap tyre as tarry species, rather than as a light gas. Such an approach is the same as that has been taken for black liquor for which the molecular weight of the side chain accounts for 128 – 148 amu. [23].

The evaluation of each kinetic parameter was done by means of curve-fitting with the primary pyrolysis rate of pulverised tyre based on the TGA analysis, as has been done in previous CPD modelling studies [23, 26, 27]. In this work, the initial guess of kinetic parameters was taken from that of the CPD simulation for coal. MATLAB R2016b was used to optimise the kinetic parameters through least-square fitting with the experimentally measured mass loss profiles at five heating rates (10, 20, 30, 40 and 50 °C/min) from TGA (Shimadzu DTG-60H) in pure argon of 100 ml/min. For each run a typical mass of 5-10 mg pulverised scrap tyre (<106 μm) was used to eliminate the heat transfer issue.

4.2.3.3 Heat Transfer Rate Coupling

Different from a TGA, the fixed-bed reactor in **Figure 4** is expected to encounter a heat transfer limitation between reactor wall/hot carrier gas and particles, as well as inside of a chip particle if it is large enough. In the modelling flowsheet in **Figure 6**, the CPD model was further coupled with the heat transfer rate in step 3. One-dimensional unsteady heat transfer controlled by intra-heat conduction and inter-convective and radiative mechanism were employed, based on the following assumptions:

a) The heat loss was n**e**gligible.
b) The intra-particle heat transfer was governed by thermal conduction, as per Equation 4.1.
c) Scrap tyre particle was heated up externally by pyrolysis gas by means of convection and radiation inside the reactor, as per Equation 4.2.
d) Scrap tyre particle was assumed to be a porous sphere, one-dimensional distribution of physical properties with uniform boundary conditions on its surface.
e) The swelling and shrinkage of tyre particles were negligible because the particle volume was found to remain almost constant (data not shown).

$$\frac{\partial}{\partial t}(\rho \cdot C_p \cdot T) = \frac{1}{r}\frac{\partial}{\partial r}\left(\frac{\partial}{\partial r}(k \cdot T)\right) + \frac{\partial}{\partial t}(\alpha \cdot \rho) \cdot \frac{1}{VM} \cdot \Delta H_{rxn} \qquad \text{Equation 4.1}$$

$$\frac{\partial}{\partial r}(k \cdot T) = h\,(T_\infty - T_s) + \varepsilon\,\sigma\,(T_\infty{}^4 - T_s{}^4) \qquad \text{Equation 4.2}$$

The reaction of heat (ΔH_{rxn}) was calculated based on the correlation of temperatures between the reference sample and ground tyre (<106 μm) in the TG/DTA analysis, which was found to be around 122 kJ/kg for an overall endothermic pyrolysis reaction. As the scrap tyre particle was subjected to pyrolysis, its composition was changed with temperature and time. In light of

this, Equations 4.3 and 4.4 together with Error! Reference source not found. were used to calculate the tyre thermal conductivity and heat capacity at each temperature and every moment. Since the mass loss fraction (α) was not calculated until the specification of thermal properties were determined (**Figure 9**), an initial guess was made by assuming that thermal properties were not changed by mass loss. The mass loss fraction was then calculated at every space and time point and the simulation was repeated with this added mass fraction using bilinear interpolation. This process was further iterated until the error between the initial guess and calculated mass loss fraction was less than 3E-5.

$$k = k_{tyre}(\frac{VM-\alpha}{VM}) + k_{carbon}(\frac{\alpha}{VM}) \quad \text{Equation 4.3}$$

$$C_p = C_{p,tyre}(\frac{VM-\alpha}{VM}) + C_{p,carbon}(\frac{\alpha}{VM}) \quad \text{Equation 4.4}$$

Table 7 Kinetic Parameters of various solid fuels for CPD modelling.

Kinetic parameters	Bituminous coal [17]	Green river oil Shale [27]	Cellulose [23]	Cellulose [26]	Black liquor [23]	Present work
E_b (kcal.mol^{-1})	55.4	23.9	55.4	59.0	55.4	60.4
A_b (s^{-1})	2.61 × 10^{15}	1.58 × 10^{10}	2.0× 10^{16}	1.0× 10^{18}	2.61 × 10^{15}	2.57× 10^{17}
σ_b (kcal.mol^{-1})	1.8	0	4.1	1.8	1.8	1.8
E_g ((kcal.mol^{-1})	69.0	21.0	61.2	43.2	62.5	60.4
A_g (s^{-1})	3.0 × 10^{15}	1.58 × 10^{10}	3× 10^{15}	8.23× 10^{12}	3.0 × 10^{15}	2.4× 10^{18}
σ_g (kcal.mol^{-1})	8.1	3.0	8.1	3.0	8.1	7.5
E_{cross}(kcal.mol^{-1})	65.0	60.0	65.0	65.0	65.0	65.0
A_{cross} (s^{-1})	3.0 × 10^{15}	1.18× 10^{15}	3.0× 10^{15}	3.0× 10^{15}	3.0× 10^{15}	3.0× 10^{15}

k_δ/k_c	0.9	0.9	100	0.9	0.9	1.34

4.2.3.4 Secondary Reaction Route of Tyre Pyrolysis

The last step in the modified CPD procedure in **Figure 6** was to quantify the secondary reaction extent of the primary species released from tyre pyrolysis inside the fixed-bed reactor. Different reaction expressions have been made by the previous modelling and experimental studies to describe the secondary reaction of tyre volatiles, such as cyclization [28], Diel-Alder reaction for the formation of aromatic compounds [29] and cracking reaction [30]. It was generally agreed that the temperature range of secondary reaction was specified at 550 – 800 °C, whereas the temperature range of 250-520 °C was deemed as primary pyrolysis reaction window where the major covalent bonds inside the parent chemical network starts to break down [30].

In the modelling study, the primary tar fraction was calculated at each point across the length of the particle. The overall primary tar fraction prior to the secondary cracking reaction was then calculated using Equation 4.5. The rate of cracking reaction for the primary tar in the fixed bed reactor, given in Equation 4.6 was assumed as a first – order Arrhenius form. The amount of tar being cracked was calculated based on Equation (7) which is based on the reaction rate and the residence time of primary volatiles inside the reactor. The residence time of tar volatiles was calculated based on the flow rate of tar/carrier gas and the actual dimension of the vertical and cylindrical reactor.

$$X_i = \frac{\sum_{i=1}^{n} x_i r_i^2}{\sum_{i=1}^{n} r_i^2} \qquad \text{Equation 4.5}$$

$$k_S = A_s\, exp(\frac{-E_s}{RT}) \quad \text{Equation 4.6}$$

$$X = X_i\, e^{(-k_S\, t_R)} \quad \text{Equation 4.7}$$

The schematic diagram of the overall reaction routes for M-CPD model is presented in **Figure 8**. The primary reactions were based on the reaction routes of the conventional CPD whereas the secondary reaction is defined as where the primary tars cracks to form light gases.

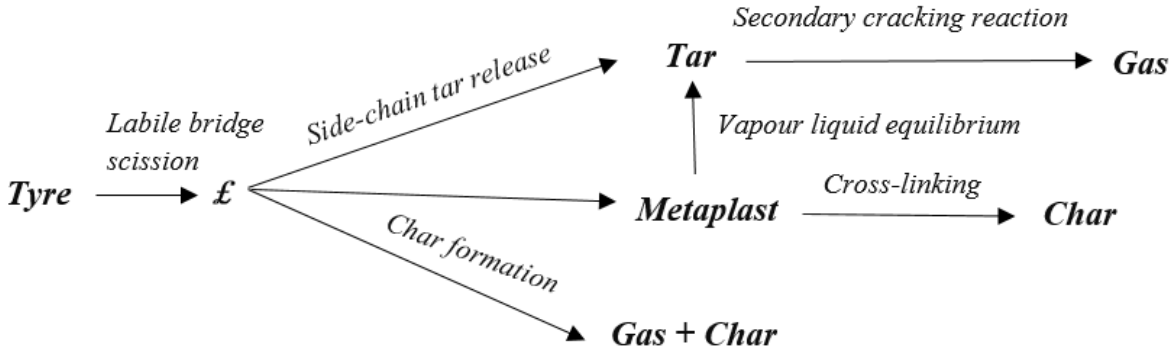

Figure 8 The schematic diagram of the reaction routes for M-CPD model, originally adapted from [17].

The extent of tar cracking is calculated based on the difference of tar yield predicted by M-CPD under the consideration of *only-primary* and *primary-secondary* reactions. The kinetic parameters for secondary cracking reaction were determined through the least-square regression method to fit with the experimental tar yields obtained from the 6-15 mm tyre size under two heating rates (slow and fast pyrolysis) and four terminal temperatures (400-700 °C). The secondary reaction is assumed to be negligible under the slow heating rate (as shown later) while it is noticeable under the fast heating scheme. Therefore, the difference of tar yield

between these two schemes were used to determine the secondary reaction extent for the tar and its kinetic parameters.

4.3 Results and Discussion

4.3.1 Effects of terminal temperature and heating rate

The intrinsic rate of tyre pyrolysis with primary reactions was first analysed by TGA. The conventional CPD model without any modification (i.e. all the default settings based on coal) was used to assess its applicability to scrap tyre pyrolysis. The experimentally measured mass loss kinetics of the ground tyre (<106 μm) are presented in **Figure 9a** and **b**, given in a solid curve. As shown in **Figure 9a**, the mass loss profile predicted by the conventional CPD model did not fit the TGA data at all. The maximum absolute error was found to be 18.21 %. Instead, upon the least – square fitting approach, the new and optimised kinetic parameters tabulated in **Table 7** were achieved, showing an improved fitting for the five different heating rates in **Figure 10b**. **Table 7** also lists the intrinsic kinetic data for other solid fuels from previous works.

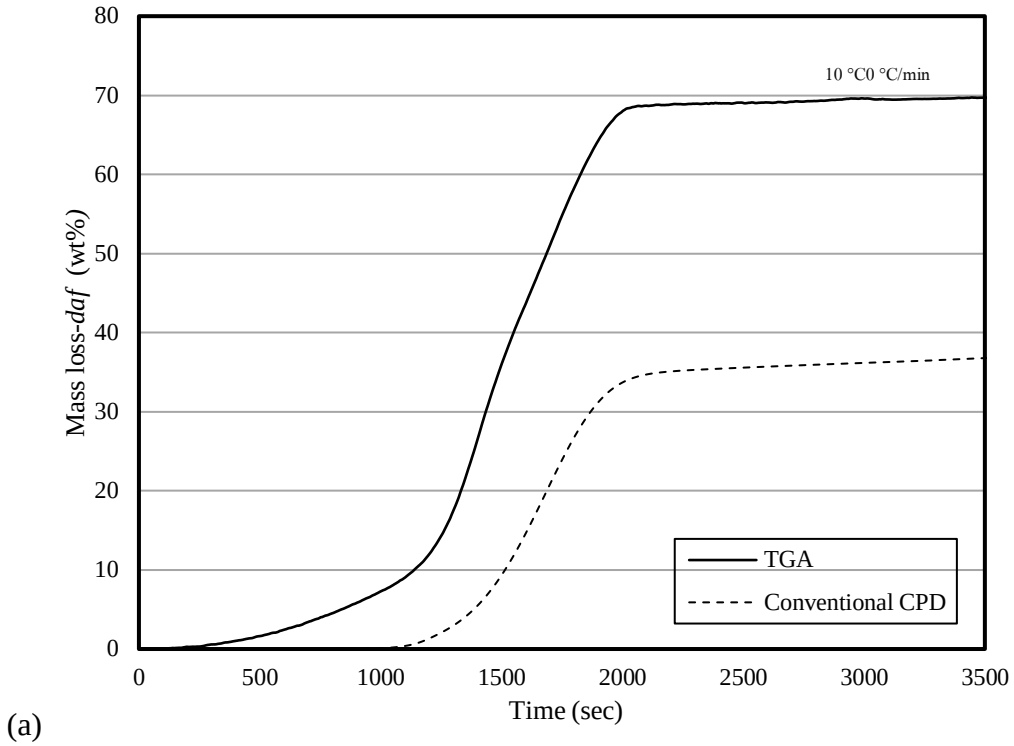

(a)

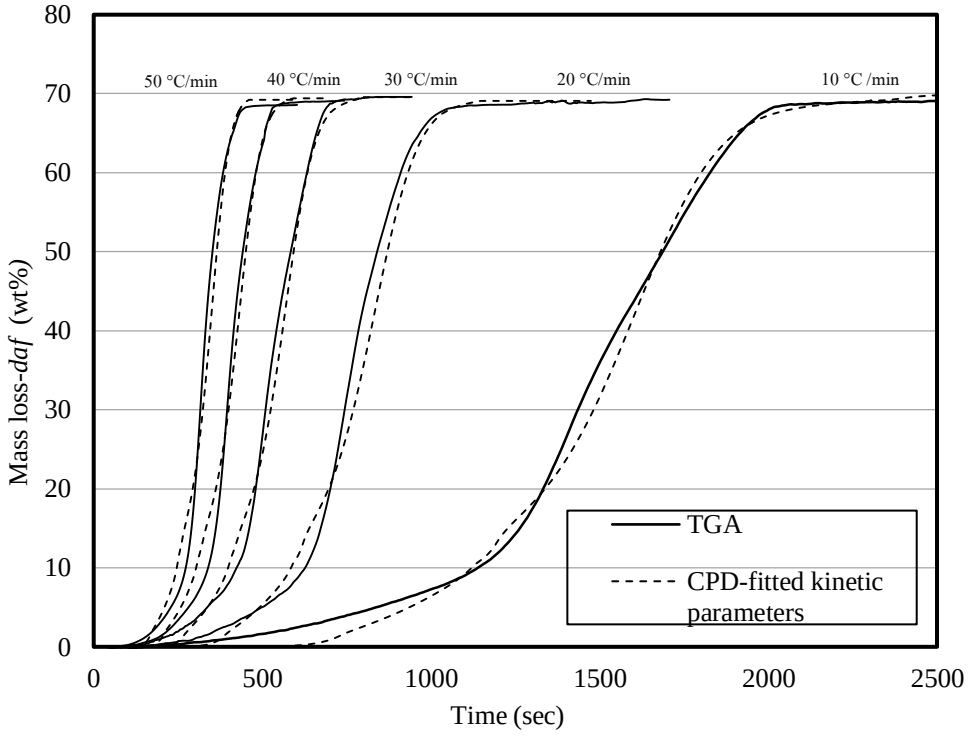

(b)

Figure 9 Comparison of the mass loss kinetics of CPD model and TGA data for various heating rates using (a) Initial kinetic parameters and (b) Optimised kinetic parameters.

Based on the optimised kinetic parameters in **Table 7**, the individual reaction rates involved in the primary pyrolysis of scrap tyre are presented in **Figure 10**. The scrap tyre started to decompose at 250 °C, predominantly contributing to the formation and release of tarry fragments that even commenced earlier than the release of light gaseous species from around 320 °C. It is in line with the previous modelling study at 300 °C revealing the formation of approximately 7 *wt%* (*daf*) tarry species, relative to a gas yield of only 0.03 *wt%* [31]. However, from 425 °C onwards, the release rates of the three products started to level off, finishing at 475 °C.

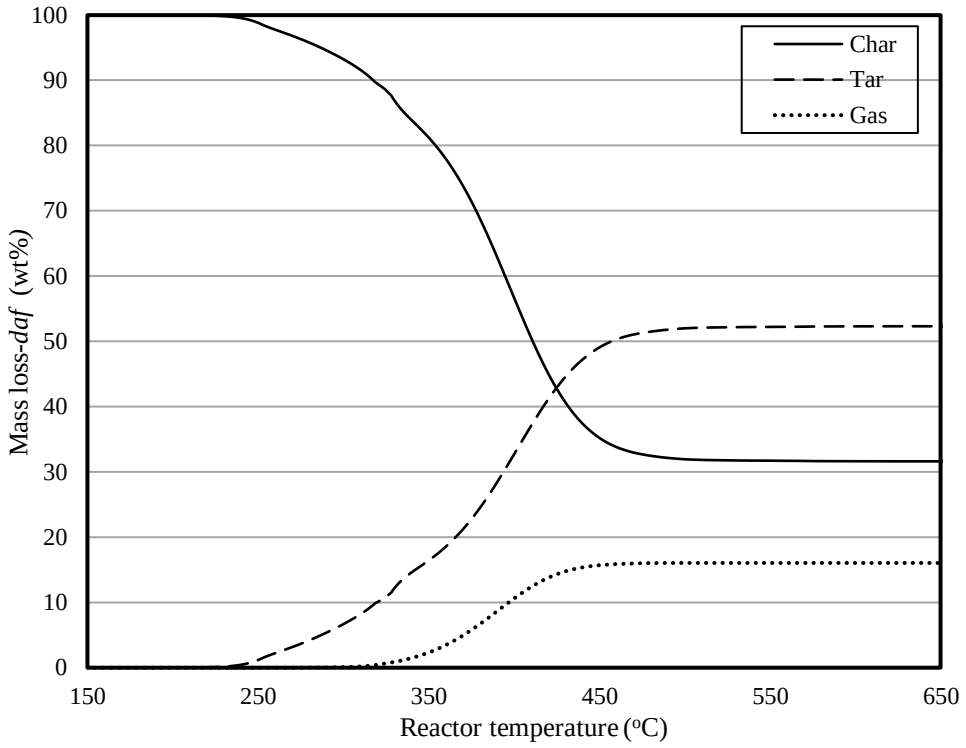

Figure 10 The rate of pyrolysis product formation during the primary pyrolysis predicted by M-CPD model.

Experiments in the lab-scale fixed-bed pyrolyzer were then conducted to evaluate the kinetic parameters achieved based on the TGA data, as well as to assess if the secondary reactions related to the primary tar and gases would occur. For these two purposes, the reactor

configuration 1 with a top flow of pure argon was used, which maximised the residence time of tar and gas inside the reactor and minimises/eliminates the interference from carrier gas on the secondary reactions of tar. The pyrolysis of tyre of the largest size band, 6-15 *mm* was also used considering that the internal heat transfer would be slower. The experimental results for product yields are presented in **Figure 11.**

In **Figure 11a**, char yield declines remarkably from 55 *wt%* to 36 *wt%* (*daf*) when the temperature increased from 400 to 500 °C, and then remains relatively constant for both heating rates. The char yields are in good agreement with above- mentioned TGA results as well as the previous findings which explained that the complete devolatilization of tyre occurred in the temperature range around 450 to 550 °C under the atmospheric pressure [30].

In **Figure 11b**, the tar fraction yield was found to reach its maximum of around 50 *wt%* at 500 °C under the fast heating rate. For the two temperatures of 400 °C and 500 °C, the tar yield increased slightly, if not negligible upon the shift from low heating to fast heating. Such an increment can be explained by the rapid relaxation of tyre particle and thus the ejection of volatiles upon a fast heating. However, compared to coal and biomass, scrap tyre has much less gaseous compounds to eject at 400 °C and 500 °C (see TGA data), thereby performing an insensible variation on the liquid tar yield upon the increase of the heating rate [19].

Increasing the terminal temperature beyond 500 °C failed to improve the tar yield, because the release of volatile was completed by 475 °C, as evident by the TGA results. This was also supported by a relatively unchanged tar yield from 600 °C and above for the slow heating

scheme. This was reasonable considering that the slow heating scheme in the fixed bed reactor bears the same heating rate as the TGA. It is also evident that the flow rate of inert argon gas was insignificant on the tar yield. This was however not the case observed for the fast heating scheme from 600 °C. A noticeable reduction in the tar yield from 45 to 36 *wt%* at 600-700 °C was observed for the fast heating scheme. Such a drop in the tar amount agreed with the increment in gas yield demonstrated in **Figure 11c**, signifying a large extent of the secondary reactions for tar. The primarily released heavy hydrocarbons tended to crack into shorter fragments while releasing light gases at a temperature around 600 °C, known as the secondary tar cracking reaction, which has been widely accepted [32]. Such a reaction was obviously facilitated upon fast heating, by which the primarily released tarry species undertook a rapid heating as well as experienced a higher temperature. Conversely, in a slow heating scheme, the tar was released before reaching the final set temperature, thereby experiencing little/no rapid temperature rise [28].

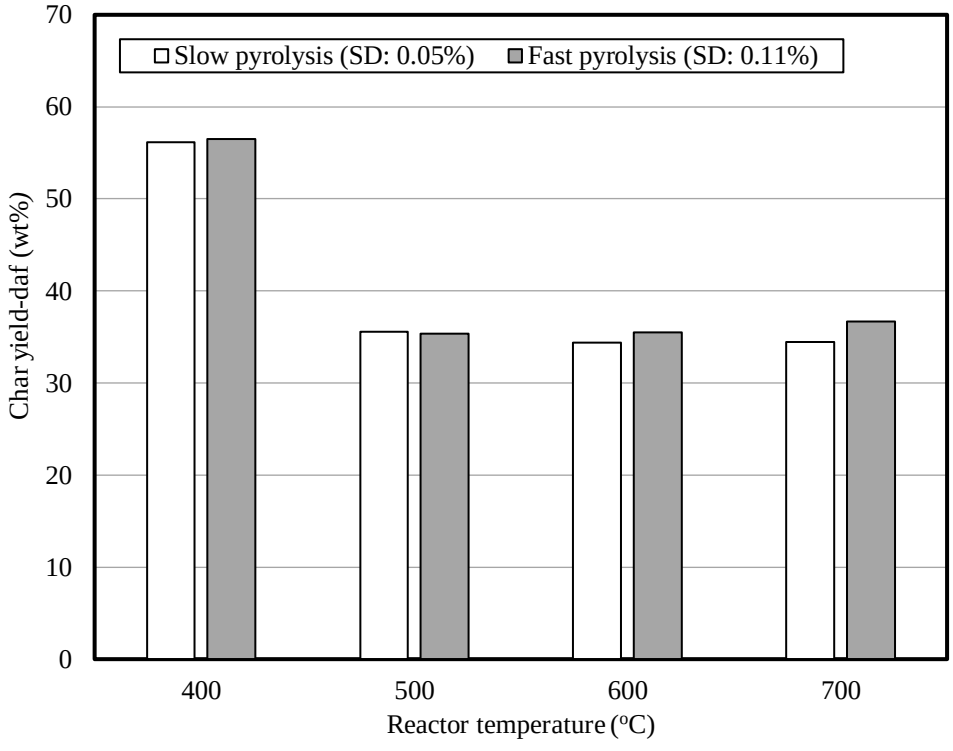

(a)

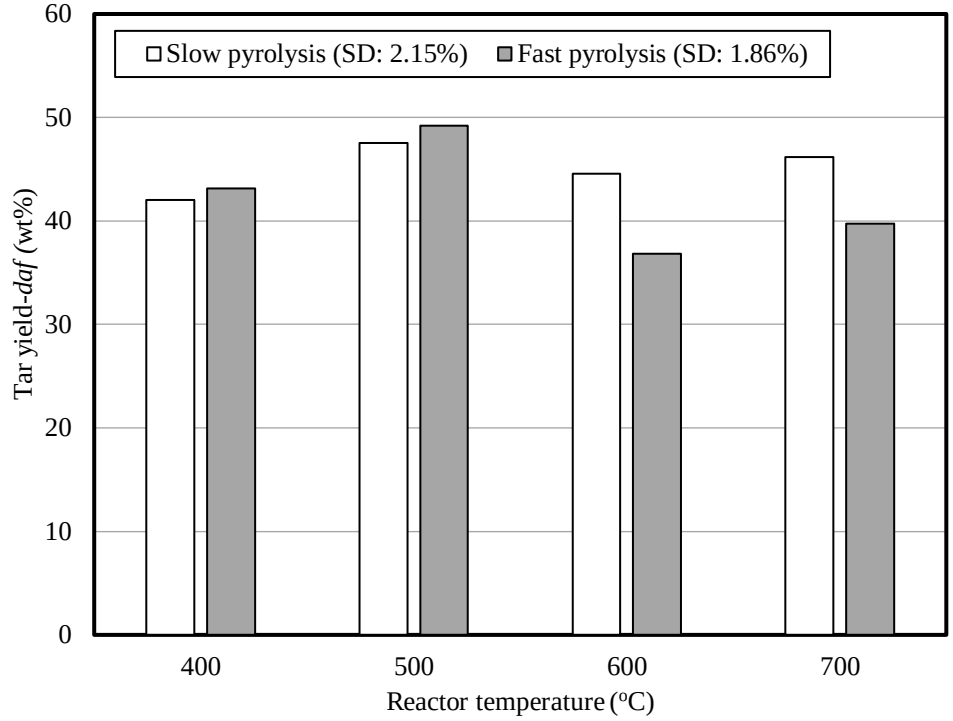

(b)

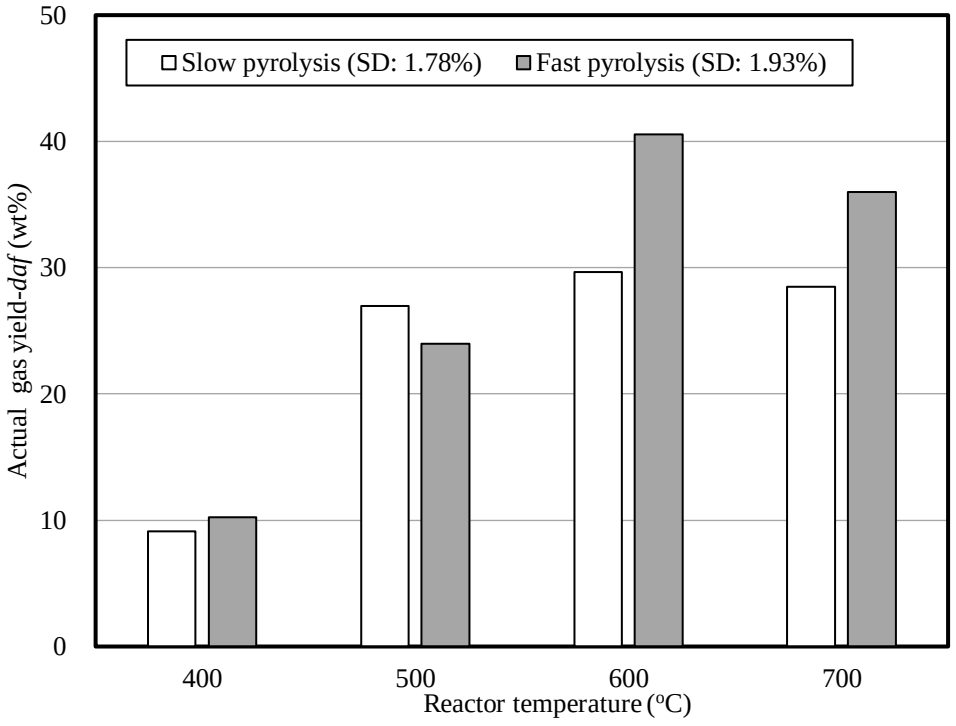

(c)

Figure 11 Experimental product yields (daf) of 6-15mm tyre on various temperature and heating rates in the fixed – bed reactor using configuration 1. Panel (a) Char yield (b) Tar yield (c) Gas yield.

The temperature-dependent profiles for the most abundant non-condensable gases (mainly CH_4) is depicted in **Figure 12**. Irrespective of the heating rate, non-condensable hydrocarbons were the most predominant species from scrap tyre pyrolysis, as has been confirmed elsewhere [33]. The amount of CO and CO_2 released were less than 1 *vol%* (data not shown), due to the low oxygen content in scrap tyre (**Table 4**) and the preferential immobilisation of oxygen into steam/water. In regard to the emission of non-condensable hydrocarbons, it was preferred upon a fast heating from 600 °C due to the secondary cracking of heavy hydrocarbons, as mentioned above.

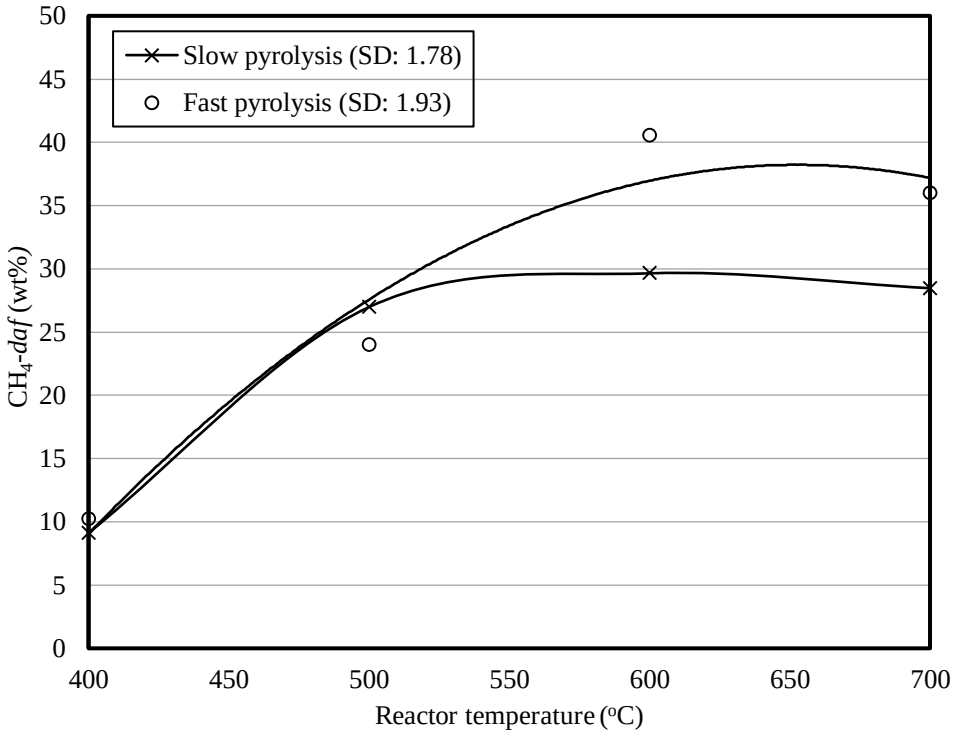

(a)

Figure 12 Yield of methane, *wt%* (daf) of 6-15mm tyre at various temperatures and heating rates.

Regarding the modelling effort using the M-CPD developed, the comparison of tar yield between experimental observation and the modelling prediction is summarized in **Figure 13**. For comparison, both the M-CPD models with and without the inclusion of secondary reactions were conducted. Clearly, without considering the secondary reaction, the predicted tar yield was far above the respective experimental value. With the method of least-square regression, the rate constants related to the secondary cracking reaction of tar are finalised in **Table 8**.

Table 8 Kinetic parameters of secondary tar cracking reactions of CPD models.

References	E_s (kcal.mol^{-1})	A_s (s^{-1})
Yan et al **[34]**	68.36	9.77×10^{10}
Present work	50.19 ± 0.48	$(5.02 \pm 3.00) \times 10^{11}$

Those values were found to differ from those obtained by Yan et al. [34] for secondary tar cracking from long flame coal-CPD in the hydrogen plasma environment. The values of activation energy and pre-exponential values were smaller and larger respectively than that of coal, indicating that the reaction rate of cracking reaction of tyre is larger at all circumstances of reaction temperatures. This might be due to the chemical nature of tar volatiles. It was reported that tar from tyre and coal mainly consists of long-chain poly-aliphatic and poly-aromatic compounds (PAH), respectively [35]. It is reasonable that higher energy is needed to crack the long-chain stable moieties.

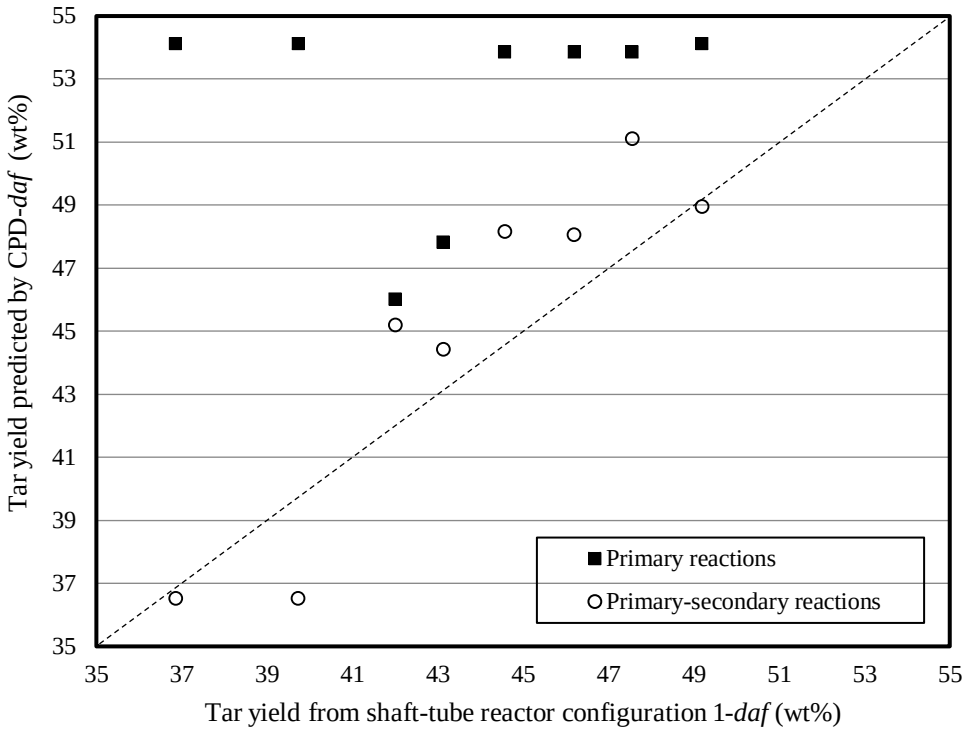

Figure 13 Comparison of tar yields between experimental results and CPD prediction for tyre in 6-15mm.

4.3.2 Effect of particle sizes on the secondary cracking reaction of tyre volatiles

To validate the accuracy of the M-CPD model which includes both heat transfer and the secondary cracking reactions of primary tar, the pyrolysis of another two tyre chip sizes were conducted using the reactor configuration 1 where the final temperature was fixed at 600 °C, via both slow and fast heating rates.

As presented in **Figure 14,** tar yield was found to decrease with increasing particle size for both heating schemes. For slow heating, one can see a slight decrease in the yield of tar by around 3 *wt% (daf)* upon the increase of size from 1 to 11 mm. The decrease was compensated by a slight increase on the gas fraction. A similar finding was reported by Barbooti et al. [36]

that less carbon black and more pyrolytic oil fraction were obtained for smaller particle sizes using a fixed-bed reactor at 400-460 °C in the slow heating scheme. This could be explained that smaller particle size provides more reaction surface for the char reduction [37].

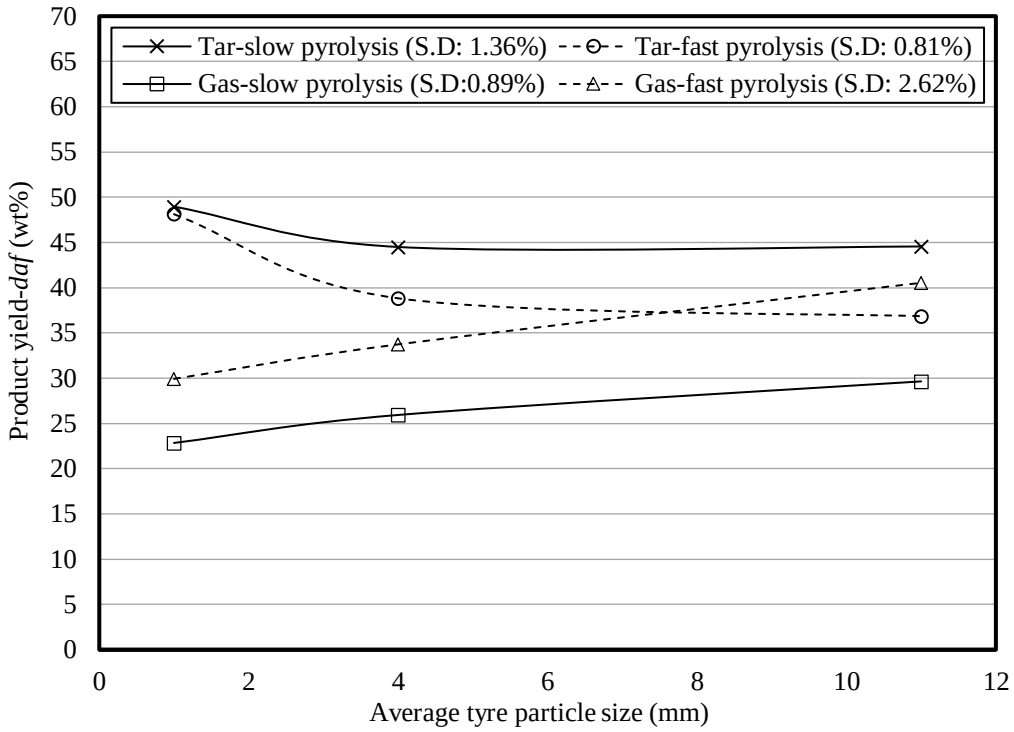

Figure 14 Experiment tar yields from different particle sizes of tyre at 600 °C in slow and fast heating schemes.

The influence of tyre size was more obvious in the fast heating scheme. As can be seen in **Figure 14,** upon the rise of the scrap tyre size from 1 to 11 mm, the tar yield was reduced remarkably by around 10 *wt%*, resulting in the rise of gas amount. Apparently, such an observed trend suggests that the secondary cracking reactions are preferred by increasing the scrap tyre feedstock size under the fast heating scheme. Considering that the cracking reactions were facilitated upon a fast heating rate (**Figure 11b and Figure 12**), it is hypothesised that the internal temperature gradient (*i.e.* temperature difference between primary tar inside the

tyre chip and reactor wall) for the released primary tarry species was further enlarged upon the increase on the scrap tyre size.

To prove this hypothesis, the temperature profiles of the three differently sized scrap tyre were predicted by the M-CPD model as well as plotted in **Figure 15** for both the slow and fast heating rates and heated to 600 °C. As expected, in the slow heating scheme, the temperature gap between the centre of a tyre particle and the reactor was relatively small, even for the particles as large as 11 mm. However, the fast heating scheme resulted in a noticeable delay in the heating of the largest size, and hence, enlarged temperature gap between the solid particle and the reactor wall. Consequently, the primarily released tarry species had to go through the largest temperature gap which facilitated their secondary cracking reactions. Besides, the internal diffusion resistance may also delay the internal release of the tar, thereby promoting the cracking reactions within the pores of the scrap tyre particle [38].

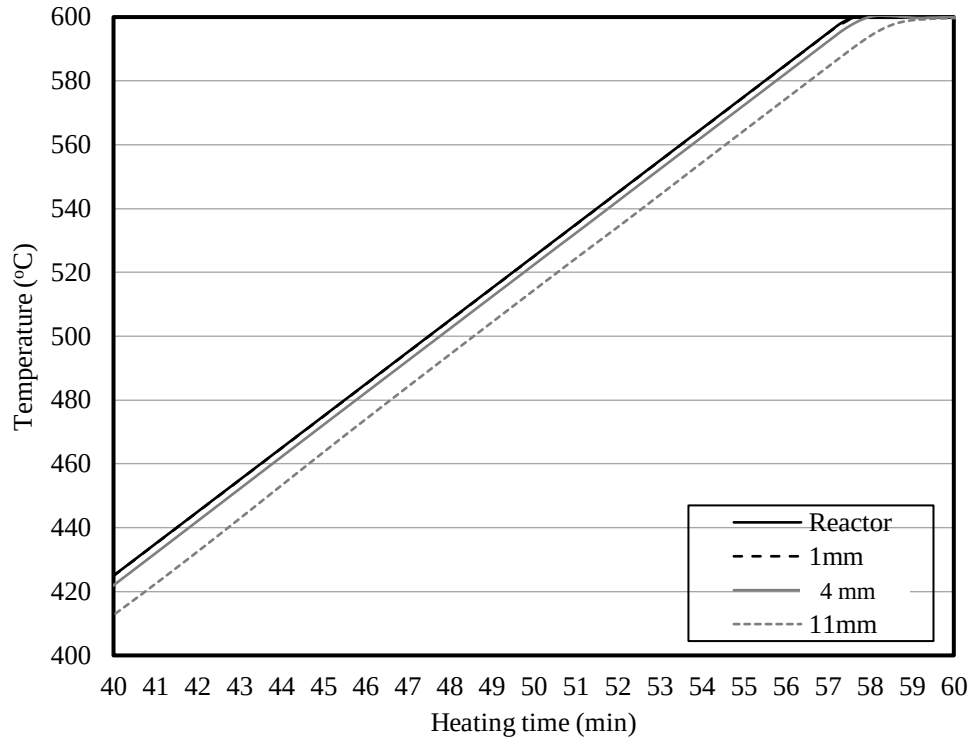

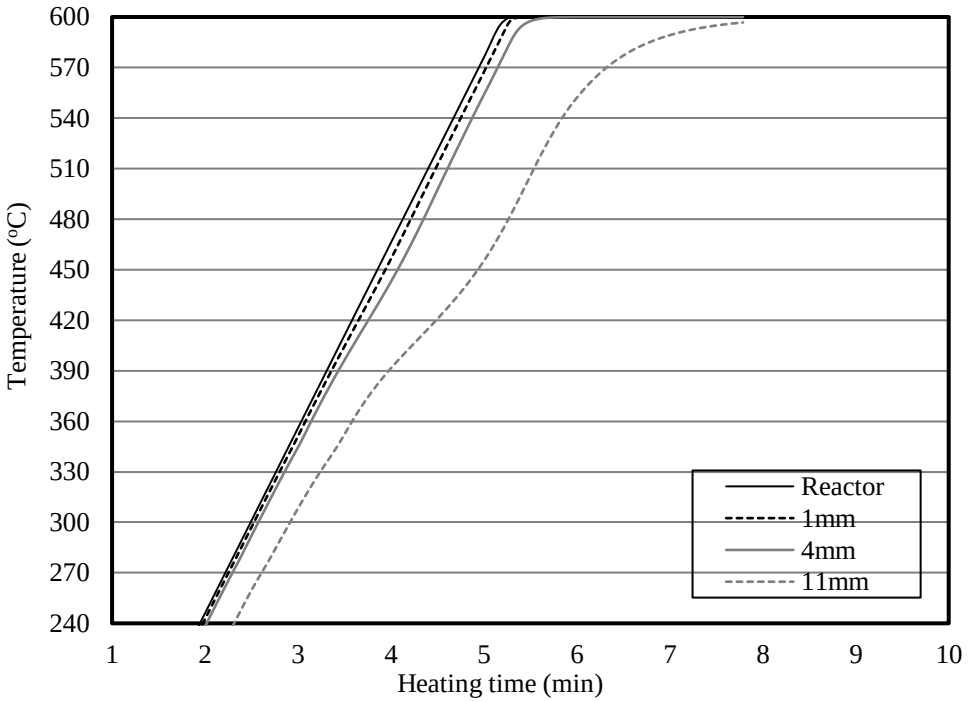

Figure 15 The predicted temperature profiles of the particles centre and the reactor in (a) slow pyrolysis; (b) fast pyrolysis.

Based on the temperature gap predicted in **Figure 15** and the secondary cracking kinetic parameters summarized in **Table 8**, effort was further made to predict and correlate the secondary cracking extent for each size under each heating rate with the respective temperature gap. The results were plotted in **Figure 16.** The temperature gap for each size under the fast heating rate was variable with the heating time, as evident in **Figure 15b**. Therefore, the average temperature gaps were calculated and used in **Figure 16**. It can be noticed that the cracking extent of volatiles was highly dependent on the temperature gap between the particle and reactor wall, raising asymptotically to 16.9 *wt%* when the predicted temperature gap reaches 115 °C obtained from large particle size and fast heating scheme. In contrast, the tar cracking extent was reduced to only 7.2 *wt%* when the temperature gap was insignificant for the smallest size under the slow heating rate.

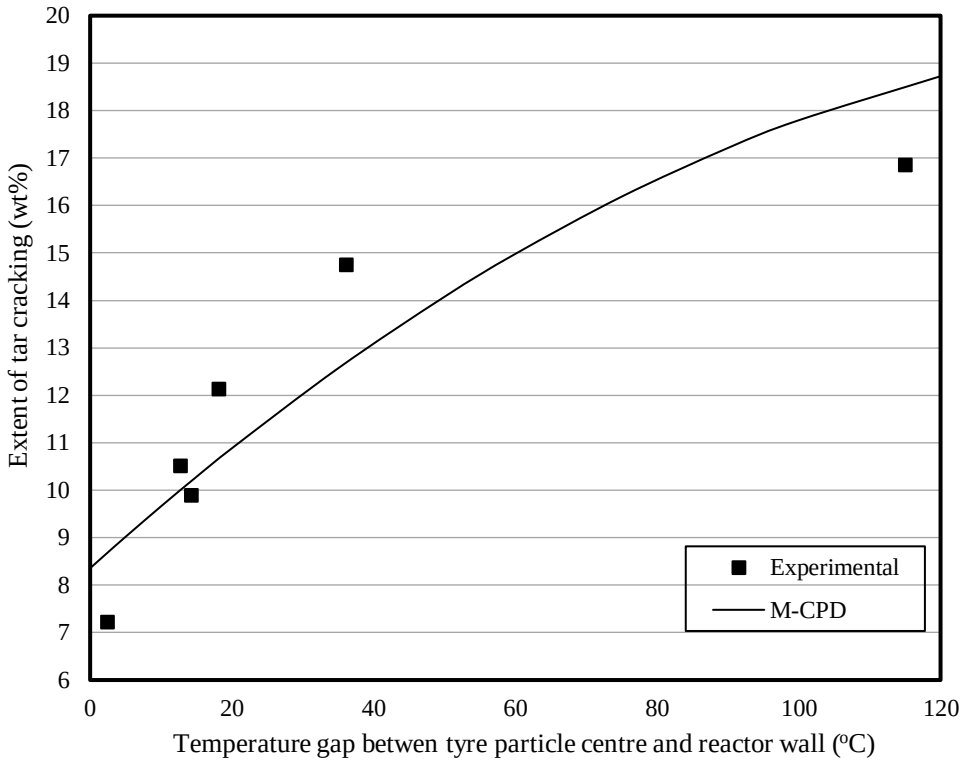

Figure 16 The relationship of the extent of tar cracking with the temperature gap of centre particle and reactor wall

4.3.3 Effect of carrier gas types and reactor configuration on the secondary cracking reactions

As mentioned previously, another option for the pyrolysis is direct heating in which a portion of the pyrolysis derived gas is sent back and burns inside the pyrolysis rig. The resultant hot flue gas was used as a heat carrier for the pyrolysis process. In light of this, the second configuration as shown in **Figure 4** was tested, through which the two major components CO_2 and steam in flue gas have been examined. To clarify the effect of CO_2, its fraction in argon balance was varied as 5, 10, 20, and 30% by volume. Similarly, as for the effect of steam, its proportion was also varied by the ratio of 10, 20, and 30% by volume, whilst both argon and CO_2 (15 *vol%*) were used as the balance gas. The total flowrate of gas mixtures was fixed at 0.8 L/min in the reactor configuration 2 where the gas mixture was fed continuously from the bottom of the reactor. The experiment was fixed at 600 °C at the slow heating rate (10 °C/min) with the use of the medium tyre chip size of 0.5-1.5 mm. Note that, only the slow heating rate was conducted here because the configuration 2 injecting the gas from the reactor bottom does not allow an injection of the whole reactor system inside a pre-heated furnace.

As shown in **Figure 17a**, the product yield for the presence of CO_2 in argon was almost unchanged, indicating that at the temperature of 600 °C tested CO_2 can be regarded as an inert gas and the carbon - CO_2 gasification reaction is insignificant, at least in terms of product yield. A similar conclusion can be drawn for the steam in **Figure 17b**, except there is a slight increment of light gas (1.68 *wt%*) at the expense of char. It is presumably due to the small

extent of char gasification and methanation of the resultant syngas. The observations were in line with the previous studies pointing that the product yield distribution was not varied upon the use of these two gases at 600 °C. Nevertheless, it was reported that lighter hydrocarbons and less long chain polymers obtained in the tar derived from steam as carrier gas compared to the tar from helium-experiment (Ogasawara et al., 1987). Also, less organic-sulphur compounds were noted in the analysis of tar composition with the use of steam during the pyrolysis of 600 °C. [33, 39]. All these will be further elucidated in a future study related to the tar properties.

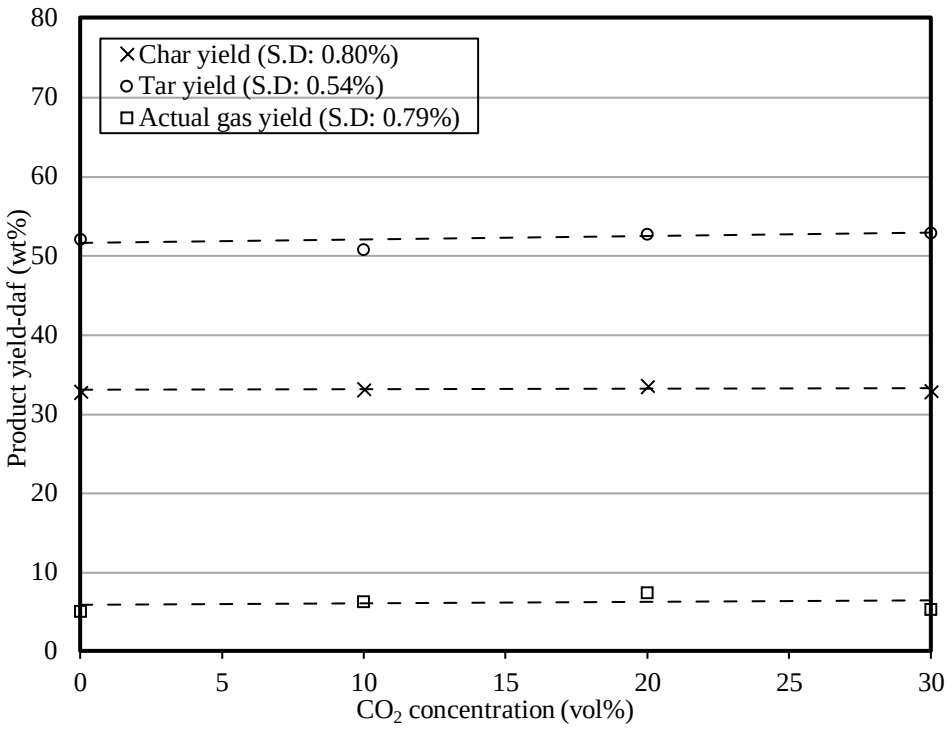

(a)

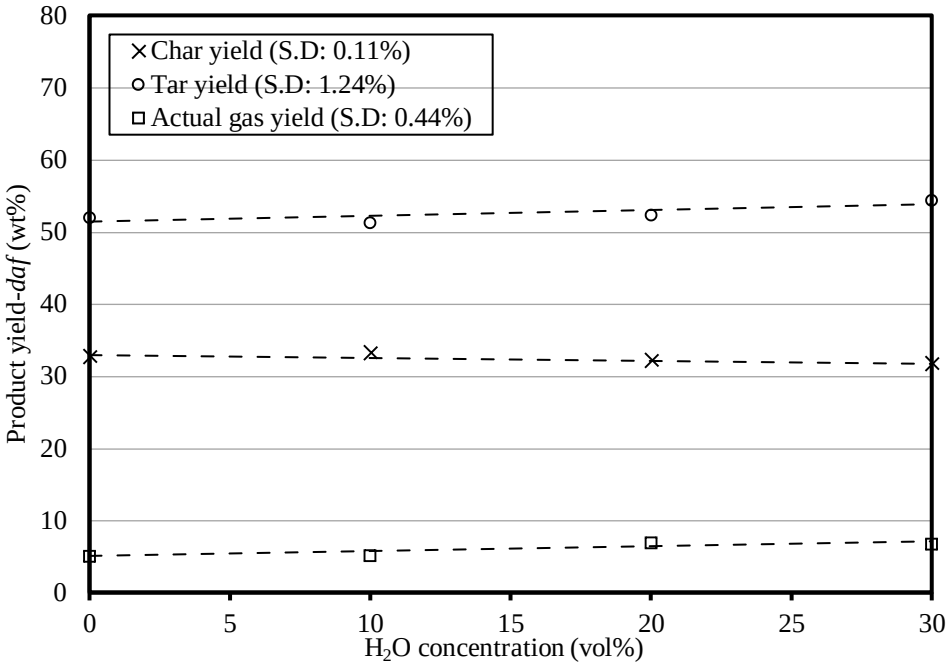

(b)

Figure 17. Experiment product yields for the experiment in which argon mixtures of (a) CO_2 and (b) H_2O (15 *vol%* of CO_2) are studied in fixed-bed reactor using configuration 2.

Regardless of the carrier gas type, it is, however, intriguing to see a rise in the tar yield up to 54 *wt%* (the maximum possible tar yield as confirmed by the TGA results in **Figure 8**) with the use of reactor configuration 2, as experimentally confirmed by varying argon flow rate and presented in **Figure 18**. Such a rise is considerable when compared to only around 48 *wt%* of tar derived from the use of reactor configuration 1 in slow pyrolysis. The rise in tar yield using the reactor configuration 2 was compensated by the drop of the gas yield, along with the slight reduction of char fraction. Such a change should be mainly attributed to the different tar cracking extent caused by the different residence time of volatiles. The injection of carrier gas from the bottom was beneficial in sweeping out the primary tar and gas quickly, thereby minimising the extent of their secondary reactions. Aylon et al. [40] found that the tar fraction was reduced significantly during tyre pyrolysis in the moving bed reactor compared to a fixed-

bed reactor. Besides, Dai et al. [37] evaluated the effect of residence time (1, 3 and 5 s) using circulating fluidized bed reactor and different feed positions. It was indicated that the fraction of light hydrocarbon components and methane were increased remarkably with the increment of volatile residence times. The secondary cracking reaction may explain the effect of residence time observed here.

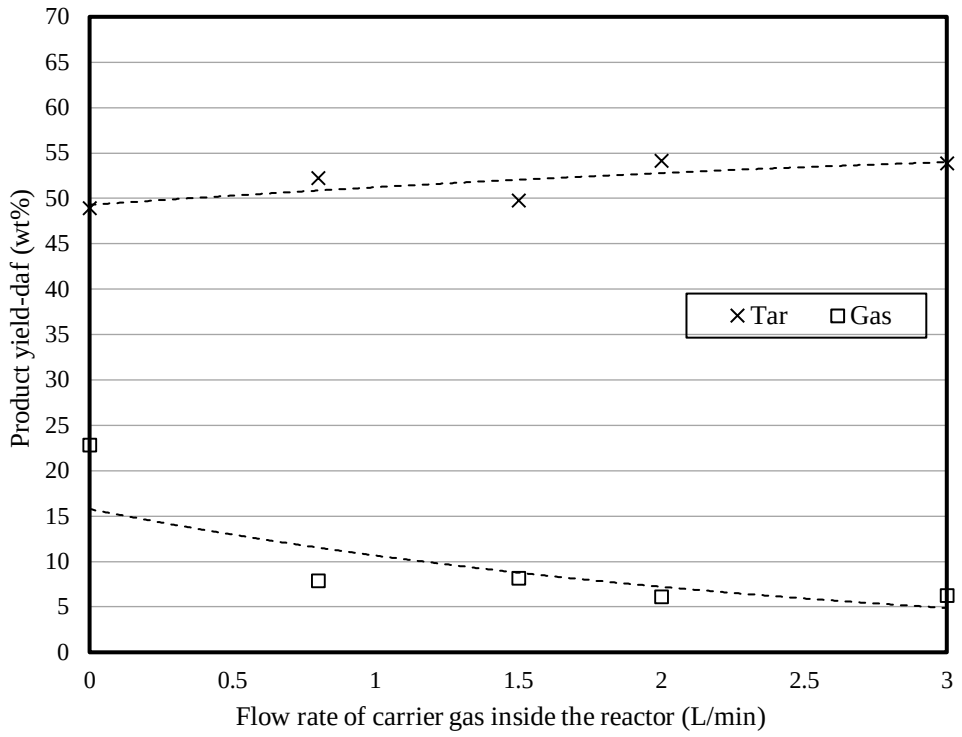

Figure 18. Experiment product yields from different reactor designs with argon as purging gas. The argon flow rate of zero refers to configuration 1 for the use of no argon in the bottom, while the other flow rates refers to configuration 2 injecting argon from the bottom of the reactor.

As witnessed in **Figure 19**, the tar cracking extent increased exponentially upon increasing the volatile residence time inside the reactor. By decreasing the residence time down to 50 s and less, the tar cracking extent can be minimised to a negligible level. In contrast, increasing the extent time to 300 s and above will considerably decrease tar yield by enhancing the tar

cracking extent up to 7 %. However, by comparing with **Figure 16**, the temperature gap caused by increasing tyre chip size and/or particle heating rate is more influential, causing a maximum possible cracking extent of ~17% of the total primary tar.

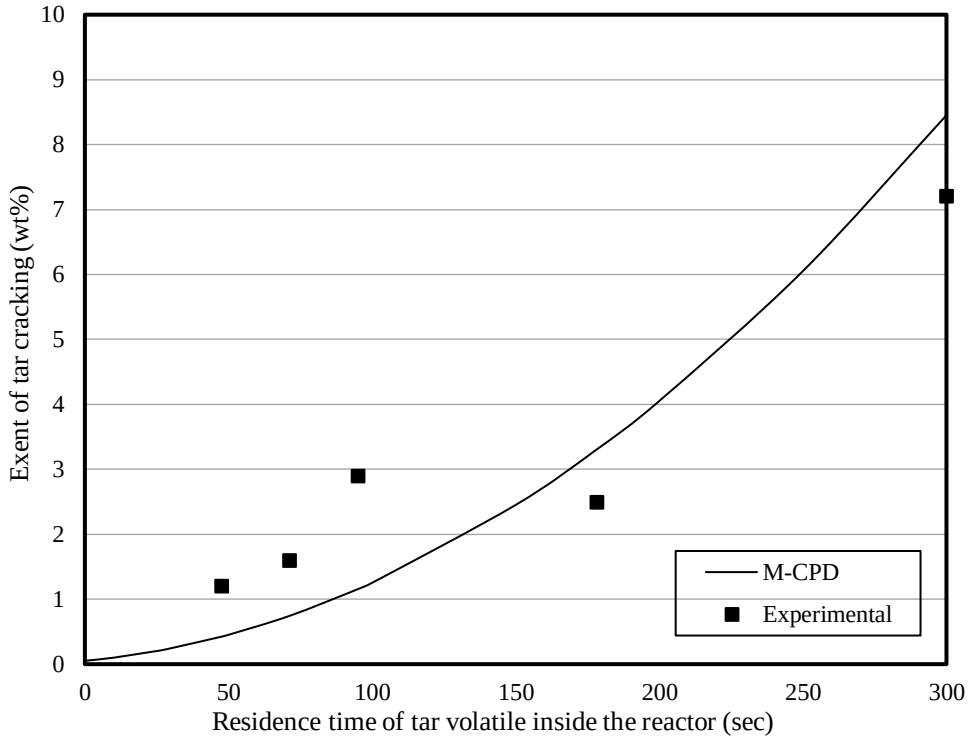

Figure 19 The relationship of the extent of tar cracking with the residence time of tar volatile inside the reactor

4.4 Conclusions

In this study, experimental investigation has been conducted to examine the pyrolysis behaviour of scrap tyre chip over a number of variables, including temperature, heating rate, carrier gas composition and flow rate, reactor configuration and chip size. In parallel, an M-CPD model, with the modification of two parameters; theoretical coordination number ($\sigma+1$) and molecular weight of side chain (MW_{side}) and the coupling of heat transfer and Secondary Cracking reaction into the original CPD model, has been successfully developed and validated

for scrap tyre pyrolysis. Attention was specifically paid to quantitatively clarify the structure of scrap tyre and the extent of its primary tar cracking. The scrap tyre pyrolysis commences at 250 °C and stabilises from 475 °C onwards in terms of volatile release. However, the secondary cracking reaction of tar was favoured from 600 °C onwards, particularly upon a fast heating scheme (~110 °C/min), increase on the chip size as well as the residence time for volatile vapour inside the reactor. A fast pyrolysis scheme results in a large temperature gap between the centre of a tyre chip and the reactor wall, noticeably resulting in the delay on the heating of the tyre chip and subsequently the release of volatiles. As the primarily released tarry species crosses a temperature gap up to 115 °C, it performances the secondary cracking with an extent of 17 %. At a pyrolysis temperature of 600 °C, the addition of CO_2 in carrier gas had an insignificant effect on the product yield distribution under the slow heating scheme. However, the addition of steam resulted in a slight increase of carbon monoxide, presumably due to the occurrence of gasification reaction. Additionally, the flow rate of carrier gas, as well as the residence time for volatiles inside the reactor is influential in the cracking extent of tar, which is noticeable in the case that the residence time is sufficiently long. At a residence time of ~300 s, the minimum cracking extent reaches around 7%, even under a slow heating mode.

4.5 Acknowledgements

This work was supported by Australian Research Council (ARC) under its Industrial Research Training Hub (150100006) scheme for the joint project between Monash and Coal Energy Australia. The scrap tyre char provided by the Tyrecycle Pty Ltd, Australia is also acknowledged.

4.6 References

1. Lopez, G., et al., *Waste truck-tyre processing by flash pyrolysis in a conical spouted bed reactor.* Energy Conversion and Management, 2017. **142**(Supplement C): p. 523-532.
2. Emma Mountjoy, D.H., Tom Freeman, *STOCKS & FATE OF END OF LIFE TYRES - 2013-14 STUDY*. 2012, Hyder Consulting Pty Ltd.
3. Purcell, A.H., *Tire recyling: Research trends and needs.* Conservation & Recycling, 1978. **2**(2): p. 137-143.
4. Shulman, V.L., *Chapter 21 - Tyre Recycling A2 - Letcher, Trevor M*, in *Waste*, D.A. Vallero, Editor. 2011, Academic Press: Boston. p. 297-320.
5. Leung, D.Y.C. and C.L. Wang, *Kinetic study of scrap tyre pyrolysis and combustion.* Journal of Analytical and Applied Pyrolysis, 1998. **45**(2): p. 153-169.
6. Martínez, J.D., et al., *Waste tyre pyrolysis – A review.* Renewable and Sustainable Energy Reviews, 2013. **23**(Supplement C): p. 179-213.
7. Quek, A. and R. Balasubramanian, *Mathematical modeling of rubber tire pyrolysis.* Journal of Analytical and Applied Pyrolysis, 2012. **95**(Supplement C): p. 1-13.
8. Zabaniotou, A., et al., *Energetic Utilization of Used Tires.* Energy Sources, 2002. **24**(9): p. 843-854.
9. Gupte, S.L. and G. Madras, *Catalytic degradation of polybutadiene.* Polymer Degradation and Stability, 2004. **86**(3): p. 529-533.
10. Unapumnuk, K., et al., *Pyrolysis Behavior of Tire-Derived Fuels at Different Temperatures and Heating Rates*. Vol. 56. 2006. 618-27.
11. Aguado, R., et al., *Kinetics of scrap tyre pyrolysis under fast heating conditions.* Journal of Analytical and Applied Pyrolysis, 2005. **73**(2): p. 290-298.
12. Seidelt, S., M. Müller-Hagedorn, and H. Bockhorn, *Description of tire pyrolysis by thermal degradation behaviour of main components.* Journal of Analytical and Applied Pyrolysis, 2006. **75**(1): p. 11-18.
13. Lah, B., D. Klinar, and B. Likozar, *Pyrolysis of natural, butadiene, styrene–butadiene rubber and tyre components: Modelling kinetics and transport phenomena at different heating rates and formulations.* Chemical Engineering Science, 2013. **87**: p. 1-13.
14. Cheung, K.-Y., et al., *Integrated kinetics and heat flow modelling to optimise waste tyre pyrolysis at different heating rates.* Fuel Processing Technology, 2011. **92**(5): p. 856-863.

15. Olazar, M., et al., *Kinetic modelling of tyre pyrolysis in a conical spouted bed reactor.* Journal of Analytical and Applied Pyrolysis, 2008. **81**(1): p. 127-132.
16. Narobe, M., et al., *Co-gasification of biomass and plastics: Pyrolysis kinetics studies, experiments on 100kW dual fluidized bed pilot plant and development of thermodynamic equilibrium model and balances.* Bioresource Technology, 2014. **162**: p. 21-29.
17. Fletcher, T.H., et al., *Chemical percolation model for devolatilization. 3. Direct use of carbon-13 NMR data to predict effects of coal type.* Energy & Fuels, 1992. **6**(4): p. 414-431.
18. De Girolamo, A., et al., *Pyrolysis of a lignite briquette – Experimental investigation and 1-dimensional modelling approach.* Fuel, 2018. **212**(Supplement C): p. 533-545.
19. Navarro, M.V., et al., *Application of a particle model to pyrolysis. Comparison of different feedstock: Plastic, tyre, coal and biomass.* Fuel Processing Technology, 2012. **103**(Supplement C): p. 1-8.
20. Garcia-Nunez, J.A., et al., *Historical Developments of Pyrolysis Reactors: A Review.* Energy & Fuels, 2017. **31**(6): p. 5751-5775.
21. Solum, M.S., et al., *13C NMR Analysis of Soot Produced from Model Compounds and a Coal.* Energy & Fuels, 2001. **15**(4): p. 961-971.
22. Kelemen, S.R., et al., *Direct Characterization of Kerogen by X-ray and Solid-State 13C Nuclear Magnetic Resonance Methods.* Energy & Fuels, 2007. **21**(3): p. 1548-1561.
23. Fletcher, T.H., et al., *Prediction of Tar and Light Gas during Pyrolysis of Black Liquor and Biomass.* Energy & Fuels, 2012. **26**(6): p. 3381-3387.
24. Yan, B., et al., *Generalized Model of Heat Transfer and Volatiles Evolution Inside Particles for Coal Devolatilization*. Vol. 60. 2014.
25. Yan, B., et al., *Generalized model of heat transfer and volatiles evolution inside particles for coal devolatilization.* AIChE Journal, 2014. **60**(8): p. 2893-2906.
26. Sheng, C. and J.L.T. Azevedo, *Modeling biomass devolatilization using the chemical percolation devolatilization model for the main components.* Proceedings of the Combustion Institute, 2002. **29**(1): p. 407-414.
27. Fletcher, T.H., D. Barfuss, and R.J. Pugmire, *Modeling Light Gas and Tar Yields from Pyrolysis of Green River Oil Shale Demineralized Kerogen Using the Chemical Percolation Devolatilization Model.* Energy & Fuels, 2015. **29**(8): p. 4921-4926.

28. Senneca, O., P. Salatino, and R. Chirone, *A fast heating-rate thermogravimetric study of the pyrolysis of scrap tyres.* Fuel, 1999. **78**(13): p. 1575-1581.
29. Williams, P.T. and D.T. Taylor, *Aromatization of tyre pyrolysis oil to yield polycyclic aromatic hydrocarbons.* Fuel, 1993. **72**(11): p. 1469-1474.
30. Li, S.Q., et al., *Pilot-Scale Pyrolysis of Scrap Tires in a Continuous Rotary Kiln Reactor.* Industrial & Engineering Chemistry Research, 2004. **43**(17): p. 5133-5145.
31. Williams, P.T., S. Besler, and D.T. Taylor, *The pyrolysis of scrap automotive tyres: The influence of temperature and heating rate on product composition.* Fuel, 1990. **69**(12): p. 1474-1482.
32. Williams, P.T., *Pyrolysis of waste tyres: A review.* Waste Management, 2013. **33**(8): p. 1714-1728.
33. Kaminsky, W., C. Mennerich, and Z. Zhang, *Feedstock recycling of synthetic and natural rubber by pyrolysis in a fluidized bed.* Journal of Analytical and Applied Pyrolysis, 2009. **85**(1): p. 334-337.
34. Yan, B., Y. Cheng, and Y. Jin, *Cross-Scale Modeling and Simulation of Coal Pyrolysis to Acetylene in Hydrogen Plasma Reactors.* AIChE Journal, 2013. **59**(6): p. 2119-2133.
35. Cunliffe, A.M. and P.T. Williams, *Composition of oils derived from the batch pyrolysis of tyres.* Journal of Analytical and Applied Pyrolysis, 1998. **44**(2): p. 131-152.
36. Barbooti, M.M., et al., *Optimization of pyrolysis conditions of scrap tires under inert gas atmosphere.* Journal of Analytical and Applied Pyrolysis, 2004. **72**(1): p. 165-170.
37. Dai, X., et al., *Pyrolysis of waste tires in a circulating fluidized-bed reactor.* Energy, 2001. **26**(4): p. 385-399.
38. Yang, J., P.A. Tanguy, and C. Roy, *Heat transfer, mass transfer and kinetics study of the vacuum pyrolysis of a large used tire particle.* Chemical Engineering Science, 1995. **50**(12): p. 1909-1922.
39. Ogasawara, S., M. Kuroda, and N. Wakao, *Preparation of activated carbon by thermal decomposition of used automotive tires.* Industrial & Engineering Chemistry Research, 1987. **26**(12): p. 2552-2556.
40. Aylón, E., et al., *Waste Tire Pyrolysis: Comparison between Fixed Bed Reactor and Moving Bed Reactor.* Industrial & Engineering Chemistry Research, 2008. **47**(12): p. 4029-4033.

This page is intentionally left blank

Chapter 5- Secondary Reactions of Volatiles upon the Influences of Particle Temperature Discrepancy and Gas Environment during the Pyrolysis of Scrap Tyre Chips

In Chapter 4, it was learnt that upon the fast heating (110°C/min) and terminal temperature of 600°C in a non-carrier gas fixed bed reactor, the average temperature gap (or discrepancy) between the centres of the coarse particle and reactor wall reached a maximum of 115 °C for the tyre chips of 6-15 mm. As a result, the primary volatiles underwent severe *secondary cracking reaction* with an overall loss of tar (and gain of light gas) by 17 *wt%*. In this work, the reactions of 'secondary-cracking' will be justified and explained in detail through the investigation of the molecular footprints of tars generated from various operating conditions including heating rate, volatile residence time, tyre particle size and non-inert gases (CO_2 and/or H_2O). This chapter has been reviewed as a manuscript by Fuel journal with minor revision.

Abstract

Pyrolysis process is one of the potential routes to convert waste scrap tyre into high-value resources such as liquid oil that is low in oxygen and high in valuable hydrocarbons. Although many studies have been conducted, the understanding of the fundamental science underpinning the pyrolysis of scrap tyre chip is still far from complete. This paper has examined the mild pyrolysis of scrap tyre chips at 600^{o}C, in an integrated manner by examining the co-effects of several key parameters including heating rate, volatile residence time, tyre chip size and non-inert gases (CO_2 and/or H_2O) on the quality of tars. In particular, we aimed to elucidate the influences of particle temperature discrepancy (to the surrounding gas environment) and reactive gas on the tar yield and properties, under the simulated fixed-bed/rotary kiln that is either heated directly by hot flue gas or indirectly by reactor wall. It has been confirmed that, in a simulated fixed-bed reactor with the absence of carrier gas, the particle temperature discrepancy can be correlated exponentially to the secondary cracking extent of the volatiles within a temperature discrepancy range of 100^{o}C. Upon an increase on the temperature discrepancy by either increasing the heating rate or tyre chip size, the inherent long-chain aliphatics preferentially underwent scission, cyclisation and polymerisation, enhancing the yields for both heavy aromatics and methane - rich light gases. The use of carrier gas is beneficial in improving the tar yield and aliphaticity. As a convective heating source, it heated particles slowly and also swept out the volatile vapours immediately, thereby minimising the secondary reactions. For the two major components, CO_2 and steam in hot flue gas, CO_2 is rather inert at 600^{o}C, while steam is reactive enough to further reduce the heavy hydrocarbons via steam reforming reaction, upon the catalytic effect of the nascent char derived from scrap tyre chips. The hydrogenation of unsaturated alkene and aromatics was also improved, and even the methanation reaction of CO on the nascent char surface, thus leading to the overwhelming dominance of CH_4 in the pyrolysis gas.

Keywords:

Scrap Tyre Chip Pyrolysis, Particle Temperature Discrepancy, Reactive Flue Gas, Secondary Reactions of Volatiles.

5.1 Introduction

The disposal of waste tyre is a global concern. Approximately 800 million used tyre is dumped annually, with a projected growth rate of 2% [1]. The traditional methods including stockpiling, illegal dumping or landfilling are only short-term solutions creating secondary hazards to the environment. In contrast, there is a renewed interest in the research and development of alternative technologies for recycling waste tyre [2]. Among these technologies, pyrolysis has been receiving increased attention, owing to its simplicity, cost-effectiveness and remarkable efficiency in transforming waste into energy. To date, a large amount of research has been conducted, as summarized in **Table 9**Table 1. However, the pyrolysis of tyre is still far from commercialisation. One major concern is the large number of polyaromatics (*e.g.* up to 20 *wt%*) within its liquid tar, which is prone to form heavy matters such as coke and asphaltene in the cooling stage [2]. In addition, for the liquid tar to be used as a fuel substitute, the abundance of polyaromatics is also associated with emission of air pollutants [3], which is of environmental concern.

From the scientific research perspective, most of the research in **Table 9** was conducted in slow heating of 5-10^{o}C/min [4-15], with some exceptions on the use of faster heating of 20-80^{o}C/min [3, 16, 17] and two cases using 200-300^{o}C/min [18, 19]. A broad range of different sizes of tyre chips have been tested, whilst the volatile residence time was limited to a maximum few minutes, mainly due to the employment of micro-scale pyro-probe and bench-scale fixed-bed reactors. With regards to the tar quality, it is unambiguous that the primary devolatilization of the scrap tyre completes at 550 - 600°C. At such temperatures, a broad variety of secondary reactions are also proposed to proceed, such as self-scission, hydrogenation, cyclisation (also known as Diel-alders), aromatisation, polymerisation and coking. In terms of the heating rate, it has been believed that slow pyrolysis is beneficial to minimise the aforementioned secondary

reactions, thereby increasing the tar yield remarkably [20]. The same argument also holds for the slow pyrolysis of coal [21]. However, as discussed intensively in a review study on coal pyrolysis [21], due to the low productivity of slow pyrolysis, the fast/flash pyrolysis has been trialled at different scales, with an ultimate goal for commercialisation. This however leads to a reduced yield for the overall tar, with a poor quality that easily plugs the volatile product line. It is mainly attributed to the widened temperature discrepancy between coal particle and the surrounding environment, namely temperature increase (TI) in the review paper [21]. The released volatile vapours are thus to experience a thermal shock leading to severe cracking and agglomeration consequently. For instance, for a hot fixed bed operating at 1100^{o}C, the coal particles fed into the reactor are rapidly heated in 12 seconds. This, in turn, reduced the overall tar yield down to only 3-4.5 *wt%*. The resultant tar was also highly viscous, consisting of 50-60 *wt%* pitch and <10 *wt%* particulates [22, 23]. However, it is unclear if this observation can be extended to the pyrolysis of scrap tyre chips. In particular, a quantitative measure has yet to be developed to correlate the particle temperature discrepancy and the secondary reaction extent for the volatiles derived from scrap tyre.

Another critical factor affecting the pyrolysis of solid fuel is the gas environment inside a furnace. In an indirectly or externally heated furnace, the furnace wall provides a fast heating for the tyre chips close to it, while the absence of carrier gas means that the volatiles released have to diffuse out on its own pressure, thereby exhibiting a relatively long residence time inside the hot furnace [24]. Alternatively, the hot flue gas from the combustion of pyrolysis gas can be fed inside the furnace to internally heat the tyre chips, which in the meanwhile to sweep out the volatile vapours quickly. This is the case for a commercial vertical Lurgi retort where the particles can enter the retort on the top and are directly heated by the hot gas generated from the upper burner [4]. It can also be achieved by a direct, counter-current injection of hot

flue gas to heat the solid particles inside a rotary kiln. To date, only a few studies have taken this factor into account for the gasification of scrap tyre under harsh conditions such as the temperatures >760^{o}C [25-27]. It is still unknown how the injection of flue gas affects the yield and properties of liquid tar, in particular at the mild temperatures of 550-600^{o}C where the tar yield is maximised.

This study aims to close the knowledge gap underpinning the influences of particle temperature discrepancy and gas environment. Upon the employment of a bench-scale fixed bed, a total of eleven different scenarios for the pyrolysis of scrap tyre chips have been conducted, by varying particle heating rate, chip size and the gas environment. The resultant liquid tar samples were characterised by several advanced instruments, including ^{1}H-NMR (Proton- nuclear magnetic resonance), FT-IR (Fourier-transform infrared spectroscopy) and GC-MS (Gas Chromatography-Mass Spectrometry). Solvent fractionation was also employed to fractionate each tar sample. Based on the results, the secondary reactions for volatile vapours were specified, and the overall cracking extents were also correlated with the particle temperature discrepancy to the surrounding environment. In addition, to examine whether or not the nascent solid char plays a catalytic role on the probable steam reforming of volatile vapours, a two-stage fixed-bed reactor was designed allowing the volatile vapours to pass through a separate bed where the nascent char wad loaded. To date, the *in-situ* char-volatile interaction has been confirmed for low-rank coal and biomass [28], which is however still unknown for scrap tyre. The results achieved by us are expected to provide some advanced insights into the secondary reactions underpinning the transformation of volatile vapours, and hence, to optimise both yield and properties of the liquid tar derived from scrap tyre, an otherwise low-value waste.

Table 9 Literature survey on the studies related to the yields, composition and properties of tyre derived tars at temperatures of 450-800°C

Heating rate (^oC/min)	Volatile residence time (min)	Particle size range (mm)	Reactor	Carrier gas type	Conclusive observation	Study
5, 20, 40, 80	1.8	14-22	Fixed-bed	N_2	The largest yield of tyre tar (55 *wt%*) was obtained at the temperature of 600°C. When the heating rate was increased from 5 to 80°C/min, the molecular mass range of the tars notably increased.	[16]
5, 20, 60	2.5	10-17	Fixed-bed	N_2	A significant increase (~600 ppm) of benzothiophenes (sulphur-polyaromatics) was noticed as the heating rate was increased from 5 to 60^{o}C/min at 550^{o}C.	[3]
5	2.0	15-30	Fixed-bed	N_2	The tars from 600°C contained a high concentration (2 *wt%*) of biologically active polyaromatics such as fluorene, phenanthrene and chrysene.	[4]
200	1.8	3	Pyro-probe	N_2	As the final temperature was increased from 450 to 550°C in 200^{o}C/min, a 7 *wt%* of tyre tar was lost, corresponding to the increment of light gas.	[18]
5, 20	9.0	0.2-1.6	Fixed-bed	N_2	A maximum of tyre yields was obtained at the temperature of 575°C in both heating rates. Further increasing the temperature resulted in the production of light gases due to strong cracking of tyre volatiles.	[17]

15	0.9	20-30	Pyro-probe	N_2	The tyre tars consisted of 10 *wt%* of the heavy tar fraction which has a boiling point of larger than 370°C.	[13]
10	7.7	-	Fixed-bed	N_2	The yields of tar and element sulphur were increased by 8.0 and 0.3 *wt%* as the temperature was increased from 350 to 550°C.	[8]
10	1.5	25-30	Fixed-bed	N_2	The tars from seven different brands of tyre showed very similar compositional properties.	[12]
12	2.4	20	Pyro-probe	N_2	A maximum of tyre yields was obtained at the temperature of 550°C and above.	[6]
300	0.8	2-5	Pyro-probe	N_2	A maximum of tyre yields was obtained at the temperature of 500°C and above in 300°C/min.	[19]
10	0.5	0.25	Pyro-probe	N_2	The concentration of single-aromatic hydrocarbons including styrene, toluene and ethylbenzene in the tars reached 120, 20 and 5 ppm at 500°C.	[11]
10	4.0	2	Fixed-bed	N_2	The tyre tars consisted of the hydrocarbons in the carbon number of 5-15 predominantly in the form of aromatics.	[9]
5, 35	2.2	1-4	Fixed-bed	N_2	No significant influence of the heating rates of 5 and 35°C/min on the physiochemical properties of the tyre tars. The fuel properties of the tars were similar to those of the commercial diesel in terms of the heating value, density and viscosity, except for sulphur content.	[5]
10	1.1	1-2	Fixed-bed	N_2	The tars from 500 to 800°C mainly consisted of limonene, xylene and sulphuric hydrocarbons such as benzothiazole which accounted for 0.9 *wt%*.	[7]

20	<2.0	10-30	Fixed-bed	N_2	Major identified hydrocarbons in the tars derived from light, medium and heavy vehicle tyre at the temperatures of 500-700°C predominantly contained benzene, toluene, xylene, *dl*-limonene and double-ring aromatics.	[10]
5, 15, 25	1.0	0.6-0.8, 2.8-3.4	Pyro-probe	N_2	Increasing the heating rates between 5 and 25°C/min led to a decrease of tar fraction due to the secondary cracking reaction of tyre volatiles.	[14]
Slow	9.8	5-6	Rotary Kiln	N_2	The tars generated from the temperature of 550°C in slow heating condition contained 47 *wt%* of heavy matters whose boiling point is larger than 200 °C.	[15]

Average volatile residence time is calculated based on the reactor dimension and the flow rate of purging gas/ volatiles (min)

5.2 Material and methods

5.2.1 Properties of the scrap tyre feedstock

The size of scrap tyre chips collected from Tyrecycle Company (Australia) was screened to 0.5-1.5, 4-6 and 6-15 *mm*. The steels and wires have been removed before received. The proximate and ultimate analyses of the tyre chips are displayed in **Table 4** in our previous chapter [29]. The total of fixed carbon and ash account for 33- 34 *wt%* while the volatile matter is around 66- 68 *wt%* on dry-and-ash free basis. As for the ultimate analysis, the content of elemental sulphur (S) is relatively high (~2 *wt%*), believing due to the introduction of organic sulphur (S) during the vulcanisation process [20].

5.2.2 Pyrolysis conditions

All pyrolysis experiments were carried out in a lab-scale fixed-bed with five different reactor configurations illustrated in **Figure 20**, with the experimental conditions detailed in **Table 10**. As for the first reactor configuration designed for the reference Scenario 1, pre-heated argon was employed as the purging gas and fed continuously (~0.8 L/min) through the tyre chip bed that was heated up with the reactor together, at a low heating rate of 10^{o}C/min and a small size of 0.5-1.5 *mm* for the tyre chip. The primary volatiles were swept away quickly once being released out, thus bearing the shortest residence time and least extent for secondary cracking [4, 21]. As for the second reactor configuration, argon was only purged from the top of the reactor to avoid the condensation of volatiles in the connecting tubes. The released volatiles in the bottom of the reactor had to flow out on their own pressure, resulting in a larger volatile residence time of 6-7 min. For this configuration, two different heating rates were employed, 10 and 110^{o}C/min. The former heating rate was achieved by temperature-programmed heating of the tyre chip-laden reactor, whilst the latter one was achieved by quickly injecting the tyre

chip-laden reactor into a pre-heated furnace. Its heating rate was estimated based on the measurement of the temperature inside the reactor. This configuration was employed for six scenarios ranging from Scenario 2 through to Scenario 7 in **Table 10**. Scenarios 2 - 4 employed a lower heating rate for three different tyre chip size varying from 0.5-1.5 to 4-6 and 6-15 *mm*, whilst Scenarios 5-7 employed a larger heating rate for the three same sizes.

As for the first and third reactor configurations, carrier gas (argon or a mixture of argon with steam and/or CO_2) was purged directly from the bottom of the reactor, the same as scenario 1. The heating rate of this reactor configuration was also fixed at 10^oC/min. For the third configuration, the tyre chips were placed at the bottom of the reactor while the carrier gas was changed from pure argon (Scenario 1) to argon with 30% CO_2 (Scenario 8) and argon with 30% CO_2 and 15% H_2O (Scenario 9). These three scenarios were tested to evaluate the influence of the gas environment inside the reactor. Note that, the fractions of CO_2 and steam used here are close to the real flue gas derived from a combustion process. Regarding the fourth configuration, the steam-argon mixture other than pure argon was employed as the purging gas to continuously feed onto the top of the reactor. The steam injected was only expected to encounter the upward flowing volatiles, and hence, this design is able to investigate the homogeneous interaction between steam and volatiles *without* the interference of tyre char. Scenario 10 employed such a confirmation.

For the fifth reactor configuration, an additional quartz frit was mounted above the tyre chip bed, where approximately 30-60 *gram* of tyre char (relative to 30 *gram* of tyre chips used for pyrolysis) was placed. Such a design was used for Scenario 11 to evaluate if the solid char is able to catalyse the homogeneous reaction of volatiles with steam/CO_2.

Approximately 30 *gram* of tyre chips were tested each run, and the terminal temperature was fixed at 600°C, which has been proven to drive out all the volatiles within the tyre chips [29]. The reactor was held for 30 *min* once reaching 600ºC to ensure a complete release of all the volatiles.

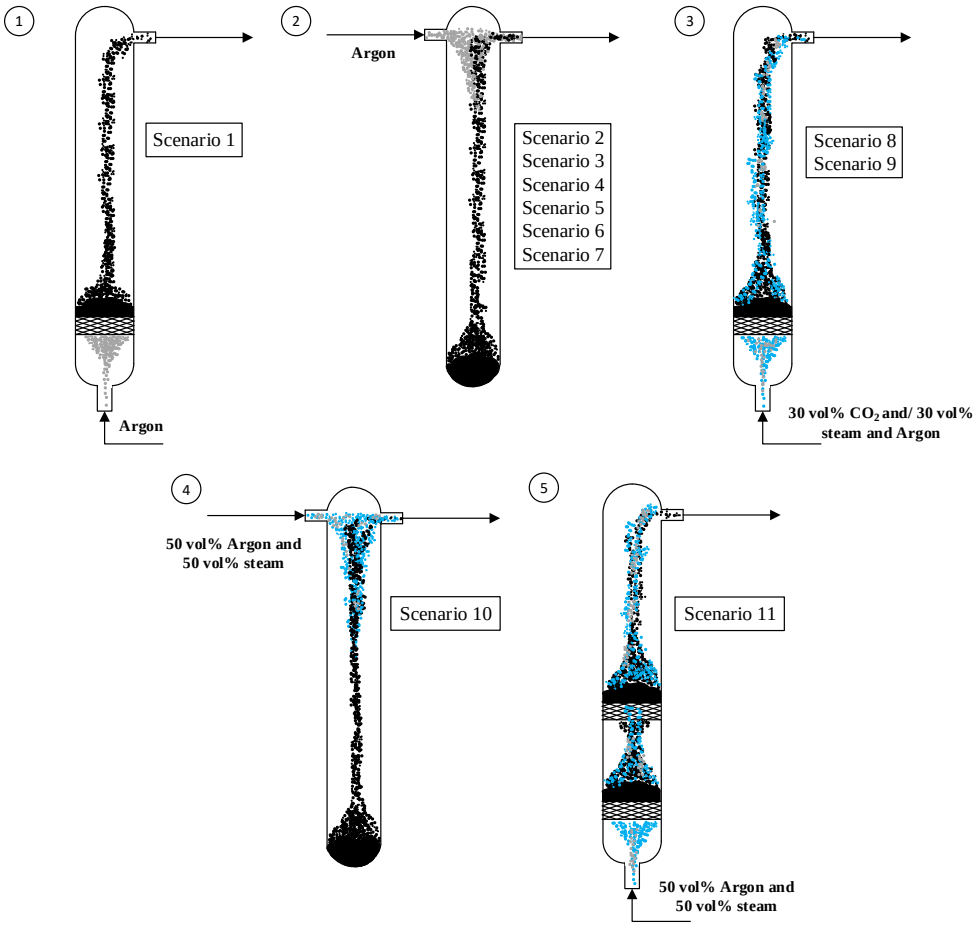

Figure 20 Schematic reactor configurations for 11 different scenarios.

Table 10 Experiment parameters of the eleven scenarios examined in this study.

Specification	Scenario 1	Scenario 2	Scenario 3	Scenario 4	Scenario 5	Scenario 6	Scenario 7	Scenario 8	Scenario 9	Scenario 10	Scenario 11
Reactor configurations	1	2	2	2	2	2	2	3	3	4	5
Material	Tyre chip only										Tyre-tyre char
Feedstock weight	Approximately 30 g										30 g tyre chip + 30-60 g char
Particle size	0.5-1.5 mm	0.5-1.5 mm	4-6 mm	6-15 mm	0.5-1.5 mm	4-6 mm	6-15 mm	0.5-1.5 mm	0.5-1.5 mm	0.5-1.5 mm	0.5-1.5 mm
heating rate	10 ˚C/min				110 ˚C/min			10 ˚C/min			
Averaged volatile residence time	45 s	~6.3-6.9 min						~45 s			

Carrier gas	Argon							30 *vol%* CO_2	30 *vol%* CO_2 (15 *vol%* H_2O)	50 *vol%* H_2O	50 *vol%* H_2O
Features	slow heating and short residence time	slow heating and long residence time	slow heating, long residence time and medium particle size	slow heating, long residence time and large particle size	fast heating and long residence time	fast heating, long residence time and medium size	fast heating, long residence time and large size	CO_2, slow heating and short residence time	Steam, slow heating and short residence time	steam-volatile, slow heating and long residence time	Char – catalysis, slow heating and short residence time
Particle Temperature Discrepancy	<2 °C	2 °C	13 °C	16 °C	26 °C	44°C	90 °C	<2 °C	<2 °C	<2 °C	<2 °C

5.2.3 Product characterisation

Elemental composition of the tar samples was determined using a CHNS Elementary Vario EL III. The chemical compositions of tars were identified by gas chromatography-mass spectrometer (GC-MS) on an HP6890 instrument in a splitless auto mode. Helium was used as the carrier gas at a flow rate of 1 mL/min. For GC analysis, the capillary column used is HP 19091S-433 (HP-5MS with 5% phenylmethyl siloxane) with a dimension of 30 *m* long, 0.25 *mm* inner diameter, and 0.25 μm nominal film thickness. The GC oven temperature was initially held at 50°C for 2 min, then heated to 200°C at 4°C/min and on hold for another 2 min. Finally, the oven was raised to 300°C at 8°C/min and on hold for 3 min. MS was operated in electron ionisation (EI) mode at 70 eV; the mass ratio scanning range is from 45-600 m/z; the accelerating voltage is 1.9 kV and the ion source is at a temperature range of 200-250°C. The chromatographic peaks were identified by using the Agilent MSD Chemstation software.

The ^{1}H-NMR spectrum of tyre tars were obtained at an H frequency of 400 MHz with a 90^{o} pulse flip angle using a Bruker AVANCE instrument. The samples were dissolved in deuterated chloroform as an internal standard. The solid-state ^{13}C-NMR spectra for the raw tyre was determined using a Bruker 400 (^{1}H)/100 (^{13}C) MHz spectrometer with cross polarisation-magic angle spinning (CP/MAS). The acquisition time was 1000 min with 20000 scans averaged and a repetition time of 3.0 s, a sample spinning rate of 30 kHz. All spectra from ^{1}H and ^{13}C-NMR were integrated based on the standard chemical shift ranges using the Topspin7.0 software.

The functional group analysis of the liquid tars was carried out by Perkin Elmer spectrum 2000 FT-IR. For each analysis, a thin uniform layer of each tar sample was placed on the sample cell, and peak heights were normalised to the major C-H peak with a normalisation order of two.

5.2.4 Solvent fractionation of tars

As outlined in **Figure 5**, the method of solvent fractionation was applied to separate the liquid tar into three major fractions, light oil, asphaltene and pre-asphaltene [30, 31]. Each tar sample was firstly mixed with n-hexane solution at a fixed ratio of 1:2 (mass: volume) in a 100 ml Erlenmeyer flask, which was subsequently stirred vigorously for 30 min at 290 rpm until a clear solid-liquid layer was formed. Vacuum filtration was conducted to filter out the n-hexane soluble, leaving the n-hexane insoluble on top of the filter paper. The n-hexane soluble was considered as light oil hereafter. The n-hexane insoluble was further mixed with toluene based on the same procedure as the mixing with hexane. The toluene-soluble and insoluble were considered as asphaltene and pre-asphaltene, respectively. After vacuum filtration, the separated insoluble products were dried in a vacuum oven at 110°C to remove the solvent for a minimum 5 hrs before weighing.

5.2.5 Modelling on the temperature discrepancy between a tyre chip particle and the surrounding gas

As has been discussed in our previous paper [29], for the tyre chips with a nominal size in millimeter scale, the intra-particle heat transfer is crucial, in particular under the fast heating scenarios. Upon the increase of both tyre chip size and heating rate, the temperature discrepancy between a tyre chip and the surrounding gas is widened, which is defined as temperature increase in the coal pyrolysis study [21]. The temperature profiles of tyre particle

were thus modelled based on one-dimensional unsteady heat transfer mechanism, along with considering a reaction of heat (ΔH_{rxn}) of around 122 kJ/kg for an overall endothermic pyrolysis reaction [29]. The time-averaged temperature discrepancies for all scenarios are also present in **Table 10**. Scenario 1 has the least temperature discrepancy of <2°C, due to use of a slow heating rate (10°C/min), smallest particle size (0.5-1.5 *mm*) and a continuous injection of pre-heated carrier gas. Whereas Scenarios 2-4 have an increasing trend of temperature discrepancy from 2 to 26°C, due to the absence of carrier gas, and the increase of particle size, even though a slow heating rate of 10 °C/min was used. Scenarios 5-7 carry larger temperature discrepancy from 44 to 90°C, due to the use of larger heating rate (110°C/min), the increase in chip size and the absence of carrier gas. Regarding the last four scenarios from No 8 through to No 11, their conditions are similar to Scenario 1. Therefore, the temperature discrepancies are the least, accounting for a maximum of 2°C.

5.3 Results and Discussion

5.3.1 Yields and composition of liquid tars derived from the scenarios without using carrier gas from the bottom of the reactor

An effort was first attempted to examine the extent of the secondary reactions for the primary volatiles in inert argon that is purged from the top of the reactor, referring to Scenarios 2-4 for the slow heating mode and Scenarios 5-7 for the fast heating mode. Scenario 1 for the injection of argon from the bottom of the reactor is also included for comparison. Its least temperature discrepancy and shortest residence time do not allow remarkable cracking of volatiles in the reactor [21]. In other words, its liquid tar collected could be deemed as the primary volatile vapours that were simply condensed into the cold impingers. **Figure 21** illustrates the product yields for these seven scenarios. Overall, a fairly good mass balance was achieved for all the

cases, with a maximum of 110% closure due to various errors derived from each step, such as pyrolysis, sampling and product characterisation.

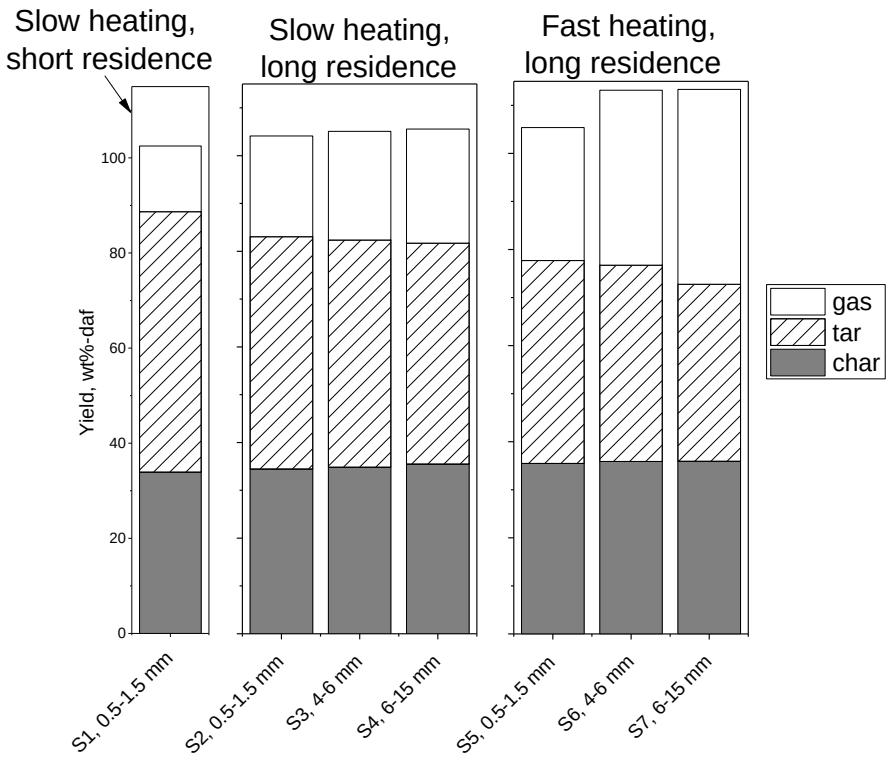

Figure 21 The overall product distributions for the first seven scenarios in dry ash free basis. For the X-axis labelling, the letter "S" in each label stands for scenario, the number after "S" refers to the Scenario number in Table 10.

As the reference, Scenario 1 was confirmed to offer the largest yield for the liquid tar, whilst the least yield for the gas. The overall yield for tar and gas together reaches 65 *wt%-daf* that is very close to 66 *wt%-daf* volatiles within this size. Upon the cessation of the carrier gas argon from the reactor bottom, the tar yield decreased whilst the yields of gas and char increased in Scenario 2, for the smallest chip size. Clearly, without a quick sweeping by carrier gas, the volatiles had to undertake the secondary cracking to produce extra gas and coke deposited on the solid char surface. With an increase of the chip size from Scenario 2 (0.5-1.5 *mm*) through to Scenario 4 (6-15 *mm*), one can see a continuing reduction on the tar yield, which is synchronised by a stable rise on the yields of non-condensable gas and solid char. Furthermore,

with the implementation of fast heating for Scenario 5 through to Scenario 7, the tar yields were reduced dramatically, demonstrating an enhanced cracking extent for the primary volatiles.

Figure 22 depicts the respective solvent fractionation results. Interestingly, the fraction for the hexane-soluble light oil decreased continually from the reference Scenario 1 through to Scenario 7, following a consistent trend with the tar yield shown in **Figure 21**. As for Scenario 1 using argon as the carrier gas, the light oil fraction is the most prevalent (93.6% of total tar), accompanied by only 4.0% hexane-insoluble and toluene-soluble asphaltene and 2.4% toluene-insoluble pre-asphaltene. The cessation of carrier gas in Scenarios 2-4 for the same slow heating caused slight reduction in the light oil fractions which are mainly accompanied by a marginal rise in the yield of heavy pre-asphaltenes. In contrast, the implementation of fast heating induced significant reduction in the light oil fractions, but remarkable increase in the fractions of the other two, in particular for the large tyre chip sizes.

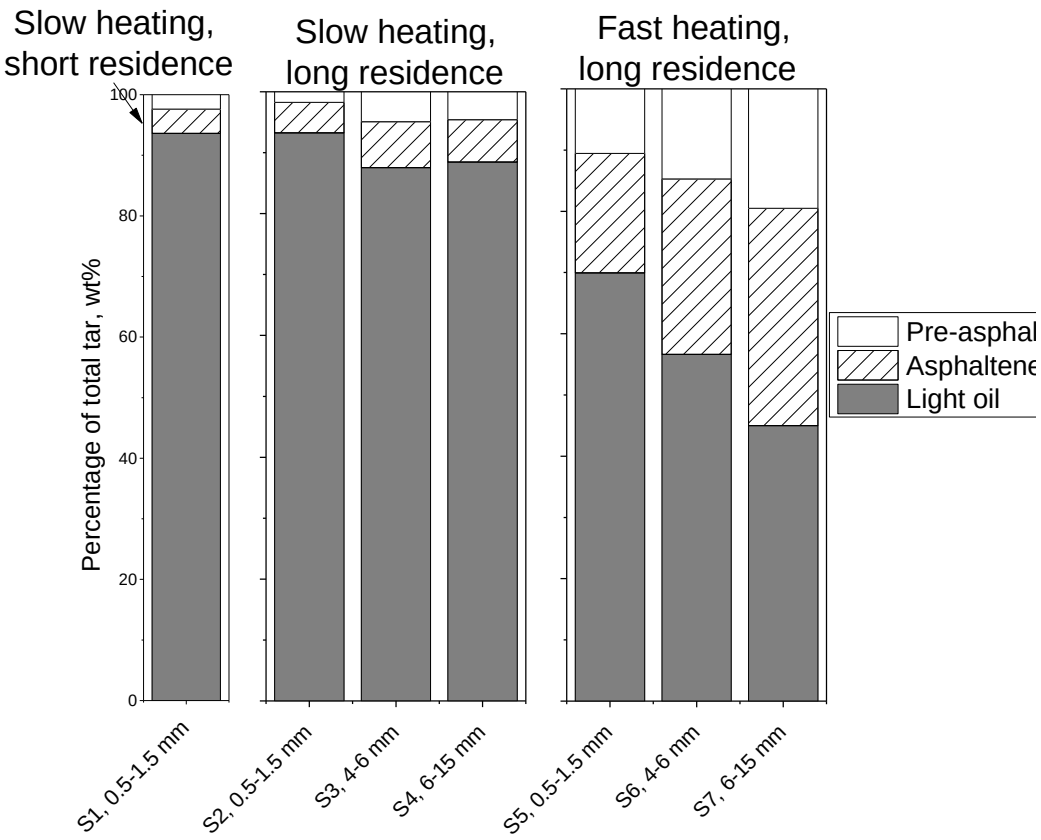

Figure 22 The liquid tar fractionation results for the first seven scenarios. The labelling for X-axis is the same as Figure 21.

On the assumption that the volatile vapours underwent insignificant cracking in the reference Scenario 1, it is reasonable that the majority of the light oil within its tar should be derived from the inherent hydrocarbons within the tyre matrix. Evidently, the light molecules preferentially underwent a variety of secondary reactions in Scenarios 2-7. **Table 11** summarises the quantified aliphatic and aromatic contents in each of the tar samples and the original tyre chips derived from ^{1}H-NMR spectra and ^{13}C-NMR spectrum, respectively. The original spectra are plotted in **Figure 23**. As noted in **Table 11**, the tar derived from the reference Scenario 1 is predominated by aliphatics with a total mass percentage of 92.6%, of which there are 67.6% of aliphatics bonded to aliphatics referring to a long-chain structure and 23.8% of aliphatics adjacent to the aromatic groups. Such a finding is in line with previous characterisation of the liquid tar samples derived from tyre [5, 16]. Regarding the source for

the abundant aliphatic, it should be assigned as the derivate from the rubber materials in the scrap tyre feedstock, as suggested in [11, 32]. ^{13}C-NMR analysis results listed in the last column of **Table 11** proved an abundance of 65 *mol%* aliphatics and 35 *mol%* aromatics for the entire carbon within the tyre chip. Considering that a higher temperature is usually required for the sublimation of aromatics [33, 34], and a tar yield of 55 *wt%* of the entire tyre in Scenario 1, it is inferable to assign the aliphatics in its tar as a derivative from the sublimation of the inherent aliphatics. These aliphatics should also account for the abundant light oil quantified for this tar sample in **Figure 22**.

Table 11 ^{1}H-NMR results for the tyre tars.

Type of hydrogen	Chemical shift (ppm)	^{1}H-NMR						^{13}C-NMR
		Scenario 1	Scenario 2	Scenario 5	Scenario 7	Scenario 8	Scenario 9	Raw tyre
Aliphatic bonded to aliphatic only	0.4-1.8	67.61	42.5	13.95	8.65	67.69	68.04	-
Aliphatic adjacent to aromatic/alkane group	1.8-3.3	23.83	44.69	42.35	41.52	24.02	24.57	-
Aliphatic adjacent to oxygen/hydroxyl group	3.3-4.5	1.18	2.71	2.88	3.18	1.13	0.75	-
Aromatics	6.0-9.0	7.38	10.11	40.82	46.65	7.16	6.64	-
Total aliphaticity	0.4-4.5	92.62	89.89	59.18	53.35	92.84	93.36	64.58

Total aromaticity	6.0-9.0	7.38	10.11	40.82	46.65	7.16	6.64	35.42

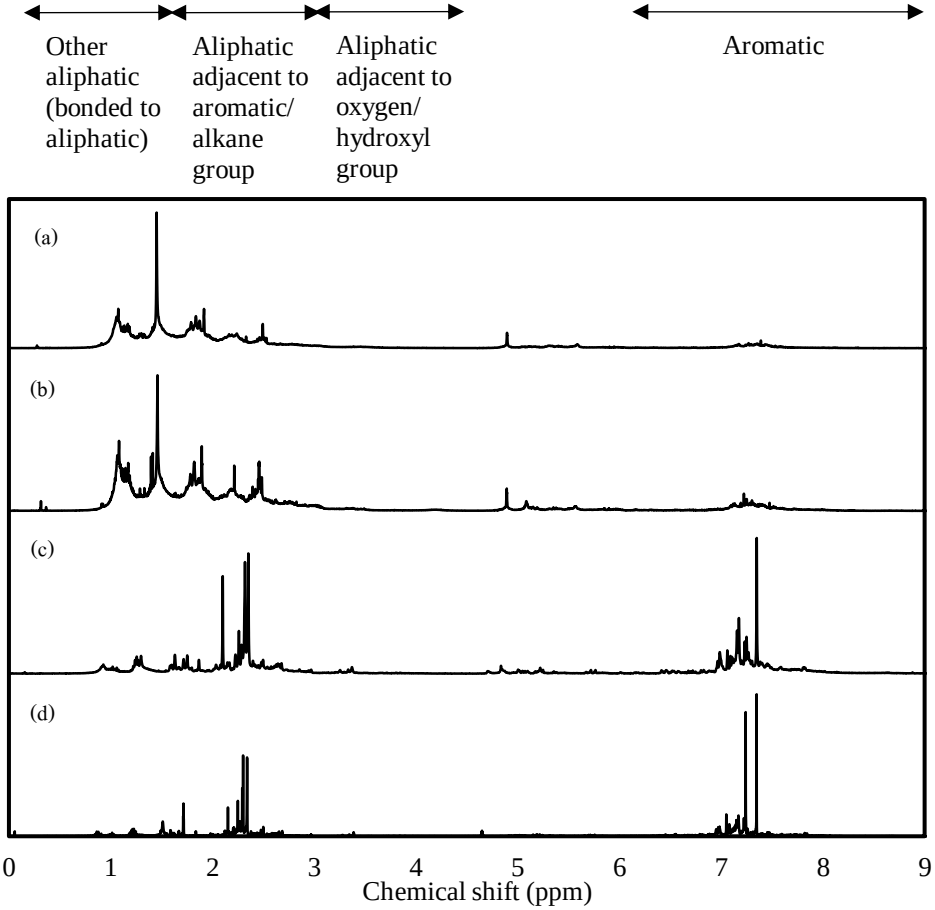

Figure 23 ^{1}H-NMR spectrum of the tyre tars obtained from (a) Scenario 1; (b) Scenario 2; (c) Scenario 5 and Scenario 7.

Upon the cessation of using carrier gas in Scenario 2, one can notice an obvious reduction in the content of the long-chain aliphatics which are accompanied by an increase in the aliphatics bonded with aromatics and pure aromatics. Since the gas yield was improved considerably, it is obvious that a portion of the long-chain aliphatics underwent the self-scission to turn into gases. It should also undertake cyclisation (also known as Diel-alder), aromatisation and polymerisation [2], thereby leading to the increased yields of heavy pre-asphaltene and even

solid char, as evident in **Figure 21** and **Figure 22**. The implementation of faster heating in Scenario 5 and coarser tyre chips in Scenario 7 further facilitated these secondary reactions, as evident by a continued increase in the fractions of aliphatic bonded as side chain to the aromatics, and even aromatics for these two scenarios in **Table 11**.

The FT-IR characterisation was further conducted to fingerprint the specific functional groups and their changes between four typical tar samples, derived from Scenarios 1, 2, 5 and 7 respectively. The identification of the FT-IR functional groups and their absorbance ranges specified for the scrap tyre are tabulated in **Table 12** [35, 36] and the respective spectra are plotted in **Figure 24**. It is further substantiated that the peaks located at 650-825 cm^{-1} assigned for aromatics are much intensified for the tars from Scenarios 5 and 7 (fast heating and different sizes). As for the other two tar samples collected from Scenarios 1 and 2 (slow heating and different sizes), the larger peaks at the region of 2800-3000 cm^{-1} suggest the abundance of alkane groups (C_{al}-C_{al}). This is, however, different from the aliphatics in the original tyre chips that is mainly made of alkene/polyisoprenes (C_{al}=C_{al}) with and without aromatics (C_{ar}=C_{ar}). These species are responsible for the production of natural and synthetic rubbers [10]. Clearly, the inherent alkene volatiles (C_{ar}=C_{ar}) have been partially saturated via hydrogenation to convert into the respective saturated alkane in the slow heating mode. This is broadly in agreement with a previous study on real-time measurement of the tyre pyrolysis products produced in the low heating rates, 10-40°C/min [11]. It demonstrated that the saturation reaction of alkenes via hydrogenation could take place at 310 ^{o}C when the release of volatiles just commenced. Since the intensity of the alkane groups (C_{al}-C_{al}) is much weaker for Scenarios 5 and 7, it is inferable that the other reactions such as cyclisation, aromatisation and polymerisation are superior to the hydrogenation reaction in the fast heating mode.

Table 12 FT-IR functional group indication.

Absorbance ranges (cm^{-1})	Type of bonds	Chemical functional groups
650-825	C-H out of plane bending	Aromatics
830-1035	C=C stretching	Alkenes
1220-1520	C-H bending	Alkanes
1525-1600	C=C stretching	Aromatics
1620-1680	C=C stretching	Alkenes
1690-1750	C=O stretching	Aldehydes/ketones
2800-3000	C-H stretching	Alkanes
3005-3095	C=C stretching	Alkenes

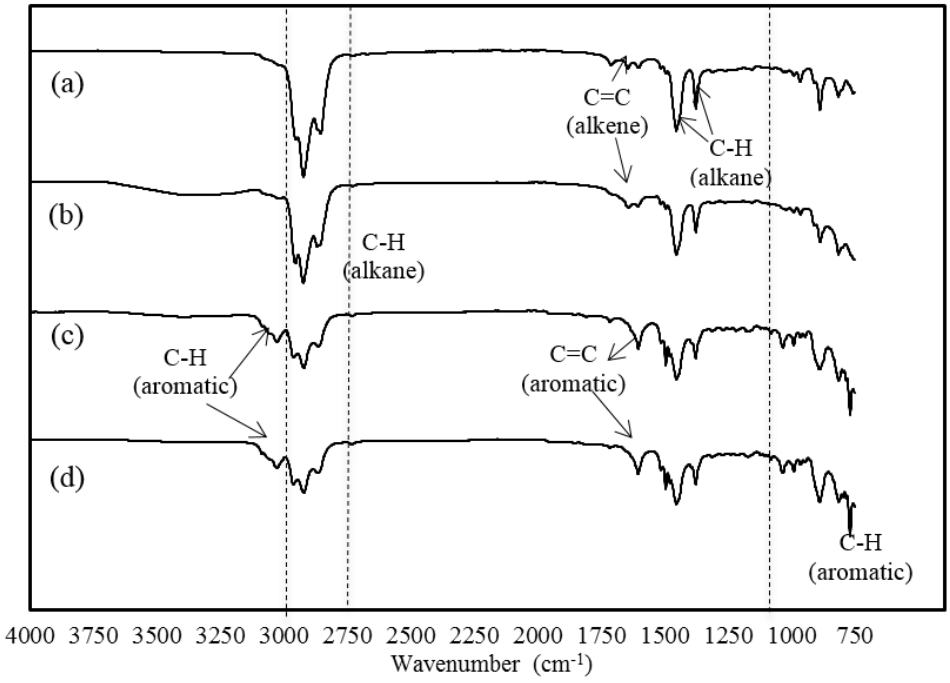

Figure 24 FT-IR spectrum for the tyre tars derived obtained from (a) Scenario 1; (b) Scenario 2; (c) Scenario 5 and (d) Scenario 7.

The GC-MS spectra in **Figure 25** further demonstrate the variation of the secondary reaction pathway for the liquid tars from different pyrolysis conditions. Here again, one can see that the tar from Scenario 1 is rich in aliphatics, with a broad variation on the chain length. The presence

of limonene ($C_{10}H_{16}$) is also confirmed by the studies in **Table 9**. Interestingly, with the cessation of carrier gas in Scenario 2, most of the aliphatics converted into 2-4 benzyl ring hydrocarbons, with a nearly complete disappearance of the C_{20-30} long-chain aliphatics. This is a strong evidence for the aromatisation of a portion of the inherent aliphatics in the free space above the tyre chip bed. The resultant hydrogen should be partially used for the hydrogenation of alkene that was observed by the FT-IR analysis. Implementation of fast heating for the smallest chip size in Scenario 5 witnessed a similar reduction in the aliphatics, whilst a further use of the larger chip size in Scenario 7 enhanced the aromatisation extent of the aliphatics and even the growth of the benzyl rings, as evident by the overwhelming dominance of 2-4 benzyl rings for comparable intensities with limonene. In a study on the biomass pyrolysis tar [37], it demonstrated a favoured ring-to-ring polymerisation at 450°C to form a large matrix of polyaromatic hydrocarbons which are also the precursors for the coke formation [37-39]. This explains the increased yields of the pre-asphaltene and solid char for Scenario 7 in **Figure 21** and **Figure 22**.

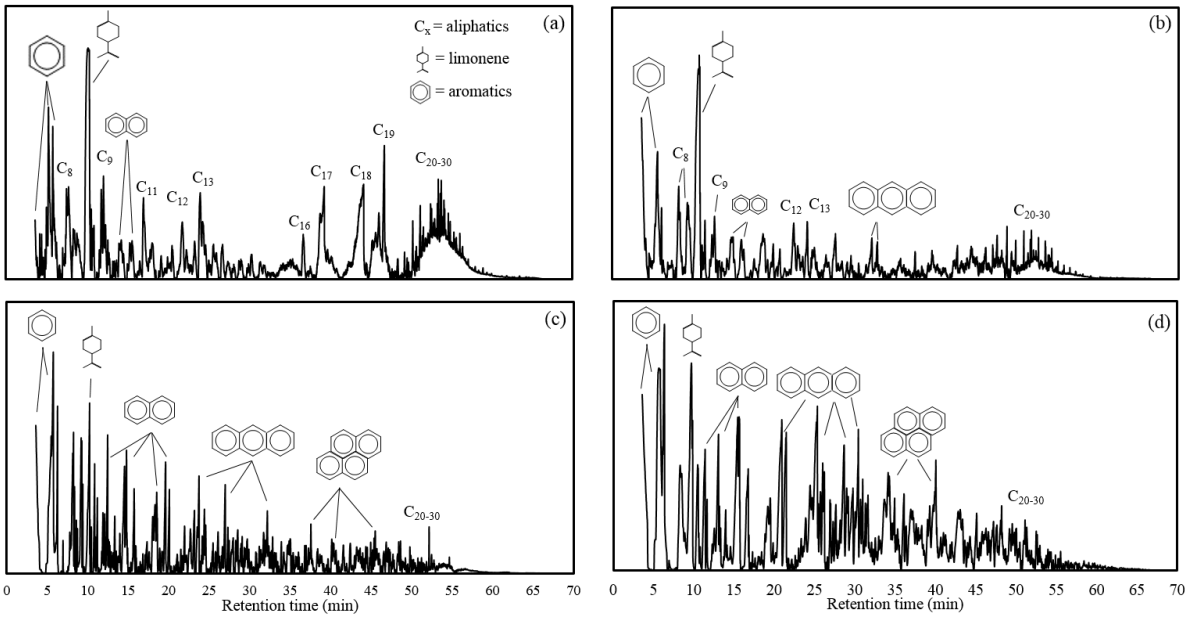

Figure 25 Normalised GC/MS spectrum for the tyre tars obtained from (a) Scenario 1; (b) Scenario 2; (c) Scenario 5 and (d) Scenario 7.

So far, the strong secondary reactions, in particular cyclisation, aromatisation and polymerisation, have been proven for the volatiles in the absence of carrier gas inside the furnace. This is the case for an industry-scale furnace such as a fixed-bed that is heated indirectly or externally from the outside. Clearly, the lack of a pre-heated carrier gas elongated the residence time for the volatile vapours inside the furnace, but it also widened the temperature difference between furnace wall and the volatile vapour, in particular for the scenarios of using large chip sizes and fast heating [29]. This is evident by the results tabulated in the last row of **Table 12. Figure 26a** plotted the yields of light oil (hexane-soluble), heavy oil (hexane -insoluble) and non-condensable gases versus particle temperature discrepancy for the first seven scenarios. Clearly, the combined influences of tyre chip size and heating rate can be elaborated as a single effect of the particle temperature discrepancy. That is, an exponential trend applies to all three products. Taking the light oil in Scenario 1 as the inherent hydrocarbons, **Figure 26b** also plotted the extent of the global secondary reaction (including all the reactions specified above) for light oil versus the particle temperature discrepancy. Clearly, the secondary reactions for the aliphatic-rich light oil are highly sensitive, the extent of which increases rapidly within a temperature discrepancy of 100^{o}C. Interestingly, although coal bears a very different nature to that of scrap tyre chips, the summary of coal pyrolysis in [21] also shows a comparable and quick reduction in the tar yield within the initial temperature discrepancy/increase of 100^{o}C. Evidently, the chemistry underpinning the secondary reaction of volatile vapours is somehow independent on the feedstock property.

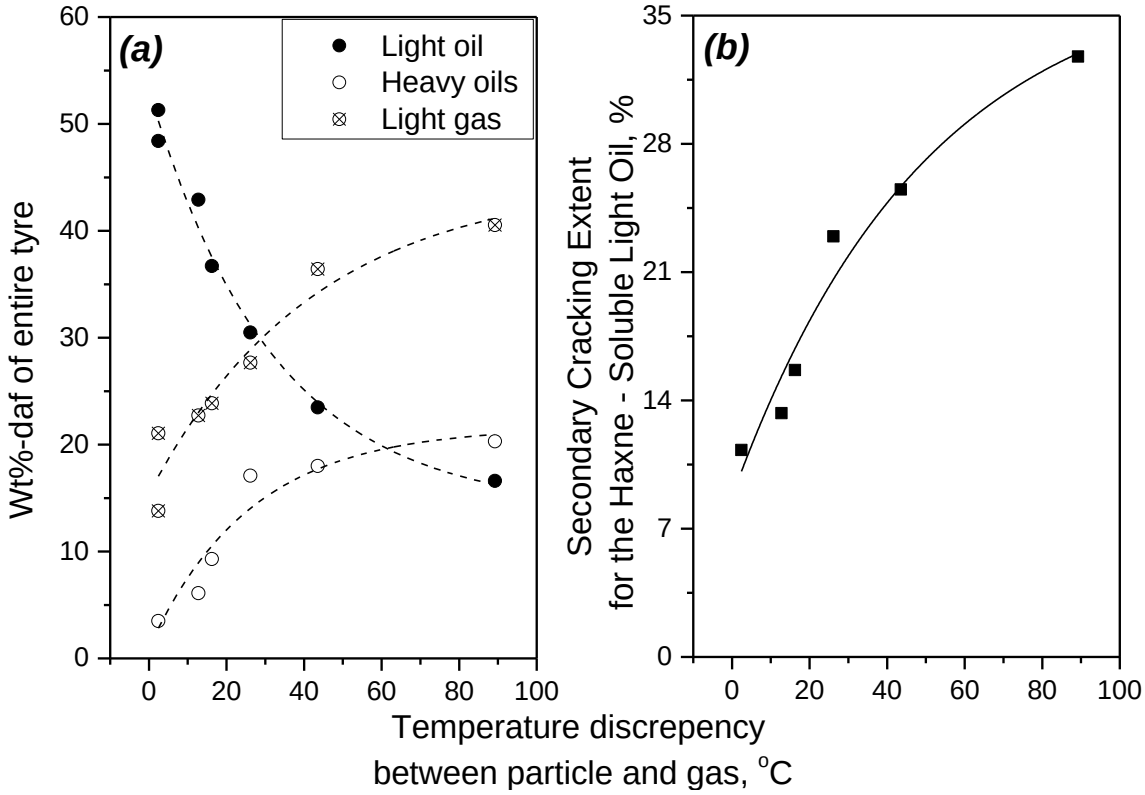

Figure 26 The relationship between the yields of light oil, heavy oils and light gas with the particle temperature discrepancy to the surrounding gas environment in Panel (a), and the global secondary cracking extent for light oil fraction in Panel (b) for the Sc

5.3.2 Yields and compositions of liquid tars derived from the non-inert gas environment

Considering that Scenario 1 using a slow heating and argon as carrier gas led to the highest tar yields and largest light oil fraction, effort was extended to investigate the influence of gas environment (Scenarios 8-11) on the properties of tar formed at 600°C, upon the employment of the same conditions but with the use of reactive CO_2 and/or steam as the carrier gas. This is to simulate the direct heating mode in an industry-scale moving bed reactor such as Lurgi-Spulgas or rotary kiln, where the hot flue gas derived from the combustion of pyrolysis gas is injected directly inside the furnace [24].

For the overall product yields and gas composition tabulated in **Table 13**, the substitution of 30% CO_2 for argon in Scenario 8 caused a marginal, if not negligible change in the product distribution. An increase in the yield of CO gas from nil to 0.47 *wt%-daf* is observed, which is accompanied by a slight drop on the char yield indicating the occurrence of the heterogeneous Boudouard Reaction 5.1 for tyre char at 600^{o}C. The extent of this reaction is extremely low here, because the temperature employed is even lower than the confirmed minimum temperature of 750^{o}C for the solid char derived from the pyrolysis of medium-vehicle tyre [10, 25].

Table 13 Overall product distribution from three scenarios using slow heating rate, carrier gas and smallest chip size, *wt%*-daf

	Carrier gas	Solid char	Liquid tar	CH_4	CO
Scenario 1	Argon	33.23	54.12	7.1	0.04
Scenario 8	30% CO_2	31.12	54.62	7.22	0.47
Scenario 9	30% CO_2 + 15% steam	32.32	52.28	7.43	0.65

The solvent fractionation results in **Table 14** also suggests little alternation between pure argon and 30% CO_2, indicating that it is reasonable to assume CO_2 as inert gas hereafter. In contrast, the introduction of 15% steam into the reactor induced a considerable reduction in the tar yield from 54.1 *wt%* in pure argon to 52.3 *wt%*, whilst increase in the CO yield up to 0.65 *wt%-daf*. Since the change in char yield is indiscernible, it is inferable that a homogeneous steam reforming reaction has taken place for the volatile vapours, as per Reaction 5.2 shown below. The solvent fractionation results in **Table 14** confirmed that the two hexane-insolubles including asphaltene and pre-asphaltene that are rich in long-chain aliphatics (C_{20-30} in the GC-MS spectra in **Figure 27**) preferentially underwent the reforming reaction.

Heterogeneous Boudouard reaction	$C+CO_2 \rightarrow CO$	Reaction 5.1
Homogenous tar reforming	$C_xH_y+xH_2O \rightarrow xCO+(y/2+1)\ H_2$	Reaction 5.2
Methanation reaction	$CO+H_2 \rightarrow CH_4+H_2O$	Reaction 5.3

Table 14 Solvent fractionation results for Scenarios 1, 8 and 9 using slow heating rate, carrier gas and smallest chip size, *wt%*-daf

	Carrier gas	Light oil	Asphaltene	Pre-asphaltene
Scenario 1	Argon	51.3	2.2	1.3
Scenario 8	30% CO_2	50.8	1.9	1.9
Scenario 9	30% CO_2 + 15% steam	51.9	0.7	0.7

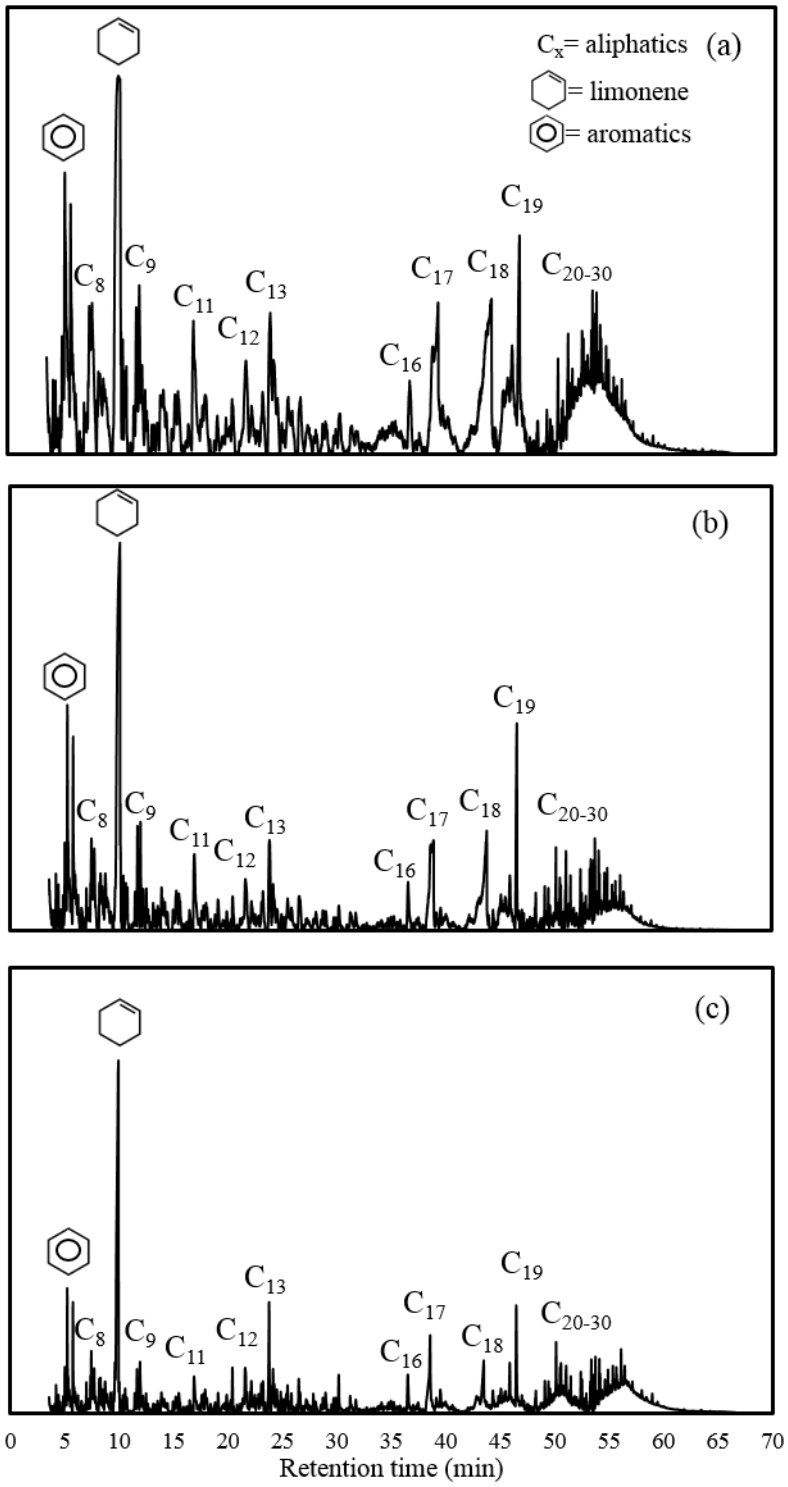

Figure 27 Normalised GC/MS spectrum for the tyre tars derived from (a) Scenario 1; (b) Scenario 8 and (c) Scenario 9.

This finding is intriguing, considering that the previous studies only confirmed the homogeneous reaction 5.2 for scrap tyre tar at the temperatures above 900°C [26, 40]. In another study on the *ex-situ* steam reforming of bio-tar upon the use of scrap tyre char [41], the increase in the yield of CO due to the catalytically enhanced decarboxylation reaction has been confirmed [41]. Moreover, through another study of ours on the catalytic cracking of bio-tar using scrap tyre char, it was even confirmed the catalytic performance of scrap tyre char for the deoxygenation of bio-tar at 500°C [42]. Following these studies, it is then hypothesised that the nascent tyre char plays a catalytic role in the *in-situ* steam reforming of heavy volatiles. To prove this, another two scenarios of experiments, Scenario 10 and Scenario 11, were designed and tested. Scenario 10 was for the injection of steam from the top of the reactor, where the steam is expected to only encounter the upward volatile vapours, whilst Scenario 11 was designed by allocating another layer of char on top of the scrap tyre chips. The upward volatile vapours were expected to flow through and encounter the char bed. Note that, the steam was also injected with argon continuously from the bottom of the reactor. The char tested was generated from Scenario 1, with two mass ratios to the tyre chips being tested in Scenario 11, 50:50 and 100:50.

As presented in

Figure 28a, it is clear that little of the volatile vapour was reactive enough to undertake the steam reforming reaction on its own, as evident by the indescribable change in the yields of overall products and tar fractions for Scenario 10, relative to two references, Scenario 1 for pure argon and Scenario 9 for 30% CO_2 and 15% steam in argon. In contrast, for the addition of an extra solid char bed in Scenario 11, one can clearly see a further increase of the CO yield

from 0.65 *wt%* (Scenario 9) to 3.22 *wt%* for a double amount of char to tyre chips. More interestingly, the solvent fractionation results shown in

Figure 28**b** confirmed a continuous reduction in the fractions of the heavy asphaltene and pre-asphaltene. The yield of the former fraction is almost indiscernible upon the doubling of the char amount, suggestive of nearly complete consumption of it by the reforming reaction. This strong evidence substantiates the catalytic role of tyre char on an *in-situ* steam reforming of the heavy tar fractions at the temperature of 600°C employed here. Such a temperature is even lower than the temperature of 700°C employed for the steam reforming of bio-oil [29], but it is in line with our study on the deoxygenation cracking of bio-tar via scrap tyre char at 500°C [42]. These results strongly demonstrate that the tyre char property is crucial for its catalytic performance, and the tyre tar is even more reactive than bio-tar upon the steam reforming reaction.

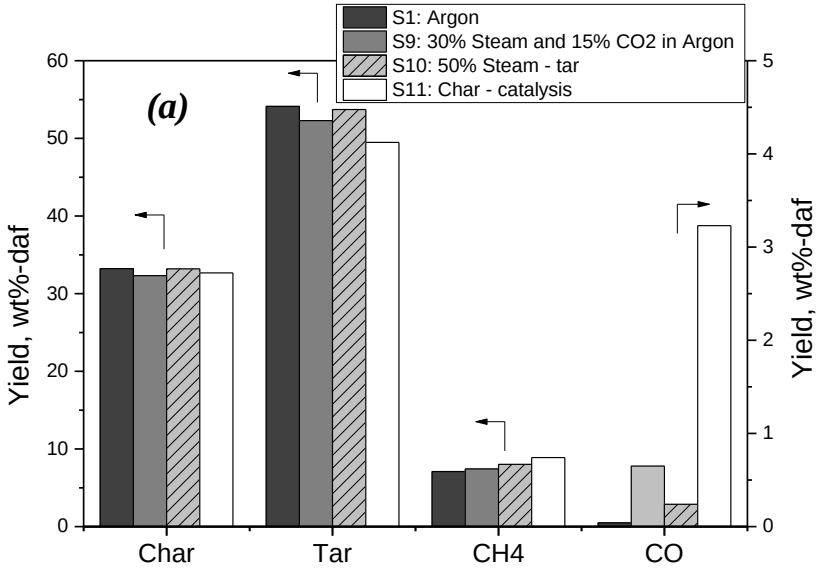

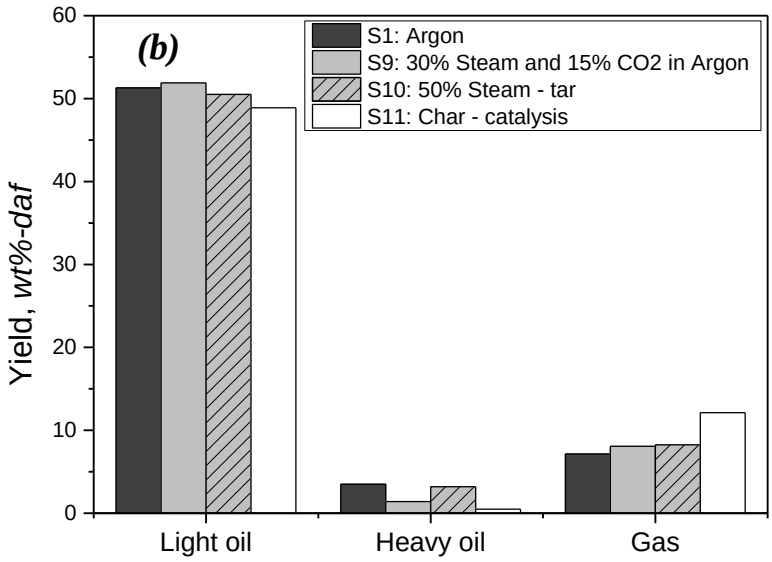

Figure 28 Influence of reactive gas on the product distribution for the Scenarios 8-11. Panel (a) for the overall product distribution and Panel (b) for the solvent fractionation results of the liquid tar samples.

With regards to the preference of heavy tar fraction over its light counterpart for the steam reforming reaction, it could be explained by a preferential trapping of the heavy molecules on the solid char surface, whereas the light molecules with a relatively larger fugacity escaped more easily into the gas phase. Once being adsorbed on the char surface, the heavy molecules should then react with the steam molecules for the reforming reactions. However, since hydrogen was not detected in the gas phase, it is inferable that this gas product or its radicals, once formed should be consumed instantly inside the reactor. It could be taken up by the light molecules for hydrogenation, by CO for methanation on the char surface (as per Reaction 5.3 above), and even by the impure elements such as sulphur and nitrogen into the respective gaseous pollutants such as H_2S and NH_3. The hydrogenation of light tar is confirmed by the ^{1}H-NMR spectrum for Scenario 9 injecting steam and CO_2 into the reactor, for the largest

aliphaticity of its tar (see **Table 11**). Regarding the methanation (Reaction 5.3), its occurrence can be partially supported by the slightly improved yields of CH_4 in Scenarios 9-11 of

Figure 28**a**. Evidently, this reaction should take place on the solid char surface, even between CO and H_2 on their respective adsorbed states on the catalyst active site. This is somehow supported by the temperature/time-resolved profiles for CH_4 emission in **Figure 29**. Compared to a bimodal distribution for Scenario 10 feeding steam onto the top of the reactor, the addition of an extra char bed in Scenario 11 clearly promoted the emission of CH_4 around the low-temperature peak. This is also confirmed in Scenario 9 when both CO_2 and steam are injected through the tyre chips. The pyrolysis-derived nascent char is fully surrounded by the volatile vapours and derivatives; thus, it promotes the secondary reactions including the methanation reaction.

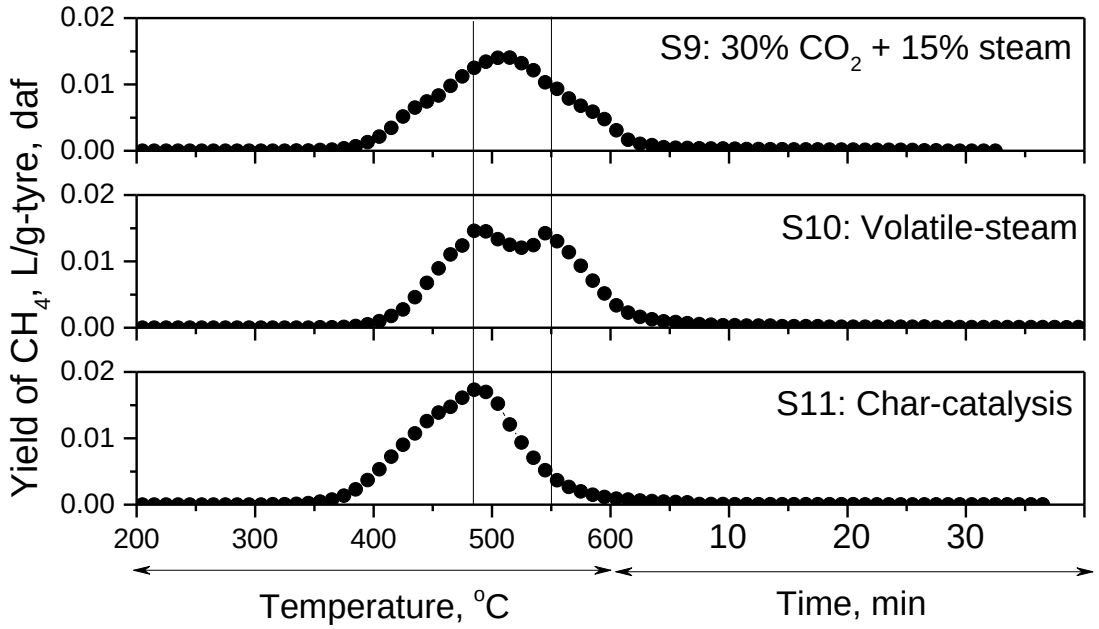

Figure 29 CH_4 emission profile for Scenarios 9-11.

The probable reaction between hydrogen and impure elements cannot be ruled out either. Instead, it is confirmed by the elemental compositions of the respective overall tar samples listed in **Table 15.** In addition, an increase in the H/C molar ratio is also discernible, which confirmed the enhanced hydrogenation reaction in the reactive gas. In contrast, the aromatisation is preferred under the fast heating condition with the presence of any carrier gas, as evident by the least H/C ratio but largest contents of impure S and N for the tar derived from Scenario 5. Clearly, the use of steam in combination with slow heating in the tyre pyrolysis environment provides multiple benefits in terms of improving the tar quality.

Table 15 Elemental analysis of three typical tyre tar samples derived from slow heating, and the use of smallest size and carrier gas. Note, the result for Scenario 5 using fast heating rate and no carrier gas was also listed for comparison.

	Carrier gas/Condition	C	H	N	S	O (diff)	H/C (molar)
Scenario 1	Argon	86.53	10.8	0.57	0.97	1.77	1.49
Scenario 8	30% CO_2	87.65	11.17	0.46	0.95	0.77	1.51
Scenario 9	30% CO_2 + 15% steam	84.76	10.8	0.44	0.69	3.31	1.52
Sceniaro 5	Fast heating, no carrier gas	89.15	7.4	0.82	1.18	1.47	0.99

5.4 Conclusions

This paper has examined the mild pyrolysis of scrap tyre in an integrated manner by examining the co-effects of several parameters including heating rate, volatile residence time, tyre particle size and non-inert gases (CO_2 and/or H_2O) on the properties of tars. In particular, the influences of particle temperature discrepancy (to the surrounding gas environment) and reactive gas on

the tar yield and properties have been explored intensively. The major conclusions are drawn as follows:

1) In a simulated fixed-bed reactor with the absence of carrier gas, the particle temperature discrepancy to the surrounding environment can be correlated positively to the secondary cracking extent of the volatiles, in an exponential increment trend within a temperature discrepancy range of 100°C. Upon an increase in the temperature discrepancy by either increasing the heating rate or tyre chip size, the inherent long-chain aliphatics preferentially underwent scission, cyclisation, aromatisation and even polymerisation, leading to the formation of abundant heavy aromatics and light gases that are rich in methane.
2) The use of a carrier gas such as in the industry-scale moving bed or rotary kiln is beneficial in improving the tar yield and aliphaticity. As a convective heating source, it heats the particles slowly and also sweeps out the volatile vapours immediately, thereby minimising the secondary reactions. Due to an elongated residence time within the reactor, the hydrogenation reaction for inherent alkene units is also enhanced. For the two major components, CO_2 and steam in hot flue gas, CO_2 is rather inert at 600°C, while steam is reactive enough to further reduce the heavy hydrocarbon fraction via steam reforming reaction.
3) At the mild pyrolysis temperature of 600°C, the nascent tyre char is catalytic enough to enhance the steam reforming reaction for heavy molecules deposited on its surface, and even the methanation reaction between CO and H_2 derived from the steam reforming reaction. Accordingly, the resultant gas product is overwhelmingly dominated by CH_4, with a maximum of 2 *wt%* CO and indiscernible contents for the other non-condensable species, whilst the heavy fractions could be largely reduced within the liquid tar product.

5.5 Acknowledgements

This work was supported by the Australian Research Council (ARC) under its Industrial Research Training Hub (170100009) scheme for the joint project between Monash and Advanced Fuel Innovation Pty Ltd. The scrap tyre used in this project was provided by the Tyrecycle Pty Ltd, Australia is also acknowledged.

5.6 References

1. Huang, H. and L. Tang, *Pyrolysis treatment of waste tire powder in a capacitively coupled RF plasma reactor.* Energy Conversion and Management, 2009. **50**(3): p. 611-617.

2. Williams, P.T., *Pyrolysis of waste tyres: A review.* Waste Management, 2013. **33**(8): p. 1714-1728.

3. Williams, P.T. and R.P. Bottrill, *Sulfur-polycyclic aromatic hydrocarbons in tyre pyrolysis oil.* Fuel, 1995. **74**(5): p. 736-742.

4. Cunliffe, A.M. and P.T. Williams, *Composition of oils derived from the batch pyrolysis of tyres.* Journal of Analytical and Applied Pyrolysis, 1998. **44**(2): p. 131-152.

5. Banar, M., et al., *Characterization of pyrolytic oil obtained from pyrolysis of TDF (Tire Derived Fuel).* Energy Conversion and Management, 2012. **62**: p. 22-30.

6. Berrueco, C., et al., *Pyrolysis of waste tyres in an atmospheric static-bed batch reactor: Analysis of the gases obtained.* Journal of Analytical and Applied Pyrolysis, 2005. **74**(1): p. 245-253.

7. Choi, G.-G., et al., *Total utilization of waste tire rubber through pyrolysis to obtain oils and CO2 activation of pyrolysis char.* Fuel Processing Technology, 2014. **123**: p. 57-64.

8. Diez, C., et al., *Pyrolysis of tyres. Influence of the final temperature of the process on emissions and the calorific value of the products recovered.* Waste Manag, 2004. **24**(5): p. 463-9.

9. Kar, Y., *Catalytic pyrolysis of car tire waste using expanded perlite.* Waste Management, 2011. **31**(8): p. 1772-1782.

10. Kumar Singh, R., et al., *Pyrolysis of three different categories of automotive tyre wastes: Product yield analysis and characterization.* Journal of Analytical and Applied Pyrolysis, 2018. **135**: p. 379-389.

11. Kwon, E. and M.J. Castaldi, *Investigation of Mechanisms of Polycyclic Aromatic Hydrocarbons (PAHs) Initiated from the Thermal Degradation of Styrene Butadiene Rubber (SBR) in N2 Atmosphere.* Environmental Science & Technology, 2008. **42**(6): p. 2175-2180.

12. Kyari, M., A. Cunliffe, and P.T. Williams, *Characterization of Oils, Gases, and Char in Relation to the Pyrolysis of Different Brands of Scrap Automotive Tires.* Energy & Fuels, 2005. **19**(3): p. 1165-1173.

13. Laresgoiti, M.F., et al., *Characterization of the liquid products obtained in tyre pyrolysis.* Journal of Analytical and Applied Pyrolysis, 2004. **71**(2): p. 917-934.

14. Mkhize, N.M., et al., *Effect of temperature and heating rate on limonene production from waste tyre pyrolysis.* Journal of Analytical and Applied Pyrolysis, 2016. **120**: p. 314-320.

15. Yazdani, E., S.H. Hashemabadi, and A. Taghizadeh, *Study of waste tire pyrolysis in a rotary kiln reactor in a wide range of pyrolysis temperature.* Waste Management, 2019. **85**: p. 195-201.

16. Williams, P.T., S. Besler, and D.T. Taylor, *The pyrolysis of scrap automotive tyres.* Fuel, 1990. **69**(12): p. 1474-1482.

17. González, J.F., et al., *Pyrolysis of automobile tyre waste. Influence of operating variables and kinetics study.* Journal of Analytical and Applied Pyrolysis, 2001. **58-59**: p. 667-683.

18. Napoli, A., et al., *Scrap tyre pyrolysis: Are the effluents valuable products?* Journal of Analytical and Applied Pyrolysis, 1997. **40-41**: p. 373-382.

19. Murillo, R., et al., *The application of thermal processes to valorise waste tyre.* Fuel Processing Technology, 2006. **87**(2): p. 143-147.

20. Martínez, J.D., et al., *Waste tyre pyrolysis – A review.* Renewable and Sustainable Energy Reviews, 2013. **23**: p. 179-213.

21. Liu, Z., et al., *Reaction of volatiles – A crucial step in pyrolysis of coals.* Fuel, 2015. **154**: p. 361-369.

22. He J, L.H., *Recovery technology of coking chemical products*, in *Metallurgical Industry Press*. 2006.

23. Shui H, Z.D., Zhang C, *Separation and refining of coal tar*, in *Chemical Industry Press*. 2006.

24. Garcia-Nunez, J.A., et al., *Historical Developments of Pyrolysis Reactors: A Review.* Energy & Fuels, 2017. **31**(6): p. 5751-5775.

25. Betancur, M., J.D. Martínez, and R. Murillo, *Production of activated carbon by waste tire thermochemical degradation with CO2.* Journal of Hazardous Materials, 2009. **168**(2): p. 882-887.

26. Ogasawara, S., M. Kuroda, and N. Wakao, *Preparation of activated carbon by thermal decomposition of used automotive tires.* Industrial & Engineering Chemistry Research, 1987. **26**(12): p. 2552-2556.

27. Hidy, G., et al., *Low-Energy and Chemical-Free Activation of Pyrolytic Tire Char and Its Adsorption Characteristics.* Journal of the Air & Waste Management Association, 2009. **59**(6): p. 747-756.

28. Li, C.-Z., *Importance of volatile–char interactions during the pyrolysis and gasification of low-rank fuels–a review.* Fuel, 2013. **112**: p. 609-623.

29. V. Tan, A. De Girolamo, T. Hosseini, J. Alhesan, L. Zhang, *Scrap tyre pyrolysis: Modified chemical percolation devolatilization (MCPD) to describe the influence of pyrolysis conditions on product yields*, Waste Manage. 76 (2018) 516–527.

30. Wei, Y. and H. Lei, *Advanced upgrading of pyrolysis oil via liquid-liquid extraction*. Vol. 2. 2013.

31. Aljariri Alhesan, J.S., et al., *Long time, low temperature pyrolysis of El-Lajjun oil shale.* Journal of Analytical and Applied Pyrolysis, 2018. **130**: p. 135-141.

32. Uçar, S. and S. Karagöz, *Co-pyrolysis of pine nut shells with scrap tires.* Fuel, 2014. **137**: p. 85-93.

33. Goldfarb, J. and E. Suuberg, *Raoult's Law and Its Application to Sublimation Vapor Pressures of Mixtures of Polycyclic Aromatic Hydrocarbons*. Vol. 25. 2008.

34. Fu, J., J.W. Rice, and E.M. Suuberg, *Phase behavior and vapor pressures of the pyrene+9,10-dibromoanthracene system.* Fluid Phase Equilibria, 2010. **298**(2): p. 219-224.

35. Williams, P.T., S. Besler, and D.T. Taylor, *The pyrolysis of scrap automotive tyres: The influence of temperature and heating rate on product composition.* Fuel, 1990. **69**(12): p. 1474-1482.

36. Li, S.Q., et al., *Pilot-Scale Pyrolysis of Scrap Tires in a Continuous Rotary Kiln Reactor.* Industrial & Engineering Chemistry Research, 2004. **43**(17): p. 5133-5145.

37. Wang, X., et al., *Soot formation during polyurethane (PU) plastic pyrolysis: The effects of temperature and volatile residence time.* Energy Conversion and Management, 2018. **164**: p. 353-362.

38. Böhm, H., H. Jander, and D. Tanke, *PAH growth and soot formation in the pyrolysis of acetylene and benzene at high temperatures and pressures: Modeling and experiment.* Symposium (International) on Combustion, 1998. **27**(1): p. 1605-1612.

39. Öktem, B., et al., *Chemical species associated with the early stage of soot growth in a laminar premixed ethylene–oxygen–argon flame.* Combustion and Flame, 2005. **142**(4): p. 364-373.

40. Donatelli, A., P. Iovane, and A. Molino, *High energy syngas production by waste tyres steam gasification in a rotary kiln pilot plant. Experimental and numerical investigations.* Fuel, 2010. **89**(10): p. 2721-2728.

41. Al-Rahbi, A.S. and P.T. Williams, *Hydrogen-rich syngas production and tar removal from biomass gasification using sacrificial tyre pyrolysis char.* Applied Energy, 2017. **190**: p. 501-509.

42. Zhou, Q., et al., *Catalytic performance of scrap tyre char for the upgrading of eucalyptus pyrolysis derived bio-oil via cracking and deoxygenation.* Journal of Analytical and Applied Pyrolysis, 2019. **139**: p. 167-176.

This page is intentionally left blank

Chapter 6- Waste Tyre Char-Catalysed *In-situ* Deoxygenation of Volatile Vapours and Production of Hydrogen – rich Syngas during the Steam-Assisted Pyrolysis of Lignite

In Chapter 5, it was discovered the self-catalytic effect of tyre char upon the steam reforming reaction for heavy hydrocarbons of tyre volatiles, and even the methanation reaction of CO and H_2 at the terminal temperature of 600ºC in the heating rate of 10°C/min. In this work, the first point of interest is to extend the catalytic potential of the char from waste tyre chips onto the pyrolysis of low-rank coals, and its performance in various operating conditions including various reactor terminal temperatures, heating rates and gas environment (argon versus steam). Besides the catalytic performance, this work also aims to grasp in-depth understanding of the catalysis mechanism triggered by tyre chars in terms of the interaction between the volatile vapours of lignites and the active metallic species of tyre chars.

Abstract

This paper examined the catalytic performance of tyre char, a waste-derived product on the catalytic pyrolysis of lignite at 600-900ºC, and the use of different gas environment (*i.e.* argon versus steam) and different catalyst to lignite mass ratios. All the resultant products (solid, gas and liquid) and spent catalysts have been characterised intensively to elucidate the specific catalytic role of tyre char and the mechanisms. As has been confirmed, the catalytic effect of tyre char is profound in the fast pyrolysis scheme, and from a minimum temperature of 700ºC. The catalyst is also highly size selective for the upgrading of primary volatile vapours. The heavy molecules are preferentially easily trapped within the catalyst matrix, and hence, upgraded via catalytic scission and decarbonylation reactions even in inert argon. The coke deposit derived from the cracking of heavy volatiles is also catalysed for the respective char-steam gasification. In contrast, the light volatiles released at the early stage of pyrolysis are preferentially upgraded via deoxygenation reaction, resulting in the formation of abundant light oils with a very low H/C molar ratio. In addition, the non-condensable gases such as methane are steam reformed on the catalyst surface too. The total H_2 yield is thus compared with the char-based catalysts tested in the literature. Regarding the catalysis mechanisms, the nano-sized Zn-bearing species are responsible for the co-production of H_2-rich syngas and upgraded liquid oil via steam-reforming reactions. In particular, the S-bearing active sites are essential and responsible for most of the decarbonylation reaction. Regarding the remaining ZnO-bearing particles, they underwent severe agglomeration upon a repeating usage, thereby losing the catalytic function rapidly.

6.1 Introduction

Pyrolysis of the low-quality hydrocarbons, including low-rank lignite, lignocellulosic biomass and industrial wastes such as sewage sludge for the production of liquid oil is one of the most promising low-emission technologies for an advanced utilisation of these fuels. However, one generic disadvantage of these hydrocarbons is the presence of abundant oxygenates within them, which makes the resultant oils corrosive, unstable and unsuitable for the current refineries [1]. Consequently, an upgrading of the pyrolytic oils via catalytic deoxygenation is essential.

To date, numerous researches have showed that the use of metallic catalysts, including precious metals [2], zeolites [3], metal oxides [4] and salts [5], demonstrated a relatively high efficiency in upgrading the quality of tar oil via various deoxygenation reactions: decarboxylation, decarbonylation and dehydration in the forms of carbon oxides and chemical water, respectively. The precious metallic catalysts have proven to carry the highest catalytic activity due to their capability of cleaving long-chains, which is dependent on the strength of their acidity, *i.e.* Lewis acid or Brønsted acid. [6- 8]. However, the excessive cracking that usually occurs induces the deposition of coke on the surface, which in turn deactivates the catalyst rapidly.

More recently, tyre char has found to be efficient to trigger not only the deoxygenation of bio-oil at 500^{o}C in argon [9], but also the steam-reforming reactions of bio-oil for the production of tar-free hydrogen-rich syngas at the temperatures up to 900^{o}C [10]. However, the mechanisms are still unclear. In particular, the role of the inherent ash-forming elements

including zinc (Zn) and sulphur (S) have yet to be specified. For the steam-reforming of bio-oil [11], the difference of hydrogen yield is marginal between the original tyre char and its acid-washed counterpart, and hence, the role of inherent ash-forming elements in tyre char is apparently insignificant, in particular at the temperatures below 800°C [11]. Similarly, in the other study concerning the steam-reforming of methylcyclohexane employing the Pt-laden tyre char as the catalyst [12], the tyre char is prior acid washed, which is thus nearly ash-free and the catalytic role is mostly attributed to the external Pt. In contrast, the studies on the test of both raw biomass and the mixture of model organic compounds confirmed the promoting effect of $ZnCl_2$ on the gasification of bio-char, and the steam-reforming of volatile vapours and even methane (CH_4) at the temperatures of 800°C and above [11,13]. Furthermore, another study on the pyrolysis of $ZnCl_2$-laden coal also confirmed its promoting effect on coal conversion, which is assigned to its strong Lewis acid and reduction potential [14]. Based on these inconsistent observations, we hypothesised that the inherent Zn^{2+} cation in tyre char could catalyse the steam-reforming/gasification reactions for the hydrogen production. Simultaneously, the inherent S-bearing active site could induce the breakage of C-O bond, thereby yielding oxygen-free oil.

To prove our hypothesis, we have examined the influence of heating rate (10, 300°C/min), terminal temperature (600-900°C) and steam environment (30 *vol%*) on the pyrolysis of three lignites with and without the presence of tyre char in a single-stage horizontal fixed bed reactor. The lignites are also named Victorian brown coals, with a reserve of approximately 500 years in Victoria, Australia [1]. The pyrolysis of these lignites usually generate around ~50 *wt%* char, ~15-35 *wt%* light gas and 15-25 *wt%* tar [15]. The tar samples are notorious for the significant content of oxygen-containing functionalities and heavy hydrocarbons [16]. The liquid tar samples collected were characterised by a variety of advanced techniques including

solvent fractionation, Karl-Fischer, elemental analysis and gas chromatography–mass spectrometry (GC/MS), whereas the fresh and used tyre chars were characterised by X-ray powder diffraction (XRD), X-ray fluorescence (XRF) and Transmission Electron Microscopy (TEM). In addition, cyclic testing on the spent tyre char was conducted for three repeats, so as to trace the change on the content and oxidation state of the elements of interest (*i.e.* Zn and S), and the acidity of the catalyst. These efforts aim to explore the catalytic potential and performance of tyre char with a deeper understanding of the mechanism, and ultimately to improve the value and stability of tyre char in the catalysis area.

6.2 Material and methods

6.2.1 Properties of lignite and tyre char feedstock

Three lignites were tested for the pyrolysis, including Yallourn (YL), Loy Yang (LY) and Morwell (MW). All the lignite samples were sieved to 2-4 mm and then dried in a vacuum oven at 110^{o}C for around 24 *h*. The tyre char was received from an industrial pyrolysis plant which operates at around 800^{o}C. Prior to be mixed with lignite, tyre char was further pyrolysed at 600°C in 10°C/min to fully remove the remaining moisture and volatiles. It was also sieved to < 2 mm for all runs throughout this study. For the simplification purpose, the tyre char is referred to as catalyst hereafter. The proximate and ultimate analyse of these samples are shown in **Table 16**. Clearly, the three lignites are all low in ash (<3 *wt%-daf*) but high in volatile fraction (54-56%), in particular oxygen. These properties are very similar to the lignocellulosic biomass. On the other hand, the fresh catalyst is high in ash content (19 *wt*%) and extremely low in volatile fraction (<0.05 *wt%*), which thus causes negligible interference on the liquid oils derived from lignite. it is also high in S (4 *wt%*), due to the addition of organic S during the tyre vulcanisation process.

Table 16 Proximate and ultimate analysis of brown coals and scrap tyre char (wt%, dry basis)

	Yallourn Lignite (YL)	Morwell Lignite (MW)	Loy Yang Lignite (LY)	Devolatilised tyre char/Catalyst
Volatile	54.57	54.65	56.70	0.04
fixed carbon	42.88	42.77	42.83	81.06
Ash	2.55	2.58	0.47	18.88
C	60.22	60.02	54.29	82.32
H	8.51	8.21	8.18	0.84
N	0.58	0.83	1.73	0.34
S	0.16	0.17	0.72	14.02
O (difference)	30.53	30.77	35.08	2.48

As for the ash composition in the fresh catalyst, XRF quantification in **Table 17** determined around 37% Zn in its oxide form, which is the second most prevalent element following SiO_2 (40.6 *wt%*). Ca and Al also account for 6.6 *wt%* (CaO) and 2.3 *wt%* (Al_2O_3), respectively. However, the other elements including Fe, Mg, Na and K are less than 2 *wt%* each, and hence, negligible. Note that, the contents of these elements are also comparable with the tyre char tested elsewhere [11]. However, the acid-solubility of the ash-forming elements is very different between our tyre char and the one in [11]. Upon the use of 5M HCl, only approximately half of the entire Zn was removed out of our catalyst [14], relative to a nearly complete removal for the tyre char studied in [11]. Apparently, the scrap tyre pyrolysis condition is crucial. The use of coarse tyre chip and a longer residence time (up to 5*h* at 800^{o}C) in our study caused the closure of voids in the carbonaceous matrix, which in turn inhibited the access of acid towards the inherent ash-forming elements. The TEM image (as shown in **Figure**

12a later) also confirmed a deep embedding of the ash-forming elements including Zn within the catalyst matrix.

Table 17 Elemental compositions of fresh and spent catalysts ash the most stable oxide form

	Fresh cat	Spent cat after one test	1st repeat	2nd repeat	3rd repeat
Overall ash content, wt% on dried catalyst basis					
	18.8	17.2	16.48	15.74	15.02
Ash composition, wt% on dried mass basis of overall ash					
SiO_2	40.6	41.18	42.48	42.71	42.84
ZnO	37	39.36	39.72	40.12	39.99
SO_3	8.5	4.62	2.58	1.98	1.42
CaO	6.6	7.54	7.84	8.12	8.21
Al_2O_3	2.3	2.36	2.89	2.02	2.03
Fe_2O_3	1.4	1.31	1.42	1.25	1.52
MgO	1.4	1.39	1.38	1.23	1.08
Na_2O	1.2	0.43	0.72	1.12	0.84
K_2O	1.0	1.03	0.97	1.45	2.07

6.2.2 Pyrolysis conditions

The pyrolysis experiment was constructed in a lab-scale horizontal fixed bed quartz tube with an inner diameter of 55 *mm* and a total length of 1 *m*. For most runs, approximately 30 g of dried lignite was physically blended with catalyst at a mass ratio of 50:50. The terminal temperature was varied from 600 to 900^{o}C, and the sample was heated up either slowly or quickly to each terminal temperature. For the slow heating, the sample was first placed in the middle of the reactor, which was then heated up at 10^{o}C/min together. The fast heating was instead achieved by a prior heating of the reactor to the set temperature, followed by a quick insertion of the sample into the middle of the reactor at an estimate heating rate of around

300°C/min. Note that, the whole reactor was fully protected by argon in the heat-up stage, while the sample was placed at the cold end of the reactor in the fast heating scheme. The holding time at a terminal temperature was kept at 20 *min* to ensure the completion of the pyrolysis reaction.

Two gas environments have been tested, including pure argon and steam-argon mixture at a volumetric ratio of 30:70, with a continuous flow rate of 400 mL/min in each run. This corresponds to a gas residence time of around 20 *s* inside the reactor. The released volatiles were cooled in four impinge trains in series, with ice and water mixture as the cooling agent in the first impinger, and dry ice/acetone mixture in the second to fourth impinger. The non-condensable gas was sent to a gas analyser (Sensotec Rapidox 5100) for on-line monitoring of the concentrations of GHC (gaseous hydrocarbons, C_1-C_4), CO, CO_2, O_2 and H_2. Note that, the GHC is mainly composed of methane (CH_4). Therefore, we simplify it as CH_4 in the reaction mechanism discussion section. Regarding the remaining chars inside the reactor, the separation of tyre char and lignite char was done by sieving into sizes of <2 mm and 2-4 mm, respectively. They were further dried in vacuum and weighed for its mass. A fairly good mass balance was achieved for all cases, with a maximum of 110% closure due to various errors generated in the individual steps, such as pyrolysis, sampling and product characterisation.

6.2.3 Coal tar analysis and characterisation

Upon the completion of each run, the resultant tar collected in the impingers was transferred and stored in a 100 ml Schott bottle. Subsequently, it was tested with a Karl Fischer Volumetric Titration to quantify the content of chemical water condensed within it. Elemental composition of the tar sample was determined using a CHNS Elementary Vario EL III. The chemical

compositions of tars were identified by gas chromatography-mass spectrometer (GC/MS) on an HP6890 instrument in a splitless auto mode, upon the conditions outlined in our previous work [16]. The identification of major compounds was conducted based on the library database shown in Appendix C.

Solvent fractionation of each tar sample was conducted to quantify the contents of light and heavy fractions within it. Same as defined previously [16], each tar sample was firstly mixed with n-hexane solution to extract out the hexane-soluble fraction, namely light oil hereafter. The n-hexane insoluble was further mixed with toluene to separate the toluene-soluble asphaltene and toluene-insoluble pre-asphaltene. Each insoluble residue was dried in a vacuum oven at 110 $^{\circ}$C to remove the solvent for a minimum 5 *h* before weighing.

6.2.4 Solid catalyst characterisation

The elemental composition within the fresh catalyst and spent ones were determined quantitatively using a pre-calibrated XRF (SPECTRO iQ II). All the elements are expressed as its most stable oxide form. X-ray Diffraction (XRD) patterns for both fresh and used catalysts were collected on a Rigaku SmartLab 3000A diffractometer with Cu Ka radiation (λ =0.15406 nm). The X-ray tube was operated at 40 kV and 15 mA. The Transmission Electron Microscopy (TEM) images and small-area electron diffraction (SAED) patterns were recorded using TEM (Model FEI Tecnai G2 T20 TWIN TEM) with an accelerating voltage of 200 kV.

The FTIR spectra of solids were recorded on a Perkin Elmer 2000 spectrometer in the 4000–400 cm^{-1} wave number range using diffuse reflectance infrared Fourier transform (DRIFT) technique. A spectrum of the solid sample was obtained using KBr dilution and finely

powdered KBr as reference. For acidity determinations by FTIR, sample of tyre char was heat-treated at 400 ºC overnight, followed by evacuation at ca. 10^{-5} Torr for 2 hrs and at the same temperature. Pyridine adsorption was performed at room temperature until saturation (60 mins). The sample was then evacuated for 10 mins at the 100 ºC and cooled to room temperature before recording the spectrum. The desorption of the probe molecule was successively monitored stepwise, by evacuating the sample for 10 mins at 150, 200, 300 and 400 ºC and cooling to room temperature between each step, to record the spectrum.

6.3 Results and Discussion

6.3.1 Pyrolysis and pyrolytic oil upgrading in inert argon

Figure 30 depicts the overall product yields of YL lignite with and without the addition of catalyst at the 600-900ºC. For the pyrolysis of YL lignite alone, its tar yield is maximised at 800ºC under both heating rates. A further increase in the temperature results in the generation of more non-condensable gases and chemical water, as an expense of the drop on tar yield. This is due to an enhanced secondary cracking of the volatile vapours [17]. Similarly, the use of fast heating rate widens the temperature discrepancy between coal particle (as well as its volatile vapour) and the carrier gas/reactor wall, thereby facilitating the secondary cracking reactions [17]. This is evident by an obvious reduction on the tar yield when the heating rate is shifted from slow to fast, especially at 700-900ºC.

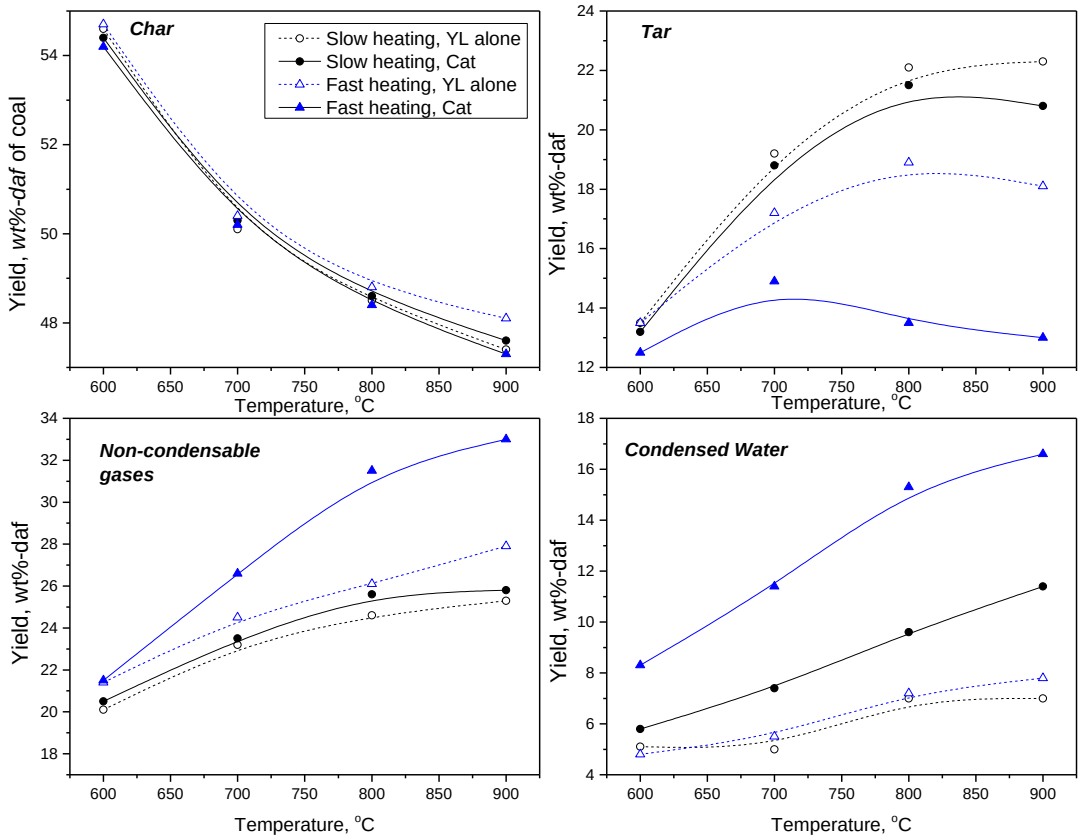

Figure 30 Product yields of YL lignite with and without catalyst (Cat:YL = 1:1, mass/mass) at a function of terminal temperature at two different heating schemes

The catalyst added into the lignite is influential in affecting all the products. Regardless of the heating rate, the solid char yields are decreased slightly in comparison to the lignite alone case. In the meanwhile, the tar yields dropped much more considerably, which is accompanied by the increase on the yields of the other two products, non-condensable gas and chemical water. Looking at the effect of reaction temperature, it is demonstrated that the catalyst effect is only pronounced from 700°C. In terms of the influence of heating rate, the fast heating scheme is clearly beneficial for the catalyst. For instance, at the terminal temperature of 800°C, the tar yield was reduced by around 5 *wt%* in the fast heating scheme, from ~ 18 *wt%* in the blank case to ~ 13 *wt%* upon the use of catalyst. However, in the slow heating scheme, the tar yield decrease only reaches around 2 *wt%*, which is rather insignificant in comparison to the tar yield

of 22 *wt%* in the blank case. The primary explanation can be assigned as a temperature – programmed gradual release of the volatile vapours in the slow heating scheme. Some of the volatile vapours are thus exposed to the catalyst surface at relatively low temperatures, e.g. <600^{o}C when the catalyst is still inactive, as demonstrated in **Figure 30**. Another reason could be the concentration or partial pressure for the volatile vapours surrounding the catalyst at a time. From the reaction rate perspective, an instant release of all the volatiles in the fast heating scheme creates a large pressure for the volatile vapours around catalyst, which in turn facilitates the surface reactions, and even the intra-particle diffusion through the catalyst voids. In contrast, in the slow heating scheme, a gradual release means there is always less momentum for the volatile vapours to undertake any catalysed reactions. Instead, they are more easily trapped on the surface of even inside the lignite char matrix [7,9], undertaking self - cracking reactions without the involvement of the added catalyst.

The GC-MS spectra for the 800^{o}C oil samples in **Figure 31** provide more information on the role of the catalyst under each heating scheme. For the slow heating scheme, both the two liquid oils have a lack of heavy hydrocarbons that are expected to elute out from the residence times above 40 min. This supports a preferential trapping of the heavy molecules within the lignite char matrix, due to their later release and smaller diffusion momentum. Nevertheless, the released small molecules from YL lignite are still upgraded by the catalyst, although they are released at relatively low temperatures. In this sense, the results here are indeed consistent with our previous observation for the bio-oil upgrading by the same catalyst at 600^{o}C [11]. For the major peaks referring to single aromatics (5.0-9.0 min), acidic compounds – aldehyde and ketone (6.5-7.4 min), phenolic compounds (9.4-10.2 and 15.3-22.8 min), and long-chain oxygenates hydrocarbons (~30 min), their intensities are clearly decreased by the use of the

catalyst. In the meanwhile, the intensity for the peaks located around 3.3-6.0 min for oxygen-free benzenic species are increased. These changes are more pronounced in the fast heating scheme, agreeing with the difference on overall product yields outlined in **Figure 30**. Another interesting point is the abundance of the heavy molecules (>40 min) derived from the fast heating of lignite alone, demonstrating an instant release of these species with the smaller ones together. Their peak intensity was effectively reduced by the catalyst. The area percentages in **Figure 32** (left panel) quantitatively proved the reduction on the major species by the catalyst. More specifically, based on the solvent fractionation result of each tar sample and its yield, the mass yields of individual fractions in a tar sample and their changes upon the addition of catalyst are further depicted in **Figure 32**. It is much clearer that the catalyst is able to cleave the heavy molecules (i.e. asphaltene and pre-asphaltene) into lighter fractions. More specifically, as indicated by the gas emission results in **Figure 33**, the oxygen-bearing volatile vapours including acids, phenols and long-chain oxygenates are upgraded into the respective aromatics, mainly via the catalytic decarbonylation for an enhanced release of CO in the gas phase. In contrast, the catalytic effect on the decarboxylation reaction should be marginal, as the yield of the resultant gas CO_2 is less affected. Furthermore, as suggested by the chemical water yield in **Figure 30**, the catalysed dehydration of phenolics is another major route for the deoxygenation of the crude tar.

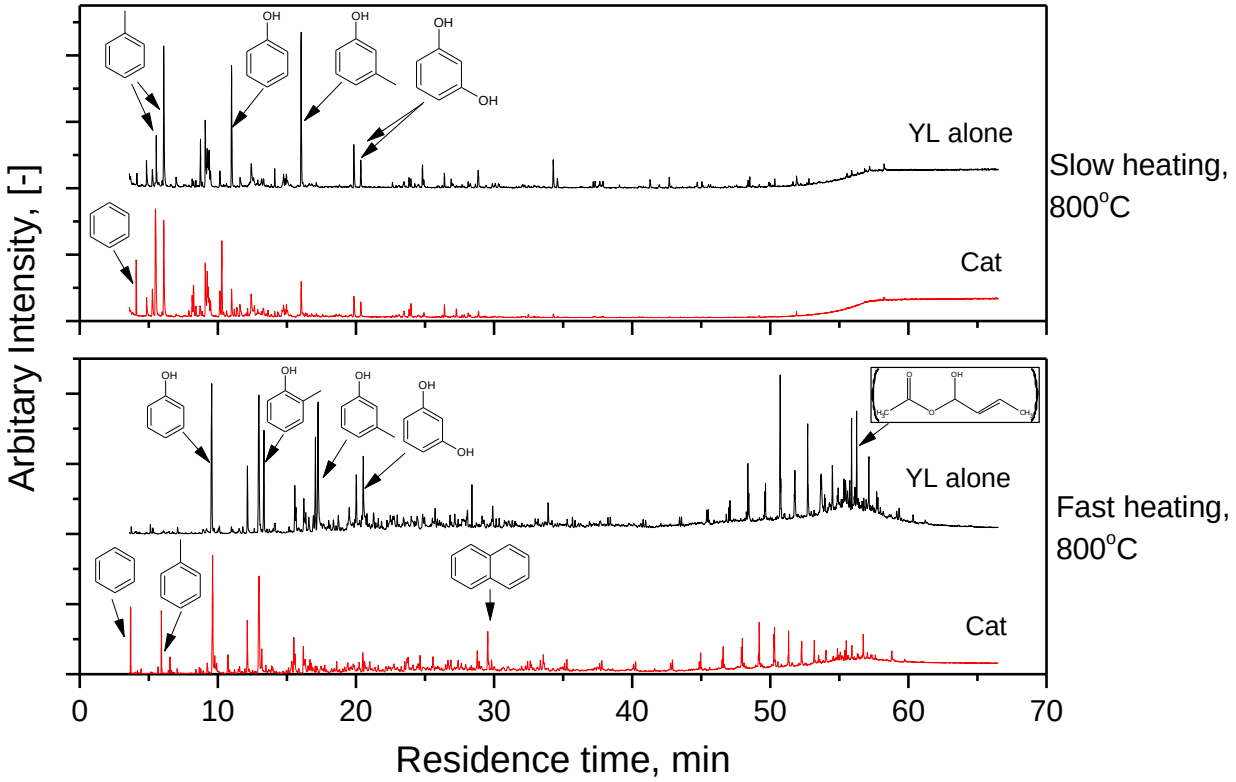

Figure 31 GC-MS spectra for the liquid tar samples collected from pyrolysis of YL lignite with and without catalyst at 800oC. The mass ratio of catalyst to YL lignite is fixed at 1:1.

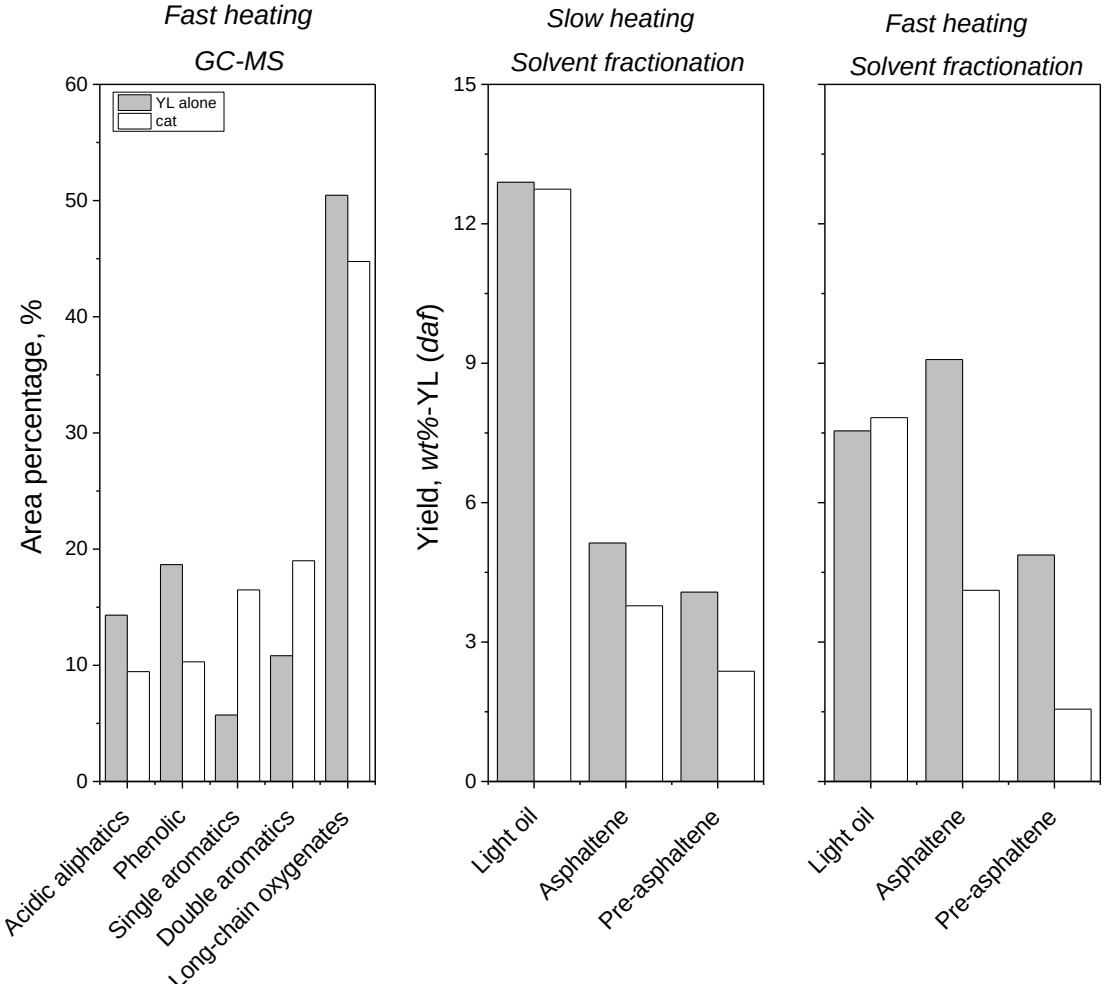

Figure 32 Solvent fractionation results for liquid tar samples and the GC-MS area-based percentages of the major species in tar. The liquid tar samples are collected from the pyrolysis of YL lignite in argon at 800°C, with and without the addition of catalyst at a mass ratio of 1:1 to YL lignite.

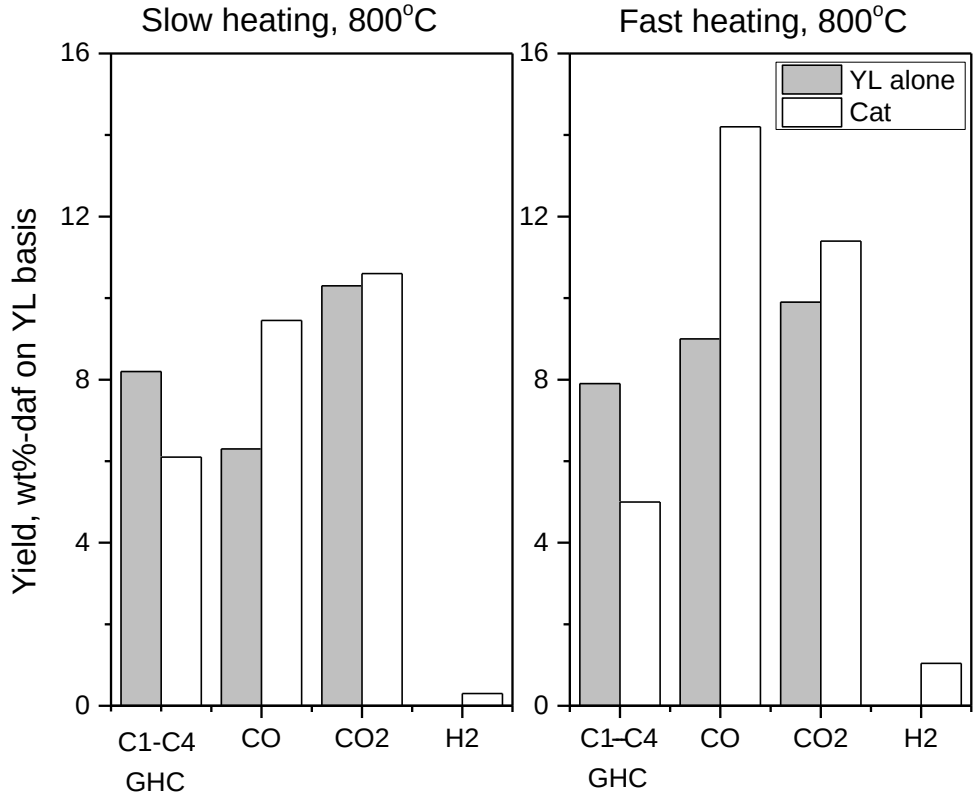

Figure 33 Gas product yields from the pyrolysis of YL lignite with and without catalyst (mass ratio of 1 to lignite) at 800°C.

The changes on the yields of another two gases including GHC and H_2 are more intriguing. Under both heating schemes, the reduction on the former species (mainly CH_4) is consistent, which should be achieved by the promoted methane-steam reforming reaction (MSR, **Equation 6.1** below). The steam should be derived from the inherent moisture and those formed from the dehydration reaction, whereas the catalytic effect of solid char on the MSR reaction is not surprising either. A number of studies have reported this phenomenon based on the test of coal char [18], $ZnCl_2$-laden biomass [11] and ZnO-laden bio-char [13] in the similar temperature window. In addition, back to **Figure 30**, the reduction on the solid char yield also suggests the catalysed char-steam gasification, as per reaction **Equation 6.2** below. This has

been proven by our previous work on a simple mixing of tyre char and lignite char for gasification tests in a thermo-gravimetric analyser (TGA) [25]. More specifically, the reduced char should be mainly the coke deposit derived from the thermal or catalytic cracking of the heavy molecules. Compared to a direct steam-reforming reaction (**Equation 6.3**) of the volatile vapour which has a very short contact with the catalyst, its coke deposit on the catalyst surface has much more chance to react with the active site and the activated $H^{\cdot}$ and $OH^{\cdot}$ from the dissociation of steam molecules [20].

Methane – steam reforming	$CH_4 + H_2O \rightarrow CO + 3H_2$	(6.1)
Char-steam reforming	$C + H_2O \rightarrow CO + H_2$	(6.2)
Tar - steam reforming	$C_xH_y + xH_2O \rightarrow xCO + (y/2 + 1) H_2$	(6.3)

The elemental compositions of the final liquid tar samples collected at 800^{o}C are shown in **Table 18**. One can clearly see a decrease on the O/C molar ratio upon the addition of catalyst, due to the aforementioned deoxygenation reactions. Here again, the stronger effect for the catalyst was confirmed in the fast heating scheme. Simultaneously, the increase on the H/C molar ratio is also achieved. However, such an achievement should not be simply attributed to the stripping of oxygen out of the tar. Instead, based on a calculation by multiplying the water-free tar yield and the content of H within it, and using the YL lignite as the reference (see **Equation 6.4** below), one can figure out the absolute amount of hydrogen (H_2) that has been stripped out from a tar by the catalyst employed here. The final calculation results are also listed in **Table 18**. It clearly demonstrates that the dehydrogenation reaction was also catalysed, in particular under the fast heating scheme. It further proved the plausibility of a direct steam-

reforming reaction for the volatile vapours that was suggested for the use of tyre char elsewhere [14], which strip the hydrogen out of the liquid tar as per **Equation 6.3**.

$$\text{Amount of } H_2 \text{ stripped out tar by catalyst} = (\text{Tar yield} * \text{H wt\%})_{\text{cat}} - (\text{Tar yield} * \text{H wt\%})_{\text{blank}} \quad (6.4)$$

Where the subscripts "cat" and "blank" refer to the pyrolysis of lignite with catalyst and without catalyst, respectively.

Table 18 Elemental analysis of YL lignite tars with and without catalyst (mass ratio of cat to coal at 1:1) at 800°C in slow and fast heating, wt% on dry-and-ash-free basis.

Elements	Slow heating		Fast heating	
	YL Lignite alone	With catalyst	YL Lignite alone	With catalyst
C	65.72	65.42	69.08	66.47
H	4.74	5.32	5.31	6.52
N	0.12	0.45	1.23	0.63
S	<0.3	<0.3	<0.3	<0.3
O	29.42	28.81	24.38	26.38
H/C	0.87	0.98	0.92	1.18
O/C	0.34	0.33	0.30	0.26
H_2 moles/100 moles-coal *(daf)*	10.0	10.9	9.6	8.4
H_2 stripped out of tar by catalyst, moles/100 moles-coal *(daf)*		-0.9	0.4	1.6

The same phenomenon was observed for the other two lignites summarised in **Figure 34**. Note that, only the results for fast heating at 800°C were provided here, considering that it is the best

condition that has been proved for YL lignite. For both lignites, upon the use of tyre char as the catalyst, the yields of tar and GHC were reduced by 8 *wt%* in total, which is compensated for a total increase of 7 *wt%* for chemical water, CO and H_2. These values are indeed quite consistent with the results observed for YL lignite. For instance, the tar yield for YL lignite also dropped by around 5 *wt%* by the use of catalyst in fast heating at 800°C (top right panel in **Figure 30**), whilst methane dropped by around 3 *wt%* (right panel in **Figure 33**). Such a large similarity between the three different lignites suggests that the catalyst employed here is insensitive to the absolute amount of volatile vapours exposed to its surface, or the limited catalyst surface is quickly saturated by the adsorption of the reactants. If that is the case, increasing the catalyst amount would be expected to further improve the reduction extent for both liquid tar and GHC.

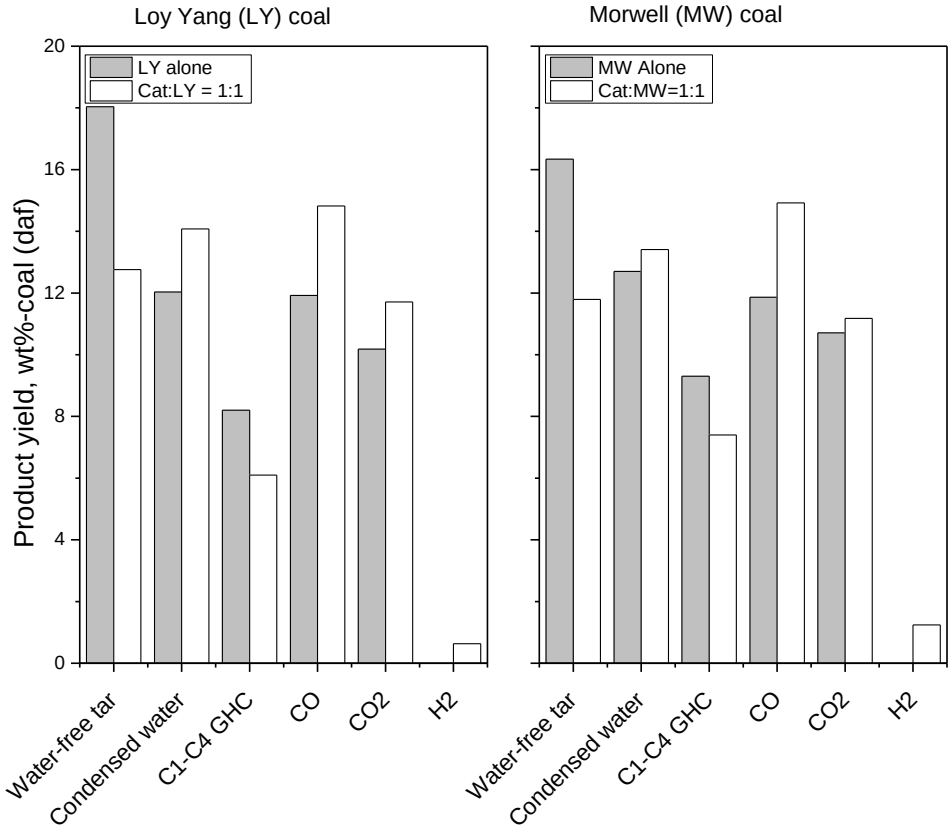

Figure 34 Comparison of product yields of Loy Yang and Morwell by the catalytic performance of tyre char at 800oC upon fast heating pyrolysis in argon. Again, the mass ratio of catalyst to lignite is fixed at 1.

6.3.2 Steam-assisted pyrolysis and pyrolytic oil reforming

Extra efforts were made by adding external steam into the system and also increasing the catalyst amount to boost all aforementioned reactions. Note that, the use of steam for pyrolysis is also reasonable in an industrial scale pyrolyser, because the combustion-derived hot flue gas is usually injected as an internal heating source inside the furnace [21]. Here again, the experiments were only conducted in fast heating and 800°C given the fact that these conditions have witnessed the best catalytic performance. In addition, only the YL lignite was tested.

Figure 35a depicts the overall product yields for four cases including the lignite alone in steam and other three cases with the catalyst to lignite mass ratio varying from 1 to 3. The results further confirmed a continual decrease on the char and tar yields with the use of catalyst and increase on the catalyst amount in the steam environment. This decrease is also accompanied by a stable increase on both gas and condensed water. Moreover, these changes are mostly attributed to the catalytic role on the first two reactions (**Equations 6.1** and **6.2**) mentioned above, rather than a simply additive effect. This is evident in **Figure 35b** where the catalyst alone only produced a tiny amount of gas (*i.e.* CO to be shown later). The additive calculation result based on the two blank runs (*i.e.* YL alone and catalyst alone in steam) is also far less than the real observation in terms of the individual product yield.

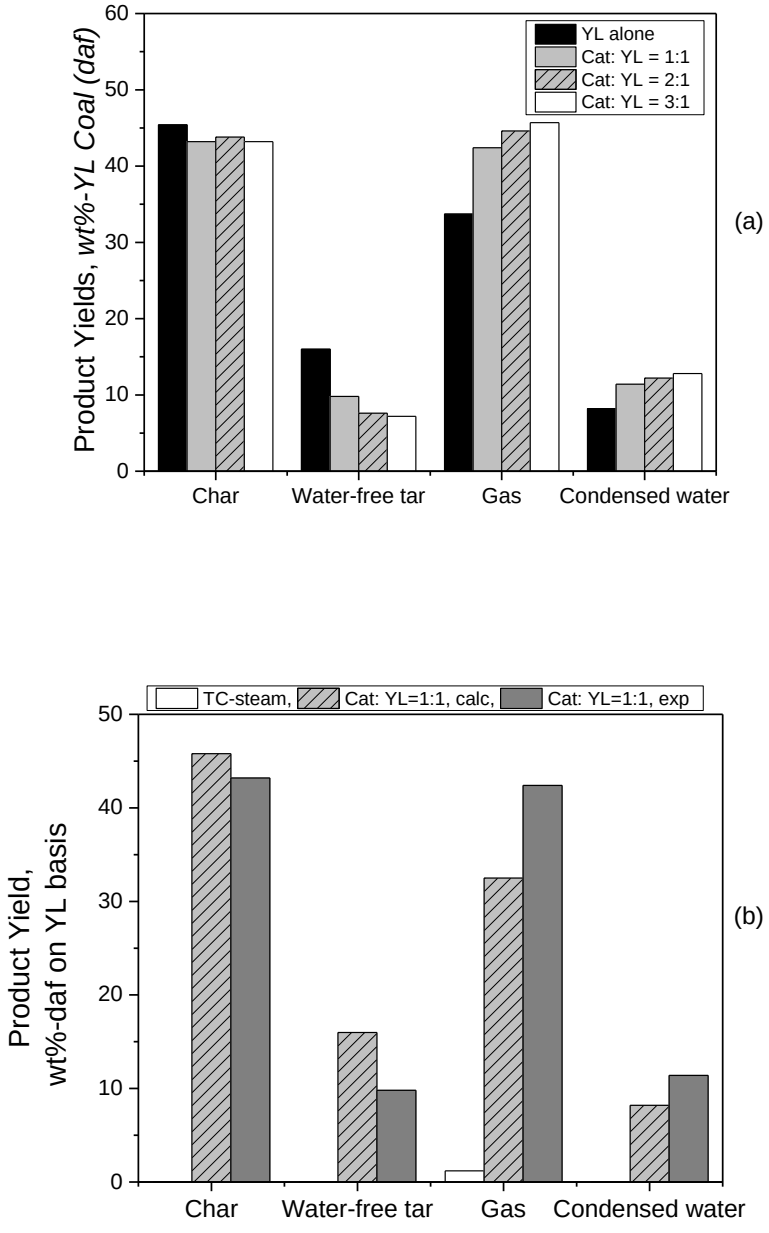

Figure 35 Overall product yields from the pyrolysis of YL lignite upon the addition of steam and varying amount of catalyst. The fast heating and a final temperature of 800oC were used.

The continual decrease on the tar yield is accompanied by a stable improvement on its quality. Their GC-MS spectra in **Figure 36** clearly demonstrates a significant increase of single aromatics at the residence time of 5.4 and 7.6 min upon the increase on the catalyst amount,

compared with the YL lignite case that contains mainly phenolic compounds and long-chain hydrocarbons. In the meanwhile, a stable decrease on the peak intensity for heavy hydrocarbons (>40 min), phenolics (9.4-10.2 and 15.3-22.8 min) and acids (6.5-7.4 min) is also evident. This is further quantitatively illustrated by area percentages in

Figure 37 (left panel). Upon the increase of the catalyst amount, the reduction on the long-chain oxygenates is most striking. In the case of using a catalyst to lignite mass ratio of 3, the area percentage for the entire long-chain oxygenates even dropped to a value which is far less than aromatics, suggesting that the catalyst is very strong at cleaving the chain length. The reduction on the long-chain species is also accompanied by phenolics and acids for an enhanced deoxygenation of these species. Quantitatively, the solvent fractionation results in

Figure 37b confirmed a significant reduction on the heaviest fraction, pre-asphaltene upon the use of three times amount for the catalyst, which is nearly fully removed that should in turn significantly alleviate the coke deposition on the catalyst surface.

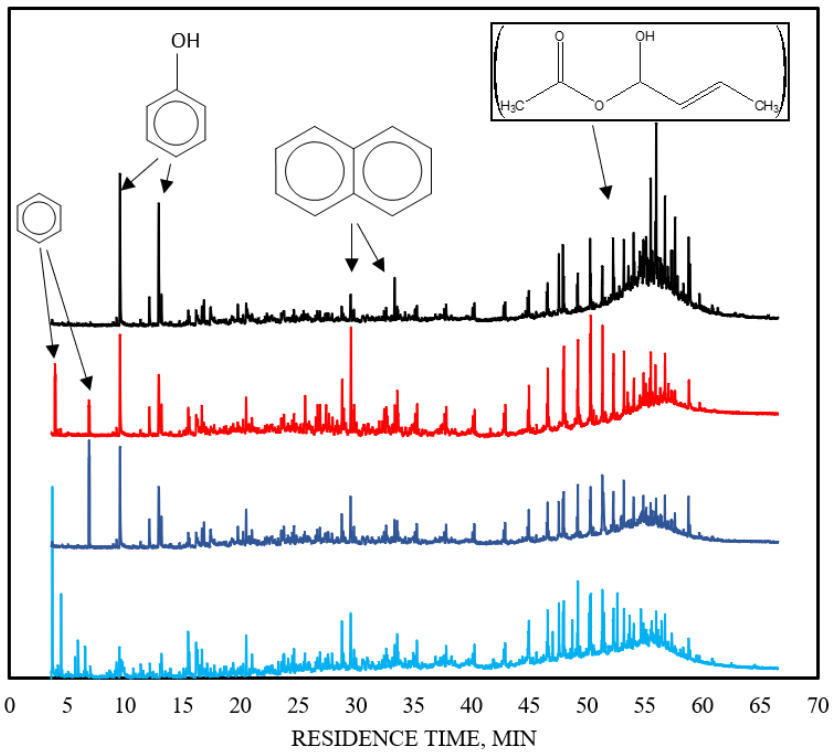

Figure 36 The GC-MS spectra for the liquid tar samples formed at upon the steam-assisted pyrolysis of YL lignite with the addition of different amounts of catalyst. The fast heating and a final temperature of 800°C were used.

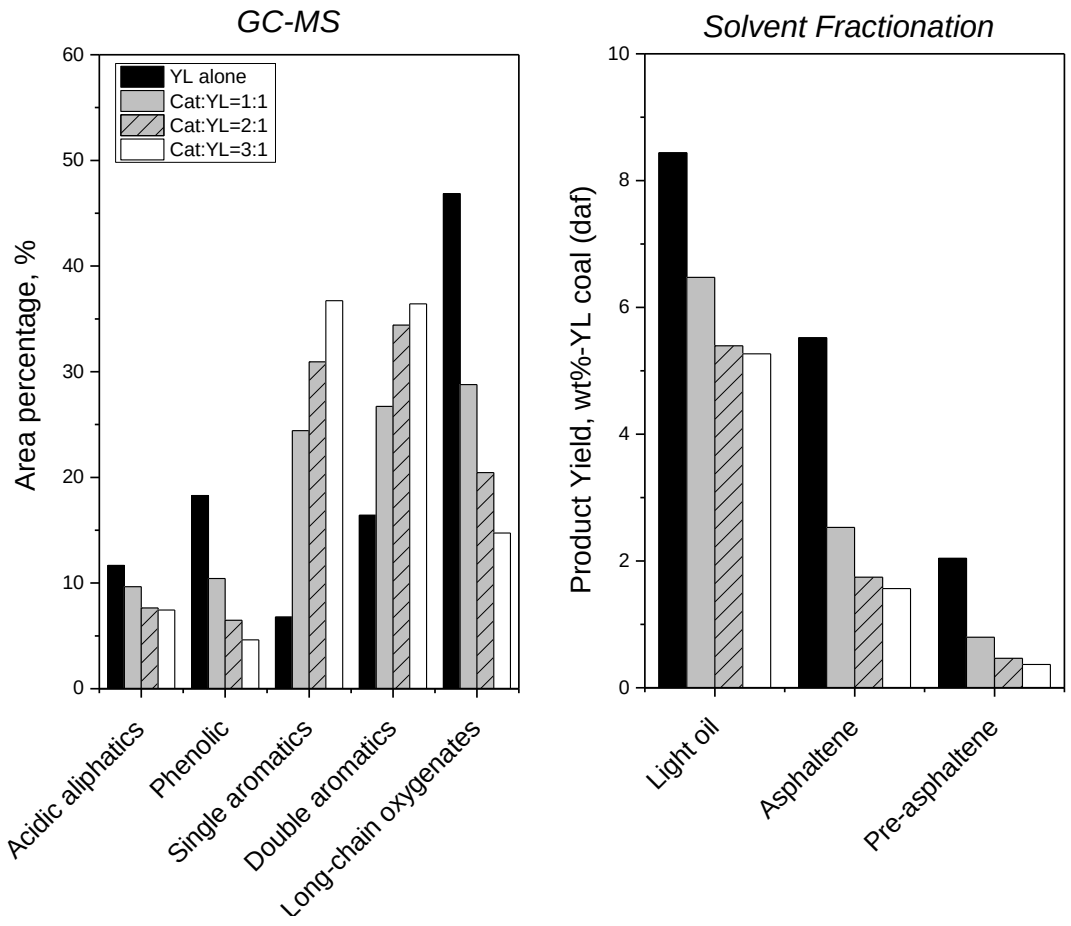

Figure 37 Solvent fractionation results for liquid tar samples and the GC-MS area-based percentages of the major species in tars. The tar samples were collected from a fast pyrolysis of YL lignite in steam at 800°C, with the addition of three different mass amounts of catalyst.

More specifically, the cumulative gas emission results in **Figure 38** confirmed a great improvement on the emission of CO from decarbonylation and even the two steam-involved reactions (**Equations 6.1 and 6.2**) mentioned above, since the yield of another product H_2 is also increased, whilst the amount of GHC is decreased continuously with increasing the catalyst amount. Here again, a portion of the new H_2 has also been stripped out by the catalytic

steam reforming of volatile vapours, as evident by the elemental analysis results for the liquid oil samples in **Table 19**, where a continual increase on the absolute amount of H_2 transferred out of the tar is clearly demonstrated.

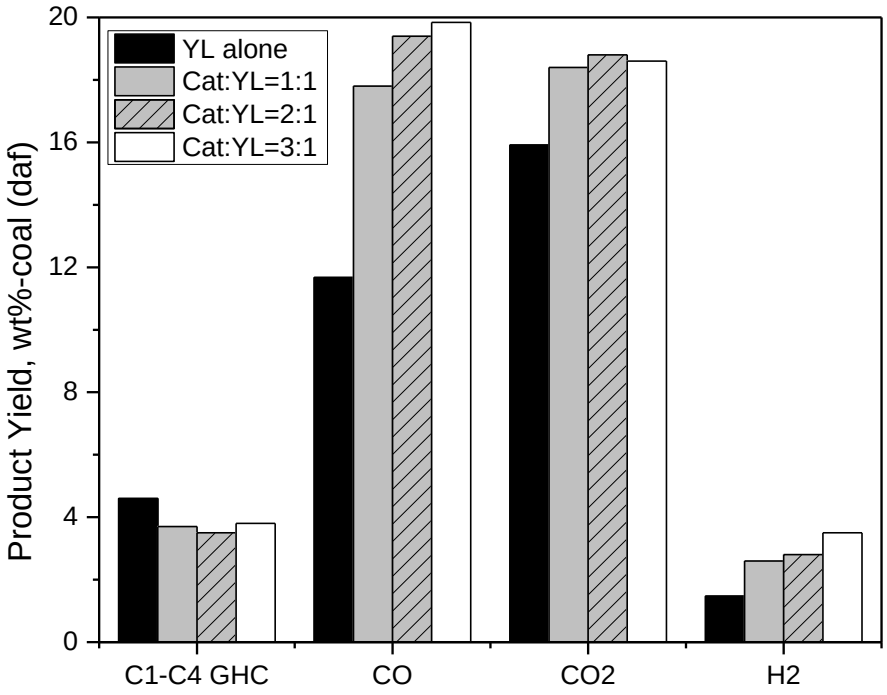

Figure 38 Individual gas product yields from the steam-assisted pyrolysis of YL lignite with the addition of different amount of catalyst. The fast heating and a final temperature of 800ºC were used.

Table 19 Elemental analysis of YL lignite tars with respect to the steam-assisted pyrolysis at 800°C in fast heating.

Elements	YL lignite alone	Cat: YL = 1:1 (mass ratio)	Cat: YL = 2:1 (mass ratio)	Cat:YL = 3:1 (mass ratio)
C	63.72	64.78	64.51	63.7
H	5.95	7.84	9.51	10.3
N	0.35	0.23	0.34	0.42

S	0.3	0.3	0.3	0.3
O	29.68	26.85	25.34	25.28
H/C	1.12	1.45	1.77	1.94
O/C	0.35	0.33	0.29	0.30
H_2 moles/100 moles-coal *(daf)*	8.5	7.4	6.9	7.1
H_2 stripped out of tar by catalyst, moles/100 moles-coal *(daf)*		1.1	1.6	1.4

6.3.3 Discussion on the Catalysis Mechanism

The time-resolved profile for the four major gases in **Figure 39** provides more details specifying the stage where the catalysed reactions had taken place. As shown for the emission of GHC, one can see a rather broad profile with a distinguishable shoulder (~12 min) for the YL lignite only in argon, suggesting the breakage of the methyl from different volatile groups. The major peak around 7 min should be assigned as light volatiles that are released quickly, whereas the shoulder one around 12 min should be derived from the relatively heavy ones, same as that has been observed elsewhere [28]. The addition of steam for YL alone clearly has no/little selectivity on the volatile size, since the peaks of both light and heavy ones are reduced. However, regardless of the use of external steam, the addition of external catalyst narrowed down the GHC profile considerably, with a significant reduction on the peak for the heavy volatiles.

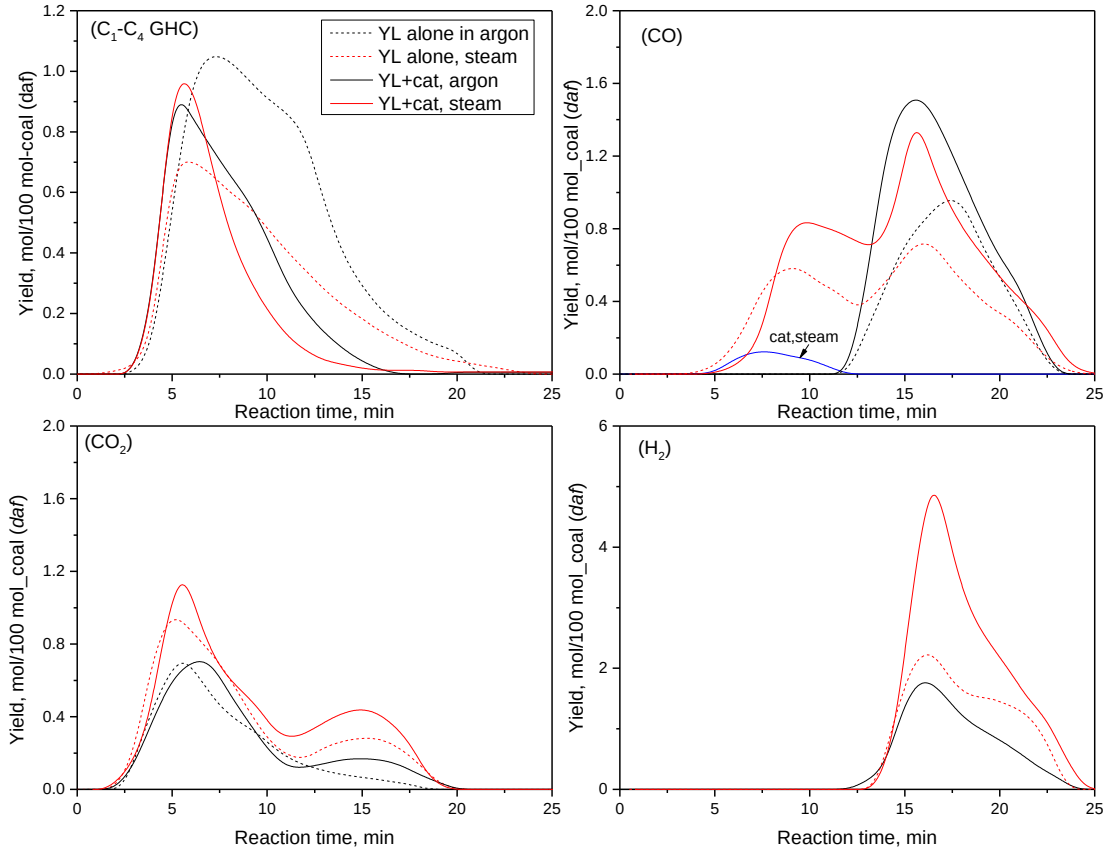

Figure 39(a) CH4; (b) CO; and (c) H2 (d) CO2 emissions from the fast pyrolysis of YL lignite in argon and steam at 800°C.

The results for the other three gases further support a two-stage release of volatiles and a preferential upgrading of the heavy ones by the catalyst tested here. As for CO_2, its abundant release before 10 min indicates a decarboxylation reaction for the light volatiles, which should be mainly occurred by thermal shocking. The addition of catalyst caused very limited changes on this peak. Instead, it is more pronounced for the change on the second peak around 15 min that can be assigned as the WGS reaction. Since the peaks of both CO and H_2 at the same residence time are enhanced greatly by the catalyst, it is referrable that the WGS reaction takes place instantly after the production of CO and H_2 on the catalyst surface. These two species are certainly mainly derived from the heavy volatiles that are easily and selectively trapped by the catalyst. Our previous study on bio-oil has confirmed the abundance of mesopores (2-50 nm)

for the catalyst employed here [14], which should be responsible for an easy trapping of the heavy volatiles. More specifically, upon an initial cracking within the catalyst, the resultant coke deposit remains on the catalyst surface, which subsequently has a relatively longer residence time and more chance to be gasified via the reaction, **Equation 6.2**.

The emission of CO for light volatiles before 12 min is also interesting. Such a peak is missing in the two argon cases, further indicating that fewer of the light volatiles had undertaken the decarbonylation reaction upon a thermal shock, even with the presence of the external catalyst. However, upon the addition of external steam, the emission of CO from the early stage was clearly promoted, in particular in the case that catalyst was blended into the lignite. This is a strong evidence for the char-steam gasification reaction (from both external tyre char and the nascent YL char generated at the early stage) that occurs at the same time span, as evident by the blank case of testing catalyst (tyre char) alone in steam.

The next question is the catalytically active site that is present on the tyre char. Our previous study on bio-oil upon the use of original tyre char and its acid-washed counterpart has indirectly proved that the inherent minerals in tyre char are catalytic [14]. More specifically, it should be the Zn-bearing species considering that it is the second most abundant element that is also unique when compared with coal char. As suggested by the classic decarbonylation theory for sulphide [7-13], the transition metal which is Zn^{2+} here should serve as the Lewis acid site for the cracking of intermolecular covalent bonds. However, the S is also suggested as the active sites to scissor the intramolecular C-O bonds. If that is the case, both Zn and S are apparently essential. As presented in **Figure 40a and b**, the nano-sized ZnS crystal is highly abundant and dispersed inside the fresh tyre char matrix, with a d-spacing of 0.31 nm (0 0 2 facet) that is the distinctive fingerprint of wurtzite. However, for the spent tyre char collected from the steam

environment in **Figure 40c and d**, the catalyst particles became more homogeneous with the individual sizes (less than 50 nm) agglomerating together. The clear fringe d-spacing value in **Figure 40d**, 0.26 nm corresponds to the crystallized ZnO (0 0 2 facet). Such a change suggests that ZnS has partially transformed into ZnO when the catalyst was exposed to the O-bearing volatile vapours. More specifically, it provided a clue that S should be involved in the cracking/cleavage reactions for the C-O bonds. As a result, a portion of S have left the catalyst surface and converted into gaseous products. This is confirmed by the XRF analysis of the spent catalysts in **Table 17**. In terms of the most stable oxide form, the SO_3 content in catalyst dropped by 1.6 *wt%* when tyre char catalyst were used in argon. Furthermore, the use of steam caused an extra drop on the SO_3 content down to 4.62 *wt%*, relative to 8.5 *wt%* in the original catalyst. This means the S should also promote the dissociation of water for the gasification reaction, and even promote the activation of the subsequent deoxygenation reaction.

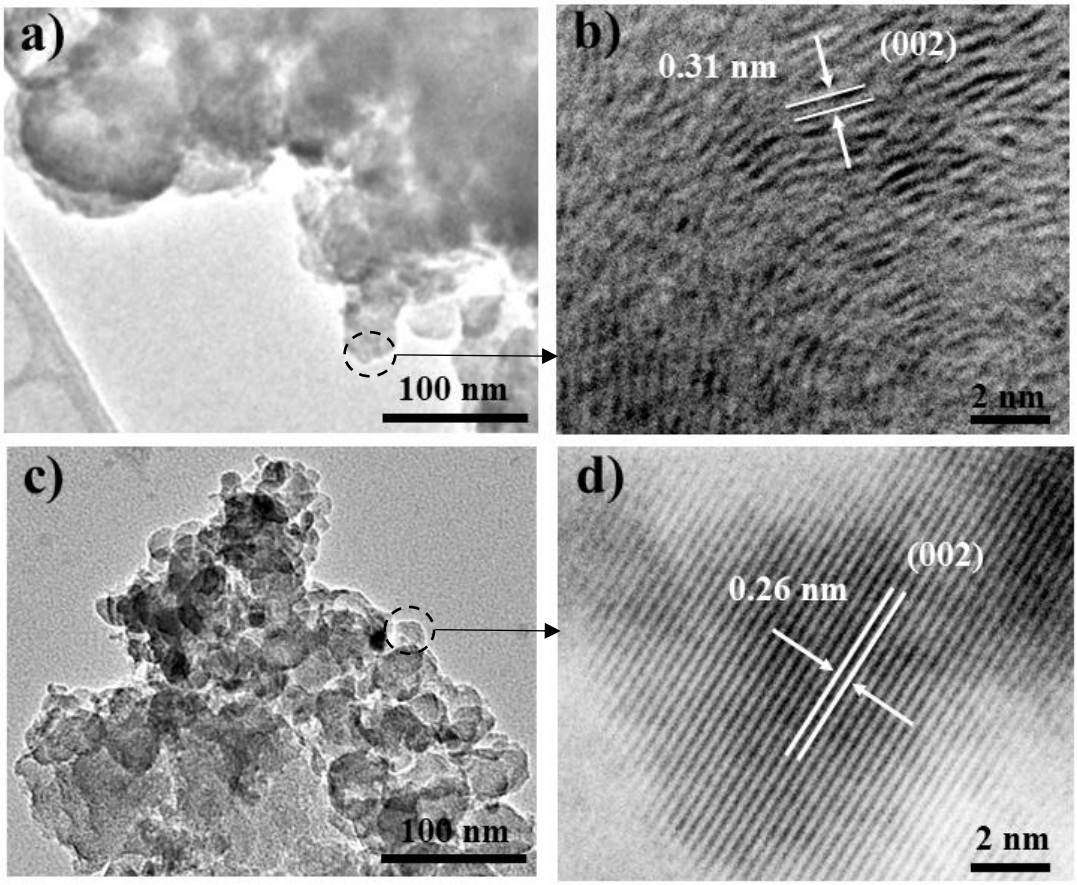

Figure 40 TEM images of fresh tyre char and used tyre char after steam catalysis condition. (a) and (b) are for fresh tyre char at different magnifications, (c) and (d) are used tyre char after steam catalysis condition at different magnifications.

If the above speculation is correct, it is thus a question regarding the role of Zn^{2+}. As a Lewis acid, it can dissociate water by preferentially adsorbing the OH^- hydroxyl [13]. If that is the case, the adsorption of O-bearing functional groups from oil and a subsequent cleavage of the C-O bond are also plausible. This in turn promotes the release of CO_x (CO and CO_2), and even H_2 derived from water gasification, as reported for $ZnCl_2$ in [11] in the gas phase. Therefore, the acidity of the catalyst played a significant role in determining the strength of the catalytic effect. Three cycle tests on the spent catalyst were further performed to prove the above hypothesis. The experimental conditions were fixed at 800°C, fast heating in steam, and use of

a mass ratio of 1 for catalyst to YL lignite. From **Table 20**, it can be observed that the Lewis acidity of tyre char, as opposed to Brønsted acid, reduced notably from 88.46 to 84.41, and from 84.41 to 60.17 upon the three further repeated use of tyre chars, due to the significant formation of ZnO and the loss of ZnS as noticed from **Figure 41**.

Table 20 The FTIR pyridine of tyre chars with respect to fresh tyre char and the used tyre chars in argon and the cyclic tests in the steam-assisted pyrolysis at 800°C, upon a fast heating.

Used tyre chars from steam experiment	Bronsted acid (μmol/g)	Lewis acid (μmol/g)	Total pyridine acidity (μmol/g)
Fresh Catalyst	0.11	32.10	38.41
Argon	6.75	33.14	39.89
Steam (1:1 mass ratio)	5.07	88.46	93.52
Steam (1:2 mass ratio)	6.08	89.76	95.84
Steam (1:3 mass ratio)	4.83	93.43	98.26
1st use in steam	5.07	88.46	93.52
2nd use in steam	4.03	84.41	88.45
4th use in steam	5.06	60.17	65.23

As for the product yields depicted in **Figure 41**, although the change on the solid char yield is a bit unclear due to the experimental error, the changes on the other three overall products are obvious. Upon increasing the repeating number, the water-free tar yield clearly increased until reaching to the level comparable to the reference case for the pyrolysis of the lignite alone in steam. In the meanwhile, both the gas product and chemical water yields dropped to the similar level with the reference case. The changes for individual non-condensable gases on the right panel also showed the same trend.

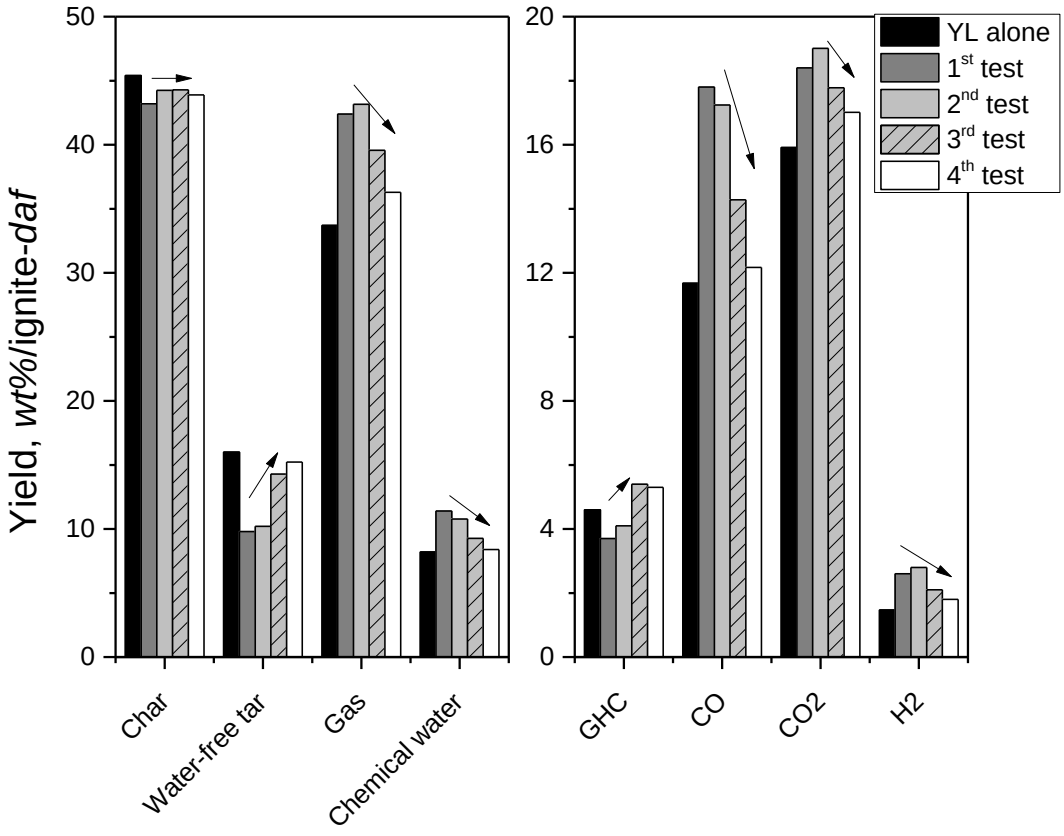

Figure 41 Changes on the product yield versus the repeating test number under the conditions of 800oC, fast heating in steam and catalyst to lignite mass ratio of 1.

Besides that, from the results of GC/MS presented in **Figure 42** and **Fig. 43**, it clearly demonstrates a notable decrease of the single aromatics at the residence time of 5.4 and 7.6 min, in the meantime, a significant increase of phenolics (9.4-10.2 and 15.3-22.8 min) and heavy hydrocarbons (>40 min), upon the repeated use of tyre char.

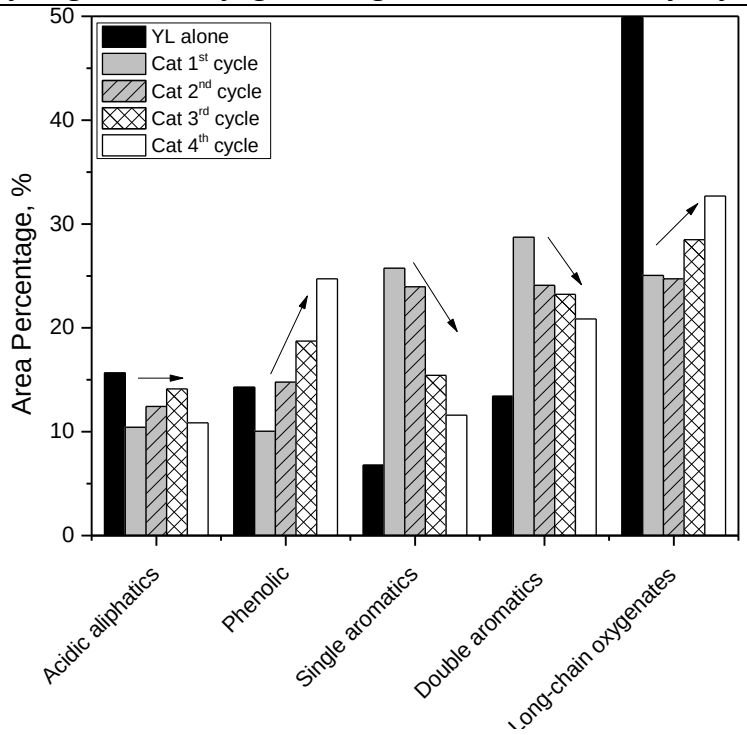

Figure 42 Changes on the liquid tar composition (GC-MS results) versus the repeating test number under the conditions of 800oC, fast heating in steam and catalyst to lignite mass ratio of 1.

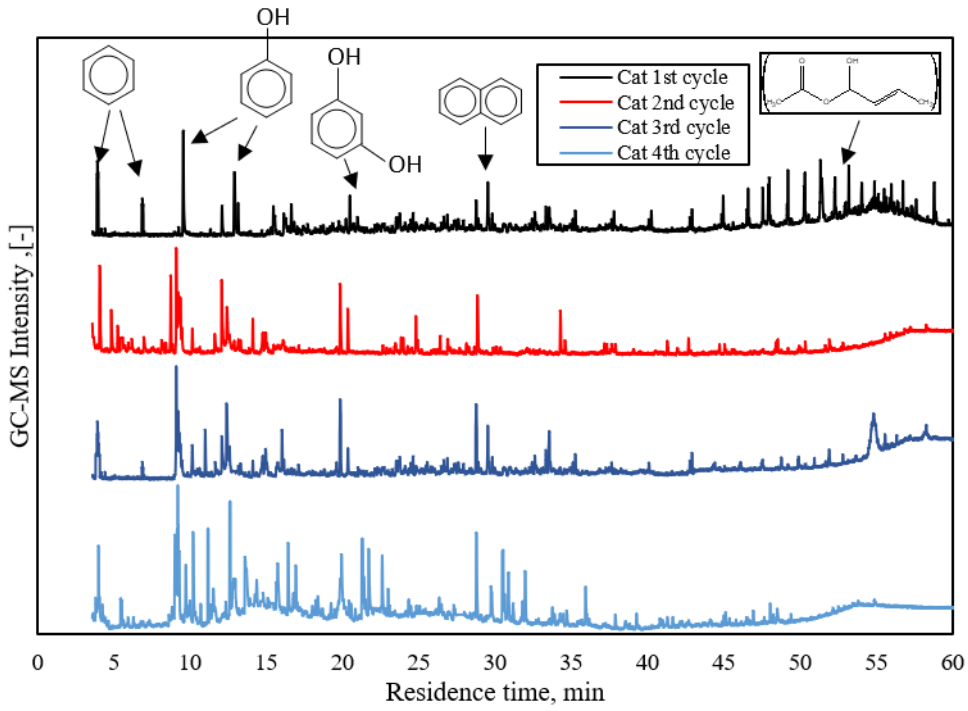

Figure 43 GC-MS spectra for the different catalyst cycle results shown in Figure 14.

Likewise, the elemental analysis of lignite oils presented in **Table 21** also showed that the O/C content of lignite oils was increasing between 0.30 and 0.33 from the first use all the way to the fourth use of catalyst. Besides, the effectiveness of the stripping of hydrogen also showed to be reduced along with the cycle tests, in which the net hydrogen stripped out was found to be reducing from 1.1 to 0.0. Clearly, these evidences demonstrated a deterioration of the catalytic function for the tyre char used under the pyrolysis conditions here. The principal factor should be attributed to the loss of S upon the repeating test, as tabulated in **Table 17**. In this sense, the presence of S within the catalyst employed here is essential, which initiates the deoxygenation reactions of volatile vapours. Compared to ZnO, ZnS was also reported to have a higher acidity that is in favour of the catalytic reactions confirmed here [23-24]. Moreover, regarding the remaining ZnO on the spent catalyst surface, its poor performance should be due to its agglomeration as evident in **Figure 40**. Upon the increase on the repeating test number, this phenomenon should become more severe, thus deteriorating the catalytic function of ZnO rapidly.

Table 21 Elemental analysis of YL lignite tars with respect to the cyclic test of tyre char in the steam-assisted pyrolysis at 800°C, upon a fast heating.

Elements	Coal alone	1st cycle	2nd cycle	3rd cycle	4th cycle
C	63.72	64.78	65.32	64.72	63.48
H	5.95	7.84	8.39	5.80	5.71
N	0.35	0.23	0.26	0.30	0.35
S	0.3	0.3	0.3	0.30	0.3
O	29.68	26.85	25.73	28.88	30.16
H/C	1.12	1.45	1.50	1.79	1.09
O/C	0.35	0.33	0.30	0.33	0.36

H_2 moles/100 moles-coal *(daf)*	8.5	7.4	8.1	8.4	8.6
H_2 stripped out of tar by catalyst, moles/100 moles-coal *(daf)*		1.1	0.4	0.1	0.0

Clearly, these evidences demonstrated a deterioration of the catalytic function for the tyre char used under the pyrolysis conditions here. The principal factor should be attributed to the loss of S upon the repeating test, as tabulated in **Table 17**. In this sense, the presence of S within the catalyst employed here is essential, which initiates the deoxygenation reactions and the hydrogenation of volatile vapours as well. Compared to ZnO, ZnS was also reported to have a higher acidity that is in favour of the catalytic reactions confirmed here [30]. Moreover, regarding the remaining ZnO on the spent catalyst surface, its poor performance should be due to its agglomeration as evident in **Figure 40c**. Upon the increase on the repeating test number, this phenomenon should become more severe, thus deteriorating the catalytic function of ZnO rapidly.

Finally, the total amounts of the three direct oxygen components: CO_2, CO and H_2O were used to quantify the deoxygenation extent for the pyrolysis of YL lignites in the condition of argon and steam with the catalysts tested here. Clearly, a positive correlation can be seen between the acidity of the catalysts and both deoxygenation extent, demonstrating a non-linear increase from 26.36 wt% for 39.89 μmol/g to 27.68 wt% for 65.23 μmol/g, and from 33.26 wt% for 88.45 μmol/g to 35.30 wt% for 93.52 μmol/g and finally to 35.60 wt% for 98.26 μmol/g. In contrast, the tar yield is reduced from 20.5 wt% for 39.89 μmol/g to 16.20 wt% for 65.23 μmol/g, and from 10.2 wt% for 88.45 μmol/g to 9.80 wt% for 93.52 μmol/g and finally to 7.60

wt% for 98.26 μmol/g. It should be noted that the overall deoxygenation extent presented here is much lower than those on the elemental analysis of liquid tar results in **Table 6** in which the O/C of tars (water-free basis) is reduced from 0.30 to 0.33% by the 1st cycle to 4th cycle of tyre char catalysts. This difference should be partially attributed to the non-condensable light moieties in the gas phase that were not included in the calculation here. In this sense, the results in **Figure 44** are rather conservative. Nevertheless, these results indicate the importance of the acidity on the catalytic effectiveness due to the fact that the transition metal serves as Lewis acid site would break down the intermolecular covalent bonds between polymers whereas sulphur acts as the active sites would scissor the intramolecular C-O bonds.

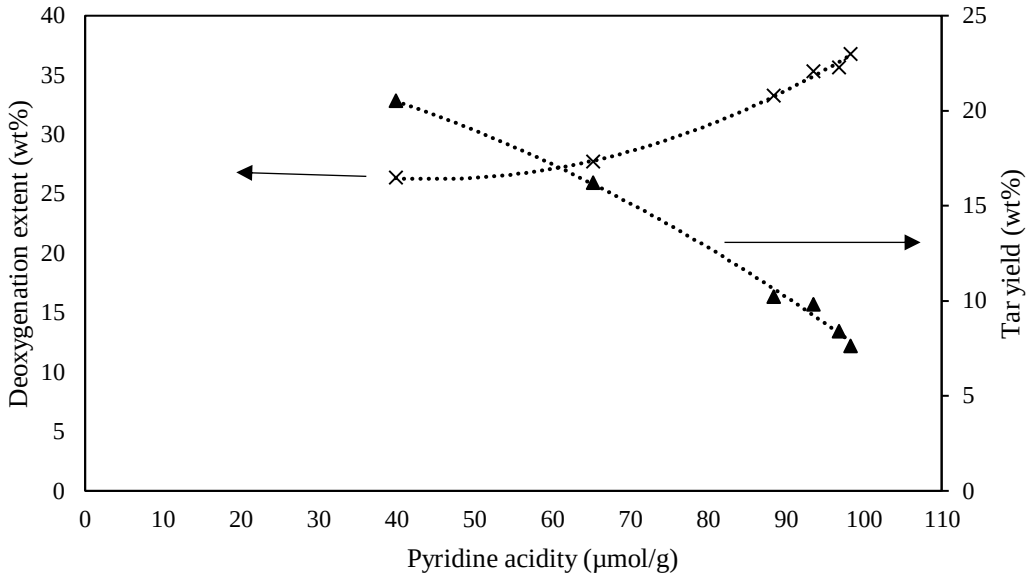

Figure 44 The relationship between the acidity of catalysts and both deoxygenation extent and tar yields.

6.4 Conclusion

This paper examined the catalytic performance of tyre char on the catalytic pyrolysis of lignite at a variety of temperatures, and the use of different gas environment (*i.e.* argon versus steam) and different catalyst to lignite mass ratios. The major conclusions can be drawn as follows:

1) The catalytic effect is more profound for the upgrading of the volatile vapours released from fast heating at a minimum temperature of 700^{o}C, although the contact time is extremely short. In an inert gas environment such as argon, the heavy molecules are preferentially upgraded via catalytic scission and decarbonylation reactions.
2) The coke deposit derived from the cracking of heavy volatiles and methane are also catalysed for the respective char-steam gasification and methane reforming reaction, respectively. The steam derived from the inherent moisture has participated into these reactions, and the resultant gaseous H_2 has a comparable yield to those reported previously. The addition of external steam and increase on the catalyst amount further promoted the gasification of lignite char and/or coke derived from the heavy volatiles, thereby improving the H_2 and syngas yields considerably.
3) The upgrading of liquid tar is favoured by both catalytic deoxygenation and the subsequent steam-reforming reactions. It is also favoured upon the contact of light volatiles with the catalyst at the early stage of the entire pyrolysis process, in particular under the inert gas. In contrast, the heavy volatiles that are easily trapped within the catalyst matrix preferentially undertook cleavage, decarbonylation and the subsequent gasification reactions (for its coke derivative).
4) The nano-sized Zn-bearing species are responsible for the co-production of H_2-rich syngas and upgraded liquid oil. In particular, the S-bearing active sites are essential and responsible for most of the deoxygenation reactions. Regarding the remaining ZnO-

bearing particles, they underwent severe agglomeration upon a repeating usage, thereby losing the catalytic function rapidly.

6.5 Acknowledgements

This work was supported by the Australian Research Council (ARC) under its Industrial Research Training Hub (150100006) scheme for the joint project between Monash and Cleantech Energy Australia (formerly Coal Energy Australia). The scrap tyre used in this project was provided by the Tyrecycle Pty Ltd, Australia is also acknowledged.

6.6 References

1. Liu C, Wang H, Karim A, Sun J, Wang Y. Catalytic fast pyrolysis of lignocellulosic biomass. Chemical Society reviews. 2014 05/07;43.
2. Wang M, Jin L, Li Y, Lv J, Wei B, Hu H. In-situ catalytic upgrading of coal pyrolysis tar coupled with CO2 reforming of methane over Ni-based catalysts. Fuel Processing Technology. 2018 2018/08/01/;177:119-28.
3. Liu Y, Yan L, Bai Y, Li F. Catalytic upgrading of volatile from coal pyrolysis over faujasite zeolites. Journal of Analytical and Applied Pyrolysis. 2018 2018/06/01/;132:184-9.
4. Han Y, Gholizadeh M, Tran C-C, Kaliaguine S, Li C-Z, Olarte M, et al. Hydrotreatment of pyrolysis bio-oil: A review. Fuel Processing Technology. 2019 2019/12/01/;195:106140.
5. Gollakota ARK, Reddy M, Subramanyam MD, Kishore N. A review on the upgradation techniques of pyrolysis oil. Renewable and Sustainable Energy Reviews. 2016 2016/05/01/;58:1543-68.
6. Rahman MM, Liu R, Cai J. Catalytic fast pyrolysis of biomass over zeolites for high quality bio-oil – A review. Fuel Processing Technology. 2018 2018/11/01/;180:32-46.
7. Baloch HA, Nizamuddin S, Siddiqui MTH, Riaz S, Jatoi AS, Dumbre DK, et al. Recent advances in production and upgrading of bio-oil from biomass: A critical overview. Journal of Environmental Chemical Engineering. 2018 2018/08/01/;6(4):5101-18.

8. Bouvier C, Romero Y, Richard F, Brunet S. Effect of H2S and CO on the transformation of 2-ethylphenol as a model compound of bio-crude over sulfided Mo-based catalysts: propositions of promoted active sites for deoxygenation pathways based on an experimental study. Green Chemistry. 2011;13(9):2441-51.

9. Zhou Q, Zarei A, De Girolamo A, Yan Y, Zhang L. Catalytic performance of scrap tyre char for the upgrading of eucalyptus pyrolysis derived bio-oil via cracking and deoxygenation. Journal of Analytical and Applied Pyrolysis. 2019 2019/05/01/;139:167-76.

10. Al-Rahbi AS, Williams PT. Hydrogen-rich syngas production and tar removal from biomass gasification using sacrificial tyre pyrolysis char. Applied Energy. 2017;190:501-9.

11. González JF, Román S, Bragado D, Calderón M. Investigation on the reactions influencing biomass air and air/steam gasification for hydrogen production. Fuel Processing Technology. 2008 2008/08/01/;89(8):764-72.

12. Zhang C, Liang X, Liu S. Hydrogen production by catalytic dehydrogenation of methylcyclohexane over Pt catalysts supported on pyrolytic waste tire char. International Journal of Hydrogen Energy. 2011 2011/07/01/;36(15):8902-7.

13. Zhang S-p, Chen Z-q, Cai Q-j, Ding D. The integrated process for hydrogen production from biomass: Study on the catalytic conversion behavior of pyrolytic vapor in gas–solid simultaneous gasification process. International Journal of Hydrogen Energy. 2016 2016/05/04/;41(16):6653-61.

14. Altuntaş Öztaş N, Yürüm Y. Effect of Catalysts on the Pyrolysis of Turkish Zonguldak Bituminous Coal. Energy & Fuels. 2000 2000/07/01;14(4):820-7.

15. Li C-Z. Some recent advances in the understanding of the pyrolysis and gasification behaviour of Victorian brown coal. Fuel. 2007 2007/08/01/;86(12):1664-83.

16. Kong J, Zhao R, Bai Y, Li G, Zhang C, Li F. Study on the formation of phenols during coal flash pyrolysis using pyrolysis-GC/MS. Fuel Processing Technology. 2014 2014/11/01/;127:41-6.

17. Nelson PF, Smith IW, Tyler RJ, Mackie JC. Pyrolysis of coal at high temperatures. Energy & Fuels. 1988 1988/07/01;2(4):391-400.

18. He T, Sun Z, Wu J, Xu Z, Zhang D, Han D. Catalytic Performance of Coal Char for the Methane Reforming Process. Chemical Engineering & Technology. 2015 01/01;38.

19. Issac M, Dai B, Zhang L. Kinetics underpinning the C-CO2 gasification of waste tyre char and its interaction with coal char upon co-gasification. Fuel. 2019 2019/11/15/;256:115991.

20. Matsuhara T, Hosokai S, Norinaga K, Matsuoka K, Li C-Z, Hayashi J-i. In-Situ Reforming of Tar from the Rapid Pyrolysis of a Brown Coal over Char. Energy & Fuels. 2010 2010/01/21;24(1):76-83.

21. Garcia-Nunez JA, Pelaez-Samaniego MR, Garcia-Perez ME, Fonts I, Abrego J, Westerhof RJM, et al. Historical Developments of Pyrolysis Reactors: A Review. Energy & Fuels. 2017 2017/06/15;31(6):5751-75.

22. Zhao H, Jin L, Wang M, Wei B, Hu H. Integrated process of coal pyrolysis with catalytic reforming of simulated coal gas for improving tar yield. Fuel. 2019 2019/11/01/;255:115797.

23. Zhou L, Yang H, Wu H, Wang M, Cheng D. Catalytic pyrolysis of rice husk by mixing with zinc oxide: Characterization of bio-oil and its rheological behavior. Fuel Processing Technology. 2013 2013/02/01/;106:385-91.

24. K Tanabe TY. Basicity and acidity of solid surfaces. Journal of the Research Institute for catalysis. 1964;11(3):179-84.

This page is intentionally left blank

Chapter 7- Conclusions and Recommendations for Future Work

This page is intentionally left blank

7.1 Conclusions and innovation of research

This thesis has for the first time presented a detailed study on the pyrolysis of waste tyre and Victorian brown coals, and the potential upgrading technologies for the resultant tar oils through the control of the operating conditions and utilisation of tyre chars as catalyst. The results provide a pathway for the design and optimisation of industrial waste tyre and Victorian brown coal pyrolysis applications, based on several major conclusions derived from the result chapters.

7.1.1 Chemical-based kinetic modelling of tyre pyrolysis

Firstly, the development of a modified chemical percolation devolatilization (M-CPD) model that includes key parameters such as the heat transfer mechanism, vapour-liquid equilibrium primary pyrolysis and cracking reactions of volatiles to describe the pyrolysis of waste scrap tyre chip, as well as to examine the influence of operating conditions on the scrap tyre pyrolysis product yields has been developed and validated. Based on the modelling and experimental results, it was found that the operating conditions such as fast heating (110°C/min), large chip size (6-15 mm) and volatile residence time (6.9 min) are conducive for severe secondary cracking of tar. This scheme results in 115 °C of temperature gap between the centre of a tyre chip and the reactor wall, noticeably resulting in the delay on the heating of the tyre chip and subsequently the release of volatiles. As a result, it performanced the secondary cracking with an extent of 17 %. By reducing the heating rate from 100 to 10°C, the temperature gap reduced from 115 to 20°C; as a result, the cracking extent was minimised to 7 *wt%* on dry basis.

7.1.2 Secondary reactions of tyre volatiles upon the influences of pyrolysis temperature discrepancy and gas environment

The use of a carrier gas such as in the industry-scale moving bed or rotary kiln is found beneficial in improving the tar yield and aliphaticity, due to the minimisation of the temperature discrepancy (i.e. gap) and the resulting secondary reactions. Upon an increase in the temperature discrepancy by either increasing the heating rate or tyre chip size, the inherent long-chain aliphatics preferentially underwent scission, cyclisation, aromatisation and even polymerisation, leading to the formation of abundant heavy aromatics and light gases that were rich in methane. CO_2 is rather inert to the tyre volatiles at 600°C, while steam is reactive enough to further reduce the heavy hydrocarbon fraction via steam reforming reaction. At 600°C, the nascent tyre char is catalytic enough to enhance the steam reforming reaction for heavy molecules deposited on its surface, and even the methanation reaction between CO and H_2 derived from the steam reforming reaction.

7.1.3 Catalytic mechanism of tyre chars and its performance on low-rank coals in various heating rates, temperatures and steam environment

Amazingly, the catalytic ability of tyre char can be further extended to the low-rank coals. Under similar volatile residence time, faster heating and/or higher temperature has brought stronger catalytic performance than slower fasting and/or lower temperature. The catalytic reactions involve the deoxygenation including decarboxylation and decarbonylation and steam reforming reactions. The deoxygenation transformed oxygen-containing phenolic compounds by reacting with self-produced H_2, and formed single aromatic molecules and chemical water, whilst the reforming reactions transformed the heavy tar volatiles by reacting with the generated H_2O to form CO and H_2. Both reactions were substantiated by the injection of extra steam into the reactor. Through TEM analysis for the crystalline footprint and XRF for the loss of sulphur in tyre char, significant amount of inherent ZnS was transformed into ZnO, strongly

evidencing that sulphur is the active sites to *steal* the oxygen and catalyse the catalytic reactions including deoxygenation and steam-reforming reactions.

7.2 Recommendations for future work

7.2.1 Further development of 1-D heat-transfer model of tyre pyrolysis

The 1-D model could effectively demonstrate the pyrolysis of a spherical or cylindrical particle. However, in an industrial scale furnace, the packing of particles is going to introduce three-dimensional effects to the process i.e. pellets or particles may be heated mainly from one side more than from the other. It is not known how much heat a pellet in the centre of a fixed bed reactor will receive. Additionally, in a 1-D model, the gas phase reactions such as tar reforming reaction cannot be resolved. This could potentially be achieved by converting the model to a 3-D CFD model. This would allow the model to be scaled up to more dimensions.

7.2.2 Costs analysis of tar upgrading process

The scope of this study included the upgrading of tar oils through the control of the operating conditions and utilisation of tyre chars as catalyst. However, it remains inconclusive if the tar oils from tyre and brown coal can be upgraded at a cost not exceeding the use of current crude oil. This could be achieved through an economic analysis of the process including capital investment and operational costs using Aspen Plus software.

7.2.3 deCatalysis mechanisms for individual tarry species

Although oxygen-containing phenolic compounds were found to be significantly reduced with the use of tyre chars as catalyst along with the increase of non-oxygen containing single aromatics, these functional groups compounds can be further clarified into the exact organic species by using model tar compounds such as phenol, cresol, BTX, aldehyde, ketone and naphthalene in order to attain deeper understanding of the catalysis mechanisms.

This page is intentionally left blank

This page is intentionally left blank

Appendix A- Chapter 4 in Publication Form

This page is intentionally left blank

Waste Management 76 (2018) 516–527

Contents lists available at ScienceDirect

Waste Management

journal homepage: www.elsevier.com/locate/wasman

Scrap tyre pyrolysis: Modified chemical percolation devolatilization (M-CPD) to describe the influence of pyrolysis conditions on product yields

Vincent Tan [a], Anthony De Girolamo [a], Tahereh Hosseini [a], Jameel Aljarin Alhesan [b], Lian Zhang [a,*]

[a] Department of Chemical Engineering, Monash University, Wellington Road, Clayton, Victoria, Australia
[b] School of Chemistry, Monash University, Wellington Road, Clayton, Victoria, Australia

ARTICLE INFO

Article history:
Received 21 December 2017
Revised 28 February 2018
Accepted 7 March 2018
Available online 17 March 2018

Keywords:
Waste tyre
Pyrolysis
M-CPD model
Secondary cracking reaction

ABSTRACT

This paper attempts to develop a modified chemical percolation devolatilization (M-CPD) model that can include heat transfer, primary pyrolysis and the secondary cracking reactions of volatiles together to describe the pyrolysis of waste scrap tyre chip, as well as to examine the influence of operating conditions on the scrap tyre pyrolysis product yields. Such a study has yet to be conducted in the past, thereby leading to a large knowledge gap failing to understand the pyrolysis of the coarse feedstock appropriately. To validate the developed model, a number of operating parameters including reactor configurations, carrier gas compositions (argon and argon blended with CO_2 and/or steam), scrap tyre chip size (0.5–15.0 mm), terminal pyrolysis temperature (400–800 °C) and heating rate (10 °C/min and 110 °C/min) were examined in a lab-scale fixed-bed pyrolyser, with a particular focus on the secondary cracking extents of the liquid tar. Through both experimental investigation and modelling approach, it was found that significant secondary cracking extent occurred upon the increase in the feedstock size, heating rate and residence time. Upon the fast pyrolysis, the average temperature gap between the centres of the coarse particle and reactor wall could reach a maximum of 115 °C for the tyre chips of 6–15 mm. Consequently, its primary volatiles underwent the secondary cracking reaction at an overall extent of 17% at a terminal temperature of 600 °C and a fast heating rate of 110 °C/min. Consequently, the yield of light gases including methane was increased remarkably. The flow rate of inert carrier gas was also influential in the secondary cracking, in which a maximum tar yield (54 wt%) was reached at a carrier gas flow rate of 1.5 L/min. This indicates the occurrence of secondary cracking has been largely minimised. At a pyrolysis temperature of 600 °C, the addition of CO_2 in the carrier gas had an insignificant effect on the product yield distribution under the slow heating scheme. In contrast, the addition of steam resulted in a slight increase of carbon monoxide, presumably due to the occurrence of gasification reaction.

1. Introduction

The disposal of waste tyres is a serious environmental issue, predominantly due to its poor biodegradability (Lopez et al., 2017). In Australia, on average 51 million of waste tyres are generated each year in which only 5% of waste tyres are properly reused whereas the rest are simply piled in large quantities (Emma Mountjoy and Freeman, 2012). Tyre fires are very difficult to control, which can create a great deal of hazardous smoke, causing a health risk through the inhalation of particles and chemicals. Various technologies have been developed to recycle waste tyres, among which, pyrolysis is receiving a great deal of attention due to its ability to recover the energy content and valuable chemicals (Purcell, 1978; Shulman, 2011). Specifically, three value-added products can be generated via tyre pyrolysis, solid semi-coke (char), liquid oil (tar) and light gases ($<C_5$).

Tyres are made of rubbers (60–65 wt%), carbon black (25–35 wt%) and the rest consists of accelerators and organic fillers (Leung and Wang, 1998). The composition of tyres is difficult to be generalised, as rubbers are mainly a blend of different types of elastomers, such as isoprene natural rubber (NR), synthetic styrene-butadiene (SBR) and butadiene (BR) polymers mixed at different ratios depending on the manufacturing requirement (Martínez et al., 2013). Regardless of the chemical composition of the tyres, a great deal of kinetic studies of the tyre upon pyrolysis process

* Corresponding author.
E-mail address: lianzhang@monash.edu (L. Zhang).

https://doi.org/10.1016/j.wasman.2018.03.013
0956-053X/

Nomenclature

Amu	atomic mass unit, 1 g/mol
A_b	frequency factor for bridge breaking (s^{-1})
A_{cross}	frequency factor for cross-linking (s^{-1})
A_g	frequency factor for gas release (s^{-1})
A_s	pre-exponential factor of secondary cracking reaction (s^{-1})
C_p	specific heat ($J \cdot kg^{-1} \cdot K^{-1}$)
$C_{p,tyre}$	tyre specific heat ($J \cdot kg^{-1} \cdot K^{-1}$)
$C_{p,carbon}$	carbon specific heat ($J \cdot kg^{-1} \cdot K^{-1}$)
C_o	initial fraction of char bridges (–)
E_{cross}	activation energy for cross-linking ($kcal \cdot mol^{-1}$)
E_b	activation energy for bridge breaking ($kcal \cdot mol^{-1}$)
E_g	activation energy for gas formation ($kcal \cdot mol^{-1}$)
E_s	activation energy for secondary cracking ($kcal \cdot mol^{-1}$)
fal	aliphaticity (fraction, [–])
fa	aromaticity (fraction, [–])
fa^C	the carboxyl and carbonyl region (fraction, [–])
fa'	the main aromatic ring region (fraction, [–])
fa^O	aldehyde and ketone region (fraction, [–])
fa^{OO}	acid, ester, amide region (fraction, [–])
fa^H	aromatic ring carbons with an attached proton (fraction, [–])
fa^N	non-protonated aromatic carbons (fraction, [–])
fa^P	aromatic ring carbons with an attached oxygen (fraction, [–])
fa^S	aromatic ring carbons with an attached alkyl group (fraction, [–])
fa^B	bridge head carbons (fraction, [–])
fal^*	methyls and methoxy methyls (fraction, [–])
fal^H	methylene and methane groups (fraction, [–])
fal^O	total aliphatic carbon bonded to an oxygen atom (fraction, [–])
k	thermal conductivity ($W \cdot m^{-1} \cdot K^{-1}$)
k_{tyre}	tyre thermal conductivity ($W \cdot m^{-1} \cdot K^{-1}$))
k_{carbon}	carbon thermal conductivity ($W \cdot m^{-1} \cdot K^{-1}$)
k_b/k_c	ratio of bridge breaking to char bridge formation (–)
MW_{cl}	average number of aromatic carbons per cluster (–)
MW_{side}	average molecular weight of a side chain (–)
h	convection coefficient ($W \cdot m^{-2} \cdot K^{-1}$)
ΔH_{rxn}	heat of reaction ($kJ \cdot kg^{-1}$)
P_o	initial number of bridges in the tyre lattice matrix (–)
r	radius of particle (m)
r_i	radius at point i (m)
R	gas constant ($kcal \cdot K^{-1} \cdot mol^{-1}$)
T	temperature (K)
T_∞	reactor temperature (K)
T_s	tyre surface temperature (K)
VM	volatile matter (daf) from proximate analysis (fraction, [–])
x_i	primary tar amount at each point i across the tyre particle (s^{-1})
X_i	averaged amount of primary tar (s^{-1})
X	tar amount after cracking (s^{-1})

Greek symbols

ρ_{tyre}	density of tyre ($kg \cdot m^{-3}$)
ε	emissivity (–)
σ	Stefan–Boltzmann constant (5.67×10^{-8} $J \cdot m^{-2} \cdot s^{-1} \cdot K^{-4}$)
α	mass loss of tyre at different pyrolysis conditions (fraction, [–])
σ+1	lattice coordination number (–)
σ_b	standard deviation in E_b ($kcal \cdot mol^{-1}$)
σ_g	standard deviation in E_g ($kcal \cdot mol^{-1}$)

has been completed, as reviewed previously (Quek and Balasubramanian, 2012).

Among the large variety of tyre modelling studies on pyrolysis, the single-kinetic-rate model is considered as the simplest kinetic model, in which the entire waste tyre pyrolysis is treated as a single reaction route (Gupte and Madras, 2004; Unapumnuk et al., 2006; Zabaniotou et al., 2002). However, this approach has been argued to only work at a high pyrolysis temperature range, while the mass loss is more diffusion limited at lower temperatures (Zabaniotou et al., 2002). Aguado et al. (2005) also indicated that different kinetic parameters were found for thirteen volatiles evolved from tyre pyrolysis under an inert atmosphere, proving that tyre is highly heterogeneous and its pyrolysis rate is not a singular reaction.

Besides the single-reaction-route, other kinetic studies proposed a series of reaction routes to account for the entire tyre pyrolysis process. It is assumed that the tyre components (additive, NR, SBR and BR) are decomposed individually without any interaction among one another. Through the comparison of thermogravimetric analyser (TGA) and differential thermos-gravimetry (DTG) profiles, the predicted results from the model showed a good fit at two ends of temperatures, though the overlapping regions around 250–500 °C did not show a good agreement (Seidelt et al., 2006), particularly under fast heating conditions. An improvement was made by Lah et al. (2013) who considered additional tyre components (volatiles, fabric and other additives), showing a satisfactory agreement with the TGA results of tyre composites. It is also acknowledged that the pyrolysis reactions are not being simple monomolecular and first-order decompositions. Another common method is to assume that the tyre pyrolysis process is competing multi-series/parallel reactions with several intermediates and products. This method is able to deconvolute the TGA/DTG data of tyre with a high fitting agreement and has been further extended to include other considerations, including heat transfer limitation and reactor designs (Cheung et al., 2011; Olazar et al., 2008). Besides that, multistep reaction kinetics can also be accounted for by the isoconversional model to predict the pyrolysis of biomass and plastics (Narobe et al., 2014).

In contrast to the empirical model, chemical based models describe the pyrolysis process by considering the chemical composition in terms of functional groups and structures, making the predictions more sensible and applicable over a wide range of solid fuels. The most renowned chemical based model, namely the chemical percolation devolatilization (CPD) works effectively to describe the devolatilization behaviour of a variety of bituminous coals (Fletcher et al., 1992). The CPD model has shown a high accuracy on the pyrolysis rate over primary devolatilization reactions. However, the secondary reactions for the primary volatiles are not included. Our previous study on the pyrolysis of low-rank brown coal (i.e. lignite) briquette discovered that the internal heat transfer is the limiting factor, which lowers the heating rate of coarse particle and leads to an increase in the cross-linking extent and a decrease in the tar fraction compared to the fine coal particles (De Girolamo et al., 2018).

This work aims to develop a modified CPD model for tyre pyrolysis based on the conventional CPD model by integrating heat transfer and the secondary reactions of primary tar, so as to make it fit for the pyrolysis of scrap tyre chips under a broad range of critical pyrolysis conditions in a lab-scale fixed bed pyrolyser, including three granule sizes (0.5–15.0 mm), carrier gas flow rate

(0–3.0 L/min), four terminal temperatures (400–800 °C), two different heating rates (10 °C/min versus 100 °C/min) and different carrier gases (pure argon versus 15–30 vol% CO_2/steam balanced by argon). All the experimental conditions are expected to be encountered in an industry-scale pyrolyser, some have yet to be tested and understood previously. In respect to the modelling approach, a first-order kinetic reaction is applied to tackle the secondary reactions of primary volatiles, incorporating the heat transfer mechanism to predict the time-resolved particle temperature as well as its radial distribution to track the overall pyrolysis rate and product yield profiles. Since the modified model has been validated by a broad range of experimental conditions, it is desirable that the modified model can be used for the scale – up and proper design of an industry-scale reactor, as well provides insights on the fundamentals underpinning the pyrolysis of scrap tyre chip, a feedstock that is far more heterogeneous than coal and biomass (Navarro et al., 2012).

2. Material and methods

2.1. Properties of the scrap tyre feedstock

The scrap tyres collected from Tyrecycle Pty Ltd (Australia) is a mixture of different tyres which were grouped into three particle size bands, 0.5–1.5, 4 and 6–15 mm. The steel and wires were removed prior to the experiments. The proximate and ultimate properties of these tyres are displayed in Table 1. As can be seen, the three sizes possess very similar properties expect the ash content. The slight differences between the three sizes are not expected to cause any considerable difference in the pyrolysis behaviour.

2.2. Pyrolysis conditions

A lab-scale fixed-bed pyrolyser shown in Fig. 1 was employed. The reactors are made of quartz with an inner diameter of 55 mm and a total length of 1 m. For the reactor configuration 1, an argon stream of 0.8 L/min was purged continuously from the top of the reactor which meets the released tar and gases from the inside of the reactor. The argon gas, in this case, is merely used to minimise the deposition of tar on the reactor wall as well inside the connecting tubes. However, it is not supposed to flow back inside the reactor once the tyre pyrolysis occurs, considering that the pyrolysis gases and the hot tar are generally ejected and flow upwards based on their concentration/pressure gradient. Such a configuration aims to mimic the indirect heating mode for an industry-scale pyrolyser without any carrier gas inside (Garcia-Nunez et al., 2017). Based on the amount and reactor configuration, the released volatiles were expected to have a residence time of approximately 300 s inside the reactor.

Table 1
Proximate and ultimate analysis of scrap tyre in different sizes.

Size bands (mm)	0.5–1.5	4	6–15
Proximate analysis, wt%			
Moisture (ar)	0.85	1.07	0.89
Volatile matter (db)	68.49	66.27	66.64
Fixed carbon (db)	25.17	29.59	30.12
Ash (db)	6.34	4.14	3.24
Ultimate analysis (db), wt%			
C	82.10	83.19	84.57
H	7.56	7.65	7.35
O (by difference)	0.75	0.74	0.70
N	1.93	1.77	2.01
S	1.32	2.51	2.13

Conversely, the reactor configuration 2 uses a continuous carrier gas flow starting from the bottom of the reactor and passing through the tyre chip bed, thus sweeping away the gaseous and tarry species instantaneously once they are released out from solid particles (Garcia-Nunez et al., 2017). This process aims to mimic the direct heating mode for an industry-scale pyrolyser inside of which a portion of the products burns to provide heat. The resultant hot flue gas flows through the reactor bed (Bergman et al., 2005). To simulate the flue gas compositions derived from the internal combustion in configuration 2, argon is also blended with 15–30 vol% CO_2 and/or steam as a carrier gas for this study.

After leaving the pyrolyser, both condensable (tar) and non-condensable (gas) species enter a three-stage impinger train. The first impinger is surrounded by ice and water mixture as a cooling agent whereas dry ice/acetone mixture is used in the second and third impingers. U-tube filled with alumino silicate wool is further used downstream to trap the remaining tarry species. The exiting gases enter a gas analyser (Sensotec Rapidox 5100) which can measure O_2, CH_4, CO, CO_2 and H_2 in real-time. Tar yield is calculated based on the mass of the condensable volatiles collected in the impinger train, plus those deposits on the reactor wall (i.e. the reactor was weighed before and after each run to calculate the tarry depositions on its wall). The content of water in each tar sample is quantified by a pre-calibrated Karl-Fischer volumetric titrator (Mettler Toledo EasyPlus). The solid char yield is calculated, on a dry-ash-free (*daf*) basis, as the weight difference of the reactor before and after each run.

Regarding the pyrolysis conditions, the final pyrolysis temperature varies between 400 °C and 700 °C at two heating rates, slow pyrolysis (10 °C/min) and fast pyrolysis (110 °C/min) under an atmospheric pressure. The slow heating rate is used to mimic the industry – scale pyrolyser such as a coking oven that bakes slowly, whereas the fast heating rate is expected to mimic particles entering a pre-heated oven or those close to the hot reactor wall that is heated up quickly. For the slow heating mode, the tyre chips are loaded inside the reactor and heated together, whereas for the fast heating mode, the furnace is pre heated to a set temperature before the tyre chips – laden reactor was quickly inserted inside. Regardless the heating mode, the total reaction time is approximately 88 min for every single run, including the time to reach the target temperature and holding time, whilst the carrier gas flow rate is fixed at 0.8 L/min. Some experiments were repeated twice and the standard deviations were averaged and listed in the corresponding figures. The average error of the overall material balance was as high as 6 wt%, presumably due to the disability of gas analyser which treats all the non-condensable C_2-C_6 hydrocarbons as methane gas (CH_4).

2.3. M-CPD model for waste tyre chip pyrolysis

Fig. 2 shows the overall calculation flow for the modelling development of the M-CPD, which is further detailed below.

2.3.1. Chemical structure parameters

The use of the CPD model requires the measurement of the chemical structure parameters (MW_{cl} MW_{side}, σ+1, P_o, C_o) of the parent tyres, which was the first step for the modelling procedure in Fig. 2. The average values of these structure parameters were measured from the solid-state carbon-13 nuclear magnetic resonance analysis (^{13}C NMR).

The solid state ^{13}C NMR spectra for samples were determined using a Bruker 400 (^{1}H)/100 (^{13}C) MHz spectrometer with cross polarization-magic angle spinning (CP/MAS). The acquisition time was 1000 min with 20,000 scans averaged and a repetition time of 3.0 s, sample spinning rate 30 kHz.

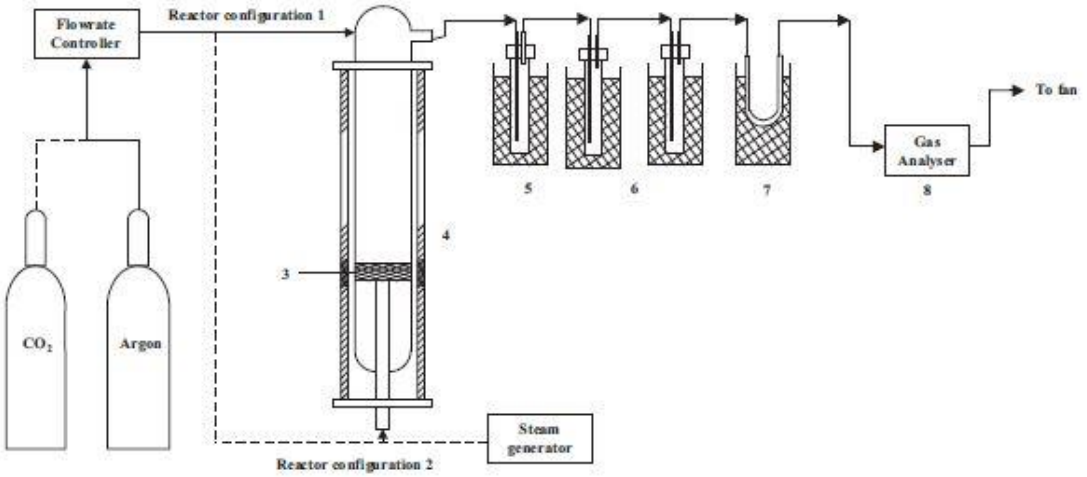

Fig. 1. Shaft furnace schematic of two reactor configurations (1–2. Reactor configurations; 3. Feed; 4. Heating furnace; 5. Condensing system with ice and water as cooling agent; 6. Condensing system with dry ice and acetone as cooling agent; 7. U-tube filled with alumino silicate wool in ice water; 8. Gas analyser).

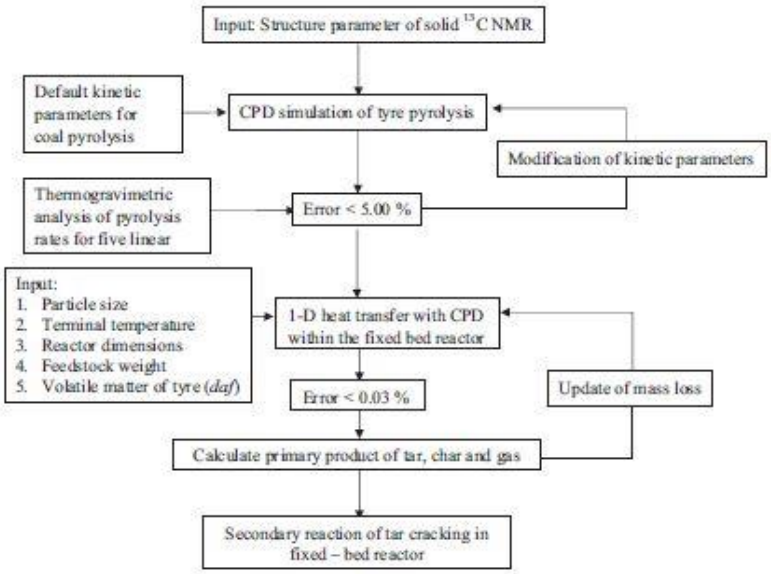

Fig. 2. The calculation flow for the M-CPD model.

Through NMR analysis, the ^{13}C NMR CP-MAS chromatograph of the tyre of 0.5–1.5 mm is presented in Fig. 3. The abundant peaks in the spectra were integrated based on the standard chemical shift ranges using Topspin 3.5 pl 7 software. The relative areas are tabulated in Table 2, corresponding to the characteristics of each peak in terms of organic structures and functional group (Kelemen et al., 2007; Solum et al., 2001). With these area fractions, the four chemical structure parameters (P_o, σ+1, MW_{cl} and MW_{side}) were determined by means of the mathematical equations by Solum et al. (2001). However, the last fifth parameter (C_o) has not been measured directly and was set to nil for this tyre sample, as most of the previous CPD work.

A modification was also made to the theoretical coordination number, σ+1 which was found to be 1.87 experimentally. According to Solum et al. (2001), the percolation threshold for a lattice is defined as $\sigma = 1/P_o$, representing the point at which the bridges are broken up to the point that no connected lattice exists. The value of σ+1 was thus calculated to be 2.30 to compromise with the value of P_o. A similar attempt was made by the CPD simulation for black liquor (Fletcher et al., 2012).

Besides the five structure parameters, there is a sixth parameter used to correct the molecular weight of side-chain of scrap tyre, MW_{side}. The molecular weight of side chain is subject to the reduction by a correlation factor as some functional groups (such as

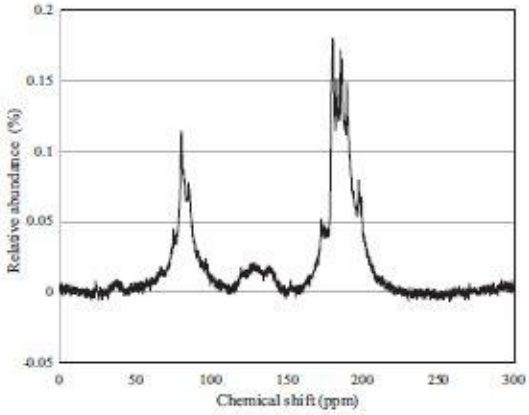

Fig. 3. NMR chromatogram of tyre rubber of 0.5–1.5 mm after deconvolution.

Table 2
The integrated peaks for the organic functional regions.

Parameters	Chemical shift range (ppm)	Area fraction
fal	0–90	0.645
fa	90–240	0.355
fa^{C}	165–240	0.042
fa'	90–165	0.313
fa^{O}	185–240	0.036
fa^{CO}	165–185	0.006
fa^{H}	90–130	0.199
fa^{N}	130–165	0.114
fa^{P}	150–165	0.018
fa^{S}	135–150	0.052
fa^{B}	130–135	0.044
fal^{*}	50–60	0.014
$fal^{'}$	0–22	0.166
fal^{H}	60–90	0.080
fal^{H}	22–50	0.385
fal^{O}	50–90	0.094

fraction of tightly-bound a-methyl groups), which were counted as side chains in the NMR measurements and should be considered as part of the aromatic clusters (Fletcher et al., 1992). To ensure a good agreement between model prediction and experimental data, this correlation factor was defaulted to be 7.0. However, this factor was noted to vary between −8.25 and 19.73 for the bituminous coals from different sources (Yan et al., 2014a). In this case, the correlation factor was found to be 49.0 for tyre CPD simulation by fitting with the TGA data (to be shown later). For comparison, the structure parameters for other solid fuels were also included in Table 3. Clearly, the structure for scrap tyre differs significantly from those that have been studied extensively.

2.3.2. Intrinsic and primary reaction routes of tyre pyrolysis

The intrinsic kinetic parameters related to the primary pyrolysis of tyre were determined after modifying its structural parameters. The conventional CPD model characterises the primary devolatilization reactions as several first-order bridge-breaking and bridge-forming reaction routes based on the theory of percolation lattice statistics (Fletcher et al., 1992). The rates of the reaction routes were defined as the rate of labile bridge scission (k_b), light gas release (k_g), cross-linking (k_{cross}) and the competing reaction coefficient of bridge breaking to char bridge formation (k_b/k_c) (Fletcher et al., 1992).

In this study, a major modification was made on the inherent reaction routes of CPD model. By definition, CPD assumes that light gas is derived from the side-chain molecules whose molecular weight was as small as around 12–52 amu (Fletcher et al., 1992). However, the molecular weight of the side chain of scrap tyre was found to be 139 amu (Table 3). A modification was thus made by taking the product derived from breakage of side-chain molecules in scrap tyre as tarry species, rather than as a light gas. Such an approach is the same as that has been taken for black liquor for which the molecular weight of the side chain accounts for 128–148 amu. (Fletcher et al., 2012).

The evaluation of each kinetic parameter was done by means of curve-fitting with the primary pyrolysis rate of pulverised tyre based on the TGA analysis, as has been done in previous CPD modelling studies (Fletcher et al., 2015, 2012; Sheng and Azevedo, 2002). In this work, the initial guess of kinetic parameters was taken from that of the CPD simulation for coal. MATLAB R2016b was used to optimise the kinetic parameters through least-square fitting with the experimentally measured mass loss profiles at five heating rates (10, 20, 30, 40 and 50 °C/min) from TGA (Shimadzu DTG-60H) in pure argon of 100 ml/min. For each run a typical mass of 5–10 mg pulverised scrap tyre (<106 μm) was used to eliminate the heat transfer effects.

2.4. Heat transfer rate coupling

Different from a TGA, the fixed-bed reactor in Fig. 1 is expected to encounter a heat transfer limitation between reactor wall/hot carrier gas and particles, as well as inside of a chip particle if it is large enough. In the modelling flowsheet in Fig. 2, the CPD model was further coupled with the heat transfer rate in step 3. One-dimensional unsteady heat transfer is controlled by convection and radiation at the particle surface, and intra-particle heat conduction, with the following assumptions:

a) The heat loss was negligible.
b) The intra-particle heat transfer was governed by thermal conduction, as per Eq. (1).
c) Scrap tyre particle was heated up externally by pyrolysis gas by means of convection and radiation inside the reactor, as per Eq. (2).
d) Scrap tyre particle was assumed to be a porous sphere, one-dimensional distribution of physical properties with uniform boundary conditions on its surface.
e) The swelling and shrinkage of tyre particles were negligible because the particle volume was found to remain almost constant (data not shown).

Table 3
Chemical structure parameters of the tyre samples determined from solid-NMR measurement.

Structure parameters	Zap coal (Fletcher et al., 1992)	Xinjiang coal (Yan et al. (2014b))	Celluloses (Sheng and Azevedo, 2002)	Green river oil Shale 1.9 (Fletcher et al., 2015)	Present work
MW_{cl}	277.00	320.96	81.00	776.00	391.00
MW_{side}	40.00	37.55	22.70	131.00	153.00
P_0	0.63	0.60	1.00	0.50	0.80
C_0	0.40	0.07	0.00	0.00	0.00
$\sigma+1$	3.90	5.11	3.00	4.50	2.30
Correlation factor of MW_{side}	7.00	14.95	7.00	7.00	49.00

$$\frac{\partial}{\partial t}(\rho \cdot C_p \cdot T) = \frac{1}{r}\frac{\partial}{\partial r}\left(\frac{\partial}{\partial r}(k \cdot T)\right) + \frac{\partial}{\partial t}(\alpha \cdot \rho) \cdot \frac{1}{VM} \cdot \Delta H_{rxn} \quad (1)$$

$$\frac{\partial}{\partial r}(k \cdot T) = h(T_\infty - T_s) + \varepsilon\sigma(T_\infty^4 - T_s^4) \quad (2)$$

The reaction of heat (ΔH_{rxn}) was calculated based on the correlation of temperatures between the reference sample and ground tyre (<106 μm) in the TG/DTA analysis, which was found to be around 122 kJ/kg for an overall endothermic pyrolysis reaction. As the scrap tyre particle was subjected to pyrolysis, its composition was changed with temperature and time. In light of this, Eqs. (3) and (4) together with Table 5 were used to calculate the tyre thermal conductivity and heat capacity at each temperature and every moment. Since the mass loss fraction (α) was not calculated until the specification of thermal properties were determined (Fig. 2), an initial guess was made by assuming that thermal properties were not changed by mass loss. The mass loss fraction was then calculated at every space and time point and the simulation was repeated with this added mass fraction using bilinear interpolation. This process was further iterated until the error between the initial guess and calculated mass loss fraction was less than 3E−5.

$$k = k_{tyre}\left(\frac{VM - \alpha}{VM}\right) + k_{carbon}\left(\frac{\alpha}{VM}\right) \quad (3)$$

$$C_p = C_{p,tyre}\left(\frac{VM - \alpha}{VM}\right) + C_{p,carbon}\left(\frac{\alpha}{VM}\right) \quad (4)$$

2.5. Secondary reaction route of tyre pyrolysis

The last step in the modified CPD procedure in Fig. 2 was to quantify the secondary reaction extent of the primary species released from tyre pyrolysis inside the fixed-bed reactor. Different reaction expressions have been made by the previous modelling and experimental studies to describe the secondary reaction of tyre volatiles, such as cyclization (Senneca et al., 1999), Diel-Alder reaction for the formation of aromatic compounds (Williams and Taylor, 1993) and cracking reaction (Li et al., 2004). It was generally agreed that the temperature range of secondary reaction was specified at 550–800 °C, whereas the temperature range of 250–520 °C was deemed as primary pyrolysis reaction window where the major covalent bonds inside the parent chemical network start to break down (Li et al., 2004).

In the modelling study, the primary tar fraction was calculated at each point across the length of the particle. The overall primary tar fraction prior to the secondary cracking reaction was then calculated using Eq. (5). The rate of cracking reaction for the primary tar in the fixed bed reactor, given in Eq. (6) was assumed as a first – order Arrhenius form. The amount of tar being cracked was calculated based on Eq. (7) which is based on the reaction rate and the residence time of primary volatiles inside the reactor. The residence time of tar volatiles was calculated based on the flow rate of tar/carrier gas and the actual dimension of the vertical and cylindrical reactor.

$$X_i = \frac{\sum_{i=1}^{n} x_i r_i^2}{\sum_{i=1}^{n} r_i^2} \quad (5)$$

$$k_S = A_s \exp\left(\frac{-E_s}{RT}\right) \quad (6)$$

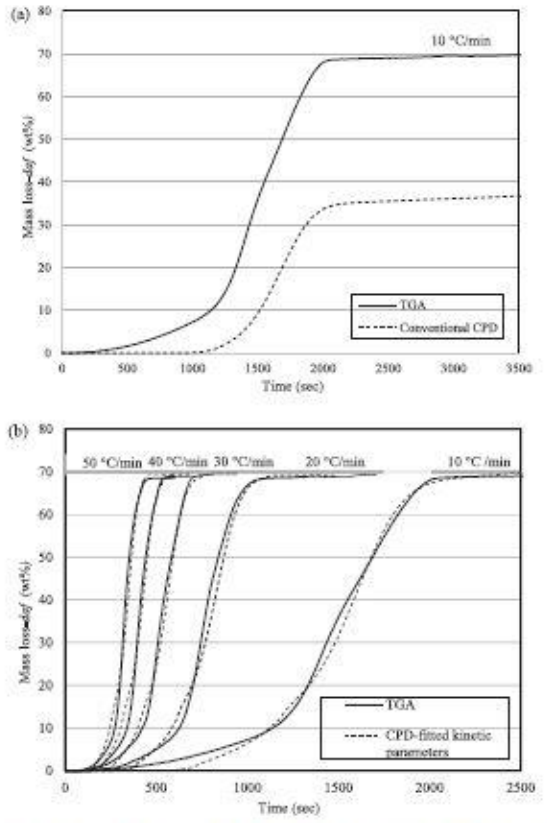

Fig. 5. Comparison of the mass loss kinetics of the CPD model and TGA data for various heating rates using (a) Initial kinetic parameters and (b) Optimised kinetic parameters.

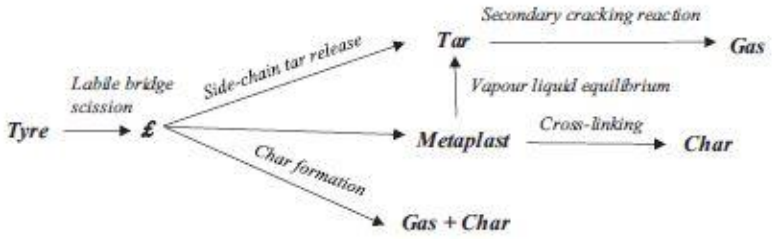

Fig. 4. The schematic diagram of the reaction routes for M-CPD model, adapted from Fletcher et al., 1992.

$$X = X_0 e^{(-k_0 t_R)} \quad (7)$$

The schematic diagram of the overall reaction routes for M-CPD model is presented in Fig. 4. The primary reactions were based on the reaction routes of the conventional CPD whereas the secondary reaction is defined as where the primary tars cracks to form light gases.

The extent of tar cracking is calculated based on the difference of tar yield predicted by M-CPD under the consideration of *only-primary* and *primary-secondary* reactions. The kinetic parameters for secondary cracking reaction were determined through the least-square regression method to fit with the experimental tar yields obtained from the 6–15 mm tyre size under two heating rates (slow and fast pyrolysis) and four terminal temperatures (400–700 °C). The secondary reaction is assumed to be negligible under the slow heating rate (as shown later) while it is noticeable under the fast heating scheme. Therefore, the difference of tar yield between these two schemes was used to determine the secondary reaction extent for the tar and its kinetic parameters.

3. Results and discussion

3.1. Effects of terminal temperature and heating rate

The intrinsic rate of tyre pyrolysis with primary reactions was first analysed by TGA. The conventional CPD model without any modification (i.e. all the default settings based on coal) was used to assess its applicability to scrap tyre pyrolysis. The experimentally measured mass loss kinetics of the ground tyre (<106 μm) are presented in Fig. 5a and b, given in a solid curve. As shown in Fig. 5a, the mass loss profile predicted by the conventional CPD model did not fit the TGA data at all. The maximum absolute error was found to be 18.21%. Instead, upon the least – square fitting approach, the new and optimised kinetic parameters tabulated in Table 4 were achieved, showing an improved fitting for the five different heating rates in Fig. 5b. Table 4 also lists the intrinsic kinetic data for other solid fuels from previous works.

Based on the optimised kinetic parameters in Table 4, the individual reaction rates involved in the primary pyrolysis of scrap tyre are presented in Fig. 6. The scrap tyre started to decompose at 250 °C, predominantly contributing to the formation and release of tarry fragments that even commenced earlier than the release of light gaseous species from around 320 °C. It is in line with a previous modelling study at 400 °C, revealing the formation of approximately 40 wt% (*daf*) tarry species, relative to a gas yield of only 4 wt% at a reactor heating rate of 5 °C/min (Williams et al., 1990). However, from 425 °C onwards, the release rates of the three products started to level off, finishing at 475 °C.

Experiments in the lab-scale fixed-bed pyrolyser were then conducted to evaluate the kinetic parameters achieved based on the TGA data, as well as to assess if the secondary reactions related to the primary tar and gases would occur. For these two purposes, the reactor configuration 1 with a top flow of pure argon was used, which maximised the residence time of tar and gas inside the reactor and minimises/eliminates the interference from carrier gas on the secondary reactions of tar. The pyrolysis of tyres of the largest size band, 6–15 mm was also used considering that the internal heat transfer would be slower. The experimental results for product yields are presented in Fig. 7a–d.

In Fig. 7a, char yield declines remarkably from 55 wt% to 36 wt% (*daf*) when the temperature increased from 400 to 500 °C, and then remains relatively constant for both heating rates. The char yields are in good agreement with above- mentioned TGA results as well as the previous findings which explained that the complete devolatilisation of tyre occurred in the temperature range around 450–550 °C under the atmospheric pressure (Li et al., 2004).

In Fig. 7b, the tar fraction yield was found to reach its maximum of around 50 wt% at 500 °C under the fast heating rate. For the two temperatures of 400 °C and 500 °C, the tar yield increased slightly, if not negligible upon the shift from low heating to fast heating. Such an increment can be explained by the rapid relaxation of tyre particle and thus the ejection of volatiles upon a fast heating. However, compared to coal and biomass, scrap tyre has much less gas-

Table 5
Thermal properties of tyres (Oyedun et al., 2012; Yang et al., 1995).

Parameters	Values	Parameters	Values
ρ tyre	1100 kg·m^{-3}	$C_{p,tyre}$	1900 + 3(T(°C)-25) J·kg^{-1}·K^{-1}
k_{tyre}	0.38 W·m^{-1}·K^{-1}	$C_{p,carbon}$	1003.2 + 2.09 T(°C) J·kg^{-1}·K^{-1}
k_{carbon}	0.20 W·m^{-1}·K^{-1}	ε	1.00 (black body)
h	50 W·m^{-2}·K^{-1}		

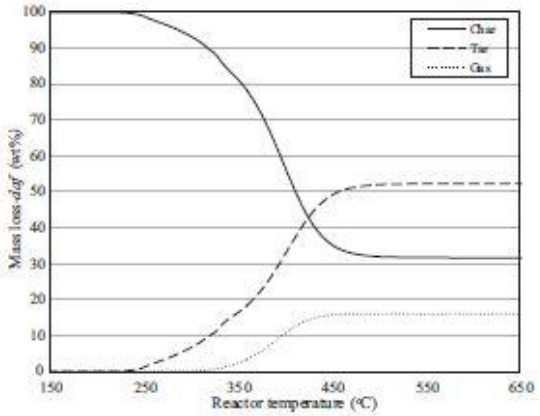

Fig. 6. The rate of pyrolysis product formation during the primary pyrolysis predicted by M-CPD model.

Table 4
Kinetic parameters of various solid fuels for CPD modelling.

Kinetic parameters	Bituminous coal (Fletcher et al., 1992)	Green river oil Shale (Fletcher et al., 2015)	Cellulose (Fletcher et al., 2012)	Cellulose (Sheng and Azevedo, 2002)	Black liquor (Fletcher et al., 2012)	Present work
E_b (kcal·mol^{-1})	55.4	23.9	55.4	59.0	55.4	60.4
A_b (s^{-1})	2.61×10^{15}	1.58×10^{10}	2.0×10^{16}	1.0×10^{18}	2.61×10^{15}	2.57×10^{17}
σ_b (kcal·mol^{-1})	1.8	0	4.1	1.8	1.8	1.8
E_g ((kcal·mol^{-1})	69.0	21.0	61.2	43.2	62.5	60.4
A_g (s^{-1})	3.0×10^{15}	1.58×10^{10}	3×10^{15}	8.23×10^{12}	3.0×10^{15}	2.4×10^{18}
σ_g (kcal·mol^{-1})	8.1	3.0	8.1	3.0	8.1	7.5
E_{cross}(kcal·mol^{-1})	65.0	60.0	65.0	65.0	65.0	65.0
A_{cross} (s^{-1})	3.0×10^{15}	1.18×10^{15}	3.0×10^{15}	3.0×10^{15}	3.0×10^{15}	3.0×10^{15}
k_b/k_c	0.9	0.9	100	0.9	0.9	1.34

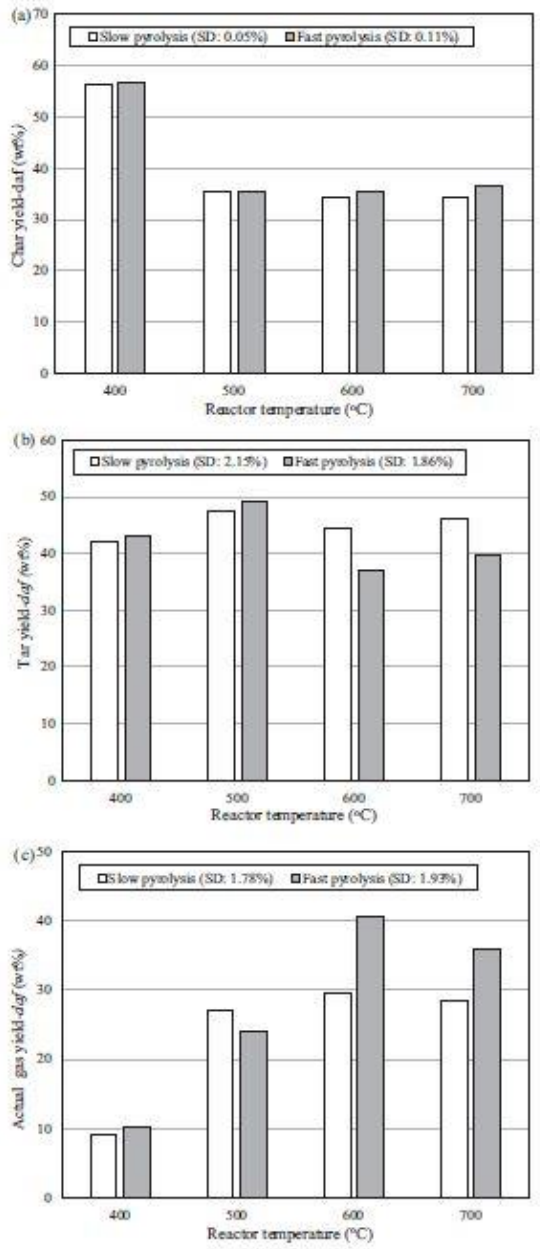

Fig. 7. Experimental product yields (*daf*) of 6–15 mm tyres on various temperature and heating rates in the fixed – bed reactor using configuration 1. Panel (a) Char yield (b) Tar yield (c) Gas yield.

eous compounds to eject at 400 °C and 500 °C (see TGA data), thereby performing an insensible variation on the liquid tar yield upon the increase of the heating rate (Navarro et al., 2012).

Increasing the terminal temperature beyond 500 °C failed to improve the tar yield, because the release of volatile was completed by 475 °C, as evident by the TGA results. This was also supported by a relatively unchanged tar yield from 600 °C and above for the slow heating scheme. This was reasonable considering that the slow heating scheme in the fixed bed reactor bears the same heating rate as the TGA. It is also evident that the flow rate of inert argon gas was insignificant on the tar yield. This was however not the case observed for the fast heating scheme from 600 °C. A noticeable reduction in the tar yield from 45 wt% to 36 wt% at 600–700 °C was observed for the fast heating scheme. Such a drop in the tar amount agreed with the increment in gas yield demonstrated in Fig. 7c, signifying a large extent of the secondary reactions for tar. The primarily released heavy hydrocarbons tended to crack into shorter fragments while releasing light gases at a temperature around 600 °C, known as the secondary tar cracking reaction, which has been widely accepted (Williams, 2013). Such a reaction was obviously facilitated upon fast heating, by which the primarily released tarry species undertook a rapid heating as well as experienced a higher temperature. Conversely, in a slow heating scheme, the tar was released before reaching the final set temperature, thereby experiencing little/no rapid temperature rise (Senneca et al., 1999).

The temperature-dependent profiles for the most abundant non-condensable gases (mainly CH_4) is depicted in Fig. 8. Irrespective of the heating rate, non-condensable hydrocarbons were the most predominant species from scrap tyre pyrolysis, as has been confirmed elsewhere (Kaminsky et al., 2009). The amount of CO and CO_2 released were less than 1 vol% (data not shown), due to the low oxygen content in scrap tyre (Table 1) and the preferential immobilisation of oxygen into steam/water. In regard to the emission of non-condensable hydrocarbons, it was preferred upon a fast heating from 600 °C due to the secondary cracking of heavy hydrocarbons, as mentioned above.

Regarding the modelling effort using the M-CPD developed, the comparison of tar yield between experimental observation and the modelling prediction is summarised in Fig. 9. For comparison, both the M-CPD models with and without the inclusion of secondary reactions were conducted. Clearly, without considering the secondary reaction, the predicted tar yield was far above the respective experimental value. With the method of least-square regression, the rate constants related to the secondary cracking reaction of tar are finalised in Table 6. Those values were found to differ from those obtained by Yan et al. (2013) for secondary tar cracking from long flame coal-CPD in the hydrogen plasma environment. The values of activation energy and pre-exponential values were smaller and larger respectively than that of coal, indicating that the reaction rate of the cracking reaction

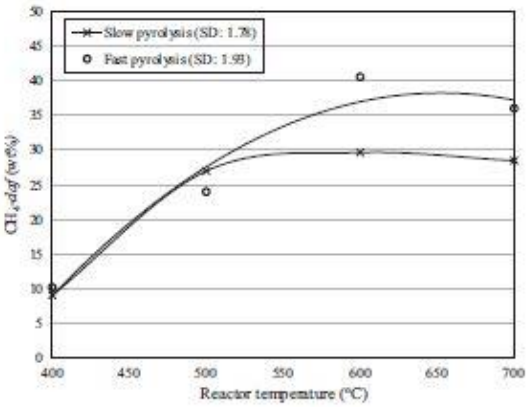

Fig. 8. Yield of methane, wt% (*daf*) of 6–15 mm tyres at various temperatures and heating rates.

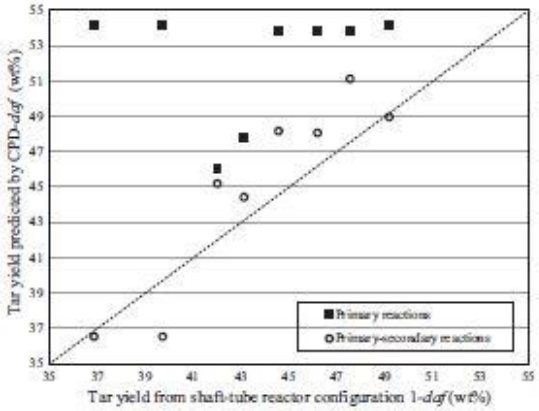

Fig. 9. Comparison of tar yields between experimental results and CPD prediction for tyres in 6–15 mm.

Table 6
Kinetic parameters of secondary tar cracking reactions of CPD models.

References	E_a (kcal mol^{-1})	A_a (s^{-1})
Yan et al. (2013)	68.36	9.77×10^{10}
Present work	50.19 ± 0.48	$(5.02 \pm 3.00) \times 10^{11}$

of tyre is larger at all reaction temperatures. This might be due to the chemical nature of tar volatiles. It was reported that tar from tyre and coal mainly consists of long-chain poly-aliphatic and poly-aromatic compounds (PAH), respectively (Cunliffe and Williams, 1998). It is reasonable that higher energy is needed to crack the long-chain stable moieties.

3.2. Effect of particle sizes on the secondary cracking reaction of tyre volatiles

To validate the accuracy of the M-CPD model which includes both heat transfer and the secondary cracking reactions of primary tar, the pyrolysis of another two tyre chip sizes were conducted using the reactor configuration 1 where the final temperature was fixed at 600 °C, via both slow and fast heating rates.

As presented in Fig. 10, tar yield was found to decrease with increasing particle size for both heating schemes. For slow heating, one can see a slight decrease in the yield of tar by around 3 wt% (*daf*) upon the increase of size from 1 to 11 mm. The decrease was compensated by a slight increase on the gas fraction. A similar finding was reported by Barbooti et al. (2004) that less carbon black and more pyrolytic oil fraction were obtained for smaller particle sizes using a fixed-bed reactor at 400–460 °C in the slow heating scheme. This could be explained that smaller particle size provides more reaction surface for the char reduction (Dai et al., 2001).

The influence of tyre size was more obvious in the fast heating scheme. As can be seen in Fig. 10, upon the rise of the scrap tyre size from 1 to 11 mm, the tar yield was reduced remarkably by around 10 wt%, resulting in the rise of the gas amount. Apparently, such an observed trend suggests that the secondary cracking reactions are preferred by increasing the scrap tyre feedstock size under the fast heating scheme. Considering that the cracking reactions were facilitated upon a fast heating rate (Figs. 7b and 8), it is hypothesised that the internal temperature gradient (*i.e.* temperature difference between primary tar inside the tyre chip and reactor wall) for the released primary tarry species was further enlarged upon the increase on the scrap tyre size.

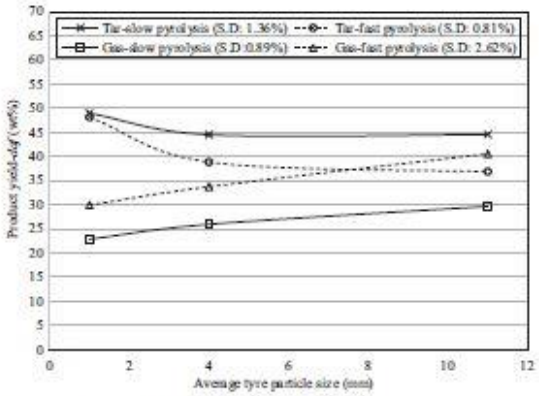

Fig. 10. Experimental tar yields from different particle sizes of tyre at 600 °C in slow and fast heating schemes.

To prove this hypothesis, the temperature profiles of the three differently sized scrap tyres were predicted by the M-CPD model as well as plotted in Fig. 11 for both the slow and fast heating rates

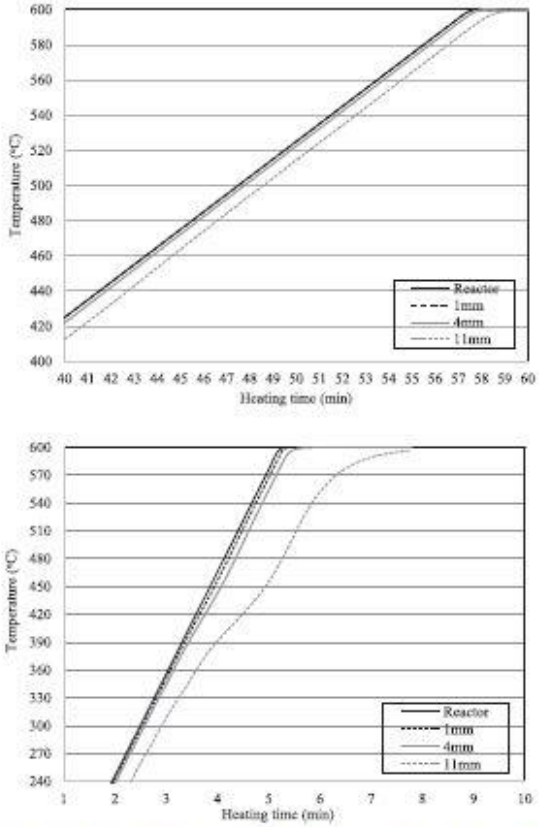

Fig. 11. The predicted temperature profiles of the particle centre and the reactor in (a) slow pyrolysis; (b) fast pyrolysis.

and heated to 600 °C. As expected, in the slow heating scheme, the temperature gap between the centre of a tyre particle and the reactor was relatively small, even for the particles as large as 11 mm. However, the fast heating scheme resulted in a noticeable delay in the heating of the largest size, and hence, enlarged temperature gap between the solid particle and the reactor wall. Consequently, the primarily released tarry species had to go through the largest temperature gap which facilitated their secondary cracking reactions. Besides, the internal diffusion resistance may also delay the internal release of the tar, thereby promoting the cracking reactions within the pores of the scrap tyre particle (Yang et al., 1995).

Based on the temperature gap predicted in Fig. 11 and the secondary cracking kinetic parameters summarised in Table 6, effort was further made to predict and correlate the secondary cracking extent for each size under each heating rate with the respective temperature gap. The results were plotted in Fig. 12. The temperature gap for each size under the fast heating rate was variable with the heating time, as evident in Fig. 11b. Therefore, the average temperature gaps were calculated and used in Fig. 12. It can be noticed that the cracking extent of volatiles was highly dependent on the temperature gap between the particle and reactor wall, raising asymptotically to 16.9 wt% when the predicted temperature gap reaches 115 °C obtained from large particle size and fast heating scheme. In contrast, the tar cracking extent was reduced to only 7.2 wt% when the temperature gap was insignificant for the smallest size under the slow heating rate.

3.3. Effect of carrier gas types and reactor configuration on the secondary cracking reactions

As mentioned previously, another option for the pyrolysis is direct heating in which a portion of the pyrolysis derived gas is sent back and burns inside the pyrolysis rig. The resultant hot flue gas was used as a heat carrier for the pyrolysis process. In light of this, the second configuration as shown in Fig. 1 was tested, through which the two major components CO_2 and steam in flue gas have been examined. To clarify the effect of CO_2, its fraction in argon balance was varied as 5, 10, 20, and 30% by volume. Similarly, as for the effect of steam, its proportion was also varied by the ratio of 10, 20, and 30% by volume, whilst both argon and CO_2 (15 vol%) were used as the balance gas. The total flowrate of gas mixtures was fixed at 0.8 L/min in the reactor configuration 2 where the gas mixture was fed continuously from the bottom of the reactor. The experiment was fixed at 600 °C at the slow heating rate (10 °C/min) with the use of the medium tyre chip size of 0.5–1.5 mm. Note that, only the slow heating rate was conducted here because the configuration 2, injecting the gas from the reactor bottom, does not allow an injection of the whole reactor system inside a pre-heated furnace.

As shown in Fig. 13a, the product yield for the presence of CO_2 in argon was almost unchanged, indicating that at the temperature of 600 °C tested CO_2 can be regarded as an inert gas and the carbon - CO_2 gasification reaction is insignificant, at least in terms of product yield. A similar conclusion can be drawn for the steam in Fig. 13b, except there is a slight increment of light gas (1.68 wt%) at the expense of char. It is presumably due to the small extent of char gasification and methanation of the resultant syngas. The observations were in line with the previous studies pointing that the product yield distribution was not varied upon the use of these two gases at 600 °C. Nevertheless, it was reported that lighter hydrocarbons and less long chain polymers obtained in the tar derived from steam as carrier gas compared to the tar from helium-experiment (Ogasawara et al., 1987). Also, less organic sulphur compounds were noted in the analysis of tar composition with the use of steam during the pyrolysis of 600 °C. (Kaminsky et al., 2009; Ogasawara et al., 1987). All these will be further elucidated in a future study related to the tar properties.

Regardless of the carrier gas type, it is, however, intriguing to see a rise in the tar yield up to 54 wt% (the maximum possible tar yield as confirmed by the TGA results in Fig. 6) with the use of reactor configuration 2, as experimentally confirmed by varying argon flow rate and presented in Fig. 14. Such a rise is considerable

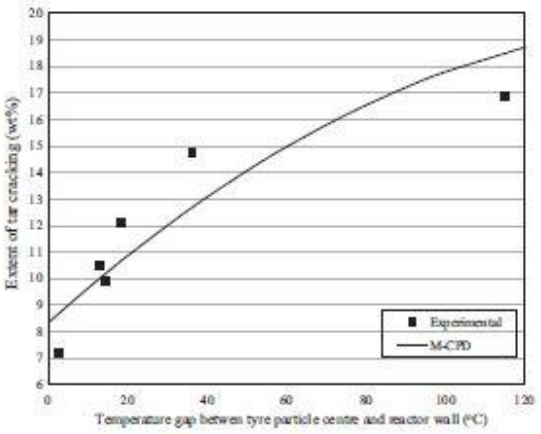

Fig. 12. The relationship of the extent of tar cracking with the temperature gap of centre particle and reactor wall.

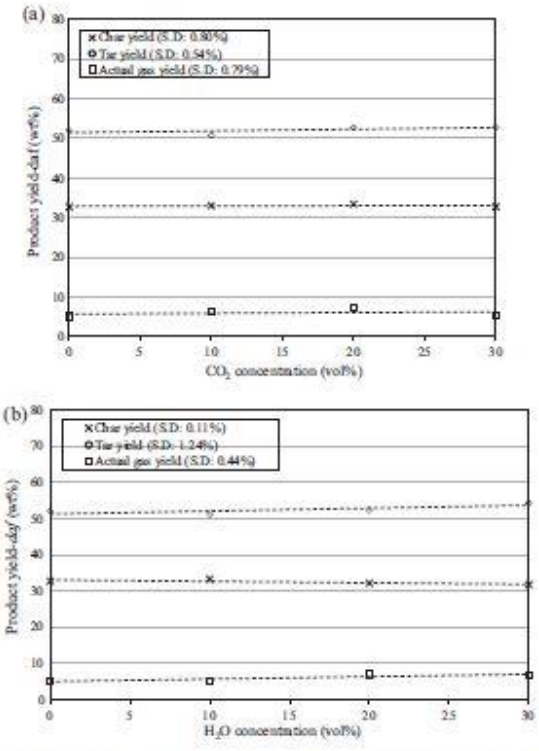

Fig. 13. Experiment product yields for the experiment in which argon mixtures of (a) CO_2 and (b) H_2O (15 vol% of CO_2) are studied in fixed-bed reactor using configuration 2.

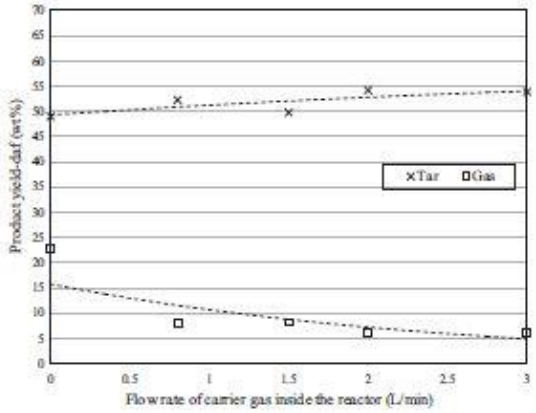

Fig. 14. Experiment product yields from different reactor designs with argon as purging gas. The argon flow rate of zero refers to configuration 1 for the use of no argon in the bottom, while the other flow rates refers to configuration 2 injecting argon from the bottom of the reactor.

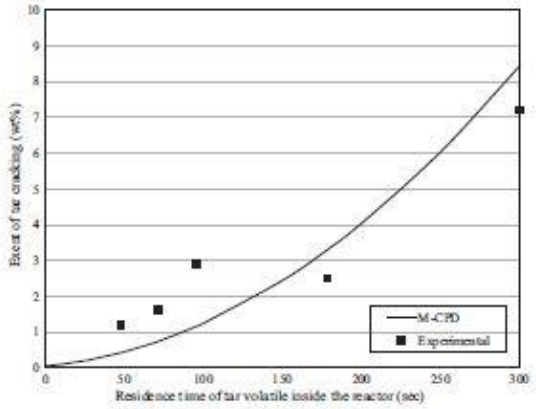

Fig. 15. The relationship of the extent of tar cracking with the residence time of tar volatile inside the reactor.

when compared to only around 48 wt% of tar derived from the use of reactor configuration 1 in slow pyrolysis. The rise in tar yield using the reactor configuration 2 was compensated by the drop of the gas yield, along with the slight reduction of char fraction. Such a change should be mainly attributed to the different tar cracking extent caused by the different residence time of volatiles. The injection of carrier gas from the bottom was beneficial in sweeping out the primary tar and gas quickly, thereby minimising the extent of their secondary reactions. Aylón et al. (2008) found that the tar fraction was reduced significantly during tyre pyrolysis in the moving bed reactor compared to a fixed-bed reactor. Besides, Dai et al. (2001) evaluated the effect of residence time (1, 3 and 5 s) using circulating fluidized bed reactor and different feed positions. It was indicated that the fraction of light hydrocarbon components and methane were increased remarkably with the increment of volatile residence times. The secondary cracking reaction may explain the effect of residence time observed here. As witnessed in Fig. 15, the tar cracking extent increased exponentially upon increasing the volatile residence time inside the reactor. By decreasing the residence time down to 50 s and less, the tar cracking extent can be minimised to a negligible level. In contrast, increasing the extent time to 300 s and above will considerably decrease tar yield by enhancing the tar cracking extent up to 7%. However, by comparing with Fig. 12, the temperature gap caused by increasing tyre chip size and/or particle heating rate is more influential, causing a maximum possible cracking extent of ~17% of the total primary tar.

4. Conclusions

In this study, an experimental investigation has been conducted to examine the pyrolysis behaviour of scrap tyre chip over a number of variables, including temperature, heating rate, carrier gas composition and flow rate, reactor configuration and chip size. In parallel, an M-CPD model, with the coupling of heat transfer and the secondary cracking reaction of tar into the original CPD model has been successfully developed and validated for scrap tyre pyrolysis. Attention was specifically paid to quantitatively clarify the structure of scrap tyre and the extent of its primary tar cracking. The scrap tyre pyrolysis commences at 250 °C and stabilises from 475 °C onwards in terms of volatile release. However, the secondary cracking reaction of tar was favoured from 600 °C onwards, particularly upon a fast heating scheme (~110 °C/min), increase on the chip size as well as the residence time for volatile vapour inside the reactor. A fast pyrolysis scheme results in a large temperature gap between the centre of a tyre chip and the reactor wall, noticeably resulting in the delay on the heating of the tyre chip and subsequently the release of volatiles. As the primarily released tarry species crosses a temperature gap up to 115 °C, it performances the secondary cracking with an extent of 17%. At a pyrolysis temperature of 600 °C, the addition of CO_2 in carrier gas had an insignificant effect on the product yield distribution under the slow heating scheme. However, the addition of steam resulted in a slight increase of carbon monoxide, presumably due to the occurrence of the gasification reaction. Additionally, the flow rate of carrier gas, as well as the residence time for volatiles inside the reactor is influential in the cracking extent of tar, which is noticeable in the case that the residence time is sufficiently long. At a residence time of ~300 s, the minimum cracking extent reaches around 7%, even under a slow heating mode.

Acknowledgements

This work was supported by Australian Research Council (ARC) under its Industrial Research Training Hub (150100006) scheme for the joint project between Monash and Coal Energy Australia. The scrap tyre provided by the Tyrecycle Pty Ltd, Australia is also acknowledged.

References

Aguado, R., Olazar, M., Vélez, D., Arabiourrutia, M., Bilbao, J., 2005. Kinetics of scrap tyre pyrolysis under fast heating conditions. J. Anal. Appl. Pyrol. 73, 290–298.
Aylón, E., Fernández-Colino, A., Navarro, M.V., Murillo, R., García, T., Mastral, A.M., 2008. Waste tire pyrolysis: comparison between fixed bed reactor and moving bed reactor. Ind. Eng. Chem. Res. 47, 4029–4033.
Barbooti, M.M., Mohamed, T.J., Hussain, A.A., Abas, F.O., 2004. Optimization of pyrolysis conditions of scrap tires under inert gas atmosphere. J. Anal. Appl. Pyrol. 72, 165–170.
Bergman P.C., Boersma A.R., Zwart R.W., and Kiel J.H., 2005. Torrefaction for biomass co-firing in existing coal-fired power stations. Energy Centre of Netherlands, Report No. ECN-C-05-013.
Cheung, K.-Y., Lee, K.-L., Lam, K.-L., Lee, C.-W., Hui, C.-W., 2011. Integrated kinetics and heat flow modelling to optimise waste tyre pyrolysis at different heating rates. Fuel Process. Technol. 92, 856–863.
Cunliffe, A.M., Williams, P.T., 1998. Composition of oils derived from the batch pyrolysis of tyres. J. Anal. Appl. Pyrol. 44, 131–152.
Dai, X., Yin, X., Wu, C., Zhang, W., Chen, Y., 2001. Pyrolysis of waste tires in a circulating fluidized-bed reactor. Energy 26, 385–399.

De Girolamo, A., Tan, V., Liu, Z., Zhang, L., 2018. Pyrolysis of a lignite briquette – Experimental investigation and 1-dimensional modelling approach. Fuel 212, 533–545.
Emma Mountjoy, D.H., Freeman, Tom, 2012. Stocks & Fate of End of Life Tyres - 2013-14 Study. Hyder Consulting Pty Ltd.
Fletcher, T.H., Barfuss, D., Pugmire, R.J., 2015. Modeling light gas and tar yields from pyrolysis of green river oil shale demineralized kerogen using the chemical percolation devolatilization model. Energy Fuels 29, 4921–4926.
Fletcher, T.H., Kerstein, A.R., Pugmire, R.J., Solum, M.S., Grant, D.M., 1992. Chemical percolation model for devolatilization. 3. Direct use of carbon-13 NMR data to predict effects of coal type. Energy Fuels 6, 414–431.
Fletcher, T.H., Pond, H.R., Webster, J., Wooters, J., Baxter, L.L., 2012. Prediction of tar and light gas during pyrolysis of black liquor and biomass. Energy Fuels 26, 3381–3387.
Garcia-Nunez, J.A., Pelaez-Samaniego, M.R., Garcia-Perez, M.E., Fonts, I., Abrego, J., Westerhof, R.J.M., Garcia-Perez, M., 2017. Historical developments of pyrolysis reactors: a review. Energy Fuels 31, 5751–5775.
Gupte, S.L., Madras, G., 2004. Catalytic degradation of polybutadiene. Polym. Degrad. Stab. 86, 529–533.
Kaminsky, W., Mennerich, C., Zhang, Z., 2009. Feedstock recycling of synthetic and natural rubber by pyrolysis in a fluidized bed. J. Anal. Appl. Pyrol. 85, 334–337.
Kelemen, S.R., Afeworki, M., Gorbaty, M.L., Sansone, M., Kwiatek, P.J., Walters, C.C., Freund, H., Siskin, M., Bence, A.E., Curry, D.J., Solum, M., Pugmire, R.J., Vandenbroucke, M., Leblond, M., Behar, F., 2007. Direct characterization of kerogen by X-ray and solid-state 13C nuclear magnetic resonance methods. Energy Fuels 21, 1548–1561.
Lah, B., Klinar, D., Likozar, B., 2013. Pyrolysis of natural, butadiene, styrene–butadiene rubber and tyre components: modelling kinetics and transport phenomena at different heating rates and formulations. Chem. Eng. Sci. 87, 1–13.
Leung, D.Y.C., Wang, C.L., 1998. Kinetic study of scrap tyre pyrolysis and combustion. J. Anal. Appl. Pyrol. 45, 153–169.
Li, S.Q., Yao, Q., Chi, Y., Yan, J.H., Cen, K.F., 2004. Pilot-scale pyrolysis of scrap tires in a continuous rotary kiln reactor. Ind. Eng. Chem. Res. 43, 5133–5145.
Lopez, G., Alvarez, J., Amutio, M., Mkhize, N.M., Danon, B., van der Gryp, P., Görgens, J.F., Bilbao, J., Olazar, M., 2017. Waste truck-tyre processing by flash pyrolysis in a conical spouted bed reactor. Energy Convers. Manage. 142, 523–532.
Martínez, J.D., Puy, N., Murillo, R., García, T., Navarro, M.V., Mastral, A.M., 2013. Waste tyre pyrolysis – a review. Renew. Sustain. Energy Rev. 23, 179–213.
Narobe, M., Golob, J., Klinar, D., Francetič, V., Likozar, B., 2014. Co-gasification of biomass and plastics: pyrolysis kinetics studies, experiments on 100 kW dual fluidized bed pilot plant and development of thermodynamic equilibrium model and balances. Bioresource Technol. 162, 21–29.
Navarro, M.V., Martínez, J.D., Murillo, R., García, T., López, J.M., Callén, M.S., Mastral, A.M., 2012. Application of a particle model to pyrolysis. Comparison of different feedstock: plastic, tyre, coal and biomass. Fuel Process. Technol. 103, 1–8.
Ogasawara, S., Kuroda, M., Wakao, N., 1987. Preparation of activated carbon by thermal decomposition of used automotive tires. Ind. Eng. Chem. Res. 26, 2552–2556.
Olazar, M., Lopez, G., Arabiourrutia, M., Elordi, G., Aguado, R., Bilbao, J., 2008. Kinetic modelling of tyre pyrolysis in a conical spouted bed reactor. J. Anal. Appl. Pyrol. 81, 127–132.
Oyedun, A., Lam, K.-L., Pittkau, M., Hui, C.-W., 2012. Optimisation of particle size in waste tyre pyrolysis. Fuel 95, 417–424.
Purcell, A.H., 1978. Tire recyling: research trends and needs. Conserv. Recycl. 2, 137–143.
Quek, A., Balasubramanian, R., 2012. Mathematical modeling of rubber tire pyrolysis. J. Anal. Appl. Pyrol. 95, 1–13.
Seidelt, S., Müller-Hagedorn, M., Bockhorn, H., 2006. Description of tire pyrolysis by thermal degradation behaviour of main components. J. Anal. Appl. Pyrol. 75, 11–18.
Senneca, O., Salatino, P., Chirone, R., 1999. A fast heating-rate thermogravimetric study of the pyrolysis of scrap tyres. Fuel 78, 1575–1581.
Sheng, C., Azevedo, J.L.T., 2002. Modeling biomass devolatilization using the chemical percolation devolatilization model for the main components. Proc. Combust. Inst. 29, 407–414.
Shulman, V.L., 2011. Chapter 21 - Tyre Recycling A2 - Letcher, Trevor M. In: Vallero, D.A. (Ed.), Waste. Academic Press, Boston, pp. 297–320.
Solum, M.S., Sarofim, A.F., Pugmire, R.J., Fletcher, T.H., Zhang, H., 2001. 13C NMR analysis of soot produced from model compounds and a coal. Energy Fuels 15, 961–971.
Unapumnuk, K., Keener, T., Lu, M., Khang, S.-J., 2006. Pyrolysis Behavior of Tire-Derived Fuels at Different Temperatures and Heating Rates.
Williams, P.T., 2013. Pyrolysis of waste tyres: a review. Waste Manage. (Oxford) 33, 1714–1728.
Williams, P.T., Besler, S., Taylor, D.T., 1990. The pyrolysis of scrap automotive tyres: the influence of temperature and heating rate on product composition. Fuel 69, 1474–1482.
Williams, P.T., Taylor, D.T., 1993. Aromatization of tyre pyrolysis oil to yield polycyclic aromatic hydrocarbons. Fuel 72, 1469–1474.
Yan, B., Cheng, Y., Jin, Y., 2013. Cross-scale modeling and simulation of coal pyrolysis to acetylene in hydrogen plasma reactors. AIChE J. 59, 2119–2133.
Yan, B., Cheng, Y., Xu, P., Cao, C., Cheng, Y., 2014a. Generalized Model of Heat Transfer and Volatiles Evolution Inside Particles for Coal Devolatilization.
Yan, B., Cheng, Y., Xu, P., Cao, C., Cheng, Y., 2014b. Generalized model of heat transfer and volatiles evolution inside particles for coal devolatilization. AIChE J. 60, 2893–2906.
Yang, J., Tanguy, P.A., Roy, C., 1995. Heat transfer, mass transfer and kinetics study of the vacuum pyrolysis of a large used tire particle. Chem. Eng. Sci. 50, 1909–1922.
Zabaniotou, A., Lagoudakis, J., Toumanidou, E., Stavropoulos, G., 2002. Energetic utilization of used tires. Energy Sources 24, 843–854.

Appendix B- MATLAB Coding for M-CPD Model

This page is intentionally left blank

```
%Primary devolatilization

para(1)=600; %maximum temperature (°C)
para(2)=88; % time (min)
para(3)=10; % heating rate (°C/min)


k_values(1)=3.78568035754162e+17; %Ag
k_values(2)=59579.1976819957; %Eg
k_values(3)=5000.00802647511; %og
k_values(4)= 5.74703753008275e+17; %Ab
k_values(5)=59104.4375266052; %Eb
k_values(6)=1583.22553268537; %ob
k_values(7)=50000; % Ecross
k_values(8)=7.83319600351109e+15; % Across
k_values(9)=1.0; % ratio

&original CPD kinetic parameters
% k_values(1)=3E15; %Ag
% k_values(2)=69000; %Eg
% k_values(3)=8100; %og
% k_values(4)=2.602E15; %Ab
% k_values(5)=55400; %Eb
% k_values(6)=1800; %ob
% k_values(7)=65000; % Ecross
% k_values(8)=3E15; % Across
% k_values(9)=0.5000; % ratio

kja(1)= 2.30; % o+1
kja(2)= 358.19; %Mw1
kja(3)= 0.80; %p0
kja(4)= 0; %c0
kja(5)= 138.50; %MwS

%TGA data
load('tga20.mat')
load('tga50.mat')
load('tga10.mat')

kja(1)= kja(1)-1;

[y,y_tar,y_char,t,c,ftar,fchar,c_temperature]=cpd_b17052017(kja,k_values,para
);
%
% plot(t,c)
% hold on
% plot(tga_10_t,tga_10_c)
% hold on
%plot(tga_10_t,tga_10_c)
```

```
function
[y,y_tar,y_char,t,c,ftar,fchar,c_temperature]=cpd_b17052017(kja,kjb,para)


xmw=zeros(21,1);
f=zeros(21,1);
ftold=zeros(21,1);


tarold=zeros(21,1);
metold=zeros(21,1);
Ecross=kjb(7);
Across=kjb(8);
R=1.987;

p0=kja(3);
c0=kja(4);
Mw1=kja(2);
MwS=kja(5)/(1.0-0);
MwS=MwS-40;

o=kja(1);
fgas0=0;
L0=p0-c0;
S0=2*(1-c0-L0);
mb=2*MwS;
ma=Mw1-(o+1)*MwS;
r=mb/ma;


alpha=87058;
beta=299;
gamma=0.5903;

hr=para(3);

tspan=[0 para(2)*60];

options = odeset('Refine',10,'NonNegative',[1 2 3 4 5 6]);
y0 = [130 L0 c0 S0 0 0];
[t,y]    =    ode15s(@(t,y)    cpd_ode_b17052017(t,y,kja,kjb,hr,para),    tspan,
y0,options);
pdash=zeros(length(y),1);
p=zeros(length(y),1);
for i=1:length(y)
    y(i,1)=min(y(i,1),para(1));
    p(i)=y(i,2)+y(i,3);
    pdash(i)=recip(p(i),o);

end
fgas=zeros(length(y),1);
ftar_2=zeros(length(y),1);
Fp=zeros(length(y),1);
phi=zeros(length(y),1);
```

```
omega=zeros(length(y),1);
Kp=zeros(length(y),1);
ffrag=zeros(length(y),1);
delfac=zeros(length(y),1);
ftar=zeros(length(y),1);
fchar=zeros(length(y),1);
fmet=zeros(length(y),1);
fcross=zeros(length(y),1);
ratecr=zeros(length(y),1);
ft=zeros(20,1);
mt=zeros(20,1);
for i=1:length(y)
     Fp(i)=(pdash(i)./p(i)).^((o+1)/(o-1));
    phi(i)=1+r*(y(i,2)./p(i)+(o-1)*y(i,4)./(4*(1-p(i))));
    omega(i)=y(i,4)./(2*(1-p(i)))-y(i,2)./p(i);
    Kp(i)=(1-(o+1)/2*pdash(i))*(pdash(i)./p(i)).^((o+1)/(o-1));
    ffrag(i)=2/(2+r*(1-c0)*(o+1))*(phi(i).*Fp(i)+r*omega(i).*Kp(i));
%     if i>1
%      if ffrag(i)<ffrag(i-1)
%          ffrag(i)=ffrag(i-1);
%      end
%     end
tarfac=1;
if i>1
    tarfac=1-ftar(i-1);
end
    fgas(i)=r.*(y(i,6)).*(o+1)./(4+2*r*(1-c0)*(o+1))*tarfac;
    ftar_2(i)=r.*(y(i,5)).*(o+1)./(4+2*r*(1-c0)*(o+1))*tarfac;

%     Pr=alpha*exp(-beta*Mi^gamma/(y(i,1)+273.15));


delfac(i) = y(i,4)/(1.-p(i));
a = 1.+r*(y(i,2)/p(i) + (o-1)/4 *delfac(i));
b = (delfac(i)/2 - y(i,2)/p(i));
ftsum=0;

for n=1:20
    tn=n*(o-1)+2;
    xm=n*o+1;
    yk = n-1;
    xm1 = xm+1;
    fg1 = gammaln(xm1);
    if fg1<1E-10
        fgam = 0;
        else
           yk1 = yk+1;
           fg2 = gammaln(yk1);
           xmyk = xm-yk+1;
           fg3 = gammaln(xmyk);
           fgam = exp(fg1-fg2-fg3);
    end
    bnn = (o+1)/(n*o+1)*fgam;
    qn = bnn*(p(i).^(n-1)).*((1-p(i)).^tn)/n;
    ft(n) = 2.*(n*a*qn+r*b*qn)/(2.+r*(1.-c0)*(o+1.));
```

```
    ftsum = ftsum + ft(n);
    if(p<1e-9)
            fac = 0;
    else
            fac = y(i,2)/p(i);
    end
    tst=1-p(i);
    if tst<1e-9
       fac1 = 0;
    else
        fac1 = y(i,4)/(1-p(i));
    end
    mt(n) = n*ma+(n-1)*r*ma*fac+tn*r*ma/4*fac1;
end
ftar(1)=0;
fcross(1)=0;
if i>1
%     fmet(i)=ffrag(i)-fcross(i-1)-ftar(i-1);
else
%     fmet(i)=ffrag(i);
end
if fmet(i)<0
    fmet(i)=0;
end
fracr=1;
if i>1
if fmet(i-1)>1e-5

        ratecr(i)     =     Across*exp(-Ecross/(R*(y(i,1)+273.15)))*(t(i)-t(i-
1))*fmet(i-1);
    fracr = 1.-ratecr(i)./fmet(i-1);
    fmet(i)=fmet(i-1)-ratecr(i);
    fcross(i) = fcross(i-1)+ratecr(i);
        if fmet(i)<0
        fcross(i)= fcross(i)+fmet(i);
        fmet(i)=0;
        fracr=0;
        end
    else
    fcross(i)=fcross(i-1);
    fmet(i)=fmet(i-1);
end
end
Ftot=0;

for j=1:20
    j1=j+1;
    xmw(j1) = mt(j);
    dif = ft(j)-ftold(j);
    dif = max(dif,0);
    f(j1) = (dif+metold(j)*fracr)/mt(j);
    ftold(j) = ft(j);
    Ftot = Ftot + f(j1);
end
ntot = 21;
gasmw=r*ma/2;
```

```
f(1) = (fgas(i)+ftar_2(i)-fgas0)./gasmw;
f(1) = max(f(1),0);
fgas0 = max(fgas(i)+ftar_2(i),fgas0);
xmw(1) = gasmw;
Ftot = Ftot + f(1);
 sum = 0.0;

 x3=0.2;
 x2=0.3;
 k=zeros(21,1);
pv=zeros(21,1);
 for ii=1:21
    sum = sum + f(ii);
    pv(ii) = alpha*exp(-beta*xmw(ii).^gamma/(y(i,1)+273.15));
    k(ii) = pv(ii);
    if k(ii)<0.001
        k(ii)=0;
    end
 end
if sum<1E-8
    ftar(i)=ftar(i-1);
    fchar(i)=1-ftar(i)-fgas(i)-ftar_2(i);
    continue
end
 z=zeros(21,1);
 for ii=1:21
     z(ii) = f(ii)/sum;
 end
 x1 = x3;
  f1 = 0;
for ii=1:21
    f1 = f1 + z(ii)*(k(ii)-1)/((k(ii)-1)*(x1)+1);
end
test = x2-x1;
if test<0.005
    x2=x1+0.005;
end
small=1E-3;
for iter=1:100
    f2=0;
    for ii=1:21
        f2 = f2 + z(ii)*(k(ii)-1)/((k(ii)-1)*(x2)+1);
    end
    if abs(f2)<small
        break
    elseif abs(f2-f1)<small^2
        break
    end
    x3 = x2-f2*(x2-x1)/(f2-f1);
    if x3>1
        x3=1-small^2;
    end
    if x3<0
        x3=small^2;
    end
```

```
    if x3==x2
        if x2>small
            x3=x2-small;
        else
            x3=x2+small;
        end
    end
    if x2<1E-5
        if x1<1e-5
            x2=1E-7;
            break
        end
    end
    if x2>0.9999
        if x1>0.9999
            x2=0.9999;
            break
        end
    end
    f1=f2;
    x1=x2;
    x2 = 0.2*x2+0.8*x3;
end
Vtot = Ftot*x2;
Ltot = Ftot-Vtot;
VoL = Vtot/Ltot;
sumx = 0.0;
sumy = 0.0;
xmwtot = 0.0;
ttot = 0.0;


x=zeros(21,1);
l=zeros(21,1);
v=zeros(21,1);
yx=zeros(21,1);
for ii=2:21
    ee = ii-1;
    l(ii) = f(ii)/(1.+k(ii)*VoL);
    v(ii) = f(ii)-l(ii);
    x(ii) = l(ii)*xmw(ii);
    yx(ii) = v(ii)*xmw(ii);
    metold(ee) = max(x(ii),0);
    tarold(ee) = tarold(ee)+yx(ii);
    xmwtot = xmwtot+tarold(ee)*xmw(ii);
    ttot = ttot+tarold(ee);
    sumx = sumx + x(ii);
    sumy = sumy + yx(ii);
end
% abc=fchar(i)
% if fchar(i)==0;
%     abc=123;
% end
if ttot>0
    xmwtot = xmwtot/ttot;
end
```

```
for ii=2:21
    if sumx>1e-28
        x(ii) = x(ii)/sumx;
    end
    if sumy>1e-28
        yx(ii) = yx(ii)/sumy;
    end
end
if fgas(i)<1E-5
    ftar(i)=0;
end
if i>1
ftar(i) = ftar(i-1)+sumy;
else
    ftar(i)=sumy;
end
 fmet(i) = sumx;
 if ftar(i)<1
    abbb=1;
else
    abbb=0;
end
fchar(i)=1-ftar(i)-fgas(i)-ftar_2(i);
if y(i,1)>500
    iaaaa=1;
end
end
c=ftar+fgas+ftar_2;

c_temperature= y(:,1);
y_tar=ftar(end)+ftar_2(end);
y_char=fchar(end);
ftar=ftar+ftar_2;
%                                                 error=mean((interp1(t,c,1:20:1024)-
interp1(pyro_50_t,pyro_50_c,1:20:1024)).^2);
```

```
function dydt = cpd_ode_b17052017(t,y,kja,kjb,hr,para)
% kj(1)=5.1937;
% kj(2)= 0.6069;
% kj(3)= 258.4986;
% kj(4)= 21.3088;
% kj(5)= 0.1259;

Eb0=kjb(5);
Ab=kjb(4);
ob=kjb(6);
Eg0=kjb(2);
Ag=kjb(1);
og=kjb(3);
Ec=0;

R=1.987;
c0=kja(4);
rho=kjb(9);
p0=kja(3);
L0=p0-c0;


dydt=zeros(6,1);
dydt(1)=hr/60; %y6= Temperature
fx1 = 1.-y(2)/L0;
if fx1>0.9997
    fx11=3.5;
elseif fx1<0.0228
    fx11=-2;
else
    fx11=norminv(fx1);
end

Eb=Eb0+fx11*ob;
kb=Ab*exp(-Eb/(R*(min(y(1),para(1))+273.15)));

fx2 = (y(5)+y(6))/(2*(1-c0));
if fx2>0.9997
    fx22=3.5;
elseif fx2<0.0228
    fx22=-2;
else
    fx22=norminv(fx2);
end

Eg=Eg0+fx22*og;
kg=Ag*exp(-Eg/(R*(min(y(1),para(1))+273.15)));

dydt(2)=-kb*y(2); %y2=L
dydt(3)= kb*y(2)/(rho+1);%y3=c
dydt(4)=(2*rho*kb*y(2)/(rho+1))-kg*y(4); %y4=S
dydt(5)=kg*y(4); %y5=g1
dydt(6)=kb*y(2)/(rho+1)*2; %y6=g2
```

```
%Secondary cracking

para(1)=700; %maximum temperature (°C)
para(2)=88; % time (min)
para(3)=100; % heating rate (°C/min)

[t,c_temperature,ftar,fchar,y_tar]=cpd_main(para);


Ecrack=202000;
Acrack=0.2317;

cross_sec_area=0.002375829;
length_reactor=0.5;
T_outside=20;
flow_rate=1;


y_tarnew=zeros(length(t),1);
c_tarnew=zeros(length(t),1);

for i=2:length(t)

T_average=(c_temperature(i)+c_temperature(i-1))/2;
residence_time_reactor=length_reactor/((T_average+273.15)/(T_outside+273.15)*
flow_rate/1000/60/cross_sec_area);
k_crack=Acrack*exp(-Ecrack/(8.3145*(T_average+273.15)));
c_tarnew(i-1)=(ftar(i)-ftar(i-1))*exp(-k_crack*residence_time_reactor);
y_tarnew(i)=y_tarnew(i-1)+c_tarnew(i-1);
end
y_gasnew=1-y_tarnew-fchar;

plot(c_temperature,y_tarnew)
hold on
plot(c_temperature,ftar)
hold off
```

```
function error=error_vincent(k_values)

k_values(1)=3.78568035754162e+17; %Ag
k_values(2)=59579.1976819957; %Eg
k_values(3)=5000.00802647511; %og
k_values(4)= 5.74703753008275e+17; %Ab
k_values(5)=59104.4375266052; %Eb
k_values(6)=1583.22553268537; %ob
k_values(7)=50000; % Ecross
k_values(8)=7.83319600351109e+15; % Across
k_values(9)=1.0; % ratio

%[1.78568035754162e+17,58579.1976819957,5000.00802647511,5.74703753008275e+17
,59104.4375266052,1583.22553268537,45000.0356087388,7.83319600351109e+15,1.03
887629085343]
kja(1)= 2.30; % o+1
kja(2)= 358.19; %Mw1
kja(3)= 0.80; %p0
kja(4)= 0; %c0
kja(5)= 138.50; %MwS

kja(1)= kja(1)-1;

para(1)=1000; %maximum temperature (°C)
para(2)=47.267; % time (min)
para(3)=9.864; % heating rate (°C/min)
error1=0;
[y_tar,y_char,t,c]=cpd_b17052017(kja,k_values,para);
error3=abs(y_tar-0.47);
load('tga10.mat')
error2=mean(abs(interp1(t,c,1:20:2800)-interp1(tga_10_t,tga_10_c,1:20:2800)));

para(1)=1200; %maximum temperature (°C)
para(2)=14.4833; % time (min)
para(3)=52.338; % heating rate (°C/min)
[y_tar,y_char,t,c]=cpd_b17052017(kja,k_values,para);
load('tga50.mat')
error4=mean(abs(interp1(t,c,1:20:800)-interp1(tga_50_t,tga_50_c,1:20:800)));

para(1)=1000; %maximum temperature (°C)
para(2)=33.65; % time (min)
para(3)=20.47; % heating rate (°C/min)
[y_tar,y_char,t,c]=cpd_b17052017(kja,k_values,para);
load('tga20.mat')
error5=mean(abs(interp1(t,c,1:20:2000)-interp1(tga_20_t,tga_20_c,1:20:2000)));

para(1)=1000; %maximum temperature (°C)
para(2)=22.07; % time (min)
para(3)=30.486; % heating rate (°C/min)
[y_tar,y_char,t,c]=cpd_b17052017(kja,k_values,para);
load('tga30.mat')
error6=mean(abs(interp1(t,c,1:20:1300)-interp1(tga_20_t,tga_20_c,1:20:1300)))
error=error1+error2+error3+error4+error5+error6;
```

Appendix C- The Matching Databases of Chemical Species of GC-MS for Lignites Tars

This page is intentionally left blank

RT	Name	Functional group
3.76	Acetic acid	Acid and others
3.82	2-Pentene, 2-methyl-	Acid and others
3.98	2,4-Pentadienenitrile	Acid and others
4.01	Pyridine	Acid and others
4.37	Propanoic acid	Acid and others
4.47	3,4-Dihydropyran	Acid and others
4.54	2-Pentene, 3,4-dimethyl-	Acid and others
4.82	Benzene, 1,3-dimethyl-	Single aromatic
5.10	Benzene, 1,3-dimethyl-	Single aromatic
5.33	Xylene	Single aromatic
5.62	p-Xylene	Single aromatic
5.92	2-Pentanone, 4-hydroxy-4-methyl-	Acid and others
6.16	Styrene	Single aromatic
6.48	Cyclopentanone, 2-methyl-	Acid and others
6.80	2-Cyclopenten-1-one, 2-methyl-	Acid and others
7.16	Pyridine, 3-methyl-	Acid and others
7.40	Pentanoic acid	Acid and others
7.49	Phenol, 3,5-dimethyl-	Phenolic
7.59	2-Cyclopenten-1-one, 3-methyl-	Acid and others
7.76	Benzene, (1-methylethyl)-	Single aromatic
7.97	Benzene, 1-ethyl-3-methyl-	Phenolic
8.25	Benzene, 1,2,4-trimethyl-	Single aromatic
8.53	Benzene, (1-methylethyl)-	Single aromatic
8.64	1-Decene	Acid and others
8.73	Benzene, 1,3,5-trimethyl-	Single aromatic
9.07	Benzene, 1,3,5-trimethyl-	Single aromatic
9.21	Phenol	Phenolic
9.30	Phenol	Phenolic
9.80	Phenol	Phenolic
9.93	Benzene, 1,2,4-trimethyl-	Single aromatic
10.19	Benzene, 1-ethenyl-3-methyl-	Single aromatic
10.36	1H-Indene, 2,3-dihydro-	Single aromatic
10.72	Indene	Single aromatic
10.87	Benzene, 1-methyl-3-propyl-	Single aromatic
10.96	Benzene, (2-methyl-1-propenyl)-	Single aromatic
11.04	Cyclohexane	Acid and others
11.10	Benzene, 1-methyl-3-(1-methylethyl)-	Single aromatic
11.43	O-Cresol	Phenolic
11.65	Benzene, (2-methyl-1-propenyl)-	Single aromatic
11.74	Acetophenone	Acid and others
11.79	Benzene, 1-methyl-4-(1-methylethyl)-	Single aromatic
11.95	o-Isopropenyltoluene	Single aromatic
12.00	Benzene, 4-ethyl-1,2-dimethyl-	Single aromatic

12.12	1-Undecene	Single aromatic
12.34	Phenol, 4-methyl-	Phenolic
12.45	Phenol, 3-methyl-	Phenolic
12.50	Phenol, 3-methyl-	Phenolic
12.63	Benzene, 1-methyl-4-(2-propenyl)-	Single aromatic
12.70	Benzofuran, 7-methyl-	Phenolic
12.77	Benzofuran, 2-methyl-	Phenolic
12.91	Benzofuran, 2-methyl-	Phenolic
13.03	Phenol, 2,6-dimethyl-	Phenolic
13.21	Benzene, 1,2,4,5-tetramethyl-	Single aromatic
13.45	Benzene, 1-methyl-4-(2-propenyl)-	Single aromatic
13.67	2,4-Dimethylstyrene	Single aromatic
13.78	2,4-Dimethylstyrene	Single aromatic
13.87	1H-Indene, 2,3-dihydro-5-methyl-	Single aromatic
13.93	Ethanone, 1-(3,4-dimethylphenyl)-	Single aromatic
14.23	1H-Indene, 1-methyl-	Single aromatic
14.30	2-Methylindene	Single aromatic
14.43	2-Methylindene	Single aromatic
14.50	2-Methylindene	Single aromatic
14.60	Phenol, 2,4-dimethyl-	Phenolic
15.04	Benzaldehyde, 4-methyl-	Acid and others
15.28	Phenol, 4-ethyl-	Phenolic
15.36	Phenol, 3-ethyl-	Phenolic
15.42	Phenol, 3,4-dimethyl-	Phenolic
15.56	Naphthalene	Double aromatic
15.81	Phenol, 2,3-dimethyl-	Phenolic
15.87	Dodecane	Double aromatic
15.98	Benzene, (2-methyl-1-methylenepropyl)-	Phenolic
16.11	2-(2-Hydroxyphenyl)buta-1,3-diene	Phenolic
16.29	Phenol, 2-ethyl-	Phenolic
16.43	Phenol, 2,4,6-trimethyl-	Phenolic
16.49	Benzofuran, 4,7-dimethyl-	Phenolic
16.61	Benzofuran, 4,7-dimethyl-	Phenolic
16.72	2,3-Dimethylbenzofuran	Phenolic
16.84	1,2-Benzenediol	Phenolic
16.94	1,2-Benzenediol	Phenolic
17.05	1,2-Benzenediol	Phenolic
17.30	Benzenamine, N,3-dimethyl-	Phenolic
17.48	Indene	Double aromatic
17.62	Ethanone, 1-(3,4-dimethylphenyl)-	Acid and others
17.84	(1-Methylbuta-1,3-dienyl)benzene	Double aromatic
17.96	1-(3-Methylphenyl)buta-1,3-diene	Acid and others
18.02	1H-Indene, 1,3-dimethyl-	Double aromatic
18.13	1H-Indene, 1,3-dimethyl-	Double aromatic

18.26	1H-Indene, 1,3-dimethyl-	Double aromatic
18.39	Pyrrolidine, 1-(1-cyclopenten-1-yl)-	Acid and others
18.62	Phenol, 2,4,6-trimethyl-	Phenolic
18.76	Phenol, 2,4,6-trimethyl-	Phenolic
19.03	1-Tridecene	Double aromatic
19.11	1H-Indene, 1,1-dimethyl-	Double aromatic
19.32	Naphthalene, 2-methyl-	Double aromatic
19.52	Benzaldehyde, 3,5-dimethyl-	Phenolic
19.61	2-Propen-1-ol, 3-phenyl-	Phenolic
19.73	Phenol, 2,4,5-trimethyl-	Phenolic
19.81	Naphthalene, 1-methyl-	Double aromatic
19.97	3-METHYLBENZALACETONE	Acid and others
20.16	1,2-Benzenediol, 4-methyl-	Phenolic
20.29	1,2-Benzenediol, 4-methyl-	Phenolic
20.37	1,2-Benzenediol, 3-methyl-	Phenolic
20.54	1,2-Benzenediol, 4-methyl-	Double aromatic
20.73	Naphthalene, 1,2,3,4-tetrahydro-2,7-dimethyl-	Phenolic
20.95	Benzofuran, 7-methyl-	Phenolic
21.14	1H-Inden-5-ol, 2,3-dihydro-	Phenolic
21.27	2-Methyl-5-hydroxybenzofuran	Phenolic
21.39	(E)-4-Methyl-1-phenyl-1,3-pentadiene	Phenolic
21.52	Benzene, 1-methoxy-4-(2-propenyl)-	Double aromatic
21.59	Benzene, 1,3,5-trimethyl-2-(1,2-propadienyl)-	Double aromatic
21.80	1,2,3-Trimethylindene	Double aromatic
21.94	1,2,3-Trimethylindene	Double aromatic
22.06	Biphenyl	Phenolic
22.14	2-Methyl-5-hydroxybenzofuran	Phenolic
22.29	1-Tetradecene	Double aromatic
22.38	Quinoline, 3-methyl-	Double aromatic
22.49	(1-Methylpenta-2,4-dienyl)benzene	Double aromatic
22.59	Benzene, 1,3,5-trimethyl-2-(1,2-propadienyl)-	Double aromatic
22.70	1,4-dimethyl-dihydro-azulene	Double aromatic
22.87	Naphthalene, 2,6-dimethyl-	Double aromatic
22.93	Naphthalene, 2,6-dimethyl-	Double aromatic
23.18	Naphthalene, 2,6-dimethyl-	Double aromatic
23.28	Naphthalene, 2,3-dimethyl-	Double aromatic
23.43	Naphthalene, 1,7-dimethyl-	Double aromatic
23.55	2-Methyl-5-hydroxybenzofuran	Phenolic
23.73	Acenaphthylene, 1,2-dihydro	Double aromatic
23.88	Naphthalene, 1,4-dimethyl-	Double aromatic
23.97	Naphthalene, 2,3-dimethyl-	Double aromatic
24.17	2-Propyn-1-ol, 3-(4-methylphenyl)-	Phenolic
24.26	Acenaphthylene	Double aromatic
24.36	Naphthalene, 2,3-dimethyl-	Double aromatic

24.63	3-Buten-2-one, 4-phenyl-	Phenolic
24.76	1H-Inden-1-one, 2,3-dihydro-5-methoxy-	Acid and others
24.95	4-Methoxycinnamaldehyde	Acid and others
25.04	3-Buten-2-one, 4-phenyl-	Acid and others
25.18	3-Buten-2-one, 4-phenyl-	Acid and others
25.23	Biphenylene, 1,2,3,6,7,8,8a,8b-octahydro-4,5-dimethyl-	Acid and others
25.40	1-Pentadecene	Acid and others
25.61	pentadecane	Acid and others
25.77	5,8-Dimethyl-1,2,3,4-tetrahydroquinoxaline	Acid and others
25.93	Naphthalene, 1,4,5-trimethyl-	Double aromatic
26.02	Naphthalene, 1,4,6-trimethyl-	Double aromatic
26.09	1H-Indene, 2,3-dihydro-1,1,2,3,3-pentamethyl-	Phenolic
26.14	Naphthalene, 1,2-dihydro-1,4,6-trimethyl-	Phenolic
26.35	Dibenzofuran	Phenolic
26.50	Naphthalene, 1,6,7-trimethyl-	Double aromatic
26.57	3-Methylcinnamic acid	Acid and others
26.72	3-Methylcinnamic acid	Acid and others
26.95	1-[2'-ethenyl-1'-cyclohexenyl]-2-propen-1-one	Acid and others
27.11	Naphthalene, 1,4,6-trimethyl-	Double aromatic
27.19	2-Naphthalenol	Phenolic
27.28	1-Naphthalenol	Phenolic
27.42	Naphthalene, 1,6,7-trimethyl-	Double aromatic
27.54	Naphthalene, 1,6,7-trimethyl-	Double aromatic
27.62	Naphthalene, 1,4,5-trimethyl-	Double aromatic
27.69	Naphthalene, 1,4,6-trimethyl- $	Double aromatic
27.91	Naphthalene, 1,4,6-trimethyl- $	Double aromatic
28.09	9H-Fluorene (CAS)	Double aromatic
28.32	Naphthalene, 1,6,7-trimethyl-	Double aromatic
28.44	2-Allyl-1-methylnaphthalene	Double aromatic
28.55	Hexadecane	Double aromatic
28.67	Naphthalene, 1-(2-propenyl)-	Double aromatic
28.76	1,1'-Biphenyl, 3,4'-dimethyl-	Double aromatic
28.81	4,6,8-Trimethylazulene	Double aromatic
28.90	9H-Fluorene (CAS)	Double aromatic
29.05	9H-Fluorene (CAS)	Double aromatic
29.18	9H-Fluorene (CAS)	Double aromatic
29.32	9H-Fluorene (CAS)	Double aromatic
29.42	9H-Fluorene (CAS)	Double aromatic
29.58	9H-Fluorene	Double aromatic
29.65	1-Naphthalenol, 3-methyl-	Double aromatic
29.79	9H-Fluoren-9-ol	Phenolic
29.99	9H-Fluoren-9-ol	Phenolic
>30.00	Oxygen-containing long-chain hydrocarbons	Long chain